For Reference

NOT TO BE TAKEN FROM THIS ROOM

Ex Libris
Universitatis
Albertaensis

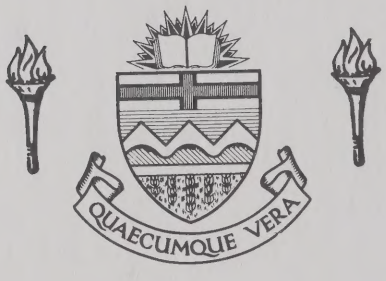

THE UNIVERSITY OF ALBERTA

THE BEHAVIOR OF THAWING SLOPES IN PERMAFROST

by

© DENNIS E. PUFAHL

A THESIS

SUBMITTED TO THE FACULTY OF GRADUATE STUDIES

AND RESEARCH IN PARTIAL FULFILMENT OF THE

REQUIREMENTS FOR THE DEGREE OF

DOCTOR OF PHILOSOPHY

DEPARTMENT OF CIVIL ENGINEERING

EDMONTON, ALBERTA

FALL, 1976

ABSTRACT

Slope instability is one of the major considerations in the choice of route location across terrain underlain by permafrost. A field reconnaissance has established the state-of-the-art of cut slope design, construction and performance in the Western Canadian Arctic and Alaska. It is apparent that limited instability of backslope cuts in fine grained frozen soils may be encountered in almost all of these regions. Emphasis has been placed on establishing the geological history, the land form, and the associated soil and ground ice characteristics.

Flow dominated failures on natural slopes and cut slopes are common in regions of permafrost. A means of stabilizing these failures is proposed. The method utilizes insulation to control the rate of thaw and the generation of excess pore water pressures. A sand/gravel surcharge load helps to stabilize the slope by increasing the normal effective stress disproportionately to the shearing stress. Design charts are provided and recommendations for installation are included.

Uncontrolled thawing of backslope cuts in fine grained ice rich soil generally results in the formation of bimodal flows common to periglacial regions. A prerequisite for the development of rational methods of control of these features is the establishment of the energetics of exposed melting permafrost. The theory is developed and verified by field experiments and thus provides the basis for controlling the rate of thaw of exposed permafrost.

Recommendations for the design and construction of cut slopes in frozen soils are outlined. Some control methods are suggested that incorporate sand/gravel and other types of higher quality insulation in a variety of different configurations.

Digitized by the Internet Archive
in 2023 with funding from
University of Alberta Library

https://archive.org/details/Pufahl1976

ACKNOWLEDGEMENTS

The activities and research presented in this thesis were carried out under the direction of Dr. N.R. Morgenstern, University of Alberta. The author is grateful and indebted to him for his suggestions regarding the topic, for his help in interpreting and presenting the data, and especially for his seemingly limitless enthusiasm for the research project. The help of Dr. Stan Thomson was also warmly received.

Sincere appreciation is extended to the University of Alberta support staff which include Messrs. O. "Woody" Woods, Roy Gitzel, Al Muir, and Don Nordheimer.

This research project was sponsored by the Department of Energy, Mines and Resources, the Defense Research Board, and the National Research Council of Canada. The Department of Public Works, Government of Can., Northwest Territories and the Yukon Territory, the Alaska Department of Highways in Fairbanks, and the State Materials Laboratory in College Alaska all receive recognition for their suggestions, participation and interest in the project.

Personal financial assistance from the Transportation Development Agency, the Roads and Transportation Association of Can., and the North American Life Canadian Council of Professional Engineers was gratefully received.

In addition the author wishes to acknowledge the support and encouragement offered by wife, Idoline Ann, during the first year and a half in Edmonton. Sincere apologies are extended to her for any economic, social or emotional deprivation that may have resulted from this undertaking.

Finally, the unflaging interest and help from Mr. Bill Roggensack during those endless miles of dust and rain and gravel will always be remembered. His editorial assistance was invaluable and the personal friendship and support provided by him and his wife, Muriel, made the completion of this thesis possible.

TABLE OF CONTENTS

		Page
Release Form		i
Title Page		ii
Approval Sheet		iii
Abstract		iv
Acknowledgements		v
Table of Contents		vii
List of Tables		xv
List of Figures		xvi
CHAPTER I	INTRODUCTION	1
	1.1 General	1
	1.2 Scope of Thesis	3
CHAPTER II	BEHAVIOR OF EXISTING CUTS IN PERMAFROST	5
	2.1 Objectives	5
	2.2 Route	6
	2.3 Alaska Highway [Mile 222 (from Dawson Creek, B.C.) 57°58'N latitude; 122°46' W longitude]	7
	2.3.1 Summary	8
	2.4 Dempster Highway	10
	2.4.1 Location and Background	10
	2.4.2 Mile 0 - Mile 80	12
	2.4.3 Mile 80 - Mile 154	14
	2.4.4 Mile 154 - Mile 178	16
	2.4.5 Fort McPherson to Arctic Red River Mile 330 to Mile 365	18
	2.4.6 Mile 178 - Mile 330	19

		Page
	2.5 Mackenzie Highway (Inuvik to Arctic Red River)	19
	2.6 Alaska Reconnaissance	20
	2.6.1 General	20
	2.6.2 TAPS Haul Road	20
	2.6.3 Copper River Basin	23
	2.7 Conclusions	24
CHAPTER III	STABILIZATION OF PLANAR LANDSLIDES IN PERMAFROST	33
	3.1 Introduction	33
	3.2 Thaw Consolidation Pore Water Pressures	33
	3.3 Stability Analysis of Infinite Thawing Slopes	37
	3.4 Numerical Procedure for Design	41
	3.5 Design Charts	46
	3.6 Example Problem	47
	3.7 Recommendations for Installation	53
	3.8 Long term Performance	55
	3.9 Choice of Insulation	55
CHAPTER IV	THE ENERGY BALANCE	70
	4.1 Basic Concepts	70
	4.2 Radiative Components on a Horizontal Surface	71
	4.2.1 General	71
	4.2.2 Direct Beam Clear Sky Solar Radiation	73
	4.2.3 Diffuse Clear Sky Radiation	76

Page

4.2.4 The Effect of Clouds 79

4.2.5 Summary of Short Wave Radiation 83

4.2.6 Short Wave Radiation Reflected by the Surface of the Earth 83

4.2.7 Net Short Wave Radiation 84

4.2.8 Longwave Radiation Emitted by The Ground Surface 86

4.2.9 Longwave Radiation From the Atmosphere to the Ground 88

4.2.10 Net Longwave Radiation 93

4.3 Radiative Components on a Sloping Surface 98

4.3.1 General 98

4.3.2 Direct Beam Radiation 99

4.3.3 Diffuse Radiation 103

4.3.4 Short Wave Component Reflected to the Surface by Surrounding Surfaces 106

4.3.5 Short Wave Component of Radiation Reflected by the Surface 108

4.3.6 Downward Longwave Component of Radiation Falling on the Slope 109

4.3.7 Downward Longwave Component Reflected to the Surface by Surrounding Surfaces 110

4.3.8 Upward Component of Long Wave Radiation Reflected onto the Slope by Surrounding Surfaces 110

4.3.9 Long wave Radiation Emitted by the Surface 111

4.3.10 Summary of Components 111

4.4 Turbulent Transfer Processes 114

4.5 Evaporation and Condensation 114

Page

4.6 Sensible Heat Transfer 120

4.7 Energy Transfer Due to Precipitation 126

4.8 Soil Heat Transfer 127

4.9 Summary of Heat Balance 128

CHAPTER V HEAT FLUX MEASUREMENTS AT THE HEAD SCARP 129

5.1 Introduction 129

5.2 Site Location and Description 129

5.3 Ablation Rates 142

5.3.1 Measurement Techniques 142

5.3.2 Magnitude and Heat Requirements 144

5.4 Radiation Balance 151

5.4.1 Short Wave Radiation 151

5.4.2 Net Short Wave Radiation 152

5.4.3 Net Long Wave Radiation 152

5.4.4 Net All wave Radiation 156

5.5 Radiation Field Instrumentation 156

5.6 Data Acquisition System 157

5.7 Measured Total Short Wave Radiation 162

5.8 Measured Net Radiation 166

5.9 Latent Heat Transfer 173

5.10 Evaporation Quantities 185

5.11 Sensible Heat Transfer 187

5.12 Ablation and the Heat Balance 189

Page

CHAPTER VI CONTROL OF THAWING IN EXPOSED PERMAFROST 205

6.1 Head Scarp Geometry of Bimodal Flows 205

6.2 Basis for Control 206

6.3 Suggested Methods of Control 209

6.4 Recommended Practice for Cut Slope Design 214

6.4.1 Self Healing Cut Slopes 214

6.4.2 Non Self-Healing Cut Slopes 217

CHAPTER VII CONCLUDING REMARKS 222

LIST OF REFERENCES 227

APPENDIX A DETAILS OF FIELD RECONNAISSANCE 236

A.1 Alaska Highway (Mile 222 (from Dawson Creek, B.C.) 57°58N Latitude; 122°46'W Longitude) 236

A.1.1 Physiography 236

A.1.2 Climate 236

A.1.3 Permafrost 236

A.1.4 Bedrock Geology 237

A.1.5 Surficial Geology 237

A.1.6 Highway Details (Mile 222) 238

A.2 Dempster Highway 238

A.2.1 Dempster Highway (Mile 0 to Mile 80) 239

A.2.2 Climate 239

A.2.3 Permafrost 240

A.2.4 Bedrock Geology 240

A.2.5 Surficial Geology 240

Page

A.2.6 Highway Details 240

A.3 Dempster Highway (Mile 80 to Mile 154) 241

A.3.1 Physiography 241

A.3.2 Climate 242

A.3.3 Permafrost 242

A.3.4 Bedrock Geology 242

A.3.5 Surficial Geology 242

A.3.6 Highway Details 243

A.3.6.1 Highway Details (Mile 80 - Mile 96) 243

A.3.6.2 Highway Details (Mile 96 to Mile 123) 243

A.3.6.3 Highway Details (Mile 114) 244

A.3.6.4 Highway Details (Mile 120.7) 244

A.3.6.5 Highway Details (Mile 123 to Mile 154) 244

A.3.7 Summary 245

A.4 Dempster Highway (Mile 154 to Mile 178) 245

A.4.1 Physiography 245

A.4.2 Climate 246

A.4.3 Permafrost 246

A.4.4 Bedrock Geology 246

A.4.5 Surficial Geology 246

A.5 Highway Details 247

A.5.1 Highway Details (Mile 168) 247

A.5.2 Highway Details (Mile 175) 247

A.5.3 Summary 248

Page

A.6 Dempster Highway (Fort McPherson to Arctic Red River, Mile 330 to Mile 365) 249

A.6.1 Physiography 249

A.6.2 Climate 249

A.6.3 Permafrost 249

A.6.4 Bedrock Geology 249

A.6.5 Surficial Geology 249

A.6.6 Highway Details 250

A.7 Dempster Highway (Mile 178 to Mile 330) 251

A.7.1 Physiography 251

A.7.2 Climate 251

A.7.3 Permafrost 251

A.7.4 Bedrock Geology 251

A.7.5 Surficial Geology 252

A.7.6 Observations 252

A.7.7 Summary 252

A.8 Mackenzie Highway (Inuvik to Arctic Red River) 253

A.9 Alaska Reconnaissance 253

A.9.1 General 253

A.9.2 Physiography 254

A.9.3 Climate 255

A.9.4 Permafrost and Vegetation 255

A.9.5 Bedrock Geology 255

A.9.6 Surficial Geology 256

A.9.7 Highway Details 256

A.9.7.1 Highway Details (Mile 14) 256

Page

A.9.7.2 Highway Details (Mile 19.6) 257

A.9.7.3 Highway Details (Mile 20.3 to Mile 20.5) 257

A.9.7.4 Highway Details (Mile 22.9) 257

A.9.7.5 Highway Details (Mile 23.4) 258

A.9.7.6 Highway Details (Mile 33.0 to Mile 33.4) 259

A.9.7.7 Highway Details (Mile 42.8) 259

A.9.7.8 Highway Details (Mile 53.5) 259

A.9.7.9 Highway Details (Mile 54.4) 259

A.9.8 Summary 260

A.10 Copper River Basin 260

A.10.1 Physiography 260

A.10.2 Climate 261

A.10.3 Permafrost 261

A.10.4 Bedrock Geology 261

A.10.5 Surficial Geology 261

A.10.6 Highway Details 261

A.11 Conclusions 262

APPENDIX B COMPUTER PROGRAM AND EXAMPLE PROBLEM OF SLOPE STABILIZATION TECHNIQUE 272

APPENDIX C

C.1 Computer program to calculate the length of a shadow cast by an obstruction on sloping ground 289

Page

C.2 Computer program to compute the direct beam and total solar daily radiation on a sloping surface from values monitored on a horizontal surface 231

C.3 Procedure for calculating the amount of reflected diffuse radiation from one surface to another 292

APPENDIX D 308

D.1 Computer program for computing vapor pressures, vapor pressure gradients and temperature gradients from wet and dry bulb temperatures 308

Radiation data in Table D-1

LIST OF TABLES

Table		Page
2.1	Summary of Soil Data	29
2.2	Summary of Cuts	30
3.1	Physical and Thermal Properties of Various Insulating Methods	42
3.2	Soil, Insulation and Climate Information for Example Problem	48
3.3	Thaw Depth and Insulation and Surcharge Requirements for Example Problem	51
3.4	Comparison of Factors of Safety by Different Methods of Computation	52
4.1	Albedo of Various Surfaces	85
4.2	Infrared Emissivities	87
4.3	Air Temperature, Relative Humidity, and Vapour Pressure	118
4.4	Snow Melt Due to Sensible & Convective Heat Transfer and Bowen's Ratio (After U.S. Army Corps of Eng., 1956)	124
5.1	Summary of Soil Data at Fort Simpson Landslide	139
5.2	Short Wave Radiation Quantities for Slopes at Different Orientations and Inclinations for Fort Simpson Region	195
5.3	Net Longwave Radiation for Different Slopes Computed from Equation 4.53	197(a)
5.4	Net Radiation for Slopes at Different Orientations and Inclinations for Fort Simpson Region	198
5.5	Daily and Accumulated Total Radiation on a Horizontal Surface at the Fort Simpson Test Site	200
5.6	Net Radiation at the Fort Simpson Test Site	201
5.7	Comparison of Predicted Values and Measured Values of Net Radiation	203
5.8	Lysimetric Data	204
D.1	Radiation Data (Fort Simpson Test Site)	

LIST OF FIGURES

Figure		Page
2.1	Transportation Facilities - 1972 Northwestern Canada	8
2.2	Permafrost in Canada (After Brown, 1967)	9
2.3	Location of the Dempster Highway, Dawson City, Yukon Territory to Arctic Red River, N.W.T.	11
2.4	Physiographic Regions of the Yukon Territory	13
2.5	Location of Mile 90 to Mile 180 of the Dempster Highway	15
2.6	TAPS Haul Road; Livengood to the Yukon River Alaska	21
3.1	Thaw Depth vs Time and Thaw Depth vs $\sqrt{\text{Time}}$ for an Insulated Thawing Slope	36
3.2	Pore Pressure at the Thaw Front of a Thawing Infinite Slope	38
3.3	Balance of Forces on a Thawing Infinite Slope	38
3.4	Pore Pressure Factor (R') for Different Thaw Consolidation Ratios (R) After Morgenstern & Nixon (1971)	40
3.5	Pore Pressure Factor (R'') for Different Thaw Consolidation Ratios (R) After Morgenstern & Nixon (1971)	40
3.6	Design Chart for Stabilization of Planar Landslides	58
3.7	Design Charts for Stabilization of Planar Landslides	59
3.8	Design Charts for Stabilization of Planar Landslides	60
3.9	Design Charts for Stabilization of Planar Landslides	61
3.10	Design Charts for Stabilization of Planar Landslides	62
3.11	Design Charts for Stabilization of Planar Landslides	63
3.12	Design Charts for Stabilization of Planar Landslides	64
3.13	Design Charts for Stabilization of Planar Landslides	65
3.14	Design Charts for Stabilization of Planar Landslides	66
3.15	Design Charts for Stabilization of Planar Landslides	67
3.16	Design Charts for Stabilization of Planar Landslides	68

Figure		Page
3.17	Design Charts for Stabilization of Planar Landslides	69
4.1	Monochromatic Emissive Power for Several Temperatures vs Wavelength (After Wiebelt (1966))	72
4.2	Atmospheric Transmission Chart (After Kimball 1928)	78
4.3	Extraterrestrial Daily Radiation Received on a Horizontal Surface (After Lui and Jordan, 1960)	80
4.4	The Ratio of the Monthly Ave. Daily Diffuse Radiation to the Monthly Ave. Daily Total Radiation as a Function the Cloudiness Index K_T (After Lui & Jordan, 1960)	80
4.5	Ratio of Direct to Diffuse Radiation Received at the Ground Surface (%) After London (1957)	81
4.6	Saturated Vapour Pressure vs Temperature	117
4.7	Convection Melt (computed) (After U.S. Army Corps of Eng., 1956)	123
4.8	Condensation Melt (computed) (After U.S. Army Corps of Eng., 1956)	123
5.1	Aerial View of Fort Simpson Landslide	130
5.2	Bank Profile of Mackenzie River Immediately East of Fort Simpson Landslide	131
5.3	Plan View of Fort Simpson Landslide	133
5.3(a)	Description of Sediments of Fort Simpson Landslide	133(a)
5.4	Aerial View of East Flank of Fort Simpson Landslide	134
5.5	Plan View and Instrumentation of Headscarp of Bimodal Flow at Fort Simpson Landslide	136
5.6	View of Headscarp (July 1974)	137
5.7	Mudflow at the Base of the Headscarp	137
5.8	Soil Profile Zone 1, 2 & 3 (Oct. 1973)	141
5.9	Soil in Zone 3	141
5.10	Frozen Core Removed From Zone 4	141
5.11	Schematic Arrangement of Ablation Measurement Technique	143

Figure		Page
5.12	Ablation Measurement Technique	145
5.13	Accumulated Ablation at Sta. 1	145
5.14	Accumulated Ablation at Sta. 2	146
5.15	Accumulated Ablation at Sta. 3	146
5.16	Accumulated Ablation at Sta. 4	147
5.17	Accumulated Ablation at Sta. 5	147
5.18	Accumulated Ablation at Sta. 6	148
5.19	Water Content vs. Relative Frequency Curve	148
5.20	Cos Λ vs. Time for a Sloping Surface	153
5.21	Cos Λ vs. Time for a Horizontal Surface	153
5.22	Net Radiometer (Fritchen Model)	158
5.23	Net Radiometers Around Headscarp	158
5.24	Typical Variation of Radiation Intensity with Time	160
5.25	Schematic Sketch of Radiation Instrumentation	165
5.26	Data Acquisition System	165
5.27	Total Shortwave Radiation on a Horizontal Surface for the Period of Observation	165
5.28	Net Radiation for the Period of Observation (Sta. 1)	167
5.29	Net Radiation for the Period of Observation (Sta. 2)	168
5.30	Net Radiation for the Period of Observation (Sta. 3)	169
5.31	Net Radiation for the Period of Observation (Sta. 4)	170
5.32	Net Radiation on a Horizontal Surface for the Period of Observation (Sta. 5)	171
5.33	Accumulated Net Radiation for the Period of Observation	172

Figure		Page
5.34	Permafrost Lysimeter	175
5.35	Permafrost Lysimeter	176
5.36	Tray from Permafrost Lysimeter (weighed with standard load cell)	176
5.37	Portable Crane and Permafrost Lysimeter	177
5.38	Product of Average Wind Speed and Relative Humidity vs. Latent Heat of Condensation	180
5.39	Wet and Dry Bulb Temperature Sensors	182
5.40	Typical Vapour Pressure Gradients Above the Headscarp	184
5.41	Daily Evaporation Rates at Test Site	186
5.42	Typical Temperature Gradients above the Headscarp	188
5.43	Heat Balance at the Headscarp of the Fort Simpson Landslide	191
6.1	Gravel Thickness, Ground Surface Thawing Index and Headscarp Retreat for Ice	212
6.2	Gravel and Artificial Insulation Configuration for Steep Slopes	218
6.3	Gravel and Artificial Insulation Configuration for Moderately Steep Slopes	218
6.4	Gravel and Rock Filled Gabions with Artificial Insulation on Moderately Steep Slope	220
6.5	Gravel and Artificial Insulation on Low Angle Slope	220
A.1	Mile 222 Alaska Highway (Backslope instability during construction, July 1973).	263
A.2	Mile 50 Dempster Highway (Headwaters of the East Blackstone River. Road built at very modest geometric design standards)	263
A.3	Mile 124 Dempster Highway (Typical view of the Ogilvie physiographic unit)	263
A.4	Mile 80 Dempster Highway (Improved geometric design standards)	264

Figure		Page
A.5	Mile 109 Dempster Highway (Biangular profile of backslope due to permafrost degradation)	264
A.6	Mile 114 Dempster Highway (Large thermal degradation scar - 150 ft. wide and 15 to 20 ft. deep)	264
A.7	Mile 120.7 Dempster Highway (Ten ft. cut with 2:1 backslopes made into ice rich organic silt)	265
A.8	Mile 153 Dempster Highway (Melting of large ice wedges caused slope degradation)	265
A.9	Mile 153 Dempster Highway (View from top dressed backslope)	266
A.10	Mile 175 Dempster Highway (Backslope and shoulder failure due to melting of a large ice lense)	266
A.11	Mile 175 Dempster Highway (Severe cracking of shoulder due to differential thermal subsidence caused by construction	266
A.12	Mile 343 Dempster Highway - Large cut between Arctic Red River and Fort McPherson (looking west)	267
A.13	Mile 343 Dempster Highway - Stabilized backslope. (Hand placed vegetation to control rate of thaw)	267
A.14	Bimodal flow in the Richardson Mountains	267
A.15	Approach cut to Mackenzie River crossing at Arctic Red River	268
A.16	Typical vegetation patterns at southern end of TAPS Haul Road	268
A.17	Mile 14 TAPS Haul Road (July 1973)	268
A.18	Mile 20 TAPS Haul Road - Typical Bore Hole Log (After Smith & Berg 1972)	269
A.19	Mile 1916 (31.6 km) TAPS Haul Road (July 1973)	269
A.20	Mile 20.3 (32.6 km) TAPS Haul Road (July 1973)	269
A.21	Mile 22.9 TAPS Haul Road (April 1970) (After Smith & Berg 1972)	270
A.22	Mile 22.9 TAPS Haul Road (July 1973)	270
A.23	Mile 23.4 TAPS Haul Road. Approach to Hess Creek (April 1970)	270

Figure		Page
A.24	Mile 23.4 TAPS Haul Road. Approach to Hess Creek (July 1973)	271
A.25	Mile 33 TAPS Haul Road (July 1973)	271
A.26	Mile 54.4 TAPS Haul Road (July 1973)	271
C.1	Shadow Cast by Obstruction on Sloping Ground	290
C.2	Relation of a Small Surface dA_2 to a Diffusely Reflecting Large Surface A_1 (After Threlkeld, 1963)	292

CHAPTER I

INTRODUCTION

1.1 General

The increased demand for energy and raw materials within the last decade has resulted in the exploitation of many frontier reserves of minerals, oil, and natural gas. The Canadian and Alaskan Arctic are presently the center for much of this activity. The development of natural resources in these regions requires the construction of various transportation facilities over terrain underlain by discontinuous and continuous permafrost. One of the major problems associated with route location for these facilities is that of slope instability.

Research activities by Capps (1919), Eakin (1919), Taber (1943), and Sigafoos and Hopkins (1952) provided a substantial quantity of qualitative information regarding slope instability in periglacial regions. The proposed pipeline construction in the Mackenzie valley added new impetus to this aspect of Arctic research. Hardy and Morrison (1972), Hughes (1972), Issacs and Code (1972) and MacKay and Mathews (1973) provided greater insight into the mechanisms of mass movements in the arctic regions.

McRoberts (1973) classified the different types of mass movements encountered along the Mackenzie River valley and its tributaries. He successfully attempted to explain the mechanisms of failure of thawing permafrost slopes in quantitative geotechnical terms. Thaw consolidation excess pore water pressures due to self weight were included in his analysis of an infinite thawing slope. This equation was

$$F_s = \gamma'/\gamma \left(1 - \frac{1}{1 + \frac{1}{2R^2}}\right) \frac{\tan \phi'}{\tan \theta} \quad - - - [1.1]$$

(After McRoberts and Morgenstern, 1974)

where F_s = factor of safety of the slope

γ' = effective unit weight of the soil

γ = total unit weight of the soil

ϕ' = angle of internal friction of the soil

θ = angle of the slope

R = thaw consolidation ratio

This relationship adequately explained soil movements on low angle slopes that would have otherwise been stable if only steady state seepage pore water pressures had been present. It was apparent that any stabilization techniques would require the alteration of the thaw-consolidation ratio (R) which includes both thermal and physical properties of the soil as well as the imposed step temperature at the surface. This thesis proposes a method for stabilizing planar landslides on thawing slopes.

The geotechnical implications of uncontrolled retreat of bimodal flows was recognized and attention was drawn to the hazards involved with artificial cuts in ice rich soil (ibid). A simple model used to relate the rate of ablation to heat flux at the surface is of the form:

$$V = F/L \quad - - - [1.2]$$

(Carslaw and Jaeger, 1947)

where V = the steady state velocity of the ablation surface

F = the heat flux available at the surface

L = the volumetric latent heat of fusion of the soil/ice mixture

This relationship indicated that a heat flux of approximately 200 to 600 ly/day was required to sustain typical rates of ablation that had been observed in the field. A comparison of these values with synoptic estimates of net radiation indicated a substantial disparity. There appeared to be an unaccountable source of heat involved in the ablation process. Kerfoot (1969) and McRoberts (1973) also noted that bimodal flows did not favor any particular aspect and that maximum retreat did not always occur on slopes with the most southerly aspect.

The questions concerning the high rate of ablation, the indifference to aspect, and the unique shape of the headscarp of bimodal flows remained unanswered. A complete analysis of the heat balance at the surface of exposed melting permafrost was considered necessary to properly explain the observed phenomena and to provide a rational basis for the design of remedial measures.

1.2 Scope of Thesis

Transportation facilities constructed across permafrost terrain necessitate the cutting of slopes in frozen soils that are not stable in the thawed state. A field reconnaissance was undertaken in order to appraise the behavior of existing road cuts. Chapter II outlines the nature of this reconnaissance, summarizes the findings, and contains the conclusions of the survey. The details of this study along with a variety of illustrated examples are contained in Appendix A.

One of the common forms of natural instability involves a surface movement or detachment failure of surficial material on reasonably planar surfaces. These flow dominated movements are evident not

only on natural slopes but on low angle back slope cuts as well. The necessity for some means of positive stabilization of these failures or incipient failures is apparent. Chapter III identifies the important variables involved in this problem and proposes a procedure to remedy this type of instability.

If rational design procedures are to be utilized to prevent excessive degradation of cut slopes or to control naturally occurring bimodal flows it is essential to establish the energetics of exposed melting permafrost. Chapter IV outlines the heat balance theory for a sloping surface of exposed permafrost and postulates the presence of substantial sources of heat other than net radiation. The theory was verified by field experiments which were performed at a large complex landslide on the Mackenzie River near Fort Simpson, N.W.T. The details of the field program and the interpretation of the results appear in Chapter V of this text. The results substantiate the theory and provide the basis for control of thawing of exposed permafrost.

Design and construction procedures for cut slopes are reviewed and a variety of methods for backslope preservation are presented in Chapter VI.

The final chapter contains the concluding remarks and suggests the form of ongoing research related to this aspect of surface transportation facilities in the Arctic.

CHAPTER II

BEHAVIOR OF EXISTING CUTS IN PERMAFROST

2.1 Objectives

Transportation facilities constructed across permafrost terrain often require cuts of varying size to maintain acceptable geometric standards. Exposure of these open cuts to thawing temperatures invariably cause degradation of the permafrost and subsequent deterioration of the backslopes. The magnitude and frequency of this deterioration was previously without documentation with the exception of the work of Smith and Berg (1972) on the Trans-Alaskan Pipeline System Haul Road.

General interrelationships regarding geological history, landform, type of material, and ground ice patterns had been emerging (Mackay and Black, 1973; Hughes, 1974 and others). Furthermore, there had been a mounting log of evidence (McRoberts and Morgenstern, 1973) to indicate that the frequency and scale of natural slope instability increased rapidly in areas containing fine grained ice rich soils. Although slope instability occasionally occurred in the till materials it was not generally characterized by continuing permafrost degradation. It was also evident that the amount and type of ground ice present in the frozen sediments played a major role in the extent and nature of the observed instability.

With these concepts in mind, a field reconnaissance program was undertaken to assess the current state-of-the-art regarding the behavior and development of design concepts pertaining to cut slopes in frozen soils.

The objectives were to establish (whenever possible):

i) the geological, climatic, permafrost and geographical setting;

ii) the soil and ice stratigraphy;

iii) the original cross-section geometry; and,

iv) the existing cross-section geometry.

This information should provide a basis for at least some tentative conclusions regarding the behavior and predicted behavior of cut slopes in arctic and sub-arctic regions under various geographic, climatic, and geologic conditions.

Economic considerations coupled with efficiency and convenience indicated that a small self-contained mobile home, towing a utility trailer, would provide the most versatile means of surface transport. The utility trailer contained a variety of equipment and support items deemed essential for the field work.

2.2 Route

During the course of the reconnaissance approximately 5,500 miles were travelled in 25 days and during that time many dozens of cuts on various highway locations in British Columbia, the Yukon Territory, the Northwest Territories and Alaska were examined, measured and photographed.

The details of these observations are contained in Appendix A while summaries and conclusions appear in the following pages. The information is presented under the sub-headings of Alaska Highway, Dempster Highway, Trans-Alaska Pipeline System Haul Road, and the Copper River Basin. It was felt that the locations could most logically be categorized according to specific projects rather than by territorial or physiographic boundaries. The main sub-divisions will,

therefore, appear in the order in which they were encountered (with minor exceptions).

The major part of the route location is shown in Figure (2-1). The field party started in Edmonton, Alberta on July 4, 1973 and travelled north through Grande Prairie to Dawson Creek, B.C. and then to Whitehorse in the Yukon Terriroty via the Alaska Highway. Travel continued north through the Yukon to Dawson City and up the Dempster Highway to its terminus at Mile 178 (1973). The route crossed the Canada-United States border at Poker Creek west of Dawson City, rejoined the Alaska Highway at Tetlin Junction and continued west to Fairbanks, Alaska. Activities in Alaska dealt primarily with the Trans-Alaska Pipeline System Haul Road, which originates near Livengood, extending fifty-five miles north west to the Yukon River. The Copper River Basin, in south eastern Alaska, was examined by travelling the loop from Fairbanks to Anchorage, east to the Copper River near Glenallen and then north to Tok Junction, and returning to Whitehorse from there.

The north end of the Mackenzie and Dempster Highways were inspected by travelling to Inuvik from Whitehorse by commercial airline and then by helicopter to Arctic Red River, Fort McPherson and the Richardson Mountains.

The field party then returned to Whitehorse from Inuvik and arrived back in Edmonton on July 29, 1973.

2.3 Alaska Highway Mile 222 (from Dawson Creek, B.C.) 57°58' N latitude; 122°46' W longitude

2.3.1 Summary

Concerns in this region regarding the instability of back slope cuts caused by permafrost degradation are slight due to the sporadic occurrence of permafrost (Figure (2-2)). North facing

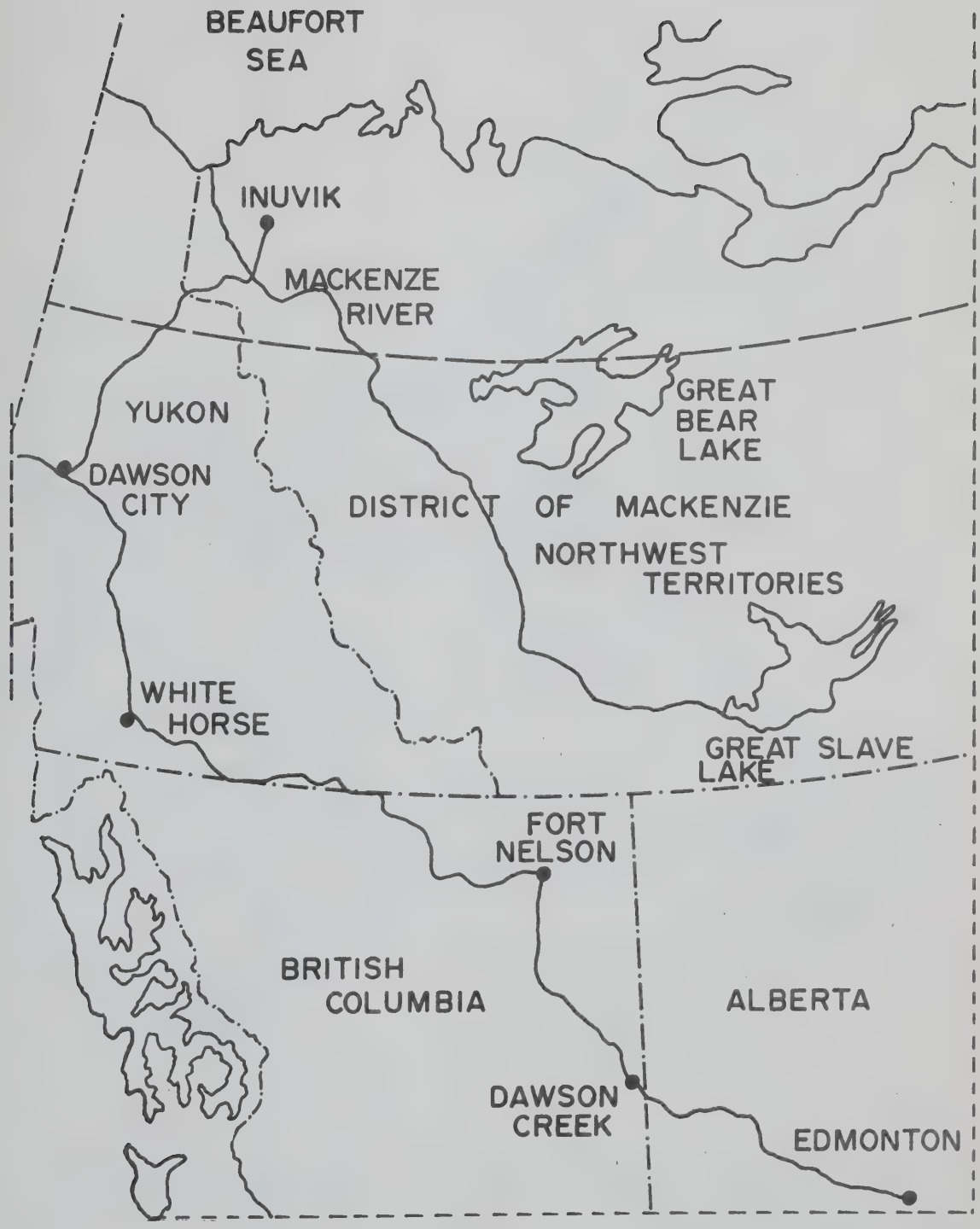

Fig. 2-1 Transportation Facilities - 1972 Northwestern Canada

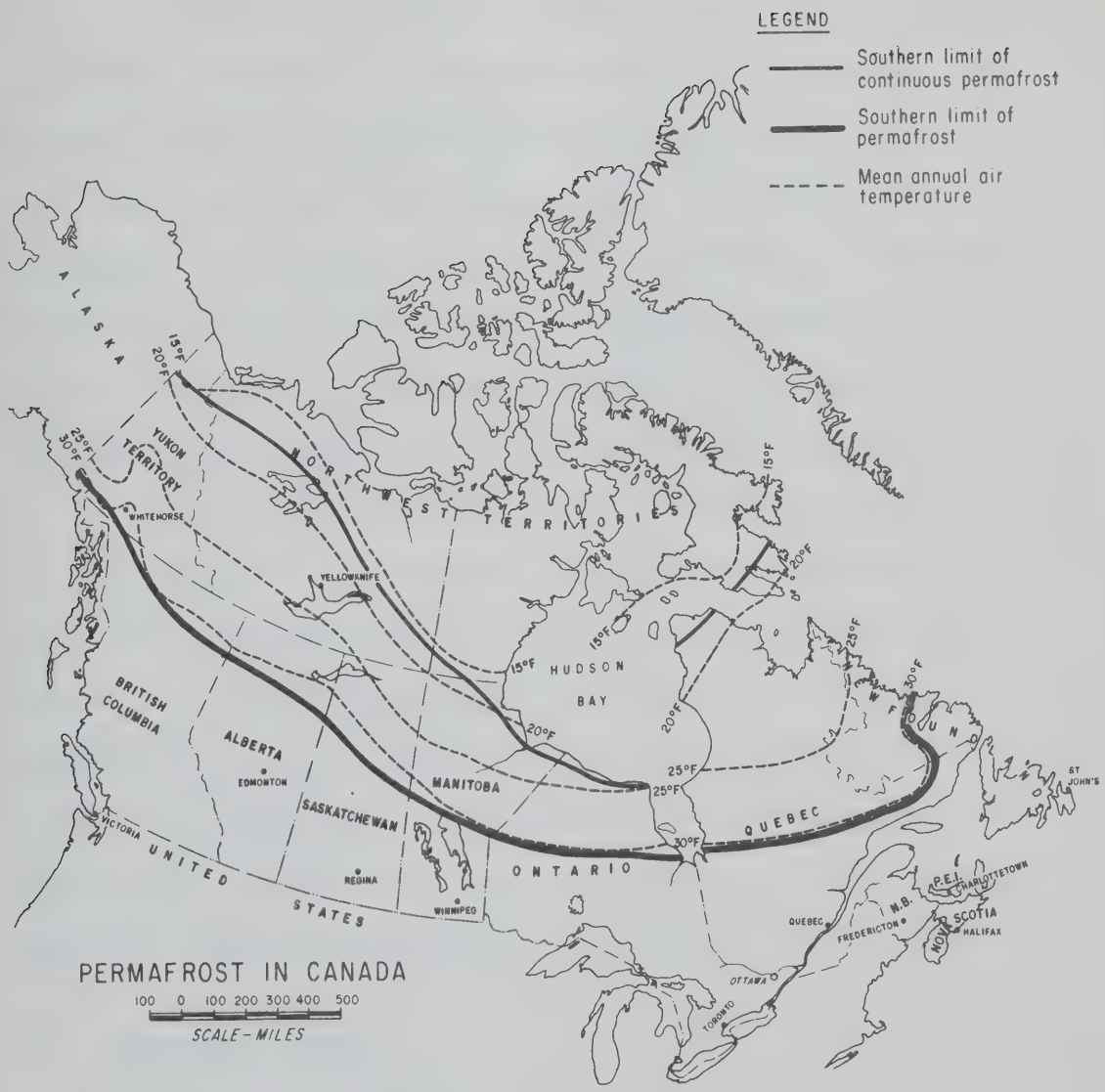

Fig. 2-2 Permafrost in Canada (After Brown, 1967)

slopes covered with heavy stands of black spruce and alder are usually avoided as are low, poorly drained areas. Encounters with permafrost are, therefore, often unexpected and as a result may lead to some particularly troublesome construction situations.

At Mile 222, a highway cut 20 to 25 ft. deep was required to maintain alignment in a reconstruction project. Very wet, fine grained partially frozen material was encountered in the fall of 1972. Cold weather, wet soil, and freezing weather conditions prompted a postponement of construction activities until spring. The material did not melt, drain, and stabilize during the following spring and summer as expected and a continuing problem of back slope instability and a wet subgrade were preventing further construction activity.

The observers felt that if the excavation had been completed and subgrade back fill consisting of select borrow had been installed, then little difficulty other than ditch maintenance would have resulted. It appeared that excavation by dragline and trucks was required to remove the saturated material from the centerline of the roadway. Subsequent back filling with free draining select borrow would provide a stable working base from which to perform ditch maintenance and the remainder of the required excavation.

2.4 Dempster Highway

2.4.1 Location and Background

The Dempster Highway follows an old overland route between the water drainage system of the Yukon and Mackenzie Rivers beginning at Dawson City, Yukon Territory $64^{o}04'$ N lat., $139^{o}26'$ W long. via Fort McPherson $67^{o}26'$ N lat., $135^{o}58'$ W long. to Arctic Red River $67^{o}27'$ N lat., $134^{o}44'$ W long. The location is shown in Figure 2-3.

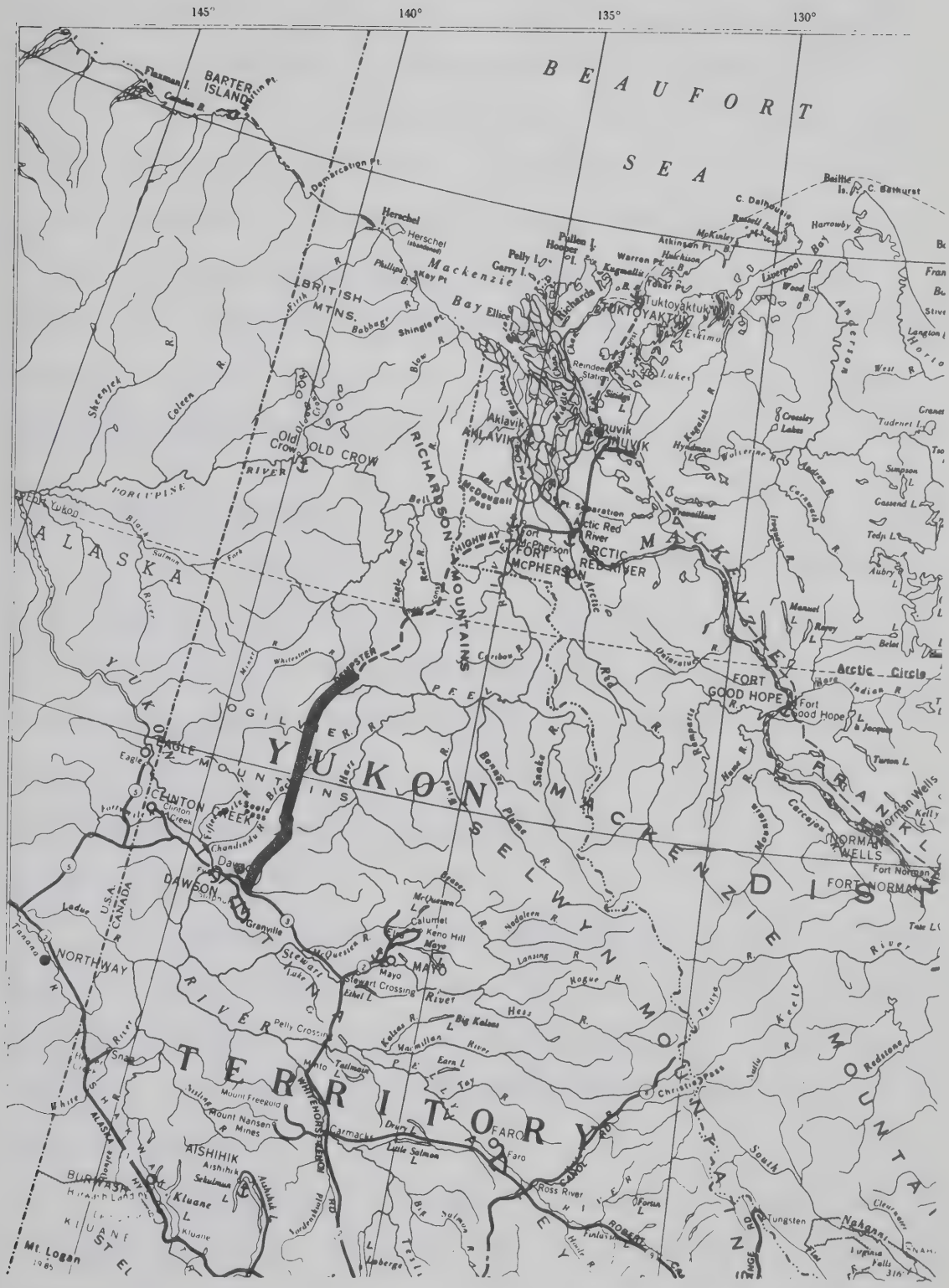

Fig. 2-3 Location of the Dempster Highway; Dawson City, Yukon Territory to Arctic Red River, N.W.T.

Construction of this highway began in 1959 and consisted largely of improving, grading and maintaining an existing tote road. Subsequently, more money was appropriated to the project with the aim of connecting Dawson City on the Yukon River to Fort McPherson on the Peel River and subsequently, the settlement of Arctic River at the confluence of the Mackenzie and Arctic Red Rivers.

The highway lies primarily within the Northern Plateau and mountain area of the Interior System of the Canadian Cordillera. Figure 2-4 indicates the different physiographic units traversed by this transportation facility.

2.4.2 Mile 0 - Mile 80

The first 45 miles of this section of highway is located along the North Klondike River and the remaining portion along the East Blackstone River. Much of this area has been glaciated and there is an abundance of sub-grade material comprised of glacial sediments along the lower portion of the route. Weathered shales and sandstones occasionally outcrop and are used extensively as surfacing materials.

Permafrost is more or less continuous and consequently the borrow pits formed in the active layer are large and shallow. Thermal subsidence of the road is common and has substantially lowered the grade line. As a result, continued maintenance has been required to sustain the road bed.

Road cuts along this eighty mile section of road were not considered significant. They were small (less than ten ft.) and were stable in all cases.

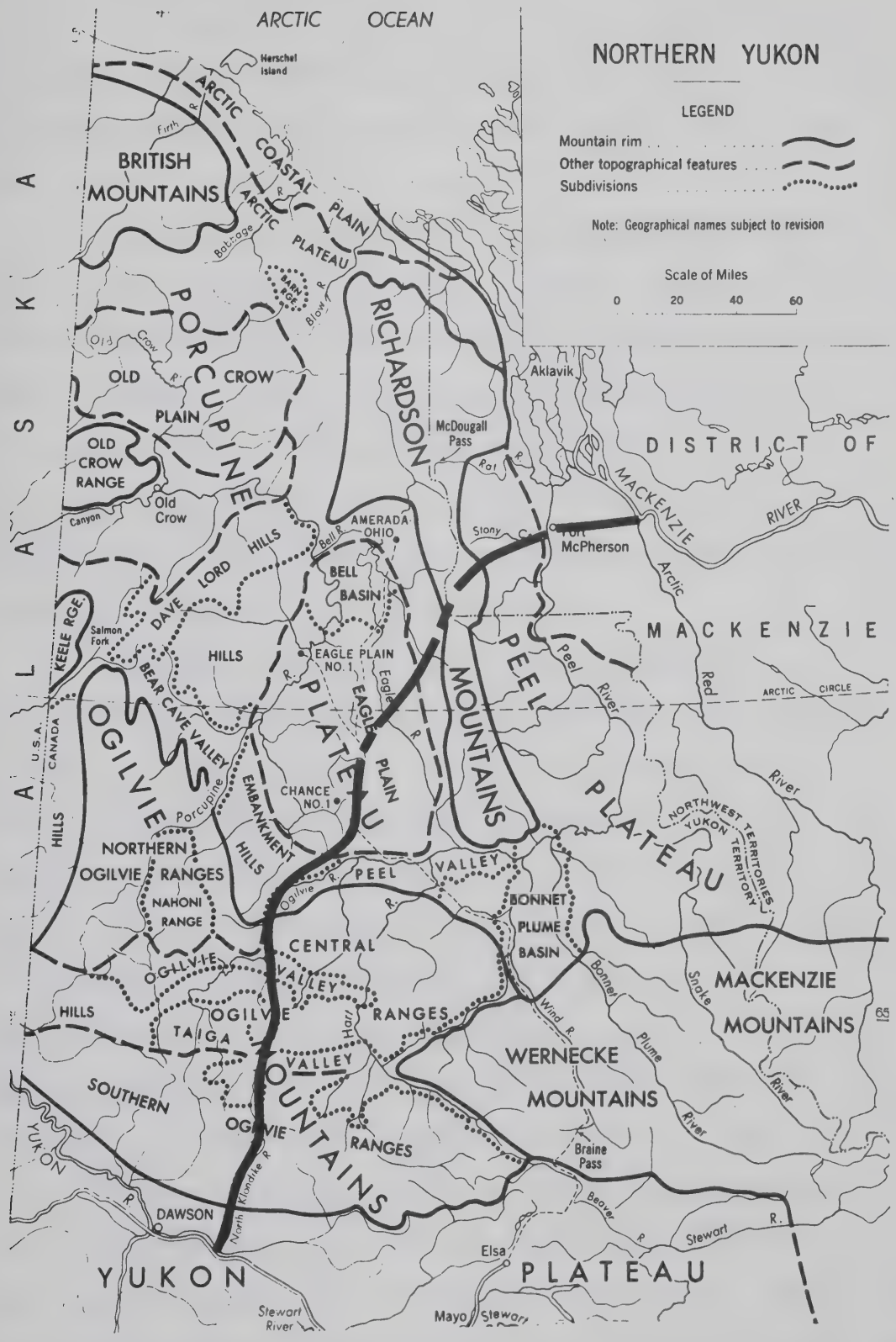

Fig. 2-4 Physiographic Regions of the Yukon Territory (Bostock, 1961)

2.4.3 Mile 80 - Mile 154

The location of this section of road is shown in Figure 2-5. The highway departs from the Blackstone River at Mile 96 and parallels Big Creek, a tributary of the Ogilvie River, to Mile 123 and from there follows the Ogilvie River to Mile 154.

The highway now lies within the unglaciated portion of the Yukon Territory and surficial deposits consist of talus covered slopes, alluvial fan deposits and active and inactive flood plain deposits. Muskeg is abundant in this area and unusually thick deposits of reworked organic matter often cover the coarse gravel of the inactive flood plains. Pediment slopes consisting of frozen colluvium and alluvial silts interspersed with rock detritus and organic matter are frequent along the flanks of the valley.

This lower sixteen mile section of sub-grade shows substantial improvement in alignment and design standards. Back slope cuts are rare, as a major portion of the road is constructed from fill material obtained from the East Blackstone River and Big Creek. The following 20 miles flank the valley walls of Big Creek and the proximity of the river bed has often forced the location onto the sides of the valley. Twenty to thirty foot cuts in colluvial silt and weathered shale are not uncommon. Construction problems and ditch blockage resulted from the melting of ice wedges and frozen soil encountered in the cuts. Small bimodal flows occurred at some locations.

Extensive disturbance was noted on an abandoned tote road located on an alluvial silt or slope wash side hill at Mile 114 directly across the valley from the present highway location. The original activity was estimated to be eight to ten years old. Large craters have formed due to thermal subsidence caused by the subsurface melting of

Fig. 2-5 Location of Mile 90 to Mile 180 of the Dempster Highway

large tabular masses of ice.

A significant and troublesome cut occurred at Mile 154 adjacent to the Ogilvie River. A bimodal flow eventually developed with a head scarp thirty feet high. Large ice wedges were exposed in a silt-weathered shale-soil mixture. The melted soil and ice caused a serious impediment to drainage and concern to maintenance personnel. After one complete thaw season, gravel was used to fill the crater formed by the loss of material and thus return the slope to its original dimensions. This remedial measure appears to have adequately prevented further degradation of the slope.

The performance of cuts along this section of highway has generally been good to excellent with little more than ditch clearing required to maintain adequate drainage.

2.4.4 Mile 154 - Mile 178

The Dempster Highway departs from the Ogilvie River and ascends the valley flank to the Eagle Plains. Unglaciated surficial deposits comprise the subgrade construction materials and consists of discontinuous felsenmeer and/or colluvium over bedrock. Extensive deposits of organic matter are common along the lower reaches of this section. The sandstone bedrock is more resistant to weathering and therefore forms the tops of ridges and escarpments. The shales, on the other hand, are softer and weaker and form smoother and more gentle slopes.

Large side hill cuts and steep grades were required to attain the ascent out of the Ogilvie River Valley to the plain above. However, since the roadbed was excavated into ice free sandstone and shale bedrock, no problem was encountered with stability. Excavation of a number of small cuts was performed without major difficulty. By

loosening the frozen soil with a ripper tooth on a large crawler tractor and rapidly excavating with conventional earth moving equipment, it was found possible to construct cuts without encountering excessively wet and muddy working conditions. Occasional encounters with residual ice rich fine grained soils caused construction delays and increased costs. However, the back slopes were not found to exhibit alarming instability.

An excellent opportunity exists to compare the difference and assess the behavior and quality of subgrade constructed in late fall and early summer along this section of road. Subgrade constructed in the spring and early summer tends to undergo substantial differential settlement and cracking as melting proceeds into the active layer during the remainder of the summer. On the other hand, subgrade that was constructed in late summer and fall tends to be more stable and exhibit less differential settlement. This behavior can be attributed to the fact that much of the settlement due to conventional consolidation occurs during the construction period rather than subsequent to the completion of grading.

Mile 178 was the construction terminus on the Yukon portion of the Dempster Highway as of July, 1973. A further 56.5 miles of road is presently being constructed to the Eagle River. No inspection of this road has been made and therefore comment is beyond the scope of this thesis. Preliminary design and location reports indicated that the location would follow summits of the ridges whenever possible and borrow material was to consist almost exclusively of weathered sandstone and shale bedrock except where limited quantities of sand and gravel were available from the Eagle River or other lesser streams convenient to the right of way.

2.4.5 Fort McPherson to Arctic Red River

Mile 330 to Mile 365

This section of highway connecting the settlements of Fort McPherson and Arctic Red River was completed during the summer of 1973. Hummocky or dead ice moraine represent the basic land form which is comprised of deposits of unsorted glacial drift occasionally draped with sorted fine grained sediments that may be water modified or reworked till. Large areas are covered with silt and organic material.

Engineering design problems involved the stability of thawed soils, embankment design and drainage structures. High moisture contents in the upper till precluded its use as a construction material and ripped sandy shales were used almost exclusively as a sub-grade material.

Excavation was generally avoided except for a large cut that was developed in a knoll at Mile 343 in order to supply borrow material for the adjacent sections. However, the material proved to have excessively high water contents and was completely unstable when thawed. Much of this material was wasted in adjacent spoil areas.

During and after completion of the cut, the back slopes exhibited reasonably serious degradation. However, the extent of the retreat was apparently limited to the areal extent of the ice. It appears that the retreat and instability of the back slopes ceased when the excess ice had melted and the water had drained away.

This is the most significant cut on the Dempster Highway and the length and width of the excavation rather than its depth make it an outstanding feature on the landscape. At the time of inspection, the back slopes appeared to have completely stabilized without det-

rimental results.

2.4.6 Mile 178 - Mile 330

A brief helicopter reconnaissance was made of the proposed location of the section of the Dempster Highway between Fort McPherson and south to Mile 178.

Several naturally occurring bimodal flow slides were noted in the Richardson Mountains near the Yukon-Northwest Territories border. Some of these flow slides have run their course or have become dormant while others are currently active. Sediments encountered at those sites consist of significant quantities of ice rich fine grained deposits. None of these slides were in close proximity to the proposed right of way.

2.5 Mackenzie Highway (Inuvik to Arctic Red River)

Two sections of the north end of the Mackenzie Highway received a cursory inspection for the presence of back slope instability. No cuts of significance were encountered in the northernmost Inuvik section. However, the north approach to the Mackenzie River warrants a short discussion as it was the only situation where measures were taken to prevent back slope degradation rather than control it.

A forty foot deep cut had exposed 15 to 20 ft. of ice-rich fine grained sediments overlying interbedded shale and sandstone bedrock. As the excavation proceeded, the ice content of the overburden increased with distance from the river bank. To prevent subsequent degradation, the slope was benched at the bedrock level and the ice-rich fine grained sediments in the upper portion of the slope were

dressed with 10 ft. of crushed shale. The slope appeared to be functioning as anticipated at the time of inspection.

2.6 Alaska Reconnaissance

2.6.1 General

Prior to 1973, the roads in Alaska had been built in the discontinuous permafrost zone except for minor activity on the Arctic Coast. The designers, for the most part, were able to choose their locations judiciously and thus avoid cuts where ice-rich fine grained soils were suspected. Even so, requirements of the oil industry have created a need for road locations that do not allow the designer as much latitude in the choice of route. The Trans-Alaska Pipeline System (TAPS) Haul Road is a typical example of such a problem.

The TAPS Haul Road begins at Livengood some sixty miles northwest of Fairbanks and extends fifty-five miles beyond to the Yukon River (1973). This road has since been completed north to Prudhoe Bay on the Arctic Coast and provides facilities for ground surface transportation of all supplies and personnel required in the construction of the Alyeska Pipeline.

The great difficulty associated with the routing of this road was that it, of necessity, crossed the grain of the country. Its origin and destination required the route to climb south facing slopes and descend north facing slopes (Figure 2-6).

2.6.2 TAPS Haul Road

The southernmost section of the TAPS Haul Road, built in 1969-70, crosses broad undulating divides and flat-topped spurs of the Yukon-Tanana Upland and descends to the Yukon River Lowland which exhibits gently rolling topography with maximum relief in the order

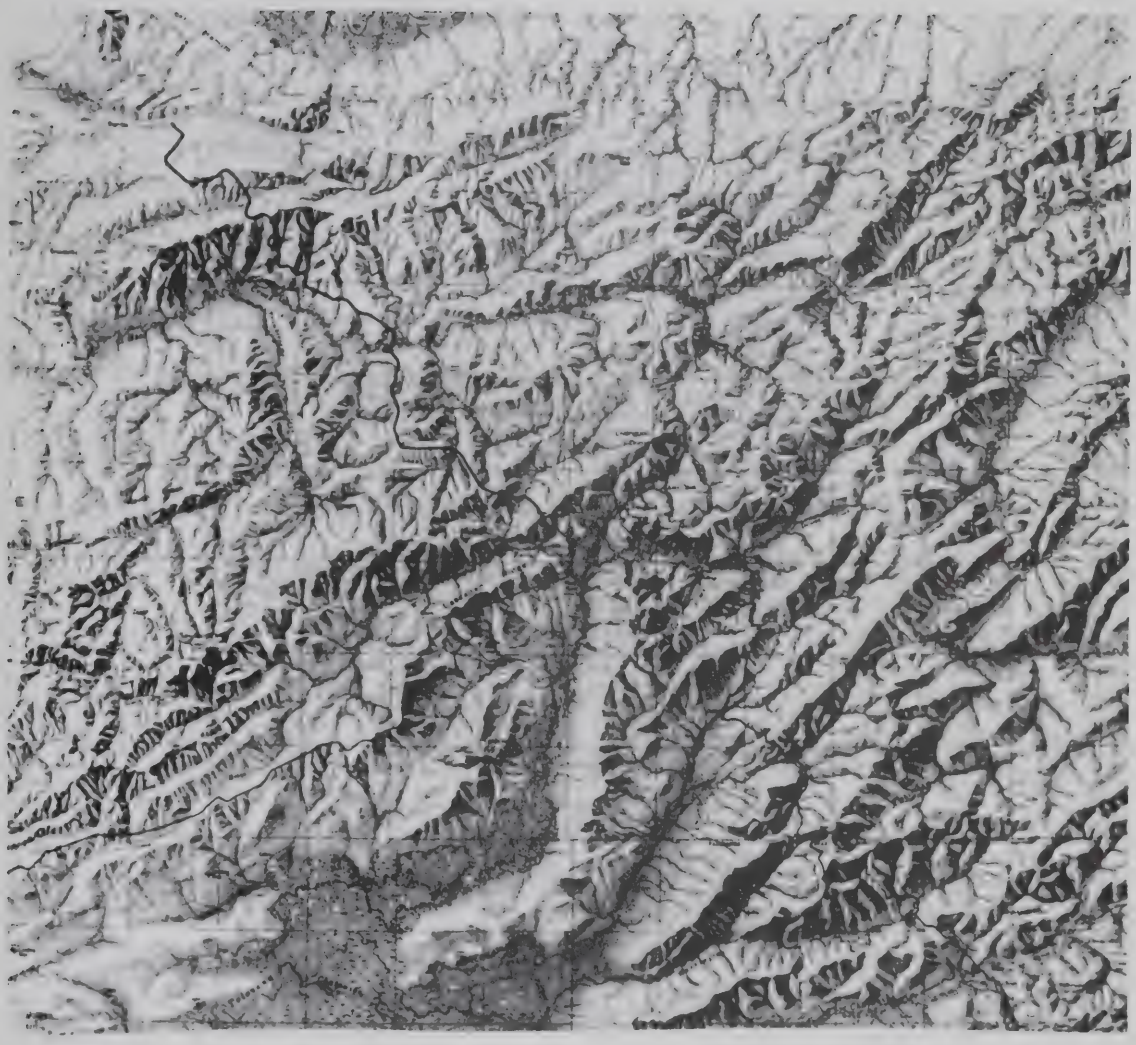

Fig. 2-6 TAPS Haul Road; Livengood to the Yukon River, Alaska (Road crosses northeast-southwest trending ridges at right angles)

of 1,000 to 1,500 feet. This entire fifty-five mile section lies within the discontinuous permafrost zone (Ferrians et al, 1969). The unglaciated surficial deposits consist of reworked aeolian silt, colluvial and alluvial silt, sand and rock fragments, dune sand, and alluvial sand and gravel and exhibits an active layer depth that varies from 18 in. to 10 ft. below the surface. These surficial sediments are unconsolidated, usually frozen, and are often very rich in ice. Ice forms include wedges, lenses, and interstitial ice.

The TAPS Haul Road has provided the first real opportunity to observe and record the performance of a significant number of road cuts in ice-rich fine grained soils. The road has many substantial cuts on north facing slopes that exposed what was termed "massive ice". Certainly the ice did appear massive in that cuts in the order of 20 ft. had 12 ft. or more of ice exposed in the section. However, the tabular extent of these ice exposures was not and has not been established.

Many of these cuts were excavated with vertical or near vertical faces with the thought that prior to any self-healing, the cuts would have to melt back to a vertical scarp. It was anticipated that the upper mantle of soil and organic mat would then slough down over the melting ice and soil and provide sufficient insulation to stabilize the slope. Vegetation would then re-establish itself preventing erosion and any further fouling of the ditches.

Inspection of these cuts in the summer of 1973 indicated that the back slopes had essentially stabilized. Many slope angles were very steep (35^{o} to 40^{o}) and the present conditions probably do not represent ultimate stable slope angles for most of the colluvial silt encountered along the route. The relatively free-draining nature

of the silt deposits, the extensive re-vegetation program, and probably the initial vertical cross section have all contributed to rapid stabilization. More important, however, may be that the ground ice occurs in the form of wedges of limited extent and that the back slopes stabilized when the exposed ice wedges melted and allowed the remaining soil to slough down forming a quasi stable slope from material with moderately low moisture contents. Summaries of the soil classification for the TAPS Haul Road appear in Table 2-1.

2.6.3 Copper River Basin

The Copper River Basin is located in southeastern Alaska in the discontinuous permafrost zone. This region has been subjected to extensive glaciation and pro-glacial lakes were common during the retreat of the ice. As a consequence, major deposits of glaciolacustrine silts and clays, fluvial silt and sand, sand and gravel, colluvium, and organic soil comprise the surficial materials. Ground ice forms and amounts are extremely variable. Ice wedges, massive tabular bodies, and interstitial ice are common. Natural water contents often exceed the liquid limit (EISTAPS, 1972).

Instability of large cuts and fills is common in this region. Slopes are designed to ensure stability in the thawed but essentially undrained case, with no excess pore water pressure considered due to thaw consolidation.

Several cuts were observed at various locations in the area. The back slopes did not exhibit any serious distress due to permafrost degradation. Many slopes along the valley wall undergo significant movements. Most of these failures are semi-rotational or block-type movements and are not necessarily related to changes in permafrost conditions.

2.7 Conclusions

The observations made during the field reconnaissance program are summarized in Table 2-2 and indicate that slope behavior varies widely in the areas that were investigated. It is also apparent that at least limited instability may be encountered in cuts in all regions which contain fine-grained, ice-rich sediments. There appear to be a number of factors which contribute to the amount of instability. These are:

(1) geological history (primarily glacial);

(2) landform and soil type;

(3) ice content of sediments;

(4) nature or type of ground ice;

(5) geometric cross-section of the back slopes.

All of these factors are inter-related and are listed in approximate order of importance.

The determination of the geological history along with the recognition of associated landforms will provide a sound basis for the preliminary design and predicted behavior of highway back slopes. Although local exceptions may exist, it appears that the greatest risk of precipitating unstable conditions arises in areas that contain significant deposits of stratified drift in the form of pro-glacial, lacustrine silts, and clays. These deposits generally contain large amounts of segregated ground ice in the form of lenses varying in thickness from a few tenths of an inch to massive sheets many feet thick (Mackay and Black, 1973).

The areal extent of these lacustrine deposits is often quite significant, varying from a few hundred feet to a number of miles. Thus, a flow slide initiated in such an extensive deposit is not likely to

terminate due to a lack of material. When these soils are thawed, large amounts of meltwater coupled with low permeabilities provide an ideal condition for the generation and maintenance of large excess pore water pressures. The thawed soil is very weak and flows at very low angles (McRoberts and Morgenstern, 1973). It is unlikely that vertical cuts would provide any great degree of stabilizing influence unless they were less than ten feet in height. Under these conditions, the intact organic cover may be able to provide a retarding effect on the rate of thaw and the subsequent generation of excess pore water pressures.

The effectiveness of the organic mat is directly related to its continuity. Tearing or ripping of the cover under self-weight can be reduced by removing the larger vegetation and in some cases reinforcing the mat with wire mesh fastened to the tree stumps.

The reconnaissance did not encounter highway or right-of-way locations in regions of extensive glacio-lacustrine deposits with the exception of the Copper River Basin in Alaska. This latter area did not exhibit the bi-modal flow slides characteristic of the Mackenzie Valley (McRoberts and Morgenstern, 1973). Although it would appear that both areas were subjected to similar glacial histories, there is a distinct difference in the ice contents of the sediments. The reasons for this deserve further study.

Conventional slope analyses using thawed, undrained strength parameters appear to provide acceptable margins of stability for most highway cuts in this region. However, there seems little doubt that route locations encountering extensive areas of pro-glacial lake basin sediments are exposed to the hazards of backslope instability. Great care must therefore be taken to avoid cuts in these regions whenever possible.

The other major classification of glacial sediments is that of unstratified drift. Till plains formed from basal or lodgement till and hummocky or dead ice moraine composed of ablation till are the two most common landorms.

Ground ice conditions in the till plains are usually not particularly severe. The ice occurs as thin subhorizontal segregated lenses. The top layer of this landform may occasionally contain significant ice lenses just below the active layer due to aggrading permafrost conditions (Hughes, 1974). These ground ice deposits usually occur within three to six feet below the surface and should, therefore, not create any sustained construction hazard. It should also be noted that this terrain has rather low relief and cuts will be uncommon.

Hummocky or dead ice moraine is common in the northern part of the Mackenzie Valley and appears sporadically along the Alaska Highway and the lower and upper portions of the Dempster Highway. This terrain unit is highly irregular and may contain lenses of silt, sand, and gravel as was witnessed at Mile 222 on the Alaska Highway and at Mile 343 on the Dempster Highway. Complex hydrologic, geologic, and topographic conditions prior to deposition of the sediments and aggradation of permafrost have produced equally complex and irregular patterns of ground ice. These forms may consist of lenses of varying thickness, wedges, and occasionally significant amounts of interstiial ice (ibid). However, it must be emphasized that these ground ice forms are usually of finite dimensions and that flow slides initiated in these sediments will be of limited (and often acceptable) extent.

Good construction practice involving wide ditches, low rock revetments, occasionally combined with minor amounts of backslope

reshaping and revegetation should provide an acceptable measure of stability and pleasing appearance.

The unglaciated regions of the Yukon and Alaska contain a variety of classic landforms consistent with the geological history and periglacial conditions. The soils are generally formed from weathered sandstones and shales and consist of colluvial and alluvial silts, sands, and gravels. Occasional deposits of medium to highly plastic residual clays are encountered in the central and northern Yukon. The ground ice conditions are again very irregular in all these deposits and occur in a variety of forms. Ice wedges and lenses of variable thickness are the most common type encountered (Kachadoorian, 1971).

The relatively high permeability of these materials coupled with low interstitical ice contents provide conditions for moderately fast stabilization under thawing conditions. Flow slides initiated in this material, with these particular ground ice conditions, will normally stabilize after two or three seasons of thaw (Davies, 1973).* Again, good construction practice should reduce the time required for stabilization and the amount of slope retreat that may be expected. Wide ditches are recommended to provide reasonable space for sloughing material. Rock revetments appear to play a significant role in retaining the soil at the toe of the backslope while drainage proceeds. Vertical cuts may be desirable in areas that contain soil and ice conditions as previously described in that they tend to expose or intersect fewer ice wedges. This aspect combined with the steep quasi-stable angles developed by the soil between and above the ice provide

* Personal communication.

encouragement for the designer in the use of steep slopes. However, it must be noted that generalization is not possible with the current state of knowledge and that steep cuts will not be desirable everywhere. There is no evidence and little rationale to suggest that vertical slopes will perform satisfactorily in ice-rich glaciolacustrine sediments except under conditions previously outlined.

The occurrence of instability of natural slopes is undoubtedly the best indicator available to assess or predict potential instability of cut slopes. If areas do not exhibit natural instability due to permafrost degradation then it is unlikely that cutting of a slope will cause serious and extensive instability in the form of flow slides.

The only reliable method encountered for preventing rather than controlling flow slides was that utilized on the Mackenzie Highway at the approach cut to the Mackenzie River near the settlement of Arctic Red River. A thick layer of crushed rock was used to dress the exposed slope before degradation of the permafrost occurred.

Procedures to prevent melting of the permafrost in colder regions are well known and are relatively simple in comparison with preventing permafrost degradation in the discontinuous zone (Lachenbruch, 1957).

The experience with cut slopes in permafrost reviewed here, albeit limited, indicates that the behavior of cuts need not be a serious impediment to the routing of transportation arteries across permafrost.

TABLE 2-1

SUMMARY OF SOIL DATA

LOCATION	SOIL TYPE	LIQUID LIMIT %	PLASTIC LIMIT %	NATURAL WATER CONTENT %	SPECIFIC GRAVITY	SAND AND GRAVEL %	SILT %	CLAY %
Alaska Highway Mile 222	Silt			23		30	60	10
Alaska Highway Mile 222	Silty-clay	50	19			10	50	40
Dempster Highway Mile 108	Silt					20	75	5
Dempster Highway Mile 114	Silt	27		25	2.71	10	80	10
Dempster Highway Mile 153	Silt					20	75	5
Dempster Highway Mile 174		54	25				40	60
Dempster Highway Mile 175		45	23	30-40		5	35	60
Dempster Highway Mile 175		48	24	30-40		5	45	50
Bi-modal Flow Richardson Mts.	Till	36	22	Dry	2.70	30	40	30
Bi-modal Flow Richardson Mts.	Alluvium	39	24	38	2.72	15	53	32
TAPS Haul Road Mile 19.6	Silt	25				0	92	8
TAPS Haul Road Mile 23.4	Silt					10	83	7
TAPS Haul Road Mile 54.4	Silt	24				0	91	9
Dempster Highway Mile 343	Upper till	26	18			25	55	20
Dempster Highway Mile 343	Lower till	23	15			30	40	30

TABLE 2-2

SUMMARY OF CUTS

LOCATION	HEIGHT (Feet)	INITIAL SLOPE (Degrees)	CURRENT SLOPE (Degrees)	SOIL TYPE	COMMENTS
Alaska Highway Mile 222	20-25	26.5	Varies from near vertical to 6^{o} frontal lobe.	Till with lenses of silt and silty clay.	The slope had retreated approximately 15 feet at the time of inspection and gave no indication of stabilizing.
Dempster Highway Mile 96	8-10	26.5	21	Till-relatively fine-grained with low ice content.	Slope is stable.
Mile 107.6	30	34	32	Colluvial silt and weathered shale with low ice content.	Organic mat tearing loose; slope is stable.
Mile 108.9	35	34	12 to 35	Colluvial silt, some weathered shale. Large ice lenses.	Slope has stabilized with small amounts of ditch maintenance.
Mile 114 Tote Road	Instability of natural slope		9 to 11	Alluvial silt and slope wash. High ice content.	Caused by locating tote road on 5^{o} side hill. Disturbance approximately 6 years old and continuing to stabilize.
Mile 120.7	Less than 10	26.5	12	Ice-rich organic alluvial and/or colluvial silts.	Slope presently quite stable. Some ditch clearing required to maintain drainage.

TABLE 2-2 (Continued)

LOCATION	HEIGHT (Feet)	INITIAL SLOPE (Degrees)	CURRENT SLOPE (Degrees)	SOIL TYPE	COMMENTS
Trans-Alaska Pipeline System Haul Road					
Mile 2	40	26.5	26.5	Weathered sandstone bedrock.	Slope is stable and revegetation is well established.
Mile 14	10 to 25	26.5	Backscarps at 35 to 45; lobes at 7 to 10.	Colluvial silt and massive ice.	Trees were removed by hand and the moss has draped itself over the retreating face. The slope is essentially stable.
Mile 19.6	15 to 20	34	20	Colluvial silt with large ice lenses and wedges.	Crushed rock revetments were used to retain the sloughed material.
Mile 20.3 to Mile 20.5	20 to 40	76	35 to 45	Colluvial silt with large ice lenses and wedges.	This section was referred to as the "ice tunnel". Vegetation is well established.
Mile 22.9	15 to 20	76	Varies from 17 to 40	4 to 6 feet of organic matter over silt and ice.	Boreholes indicated massive ice in excess of 32 feet. Slope degraded 75 feet in localized areas.

TABLE 2-2 (Continued)

LOCATION	HEIGHT (Feet)	INITIAL SLOPE (Degrees)	CURRENT SLOPE (Degrees)	SOIL TYPE	COMMENTS
Mile 153	40	40 to 45	Angle of repose of coarse gravel	80% silt; 20% shale; no interstitial ice. Large lenses or wedges exposed.	Backslope retreated until a 35 foot vertical section was formed. Gravel placed on face to control melting. Slope appears stable.
Mile 168	Less than 10	34	11	Sandy silt with angular weathered rock. Ice-rich.	Backslope has retreated 20 to 25 feet. Appears to be stabilizing under present conditions.
Mile 175	8 to 10	34	40 to 50	Silt and silty clay with shale fragments.	Activity due to melting of large ice lense, slope has retreated 25 feet at time of inspection.
Mile 343	35	34	17	Silty clay till; ice lenses up to 4 feet in thickness.	Cut is 1/2 mile long. Backslopes are essentially stable; some ditch clearing and backslope reshaping has been done.
Mackenzie Highway Mile 894	45	34 on upper slope to 45 on lower slope	45	Upper 25 feet is ice-rich and fine-grained Lower 20 feet is bedrock.	Upper 25 feet was benched and dressed with 10 foot thick layer crushed shale slope is completely stable.

CHAPTER III

STABILIZATION OF PLANAR LANDSLIDES IN PERMAFROST

3.1 Introduction

Flow dominated land slides in periglacial regions have been documented by numerous researchers (Capps, 1919; Eakin, 1919; Sigafoos and Hopkins, 1952; and others). Skin flows or planar landslides involving the detachment of vegetation and thawed soil from the underlying frozen soil are abundant in the Mackenzie Valley and have been described by Hardy and Morrison (1972), Hughes (1972), Issacs and Code (1972), Mackay and Mathews (1973), and McRoberts and Morgenstern (1973).

Since skin flows are common, a method of stabilizing them or inhibiting their occurrence is of interest.

A technique for the analysis of thawing slopes of infinite extent has been developed which incorporates pore water pressure components due to steady state seepage as well as those resulting from self weight and surcharge loading during thaw consolidation. Insulation used in conjunction with a surcharge load reduces the rate of thaw, decreases the induced pore water pressures and may effectively stabilize the slope.

3.2 Thaw-Consolidation Pore Water Pressures

Excess pore pressures in thawing soils may be predicted from the theory given by Morgenstern and Nixon (1971). The magnitude of these water pressures at a horizontal thaw front in a homogeneous single layer soil due to self weight and surcharge loading are given by the following equations:

$$U_{\gamma}' = \gamma' \; X(t) \frac{1}{1 + \frac{1}{2R^2}} \qquad - - - [3.1]$$

$$U_{p_o} = \frac{(P_o - \sigma_o')\, \mathrm{erf}(R)}{\mathrm{erf}(R) + \frac{e^{-R^2}}{\sqrt{\pi R}}} \qquad - - - [3.2]$$

where γ' = effective unit weight of the soil

$X(t)$ = depth of the thaw front, predicted by

$X(t) = \alpha \sqrt{t}$ (Carslaw & Jaeger, 1947) - - - [3.3]

where $\alpha = \sqrt{\frac{2K_u Ts}{L}}$ (Stefan, 1891) - - - [3.4]

K_u = thermal conductivity of the unfrozen soil;

Ts = surface step temperature;

L = latent heat of fusion of the soil/ice mixture;

t = time

$R = \frac{\alpha}{2\sqrt{C_v}}$ (thaw consolidation ratio) - - - [3.5]

erf ( ) = error function

P_o = surcharge load

σ_o' = residual effective stress (assumed to be zero at shallow depths in ice rich fine grained soils). The solution for equations [3.1] and [3.2] have been given in graphical form by Morgenstern and Nixon (1971).

The depth of thaw in a two layer medium is given by Nixon and McRoberts (1973):

$$X(t) = \sqrt{\left(\frac{K_2}{K_1} H\right)^2 + \frac{2K_2 \, Ts(t - t_o)}{L_2}} - \left(\frac{K_2}{K_1} H\right) \qquad - - - [3.6]$$

where $X(t)$ = depth to the thaw front measured from the interface of the two layers.

K_1 = thermal conductivity of the upper layer

K_2 = thermal conductivity of the lower layer

H = thickness of the upper layer

t = length of the thawing season

$t_o = \frac{H^2 L_1}{2K_1 T_s}$; (time to thaw layer 1)

L_2 = latent heat of fusion of the soil/ice mixture in the lower layer.

$$L_{(1,2)} = \gamma_t (W - W_u) L' \qquad - - - [3.7]$$

where γ_t = total unit weight of the soil

W = water content of the soil

W_u = unfrozen water content of the soil expressed as a ratio of gms. of water to gms. of dry soil

L' = latent heat of fusion of ice (79.6 cal/gm.)

If the upper layer consists of an insulating material or incompressible surcharge loading, a measure of the pore pressure in the soil below the insulation may be determined by computing $X(t)$ from equation [3.6], substituting into equation [3.3] and obtaining an equivalent α_e. R can then be evaluated from equation [3.5] and the pore pressures evaluated for this modified rate of thaw.

The above procedure is not strictly correct because the thaw depth as computed from equation [3.6] will in general not be linear with the square root of time. Figure 3.1 indicates the manner in which the thaw depth varies with time for a typical problem. It is apparent that this technique will slightly underestimate the thaw-

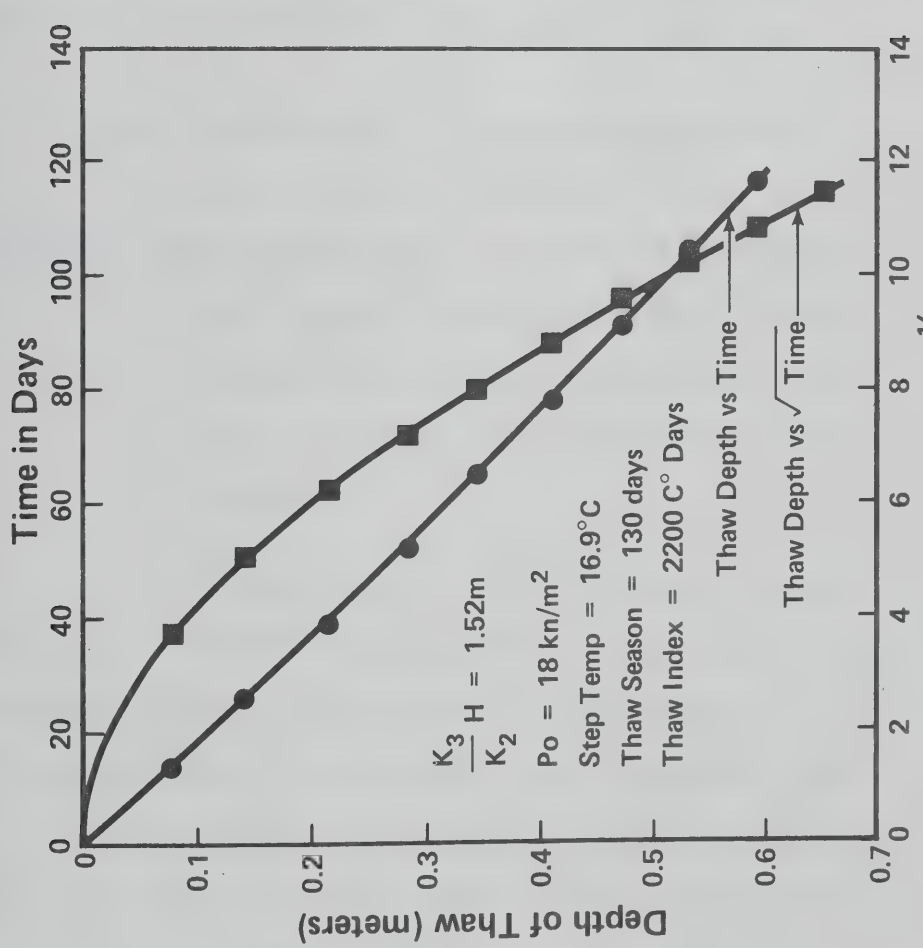

Fig. 3.1 Thaw Depth vs Time and Thaw Depth vs $\sqrt{\text{Time}}$ for an Insulated Thawing Slope

consolidation pore pressures generated in this particular two layer medium. A better estimate of these water pressures can be made either by numerical techniques or by modelling the thaw rate from:

$$X(t) = B(t)^n \quad \text{(Nixon and Morgenstern, 1973)} \quad - - - [3.8].$$

The thaw depth must be calculated for various times from equation [3.6] and a suitable value of n determined for equation [3.8]. Graphical procedures may then be used to properly evaluate the pore pressures at the thaw front at different periods of time (ibid).

3.3 Stability Analysis of Infinite Thawing Slopes

The pore pressure term in the stability analysis of an infinite slope with surcharge loading will be composed of:

1) Pore pressure due to steady state seepage.
2) Thaw-consolidation pore water pressure due to self weight.
3) Thaw-consolidation pore water pressure due to surcharge loading.

These three components may be evaluated separately as shown in Figure 3.2 and then added numerically to obtain the total pore water pressure acting at the thaw front. This procedure is similar to that of McRoberts (1972), and McRoberts and Morgenstern (1974).

The condition for steady state seepage is shown in Figure 3.2(a). This is a well known solution and the pore pressure term is:

$$U_s = X(t) \cos i \, \gamma_\omega \quad - - - [3.9(a)]$$

Figure 3.2(b) indicates the condition for the pore pressure due to self weight generated from one dimensional thaw-consolidation. This magnitude is expressed by:

$$U_{\gamma'} = \gamma_3' \, X(t) \cos i \, \frac{1}{1 + \frac{1}{2R^2}} \quad - - - [3.9(b)]$$

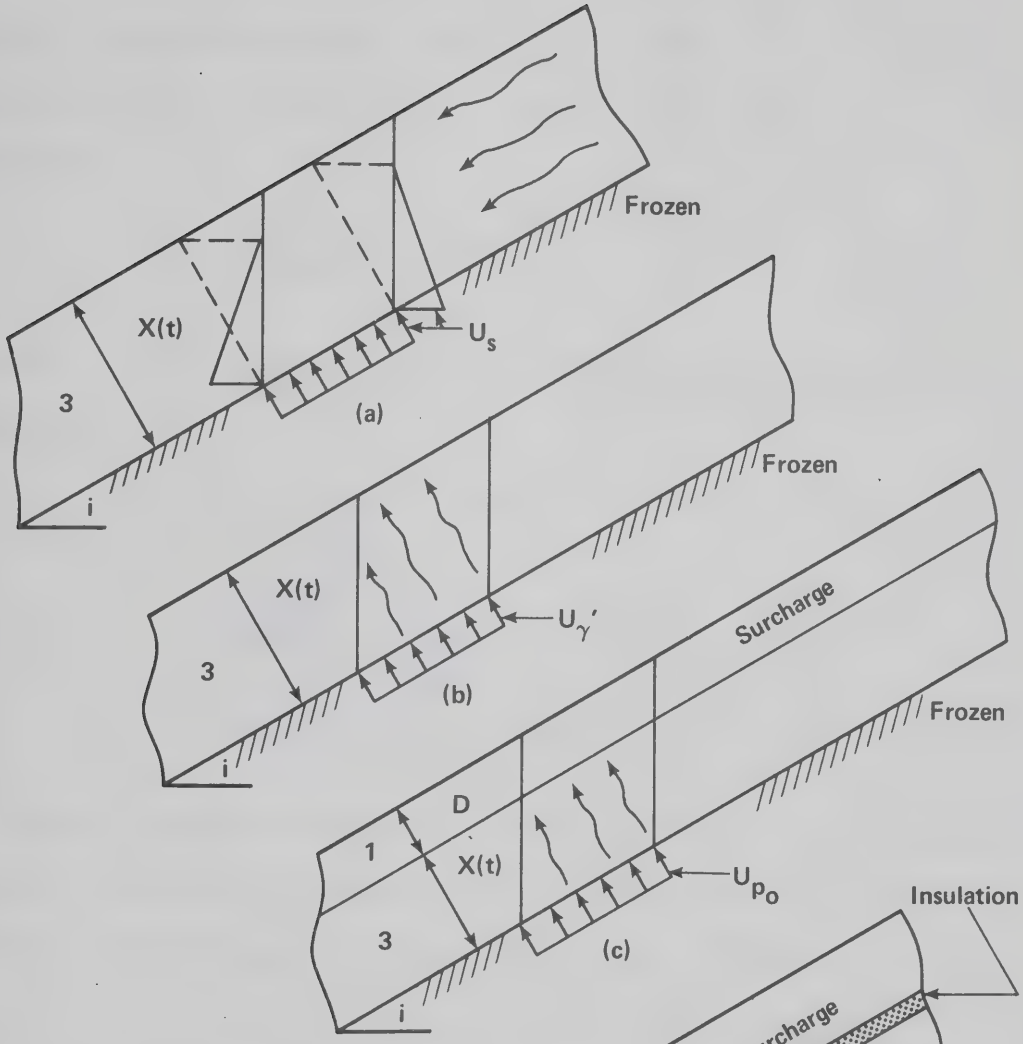

Fig. 3.2 Pore Pressure at the Thaw Front of a Thawing Infinite Slope

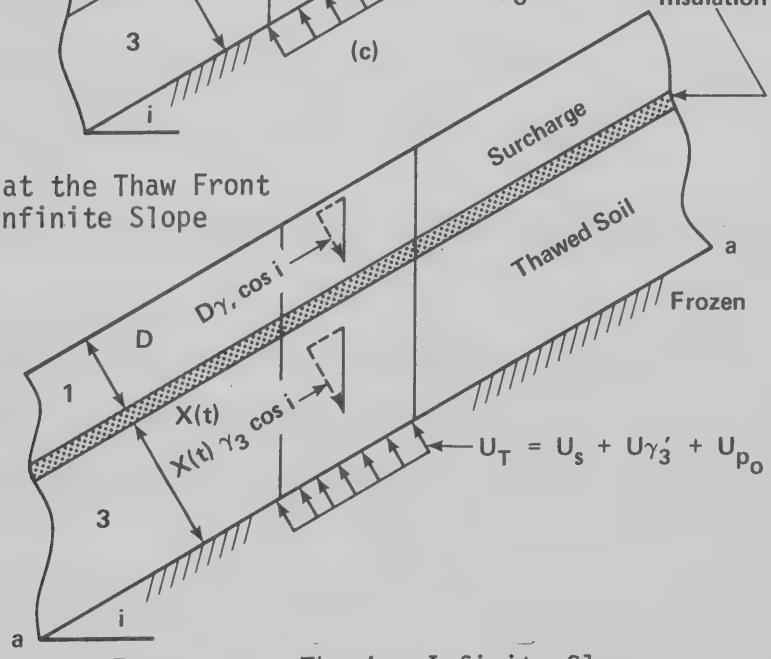

Fig. 3.3 Balance of Forces on a Thawing Infinite Slope

where γ_3' X(t) cos i is the normal stress on the thaw plane produced by the effective unit weight of the thawed soil. The pore pressure due to the surcharge is shown in Figure 3.2(c) and is given by:

$$U_{P_o} = \frac{P_o \cos i \, \text{erf}(R)}{\text{erf}(R) + \frac{e^{-R^2}}{\sqrt{\pi R}}} \quad - - - [3.9(c)]$$

where P_o cos i is the normal pressure exerted by the surcharge on the thaw plane.

If $R' = \frac{1}{1 + \frac{1}{2R^2}}$ and

$$R'' = \frac{\text{erf}(R)}{\text{erf}(R) + \frac{e^{-R^2}}{\sqrt{\pi R}}}$$ then

$$U_T = X(t) \cos i \, \gamma_\omega + \gamma_3' X(t) \cos i \, R' + P_o \cos i \, R'' \quad - - - [3.9(d)]$$

R' and R'' may be evaluated from Figure 3.4 and 3.5 respectively. A statical balance of forces applied at the thaw front as indicated by section a-a in Figure 3.3 results in a factor of safety:

$$F = \frac{\{D\gamma_1 (1 - R'') + \gamma_3' X(t) (1 - R')\}}{D\gamma_1 + \gamma_3 X(t)} \frac{\tan\phi'}{\tan i} \quad - - - [3.10]$$

where γ_1 and γ_3 = total unit weights of the surcharge and the thawed soil respectively.

γ_3' = effective unit weight of the thawed soil.

i = angle of inclination of the slope.

If the depth or unit weight of the surcharge is zero, the equation becomes:

$$F = \frac{\gamma_3'}{\gamma_3} (1 - R') \frac{\tan \phi'}{\tan i} \quad - - - [3.11]$$

which is in agreement with McRoberts (1972) and McRoberts and Morgen-

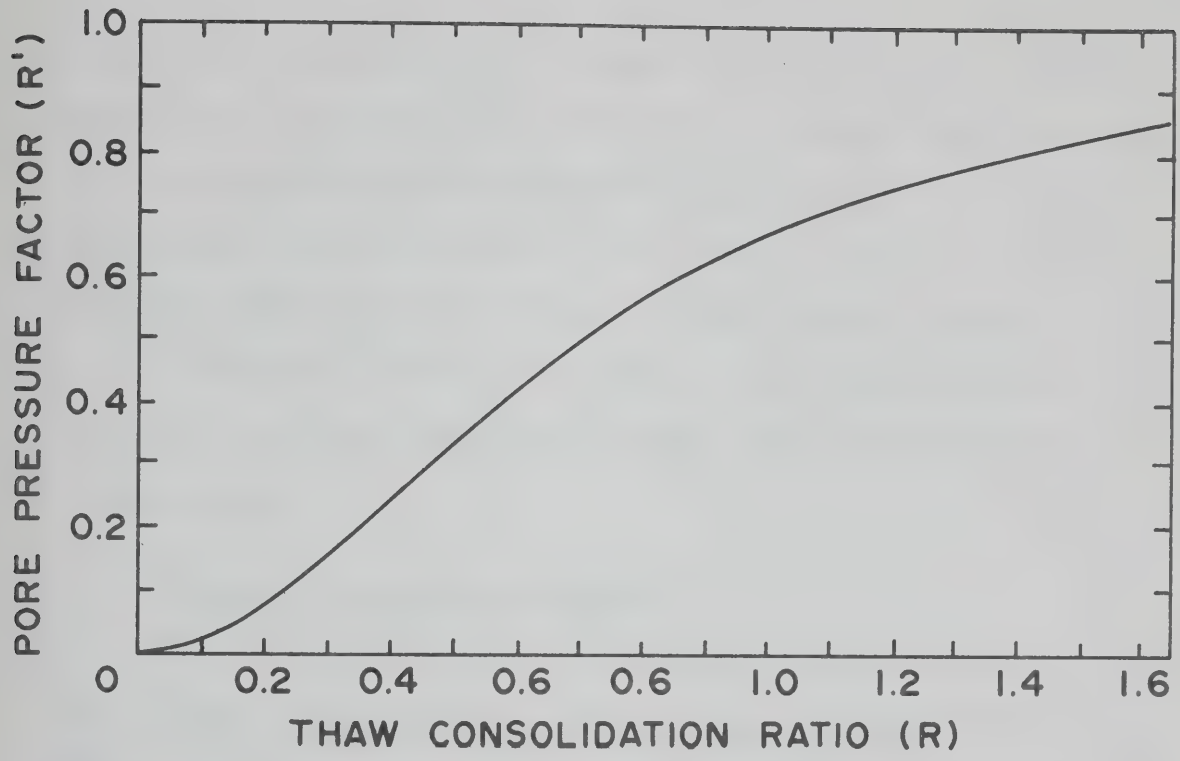

Fig. 3.4 Pore Pressure Factor (R') (self weight only) for Different Thaw Consolidation Ratios (R). After Morgenstern & Nixon (1971).

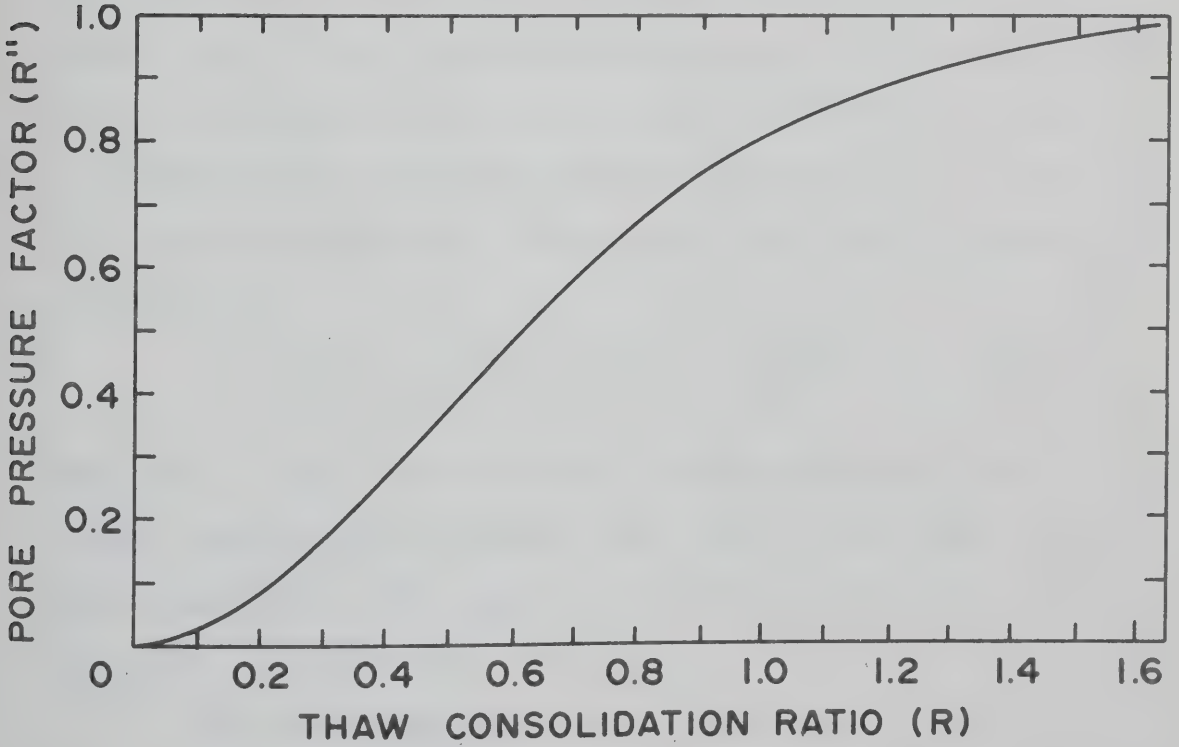

Fig. 3.5 Pore Pressure Factor (R") (surcharge only) for Different Thaw Consolidation Ratios (R). After Morgenstern & Nixon (1971).

stern (1974). Equation [3.10] produces an approximate and slightly unconservative solution because the procedure underestimates the pore water pressures and therefore overestimates the factor of safety. If the rate of thaw is plotted as in Figure 3.1 and modelled from equation [3.8], R' and R'' as obtained from Nixon and Morgenstern (1973) will be larger and the factor of safety will be proportionately smaller. The relative magnitude of these safety factors will be compared later.

3.4 Numerical Procedure For Design

The need for a numerical procedure to analyze the stability of a thawing slope covered with insulation and surcharge load is based on the lack of a suitable analytical method to evaluate pore water pressures for rates of thaw that are not proportional to the square root of time. A program was developed to compute the depth of thaw from equation [3.6] and uses a Crank-Nicholson finite difference procedure to solve the equation of consolidation subject to the boundary conditions at the thaw line (Nixon, 1973). The factor of safety is computed from:

$$F = \left[\frac{D\gamma_1 + \gamma_3' X(t) - U(N)/\cos i}{D\gamma_1 + \gamma_3 X(t)}\right] \frac{\tan \phi'}{\tan i} \quad - - - [3.12]$$

where U(N) is the pore pressure due to thaw consolidation and surcharge loading acting at the thaw front, and the other terms are as defined previously. This equation is identical to equation [3.10], except for the pore pressure term (U(N)).

The input parameters are:

1) thermal conductivities of layers 1, 2 and 3 (cal/C^o cm sec) (Kersten, 1949 and Table 3.1);

TABLE 3-1

PHYSICAL AND THERMAL PROPERTIES OF
VARIOUS INSULATING MATERIALS

Material	Moisture Content %	Density gm/cc	Specific Heat cal/gm ^{o}C	Thermal Conductivity cal/^{o}c cm sec
1) *Styrofoam HI	Dry	0.052	0.28	7.9×10^{-5}
2) *Polyurethane	Dry	0.03 to 0.08	0.28	5.5×10^{-5}
3) *Fibreglass	Dry	0.048	0.16	8.2×10^{-5}
2) *Woodchips	37	0.26	0.33	3×10^{-4}
3) *Sawdust or shavings	Dry	0.19	0.33	1.6×10^{-4}
4) *Peat	Varies with water content			

1)* Dow Chemical (1972)

2)* Smith, Berg and Muller (1973)

3)* ASHRAE (1963)

4)* Dept. of Army (1966)

2) trial thickness of insulation (m);

3) the equivalent step temperature (^{o}C);

4) the length of the thawing season (days);

5) the coefficient of consolidation of the parent material (cm^2/sec);

6) the grid spacing in the parent material (a suitable depth increment is $\simeq$ 0.040 m);

7) the thickness and unit weight of the surcharge respectively (m and kN/m^3);

8) the specific gravity of the soil solids in the parent material;

9) the total and unfrozen water contents of the parent material (expressed as a ratio of gms of water/gms of dry soil);

10) the effective angle of internal friction of the parent material;

11) the angle of the slope with the horizontal (^{o}); and,

12) the number of times output is desired over the length of the thaw season.

The output information consists of elapsed time, the depth of thaw, the pore pressure depth increment profile, the effective normal and shearing stress at the thaw front, and the factor of safety against failure.

If pore pressures and corresponding factors of safety are to be computed throughout the thaw season, then an equivalent surface step temperature must be used in equation [3.6]. This temperature is a function of the air thawing index (Thompson, 1963), a surface index factor (N) (Dept. of U.S. Army, 1966), and the length of the thaw

season (Burns, 1973).

Thus $$Ts = \frac{ATI \times N}{\text{Length of thaw season}} \quad - - - [3.13]$$

On the other hand, if pore pressures and factor of safety are desired only at the end of the thaw season when the thaw depth is at its maximum value and the factor of safety is at its minimum value, then only the surface thawing index need be used in equation [3.6]. The surface thawing index is the product of the surface temperature Ts and the total length of the thaw season. Generally, the time (t_o) required to thaw through the gravel surcharge will not be significant and may, therefore, be ignored. This simplifies the computations and provides a more conservative answer. The number of days that are chosen to represent the length of the thaw season is not particularly critical, for it is the product of the length of the thaw season and the step temperature which governs the maximum depth of thaw and is, therefore, of interest in the final analysis. It is, however, conservative to choose a slightly shorter thaw season and a correspondingly larger step temperature. Under these conditions larger pore pressures are generated in the early stages of the thaw season and therefore accentuate any critical condition that may occur at that time.

The actual temperature boundary conditions are approximated more closely by a sinusoidal variation rather than a surface step temperature. It is of interest to note that this former temperature variation will produce larger rates of thaw and therefore larger pore water pressures in mid-season than does an equivalent step temperature boundary condition (Nixon and McRoberts, 1973). At late stages in the thaw season the velocity of the thaw front is

reduced and eventually goes to zero when the thaw depth reaches its maximum value. Although the factor of safety of the slope decreases with increasing thaw depth, it is unlikely that the increase in the velocity of the thaw front at mid-season combined with a relatively shallow depth of thaw would seriously decrease the factor of safety at that time. On the other hand, the reduction in the velocity of the thaw front at the end of the thaw season diminishes the severity of the condition of decreasing factor of safety with increases in depth of thaw.

Estimates of thermal conductivity for the surcharge (K_1) and in situ material (K_3) may be obtained from Kersten (1949). These values must be multiplied by 4.13×10^{-3} to change the units to cal/cm ^{o}C sec. Table 3.1 lists the thermal conductivities (K_2) of various insulation materials that may be used. The surcharge material will provide some small but significant insulative value. The U.S. Army and Air Force (1966) suggest that one layer of material may be converted to an equivalent thickness of another from the ratio of their diffusivities. If the simple Stefan solution is employed to calculate the rate of thaw, then the ratio of the conductivities may provide a reasonable and conservative evaluation of the insulating effect of the sand/gravel surcharge. It should also be noted that the latent heat effects of the surcharge and insulation have been omitted from the computations. This term acts to retard the rate of thaw through these upper layers and therefore essentially reduces the length of the thaw season. On the other hand, the large water contents associated with significant magnitudes of latent heat increase the thermal conductivity of these materials and reduce their insulating

value. It was, therefore, considered preferable to neglect the latent heat effects of the upper layers and assume that the time to thaw through these upper two layers (to) in equation [3.6] be equal to zero.

Values of the coefficient of consolidation (Cv) may vary from 1×10^{-2} to 5×10^{-2} cm.^{2}/sec. for materials encountered in the active layer at a number of sites in the Mackenzie Valley (Roggensack, 1975).* Test results also indicate that Cv will decrease with depth to values in the order of 3×10^{-3} cm.^{2}/sec. when tested at pressures equal to or greater than the effective overburden. The minimum value that may be encountered will not likely be less than 5×10^{-4} cm.^{2}/sec. (ibid). However, when cuts are made in this material, the soil will be thawing under low normal stresses and the tendency for consolidation will be minimal. The values of Cv quoted for the active layer are therefore considered to be appropriate for the majority of the situations encountered in this region of the Arctic.

Values of ϕ' will vary from 20 to 24 degrees for the predominantly illitic clays found in this region (ibid). The effective cohesion intercept has been considered as zero for the purposes of computation.

3.5 Design Charts

A series of design charts have been prepared for use in determining the appropriate thicknesses of insulation and surcharge that may be required to stabilize thawing slopes in frozen soils (Figures 3.6 to 3.17). These charts establish the relationship between the factor of safety of a thawing slope and the factor of

* Personal communication

safety of the same unfrozen slope with steady state seepage pore pressures only. The ratio F thaw/F seepage is plotted against the coefficient of consolidation. Four curves appear on each plot indicating conditions for surcharge loads varying from 0 to 18.0 kN/m^2 (0 to 375 psf).

Three surface thawing indices, (1,500; 2,500 and 3,500 C^o days) were chosen to embrace thawing conditions extending from the latitudes of Fort Simpson to the Beaufort Sea. Four water contents varying from 20 to 50% span the range likely to be encountered for most problems. The ratio of K_3/K_2 H indicates the effective insulation thickness. The three values of 0, 1.52 m (5.0 ft.) and 3.05 m (10.0 ft.) provide the necessary range for typical conditions.

The factor of safety varies with time, decreasing with increasing time and thaw depth. Therefore, only the minimum values that correspond to the maximum thaw depths have been considered.

The total unit weight of the surcharge was taken as 19.6 kN/m^3 (125 pcf) with a water content of 12% and a thermal conductivity (K_1) of 0.0065 cal/^oC cm. sec. The permafrost was assumed to be saturated and the soil grains to have a specific gravity of 2.70. Thaw depths were computed using unfrozen thermal conductivities (K_3) that vary with water content according to Kersten (1949). The unfrozen water content was assumed to be zero.

3.6 Example Problem

The information for the example problem regarding soil, insulation, climate, and desired factor of safety appears in Table 3-2. The solution is obtained by referring to Figures 3-6 to 3-17.

Trial I determines the thaw depth and the F ratio for the

TABLE 3-2

SOIL, INSULATION AND CLIMATE INFORMATION FOR EXAMPLE PROBLEM

SOIL PROPERTIES	INSULATION PROPERTIES	CLIMATE	F_1 (SEEPAGE) $\frac{\gamma_3}{\gamma_3} \frac{\tan \phi'}{\tan i}$	F_R
W = 35%	wood chips:	Air thawing Index: 1260 C^o days (Thompson, 1963)	0.89	$\frac{1.3}{0.89} = 1.46$
Wu = 0	K_2 = 0.003 cal/^{o}C cm sec			
Cv = 0.002 cm^2/s	Styrofoam:	Surface Thawing Index Factor: 1.75 (U.S. Dept of Army, 1966)		
ϕ' = 22^o	K_2 = 0.000079 cal/^{o}C cm sec			
K_3 = 0.003 cal/^{o}C cm sec		Surface Thawing Index: 1260 x 1.75 = 2200 C^o days		
Slope Angle = 12^o				

* Assume F (Thaw) required = 1.3

slope after disturbance, but without insulation or surcharge. The results are obtained by linear interpolation between soil water contents of 30 and 40% and surface thawing indices of 1,500 and 2,500 C^{o} days.

Trial II determines the thaw depth and F ratio for a $\frac{K_3}{K_2}$ H ratio of 1.52 m (5.0 ft.) and a surcharge load of 18.0 kN/m^2 (375 psf) (1 m of surcharge) for the same water content and surface thawing index. An F ratio of 1.47 was obtained for this combination of insulation and surcharge.

Trial III produces results for a $\frac{K_3}{K_2}$ H value of 2.3 m (7.5 ft.) and a surcharge load of 12 kN/m^2 (250 psf) ($\simeq$ 0.6 m of sand/gravel). An adequate F ratio is obtained with this combination of surcharge and insulation.

Linear interpolation for thaw depth between thawing indicies produces negligible error. However, linear interpolation between $\frac{K_3}{K_2}$ H values of 0 and 1.52 m causes a maximum of 8% overestimation of the thaw depth. Overestimation of thaw depth between $\frac{K_3}{K_2}$ H values of 1.52 m and 5.05 m is not significant.

Both Trial II and Trial III solutions are viable but it is probable that Trial II would be more economical depending on the relative availability of surcharge and insulating materials. However, the thaw depth in Trial II is approximately 20% greater than in Trial III. This may be a distinct disadvantage if the lower material is significantly inferior to the surficial deposits. Trial II would require approximately 15 cm. (6 in.) of woodchips along with 1 m (3 ft.) of sand/gravel surcharge. If styrofoam board were used approx-

imately 4 cm. (≃ 1.51 in.) would provide the same $\frac{K_3}{K_2}$ H value.

If the same problem is solved by direct hand computations, the thaw depth is computed from equation [3.3]. The modified thickness of insulation is determined from:

$$HE = H + \frac{K_2}{K_1} DEP \qquad - - - [3.14]$$

where H = thickness of insulation

DEP = thickness of sand/gravel surcharge

K_1 and K_2 are the thermal conductivities of the surcharge and insulation respectively. α_e is determined from equation [3.3], R from equation [3.5], R' and R'' from Figures 3.3 and 3.4 and F from equation [3.10]. The results are shown in Table 3-3.

Figure 3-1 illustrates the manner in which the thaw depth varies with time for the combination of insulation and surcharge represented by Trial II. The thaw depth is almost linear with time, indicating a reasonable value of n (in equation [3.8]) equal to 1. R' and R'' may be evaluated from Nixon and Morgenstern (1973) and F computed from equation [3.10]. The results appear in Table 3-4.

A comparison of the values for factor of safety in this example indicate a slight variance in the magnitude depending on the method chosen for evaluation. The maximum value of the difference in this example is less than 10%. Since it is impossible to predict the various soil and climatic parameters required for the solution within this tolerance, it may be concluded that all methods produce acceptable values for design. The design charts are favoured in a choice of methods because of their convenience. The numerical procedure provides a more exact solution and generates data throughout

TABLE 3-3

THAW DEPTH AND INSULATION AND SURCHARGE REQUIREMENTS FOR EXAMPLE PROBLEM

Surface Thawing Index C^o Days	Water Content %	$\frac{K_3}{K_2}$ H (m)	Po (kN/m^2)	Thaw Depth (m)	F_R
TRIAL I					
1500	30	0	0	1.57	0.64
1500	40			1.33	0.71
1500	35			1.45	0.68
2500	30			2.03	0.54
2500	40			1.71	0.63
2500	35			1.87	0.59
2200	35	0	0	1.74	0.62
TRIAL II					
1500	30	1.52	18	0.53	1.50
1500	40			0.38	1.77
1500	35			0.45	1.63
2500	30			0.82	1.25
2500	40			0.61	1.54
2500	35			0.71	1.40
2200	35	1.52	18	0.64	1.47
TRIAL III					
1500	30	1.52	12	0.57	1.37
1500	40			0.42	1.63
1500	35			0.49	1.50
2500	30			0.94	1.13
2500	40			0.71	1.39
2500	35			0.82	1.26
2200	35	1.52		0.72	1.33
1500	30	3.05		0.34	1.60
1500	40			0.25	1.84
1500	35			0.30	1.72
2500	30			0.58	1.39
2500	40			0.40	1.66
2500	35			0.49	1.53
2200	35	3.05		0.43	1.59
2200	35	2.3	12	0.59	1.46

TABLE 3-4

COMPARISON OF FACTORS OF SAFETY BY DIFFERENT METHODS OF COMPUTATION

FOR $\frac{K_3}{K_2}$ H = 1.52 m Po = 18 kN/m^2 (TRIAL II)

$X(t) \alpha \sqrt{\text{Time}}$ Equation (3-10)	$X(t) \alpha$ Time Equation (3-8)	Design Charts	Numerical Methods
	n = 1.0		
Max. Thaw Depth 0.649 m (2.13 ft)	Max. Thaw Depth 0.649 m (2.13 ft)	Max. Thaw Depth 0.64 m (2.10 ft)	Max. Thaw Depth 0.649 m (2.13 ft)
α_e = 0.0194 cm/sec$^{1/2}$	α_e = 0.0194 cm/sec$^{1/2}$	F = 1.31	F = 1.28
R = 0.217	R' = 0.14		
R' = 0.086	R'' = 0.16		
R'' = 0.090	F = 1.28		
F = 1.36			

the complete thaw season. The choice between the latter two methods will, therefore, depend upon the extent of the information required in the design project.

3.7 Recommendations For Installation

Since there is little documented experience regarding the actual performance of such installations, the following section is not intended to provide a detailed contract specification, but rather to highlight some of the more important aspects of the topic. Each site will demand innovative methods depending upon location, geographical setting, accessibility and a host of other logistic problems.

The ideal time for installation of the stabilizing materials would be in late winter or early spring when the permafrost is at its minimum temperature. It is intended that the placement of the insulation precede that of the surcharge. It may, however, be necessary to dress the slope with a layer of sand and gravel to provide a uniform surface for the insulation.

It is imperative that adequate drainage be provided directly above the permafrost to prevent the possibility of impeding the dissipation of excess pore water pressures. This may be most readily achieved by placing a four to six inch granular inverted filter or perforated plastic drainage pipe embedded in a herringbone pattern within a layer of sand immediately adjacent to the base material.

Insulation in the form of styrofoam board, wood chips, sawdust or planer shavings would then be placed over this drainage facility. Some consideration might be given to prevent these insulating materials

from absorbing excessive surface run-off and thus increasing their thermal conductivities. Styrofoam board will absorb 0.25% water by volume (Dow Chemical, 1972) and this small amount of moisture retention will not measurably affect the thermal characteristics of this material. Similar data is not available for foamed in place polyurethane but it is reasonable to assume that its water retention characteristics would be somewhat greater than the extruded styrofoam board. Increases in thermal conductivity with increasing water content in planer shavings and wood chips are also not known. However, these materials may be protected with an overlay of polyethylene plastic that would help to prevent substantial increases in water content. Surface runoff should be diverted by construction of small diversion dykes above the slope rather than by ditching.

The surcharge material, consisting of a sand/gravel mixture capable of sustaining plant growth forms the upper layer of the stabilizing components. This material must be end dumped and worked down the slope using all reasonable care to prevent disturbance of the underlying materials. It is necessary to ensure that this material is sufficiently resistant to erosion to maintain it in place prior to re-establishing vegetation on the slope.

Re-vegetation procedures should take place subsequent to the final trimming of the slope. It would be desirable to apply the seed in the form of hydro seed at the beginning of the growing season. The choice of plant species should be made in accordance with the results of on-going research experiments being conducted in the arctic and sub-arctic regions.

3.8 Longterm Performance

The most critical conditions regarding pore water pressures and stability will not necessarily occur during the first season of thaw. During this period of time, the soil will be consolidating under the imposed surcharge load and the water content will be reduced accordingly. Freeze back in the fall will not occur until movement of the thaw front has ceased and the pore water pressure has essentially dissipated. Therefore, there does not appear to be any danger of impeded drainage due to freeze back from the surface. During the second season of operation the $\frac{K_3}{K_2} H$ ratio will be increased because of the increased thermal conductivity of the soil due to the decrease in water content. However, this increase is not large enough to limit the melting to the same level during the first year. As a consequence, the thaw line will be penetrating the material below the maximum thaw depth of the preceding year, resulting in a smaller factor of safety. The magnitude of the decrease is less than 10% for the extreme condition, where the water content is reduced from 50 to 20%. These changes in factor of safety from one season to another are generally not considered to be significant. However, the designer may wish to choose a slightly larger initial value for the factor of safety in view of the foregoing. Increased thaw depth during subsequent years will not be significant. As vegetation is developed on the slope the surface heat balance will change and the surface will experience cooler temperatures, resulting in a decreased thaw depth and increased stability.

3.9 Choice of Insulation

A number of different insulating materials have been listed

in Table 3-1 for consideration. The final choice of material for each location will be made on the basis of availability of the material, the ease of placement and ultimately, the cost in place. A detailed economic analysis is beyond the scope of this presentation and the following discussion is only meant to provide guide lines for the designer in his choice of material.

Styrofoam board is readily available in southern Canada and may be shipped by rail f.o.b. Hay River, N.W.T. for approximately 17 cents per board foot (1974 quotation). This material is easy to place but requires a significant amount of unskilled hand labour. It has a low value of thermal conductivity, low water retention characteristics and a high compressive strength. It is not biodegradable, which may or may not be an advantage.

Polyurethane (foamed in place) has insulative qualities similar to those of styrofoam. It requires a high level of expertise and sophisticated equipment for placement. As a comparative cost, this option has been quoted (Edmonton, 1974) at 25 cents per board foot for material and $1.00 per square foot for placement. Mobile equipment is available for transport into remote regions.

Large quantities of planer shavings are available at points as far north as High Level, Alberta. Small quantities may be available from local saw mills in the southern part of the Yukon and Northwest Territories. The cost of this material is very low. On the other hand, transportation costs may be very high. Placement is simple, requiring combined machine and hand operations. Plastic sheeting should be used to encapsulate the shavings and prevent excessive increases in the water content. This insulating material may undergo a substantial

amount of compaction under the influence of the surcharge load. Some reduction in insulative quality will undoubtably result. Placing 50-75% of the surcharge below the shavings would help to alleviate this problem. Planer shavings and sawdust are biodegradable which may be a desirable aspect.

Woodchips, as used in the example, appear to possess considerable merit as an acceptable form of insulation. They would be manufactured near or on site with a commercial wood chipper using trees cleared from the right of way. However, careful assessment must be made of the quantity of trees available for this purpose. For example, a 100 foot wide right of way might require 9 in. of wood chips for insulation. One hundred lineal feet of this right of way would require 7,500 ft^3. At 17 pcf, 12,750 lbs. of wood chips are required. Assuming green spruce or poplar weighs approximately 40 pcf, then 3,200 ft^3 of wood are required. If a cord of wood has a porosity of 20%, then the volume of solids per cord of wood is approximately 100 ft^3. Therefore, 32 cords of wood per 10,000 sq. feet of area are required. This is a substantial amount of wood and forestry personnel should be consulted regarding estimates of the availability of these quantities in the areas where they are required.

Environmental restrictions will generally make the on-site mining of peat moss impractical. If the material is gathered locally, it must be dried to obtain a suitable moisture content and correspondingly low coefficient of thermal conductivity. Transporting processed peat moss from southern Canada to northern regions is generally considered to be impractical when compared with artificial insulation materials. It, therefore, seems reasonable to conclude that wood chips, planer shavings or styrofoam board are the three prime contenders in the choice of insulation.

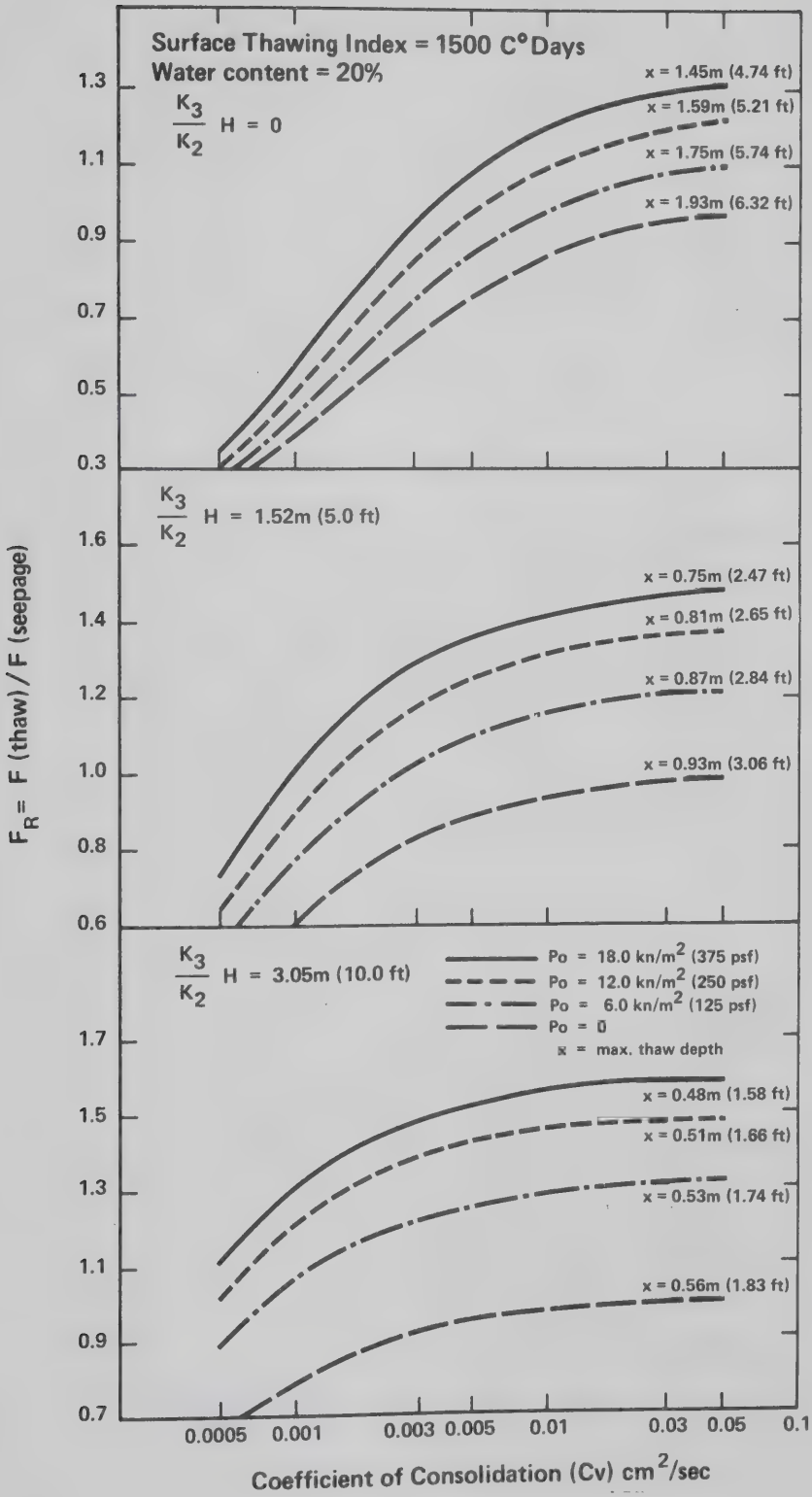

Fig. 3.6 Design Chart for Stabilization of Planar Landslides

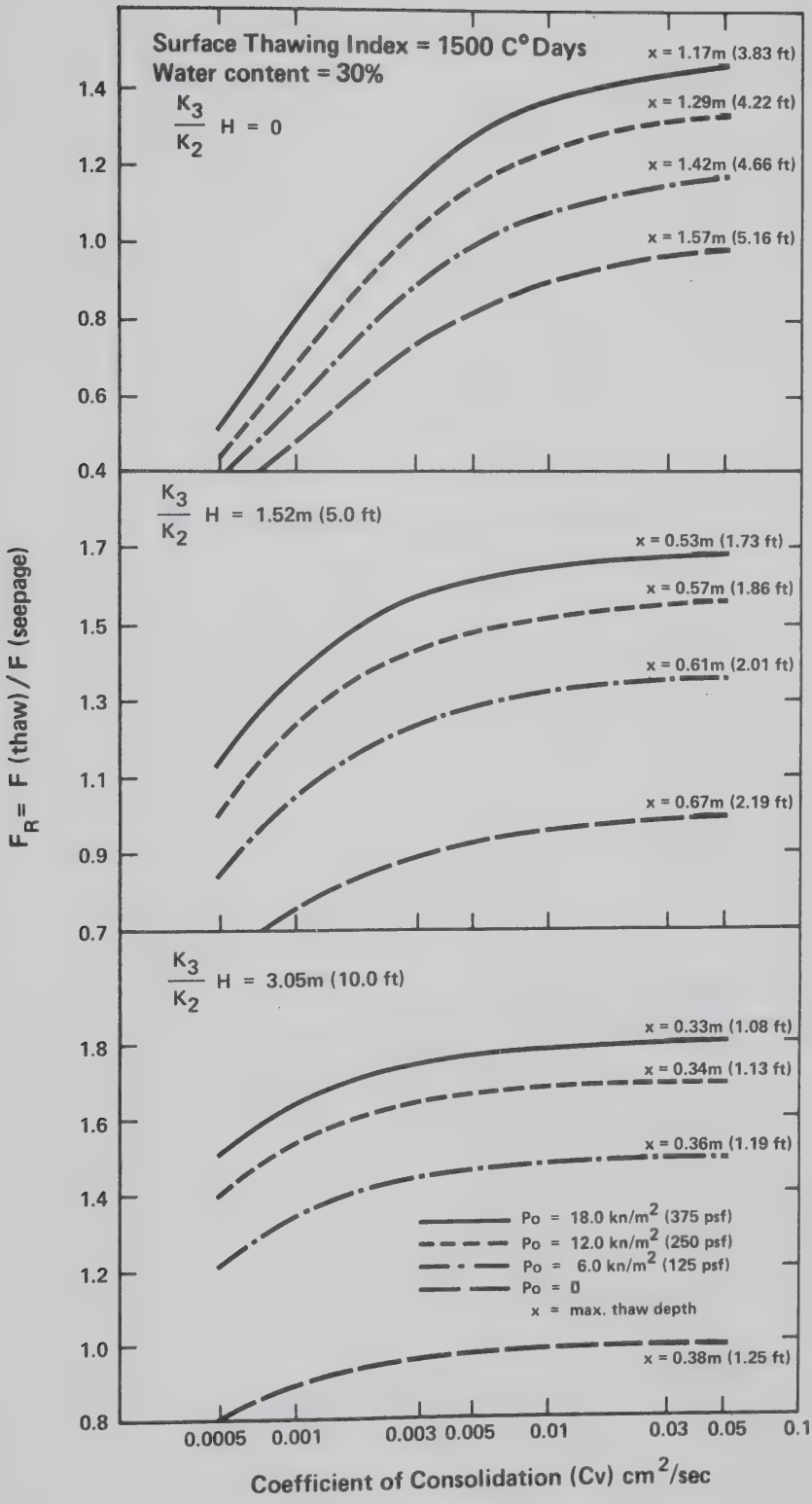

Fig. 3.7 Design Charts for Stabilization of Planar Landslides

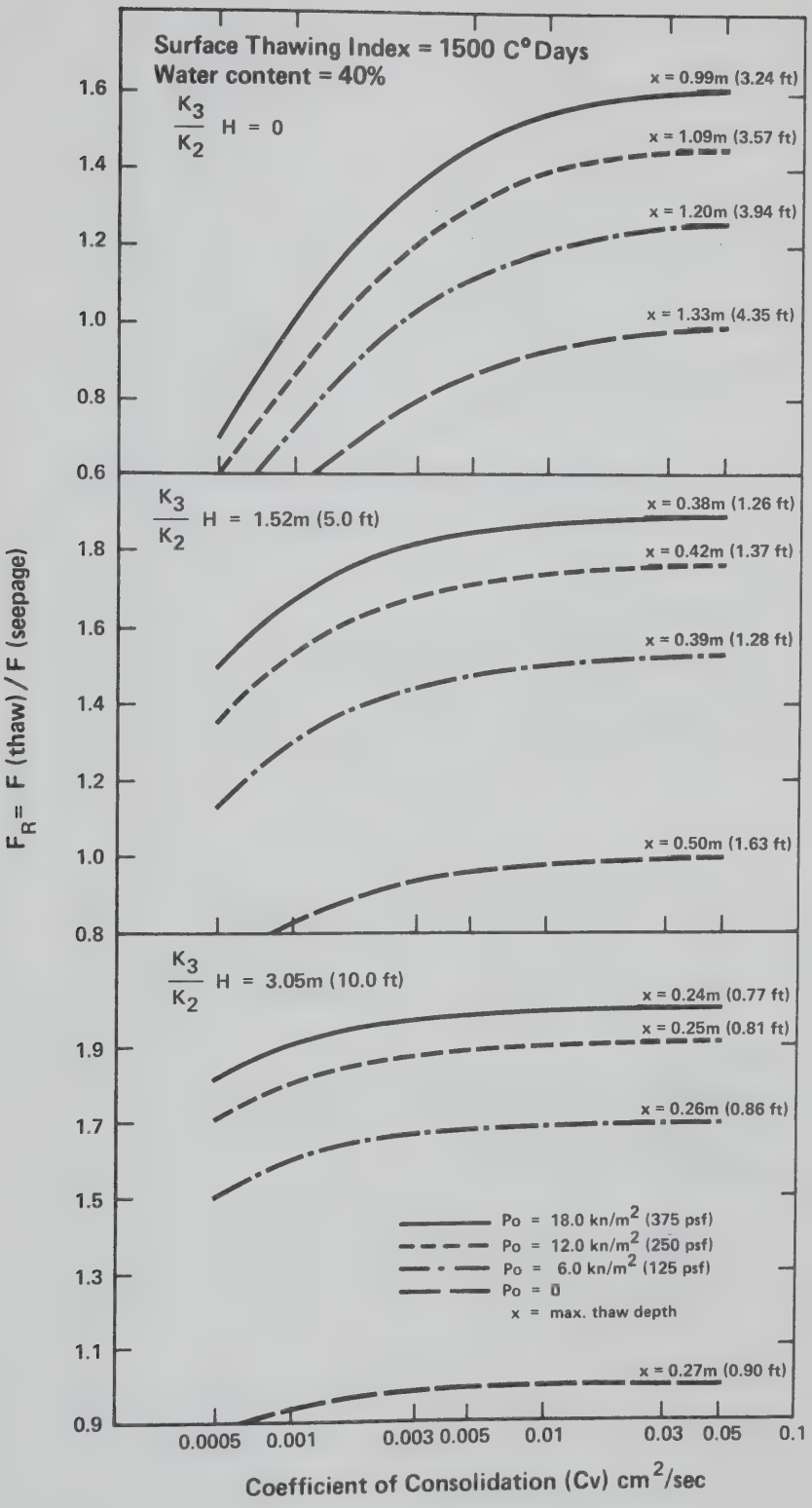

Fig. 3.8 Design Charts for Stabilization of Planar Landslides

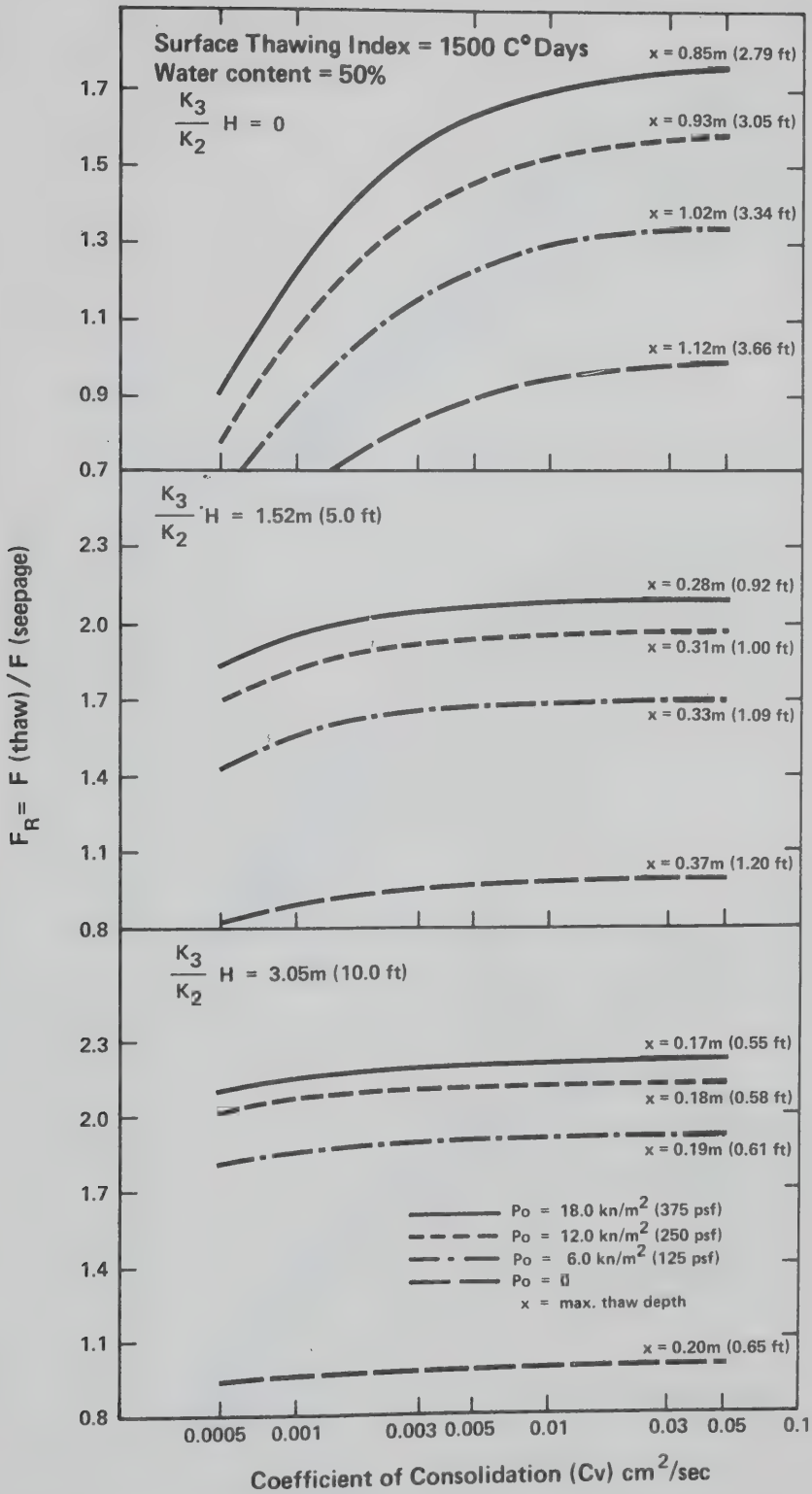

Fig. 3.9 Design Charts for Stabilization of Planar Landslides

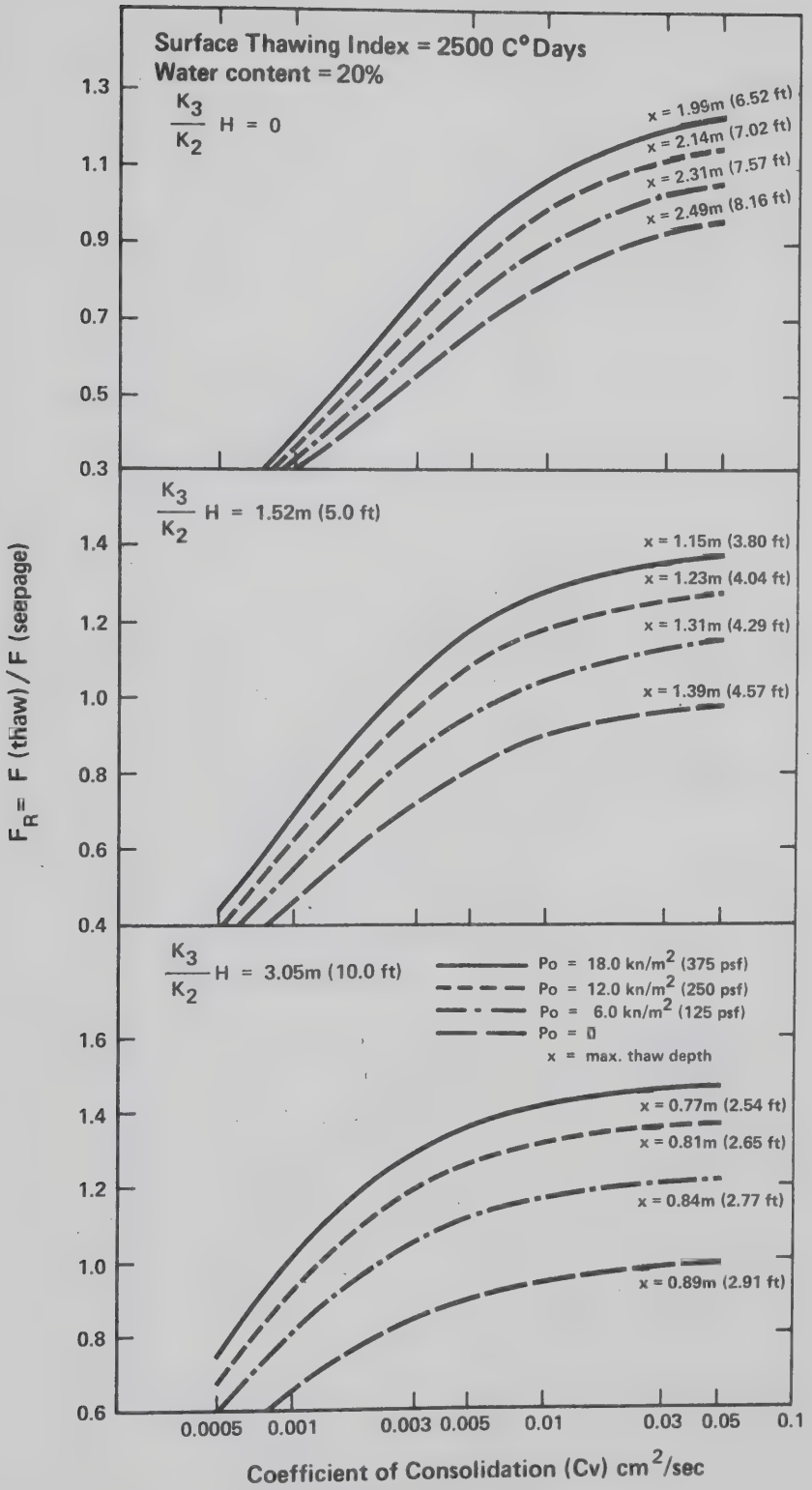

Fig. 3.10 Design Charts for Stabilization of Planar Landslides

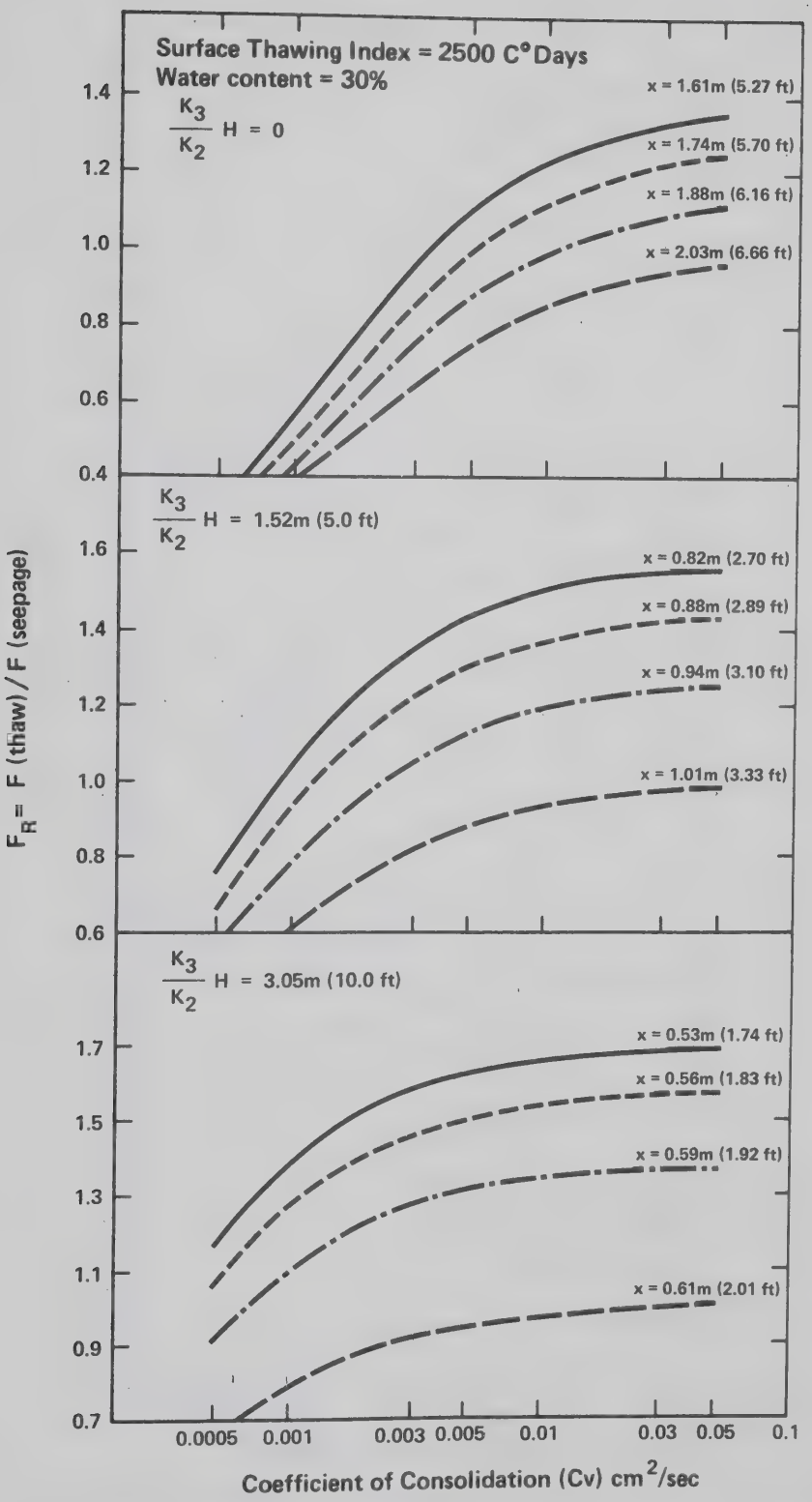

Fig. 3.11 Design Charts for Stabilization of Planar Landslides

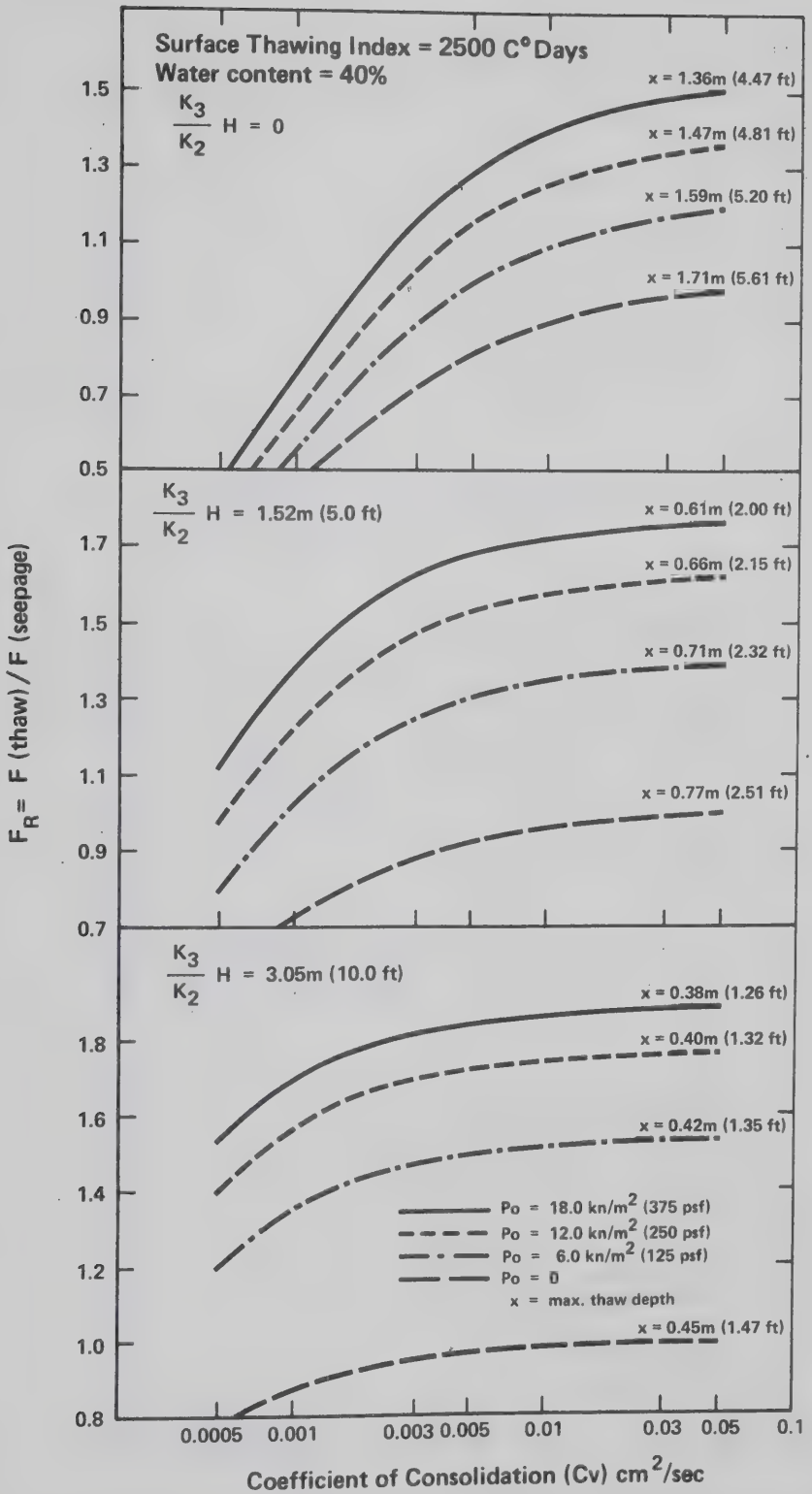

Fig. 3.12 Design Charts for Stabilization of Planar Landslides

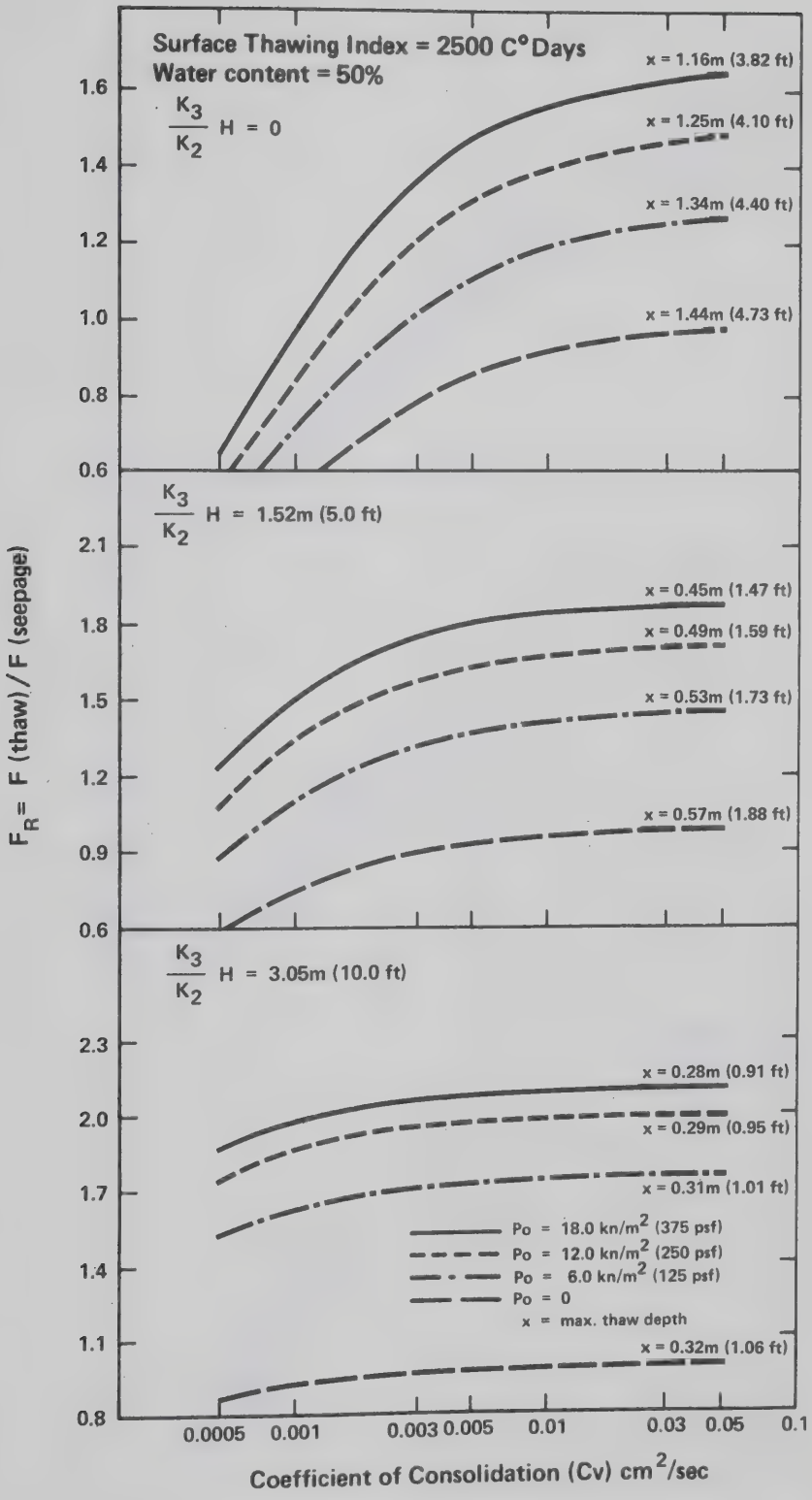

Fig. 3.13 Design Charts for Stabilization of Planar Landslides

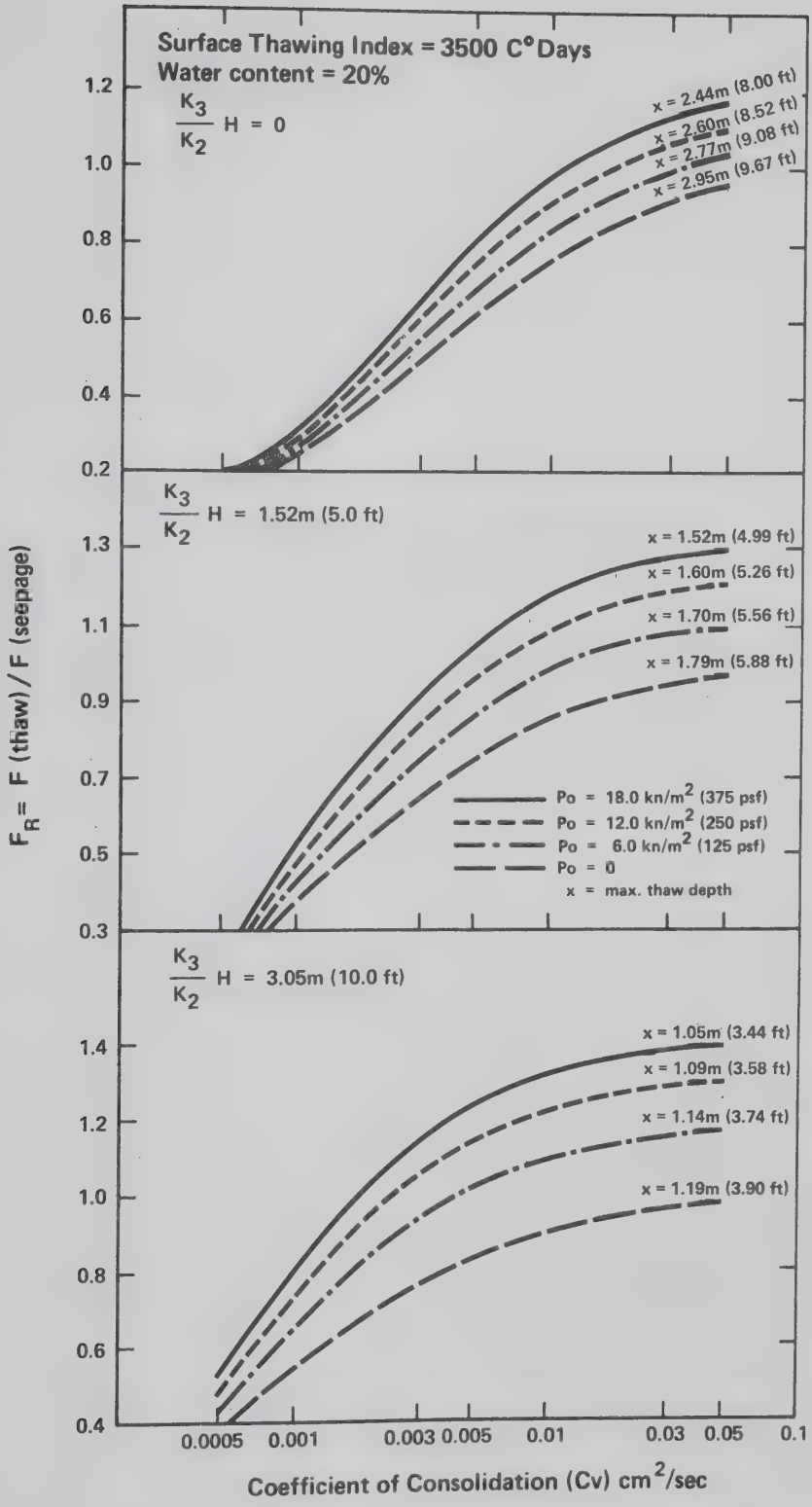

Fig. 3.14 Design Charts for Stabilization of Planar Landslides

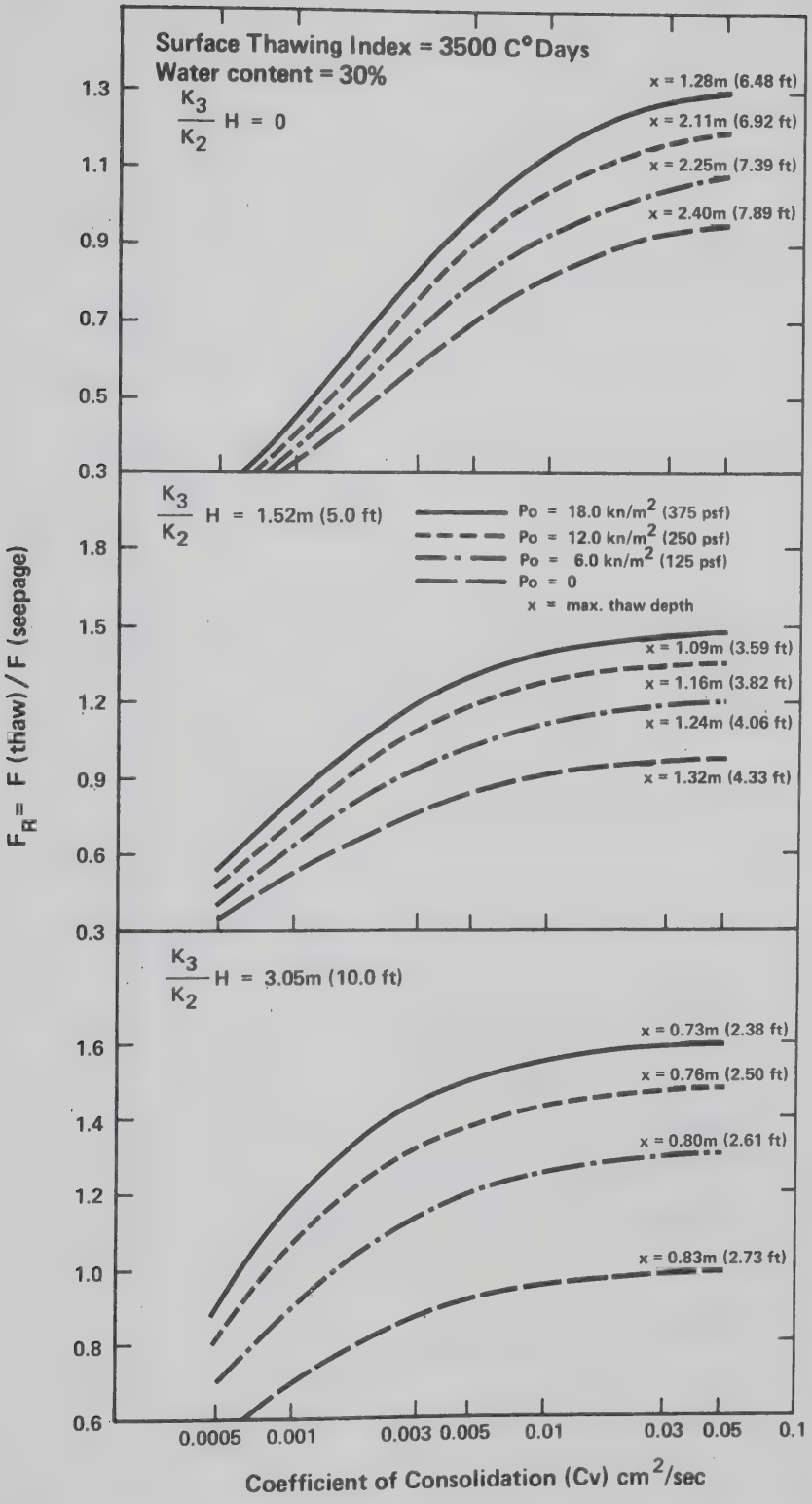

Fig. 3.15 Design Charts for Stabilization of Planar Landslides

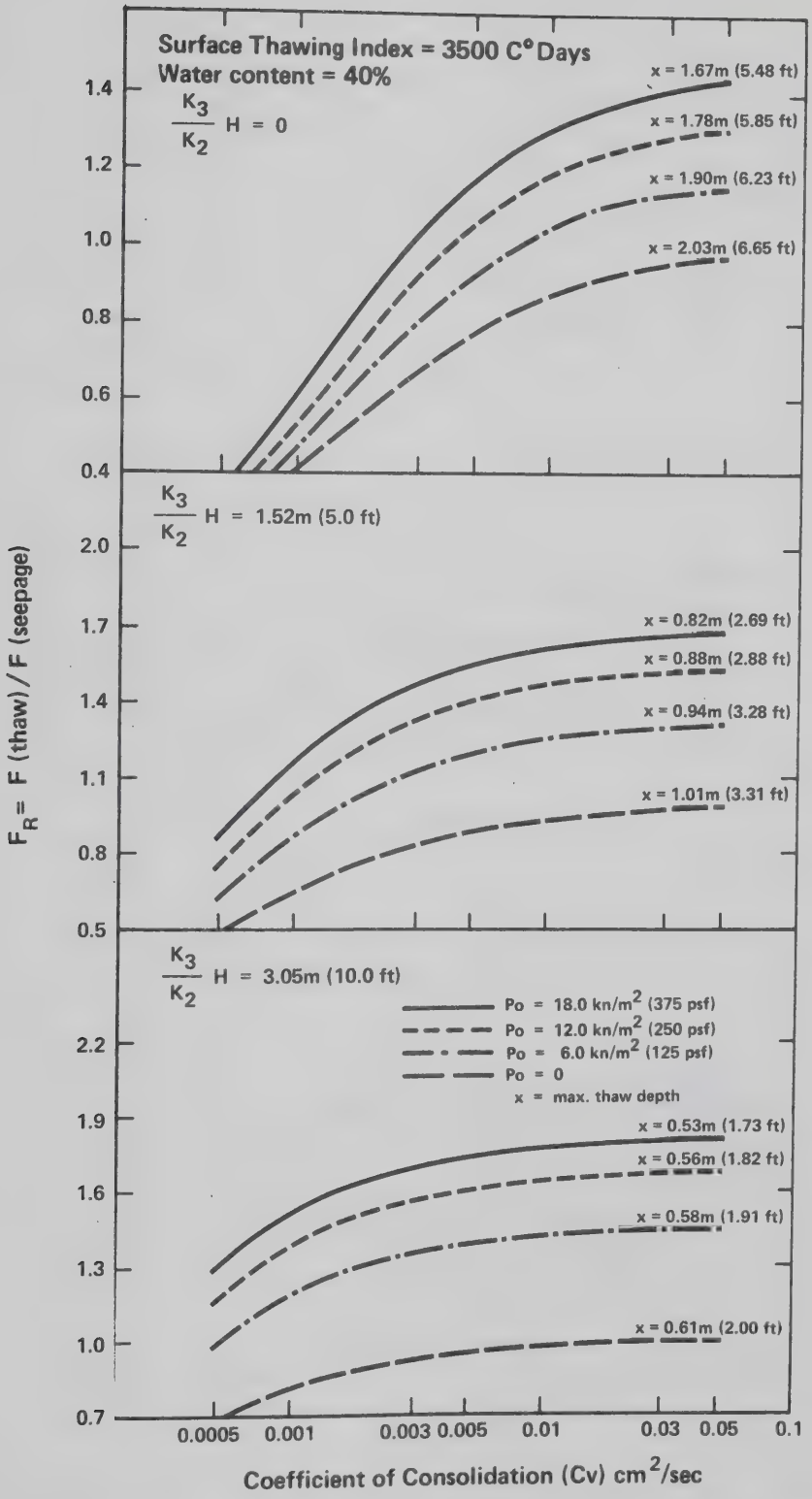

Fig. 3.16 Design Charts for Stabilization of Planar Landslides

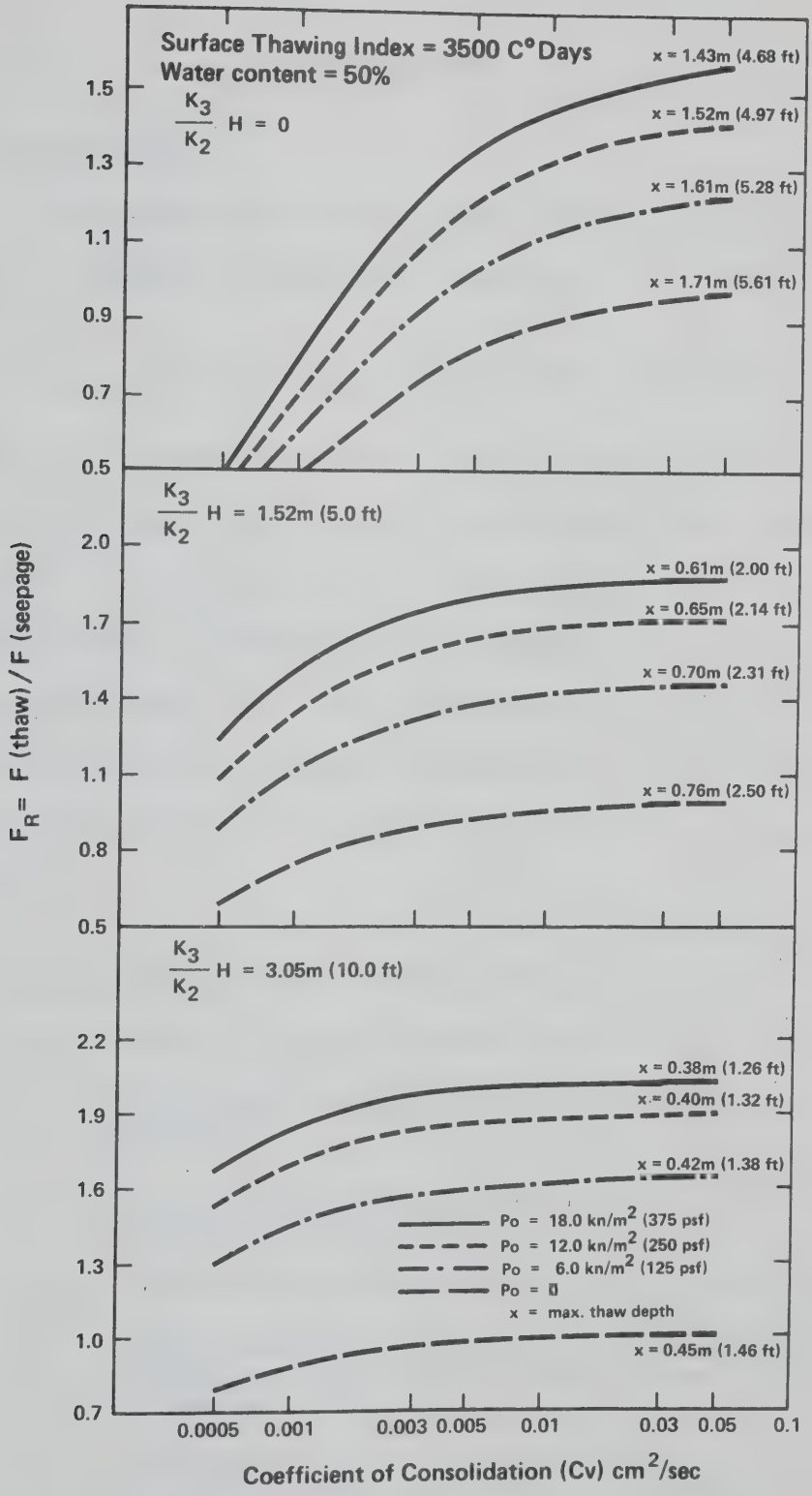

Fig. 3.17 Design Charts for Stabilization of Planar Landslides

CHAPTER IV

THE ENERGY BALANCE

4.1 Basic Concepts

The energy balance at the surface of the earth may be expressed in terms of a mathematical equation:

$$q_{DS} + q_{dS} + q_{RS} + q_{LU} + q_{LD} + q_L + q_H + q_P + q_G = 0 \quad - - - [4.1]$$

The symbol q represents energy per unit of area per unit of time and has units of gm. cal/cm^2 min. or simply ly/min. The subscript refers to the source of this energy. The equation is written with all terms positive. If the direction of energy flow is toward the surface of the ground, the sign will be positive and if energy flow is directed away from the surface, the sign will be negative. This convention also applies to heat flow below the surface. In equation [4.1]:

q_{DS} = direct beam short wave energy from the sun.

q_{dS} = diffuse short wave energy from the sky.

q_{RS} = short wave radiation reflected by the earth's surface.

q_{LD} = long wave radiation directed downward from the atmosphere to the ground.

q_{LU} = long wave radiation emitted by the ground surface.

q_L = the transfer of energy to or from the surface through the latent heat of vaporization or condensation.

q_H = the transfer of energy by sensible heat to or from the surface by turbulent or convective processes.

q_P = the gain or loss of energy through the addition of sensible heat due to precipitation on the surface.

q_G = the transfer of energy to or from the surface through the ground.

4.2 Radiative Components on a Horizontal Surface

4.2.1 General

All bodies radiate thermal energy, the intensity and spectral distribution of which is a function of the temperature and emissivity of the body.

A "black body" is a body or object that completely absorbs all radiation (at all angles) incident upon its surface. It is also a perfect emitter at all wave lengths. The emissivity (ε) of a body is the ratio of the emissive power (E) of a body at absolute temperature (T) to the emissive power of a black body (E_b) at the same absolute temperature (T). Thus,

$$\varepsilon = E/E_b \qquad - - - [4.2]$$

Radiation is characterized according to wave length (λ) usually measured in microns (μ). The spectral distribution ranges from some small, but finite value (.10μ) to wave lengths in excess of 50μ.

Planck (1959) used quantum theory to derive the hemispherical emissive power of a black body.

$$E_{b\lambda} = \frac{C_1}{\lambda^5 (e^{C_2/\lambda T} - 1)} \qquad - - - [4.3]$$

where C_1 and C_2 are constants and $E_{b\lambda}$ is the emissive power at wave length λ and absolute temperature (T) expressed in ^oK. Figure 4.1 indicates the manner in which black bodies emit energy at different temperatures and wave lengths. It also shows that the maximum energy emitted by a black body occurs at some unique wave length

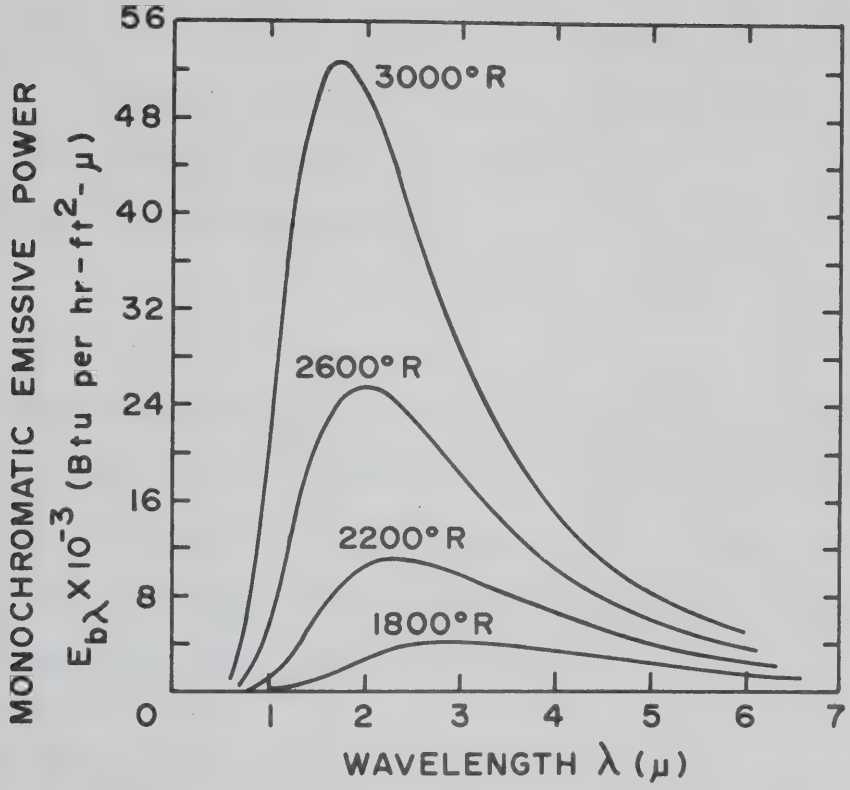

Fig. 4.1 Monochromatic Emissive Power for Several Temperatures vs Wavelength (After Wiebelt (1966))

associated with some unique temperature. If equation [4.3] is differentiated partially with respect to wave length and set equal to zero, the equation $\lambda_{max} T$ = constant emerges where λ_{max} is the wave length corresponding to the maximum emissive power (Wien, 1894). The Wien's Displacement Law indicates that the peak intensity of emitted radiation occurs at a wave length which is inversely proportional to the absolute temperature. It is evident that so called "hot bodies" radiate maximum amounts of energy at short wave lengths and cooler bodies radiate at longer wave lengths. The sun, at approximately 6,000^0 K, has its peak emissive power in the 0.47 to 0.49 μ range, whereas the earth at approximately 300^0 K emits at a peak intensity of 11 to 12 μ. It is of interest to note that 45% of the emitted energy in the solar spectrum falls within the visible range of 0.4 to 0.74 μ (Sellers, 1965). Short wave radiation is generally

considered to be all that radiation less than 4 μ in length.

The Planck equation for emissive power in monochromatic wave lengths may be recast and integrated over all wave lengths to form the Stefan-Boltzman equation.

$$E = \sigma T^4 \qquad - - - [4.4]$$

This equation describes the energy emitted by a black body in all wave lengths at absolute temperature (T) and where the Stefan-Boltzman constant (σ) equals 8.26×10^{-11} ly/min. $^oK^4$. If the emissivity (ε) is included, then the equation describes the manner in which bodies other than black bodies emit radiation.

4.2.2 Direct Beam Clear Sky Solar Radiation

As solar radiation passes through the atmosphere it is selectively scattered and/or absorbed by gases and impurities in the air. Ozone absorbs all the energy at wave lengths less than 0.3 μ and selectively up to 0.35 μ. Water vapour effectively prevents solar radiation longer than 4.0 μ from reaching the ground. It selectively transmits in the 11 to 13 μ range and this accounts for the significant influence of long wave radiation.

Carbon dioxide is the only other gas in the atmosphere that absorbs radiation. It will, however, absorb only in two narrow bands. The first band occurs between 0.29 and 4.0 μ and the second between 12 and 16 μ (Simpson, 1929).

Actual depletion of a direct ray of radiation is a function of the composition and thickness of the medium through which it passes. The quantity of direct beam radiation (on a plane normal to the beam) reaching the earth's surface is commonly expressed by Beer's Law.

$$q_{DSN} = J_o e^{-\beta m} \quad - - - [4.5]$$

where q_{DSN} is the flux of energy transmitted to the earth by direct short wave radiation.

β = coefficient of extinction.

m = thickness of the medium traversed by the beam or commonly called the optical air mass.

This quantity m may be adequately approximated by $^1/\cos z$ (where z equals the zenith angle of the sun) for angles of z less than 80 degrees. The solar constant (J_o) is defined as the intensity of solar radiation received on a unit area of a plane normal to the incident radiation at the outer limit of the earth's atmosphere with the earth at its mean distance from the sun. The magnitude of this constant varies within limits of ± 1.5%. List (1968) proposes a value of 1.94 ly/min. Occasionally adjustments are made to J_o that take the form of J_o/r^2 where r, the radius vector of the earth, is the distance from the center of the earth to the center of the sun expressed in terms of the length of the semi-major axis of the earth's orbit (ibid). This variation in distance produces a variation in intensity of ± 3.5%.

The term $e^{-\beta}$ is alternately called the transmittance (a). This parameter is a function of scattering due to air molecules and water vapour as well as absorption of radiation by water vapour. The amount of radiation reaching a horizontal plane on the earth's surface may then be written as

$$q_{DSH} = J_o a^m \cos z \quad - - - [4.6]$$

where z again represents the zenith angle of the sun and can readily be expressed in terms of the declination, latitude and the hour angle.

If the designer wishes to calculate or estimate the amount of direct beam radiation reaching the surface of the earth, he must in some way be able to evaluate the transmittance (a).

The classical approach to calculating direct beam radiation at the surface of the earth has been to express it as some fraction of the direct beam radiation incident upon a horizontal surface at the outer limits of the atmosphere. Thus the ratio $q_{DSH}/q_{DSHE} = a^{11}$ (and $a^{11} = a^{m}$) must be determined. a^{11} is defined as the atmospheric transmission coefficient. The subscript E indicates extraterrestrial. Kimball (1928) has prepared charts which allow the evaluation of a^{11} for different values of the precipitable water in the air (w) and various values of the optical air mass (m).

For example, if the amount of precipitable water is 30 mm and a low to moderately dusty atmosphere prevails, the transmission coefficient (a^{11}) for m = 1 is 0.63 and for m = 5, a^{11} = 0.28. Thus the length of path of the sun's rays through the atmosphere is of extreme importance in affecting the reduction of solar intensity. The reader is referred to Klein (1948) for the most lucid presentation of the technique.

The amount of precipitable water in the atmosphere is that amount of water that would be obtained from a column of air extending from the earth's surface to the top of the atmosphere. The magnitude of this parameter can be related to the moisture in the air at the surface of the earth which in turn is a function of the dew point temperature. Reitan (1963) suggests the relationship

$$\ln w = a + b\,(t_d) \qquad - - - \ [4.7]$$

where w = the amount of precipitable water vapour in the air (cm).

t_d = dew point (^oC).

a = 0.110 and b = 0.614.

Similar equations have been suggested by Threlkeld and Jordan (1958), Brooks (1959), Stephenson (1967), and ASHRAE (1967). The amount of precipitable water may be adjusted for elevation when sites are in excess of 2,000 feet above sea level (Klein, 1948, Threlkeld and Jordan, 1958).

Direct evaluation of the precipitable water may be omitted if published values of the apparent extention coefficient (β) are available (ASHRAE, 1967, Sadler, 1970). The precipitable water and scattering are considered as a monthly average and the values have been determined experimentally and tabulated for each month of the year.

The accuracy of computed values of clear sky radiation is reasonably good for most unindustrialized areas of the world. However, the value of such computations is not always evident in most micrometeorological problems. Cloud cover has a profound effect on direct beam radiation and must be considered in most practical problems.

4.2.3 Diffuse Clear Sky Radiation

A significant part of the direct solar radiation which has been scattered and diffusely reflected in the atmosphere by molecules of air, water vapour and dust arrives at the earth's surface unchanged in wave length. This portion of short wave radiation is known as diffuse radiation and is in excess of the direct beam radiation.

Kimball (1935) has suggested that -- "about half the radiation lost from the incoming rays through scattering and diffuse reflection is finally received at the ground as diffuse radiation from the sky". The total depletion by atmospheric scattering and diffuse reflection

can be expressed as:

$$s = 1 - a^{1} \quad - - - [4.8]$$

where a^{1} is the transmission coefficient after scattering by air and water molecules. It differs from the previous transmission coefficient a^{11} in that it does not include water vapour absorption. Thus for a given amount of precipitable water in the atmosphere a value for a^{1} may be obtained from Figure 4.2 and a scattering coefficient calculated from equation [4.8]. The quantity of short wave diffuse radiation incident upon a horizontal surface may be estimated as:

$$q_{ds} = J_o \cos z \, S \, (0.5) \quad - - - [4.9]$$

Typical values of S range from 0.11 to 0.20. These values agree reasonably well with Stephenson (1967).

A technique devised by Lui and Jordan (1960) to estimate diffuse radiation appears to have significant merit. They suggest the equation:

$$\tau_d = 0.2710 - 0.2939\tau_D \quad - - - [4.10]$$

where $\tau_d = q_{dSH}/q_{DSHE}$ and

$\tau_D = q_{DSH}/q_{DSHE}$.

If a value of total short wave radiation is available the equation may be written as:

$$\tau_d = 0.3840 - 0.4160\tau_T \quad - - - [4.11]$$

where $\tau_T = (q_{DSH} + q_{dSH})/q_{DSHE}$.

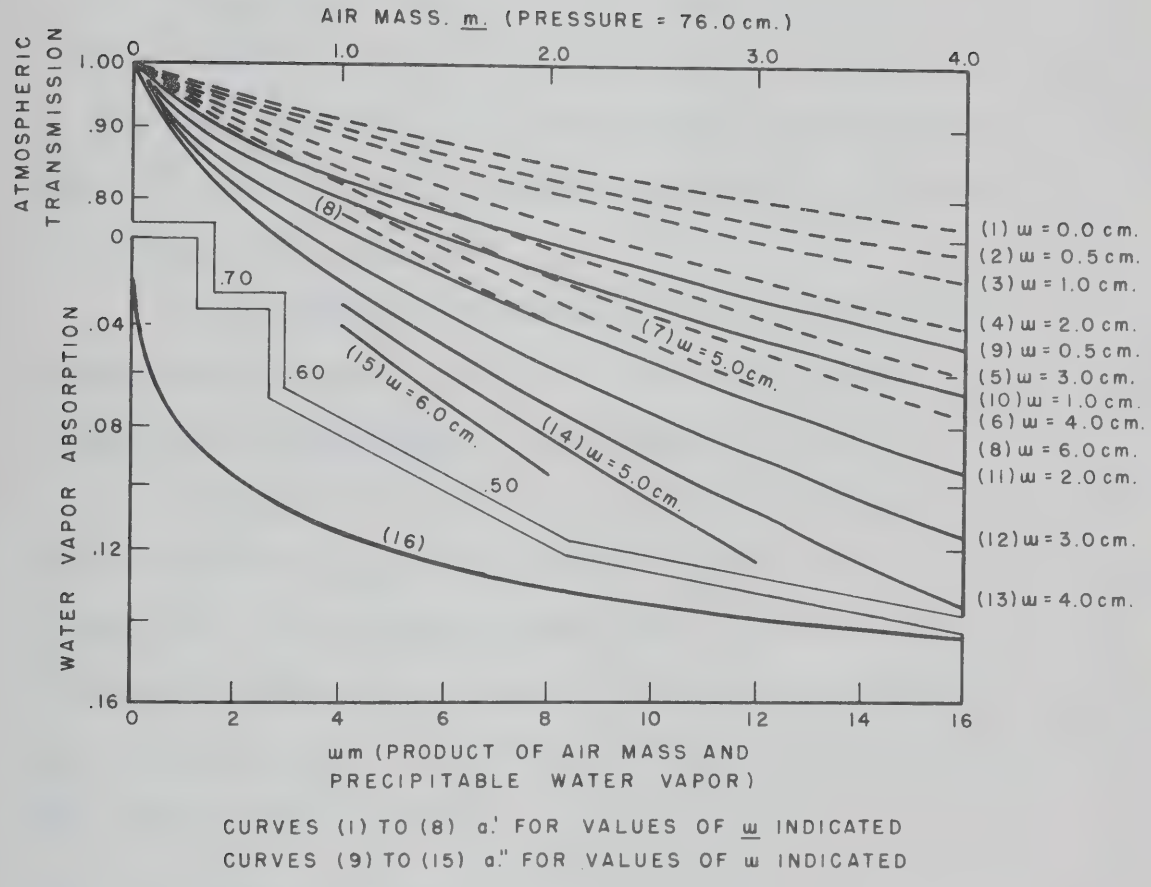

Fig. 4.2 Atmospheric Transmission Chart (After Kimball 1928)

A better procedure, also by Lui and Jordan (1960), is to use Figures 4.3 and 4.4 which relate the ratio

$$K_T = (Q_{DSH} + Q_{dSH})/Q_{DSHE}$$ to

$$Q_{dSH}/(Q_{DSH} + Q_{dSH})$$ where Q

represents monthly average daily totals and the subscripts are as before. It is assumed that $(Q_{DSH} + Q_{dSH})$ is available from measurements. With this information the diffuse component can readily be estimated on an average monthly daily basis.

Partitioning of diffuse and direct radiation may also be accomplished by relating the ratio of direct beam to total radiation relative to the sun's zenith distance (List, 1968).

London (1957) also provides a chart relating the ratio of direct to diffuse radiation for various latitudes and months of the year (Figure 4-5). The advantage gained in using London's chart is that it considers the effect of latitude. It is, however, interesting to note that Figure 4.4 shows no significant difference in results from latitudes ranging from 42^{o} to 60^{o} N.

4.2.4 The Effect of Clouds

All discussion to this point has referred to clear sky radiation only, except for the treatment of diffuse radiation by Lui and Jordan (1960). By using the proper transmittance with adjustments made for dust particles reasonable values of clear sky direct beam radiation are readily obtainable from one or more of the previous references. However, by far the largest variation in the portion of solar radiation transmitted to the earth through the atmosphere is caused by cloud cover.

Different relationships involving estimated cloud cover have

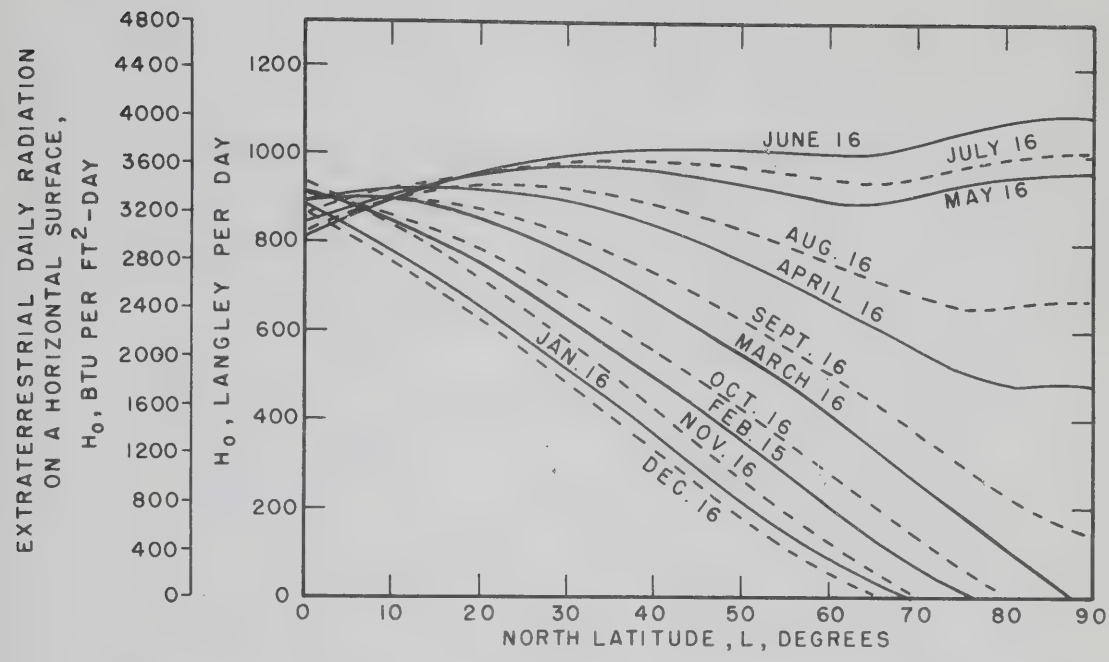

Fig. 4.3 Extraterrestrial Daily Radiation Received on a Horizontal Surface (After Lui and Jordan, 1960)

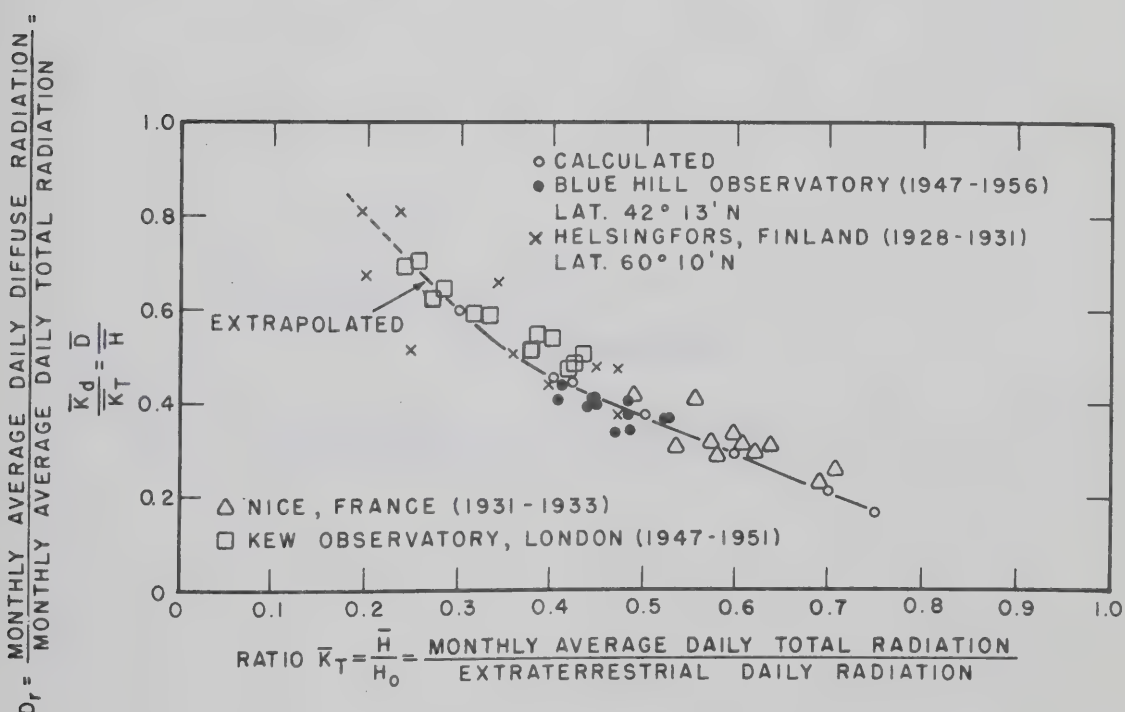

Fig. 4.4 The Ratio of the Monthly Ave. Daily Diffuse Radiation to the Monthly Ave. Daily Total Radiation as a Function the Cloudiness Index K_T (After Lui & Jordan, 1960)

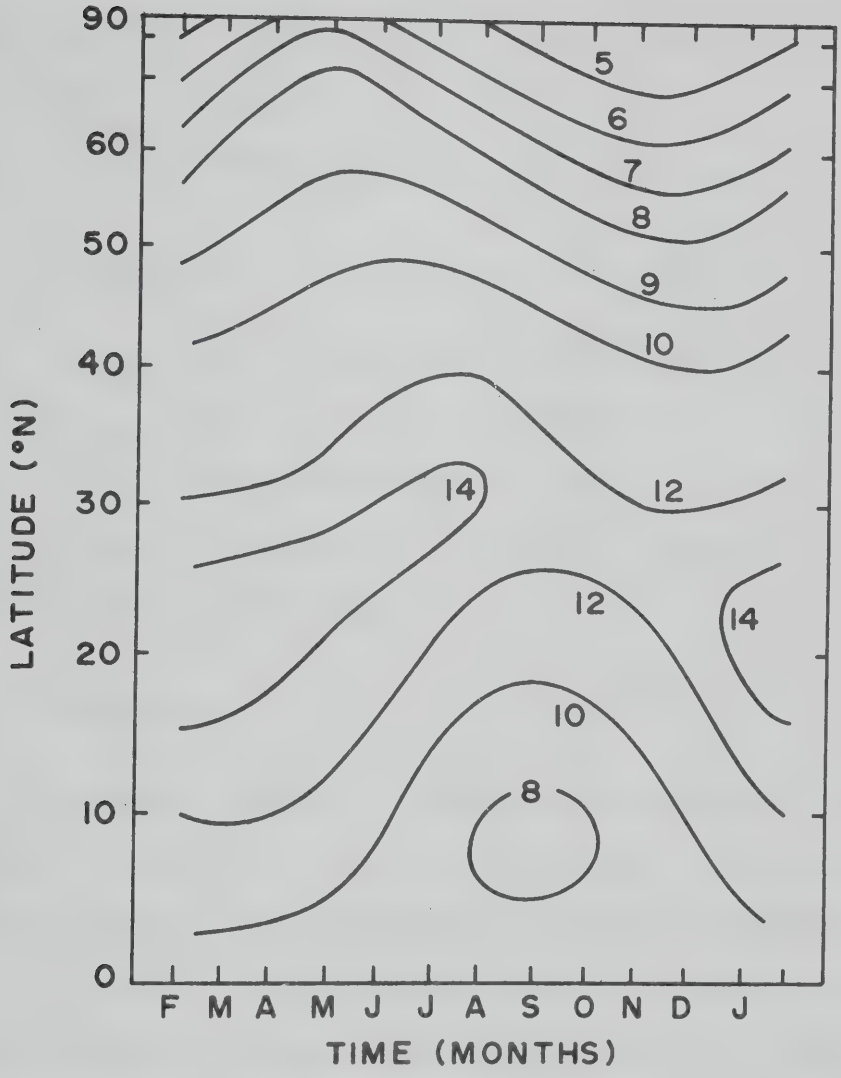

Fig. 4.5 Ratio of Direct to Diffuse Radiation Received at the Ground Surface (%) After London (1957)

been suggested by various authors. Difficulties arise with these methods because of variations in the height, type and distribution of the clouds. The subjective nature of such estimates tend to detract from this approach.

Kimball (1928) suggested:

$$q_{STHA}/q_{STHC} = a + b\,(1-n) \quad - - - [4.12]$$

where q_{STHA} = actual total short wave radiation.

q_{STHC} = clear sky short wave radiation.

a and b are constants and n is the cloud cover in tenths.

Quadratic functions of n have been suggested by Mateer (1955). Budyko (1956) suggests:

$$q_{STHA}/q_{STHC} = 1 - (1-k)n \quad - - - [4.13]$$

where k depends on latitude, climatic region and season of the year. The reader is referred to Sverdrup (1942), Newman (1954), and Haurwitz (1948) for more details on cloud cover in relation to total radiation.

The other approach commonly used is an equation expressing the actual radiation to total radiation as a function of sunshine. The general form of these relationships are:

$$q_{STHA}/q_{STHC} = a + b.S \quad - - - [4.14]$$

(List, 1966).

where a and b are empirical constants

S = ratio of actual hours of sunshine to the total possible hours of sunshine.

Typical values of a and b are 0.35 and 0.61 respectively. Additional details regarding similar equations may be obtained from Fritz and

MacDonald (1949), Hamon et al (1954), Vowinckel and Orvig (1962) and others.

4.2.5 Summary of Short Wave Radiation

It is apparent that accurate calculations of solar radiation quantities other than clear sky values may be somewhat futile. However, weather bureaus throughout the world provide meteorological stations that record various and sometimes all of the components of short wave radiation. Summaries of radiation in Canada and the United States are contained in Monthly Radiation Summaries published by the Meteorological Service in Canada and National Summary of Climatological Data by the U.S. Weather Bureau.

However, many of the remote stations only record total short wave radiation on a horizontal surface (q_{STHA}) and it may be necessary to separate the two components when considering the amount of radiation incident upon a sloping surface.

The direction of the flow of energy associated with short wave radiation is always positive, i.e. the energy flows from the atmosphere to the ground. Typical clear sky intensities of solar radiation as the sun approaches the zenith at elevations of 2,000 ft. or less above sea level during the summer in the middle north to north latitudes are about 1.3 to 1.5 ly/min. Daily values in the same regions range from 400 to 600 ly/day in the summer months for average cloud conditions (Mateer, 1955).

4.2.6 Short Wave Radiation Reflected by The Surface of the Earth (q_{RS})

All the short wave radiation transmitted through the atmosphere is not absorbed by the surface of the earth. A significant portion may be reflected back to space, depending primarily on the

color and composition of the surface. Most of this radiation will be lost to space but part of the diffuse component may again be scattered with half of this amount again returning to the ground. Generally this portion is quite small and can usually be neglected. However, studies involving solar heat gain may include this factor (Klein, 1948).

The ratio of the amount of short wave radiation reflected by a surface to the amount incident upon it is defined as the albedo (α). Thus the albedo of a perfect reflector and a perfect absorber would be 1 and 0 respectively.

$$q_{RS}/q_{STHA} = \alpha \quad - - - [4.15]$$

Values of albedo for different surfaces are shown in Table 4-1.

Albedo is not necessarily a constant value for a given material. Changes in moisture content can change the albedo of a surface by as much as 30% (Table 4-1). Variations also occur with solar altitude and spectral changes in the radiation flux. Geiger (1961) indicates values may vary from 35 to 100% for dry sand and 7 to 100% for water, depending on the solar altitude of the sun. Spectral changes cause much less variation in albedo and are probably not significant in most instances.

4.2.7 Net Short Wave Radiation

The amount of short wave radiation absorbed by the ground or made available for heat gain of the soil is given by:

$$q_{STHA} - q_{RS} = q_{STHA}\,(1-\alpha) \quad - - - [4.16]$$

It is only this net amount of short wave radiation that can

TABLE 4-1

ALBEDO OF VARIOUS SURFACES

Surface	Albedo (%)	Source
Dry sand	35 - 45	Sellers (1965)
Wet sand	20 - 30	Sellers (1965)
Light sand	30 - 60	Geiger (1965)
Sandy soil	15 - 40	Geiger (1965)
Fields	12 - 30	Geiger (1965)
Woods	5 - 20	Geiger (1965)
Dark soil	7 - 10	Geiger (1965)
Water Surfaces	3 - 10	Geiger (1965)
Tundra Surfaces:		
1. Shrub	16 - 17	Haag and Bliss (1974)
2. Wet sedge	18 - 25	Haag and Bliss (1974)
3. Winter road	7 - 11	Haag and Bliss (1974)
4. Burn	10	Haag and Bliss (1974)
Borel Forest:		
1. Forest	14	Haag and Bliss (1974)
2. Seismic line	13	Haag and Bliss (1974)
Seeding Experiment on Winter Road:		
Control	15	Haag and Bliss (1974)
Spring after use	8	Haag and Bliss (1974)
1st growing season	11.5	Haag and Bliss (1974)
2nd growing season	13.2	Haag and Bliss (1974)
3rd growing season	14.0	Haag and Bliss (1974)

be used to warm the surface, melt snow, evaporate water or be transferred as heat to the soil below.

The sign of this term is always positive as the albedo is always less than 1. The magnitude of this term varies from 20 to 85% of the incident radiation depending on the nature of the surface and the time of year.

4.2.8 Longwave Radiation Emitted by the Ground Surface

The earth is a source of terrestrial or longwave radiation. Since the temperature range is usually within 230 to 300^{o} K, the infrared spectral range is from 3 or 4 to 100 μ.

The earth's surface is assumed to be either a black body or a grey body within the spectral range quoted above. A grey body is one that emits a fixed proportion of the black body radiation in all wave lengths. Suggested values of infrared emissivity for naturally occurring materials on the earth range from 85 to 100%, with more commonly accepted values of 95 to 97% (Table 4-2).

The equation:

$$q_{LU} = \varepsilon_s \sigma T_s^4 \qquad - - - [4.17]$$

where ε_s = infrared emissivity,

T_s = surface temperature in ^{o}K,

adequately describes the transfer of radiant energy from the earth to the atmosphere. The magnitude of this term ranges from 320 ly/day to 920 ly/day for temperatures of 230 and 300^{o}K respectively. The sign of this component of the heat balance equation is always negative.

TABLE 4-2

INFRARED EMISSIVITIES

(Percent)

A. WATER AND SOIL SURFACES

Water	92-96
Snow, fresh fallen	82-99.5
Snow, ice granules	89
Ice	96
Soil, frozen	93-94
Sand, dry playa	84
Sand, dry light	89-90
Sand, wet	95
Gravel, coarse	91-92
Limestone, light gray	92-92
Concrete, dry	71-88
Ground, moist, bare	95-98
Ground, dry plowed	90

B. NATURAL SURFACES

Desert	90-91
Grass, high dry	90
Fields and shrubs	90
Oak woodland	90
Pine forest	90

C. VEGETATION

Alfalfa, dark green	95
Oak leaves	91-95
Leaves and plants	
0.8μ	5-53
1.0μ	5-60
2.4μ	70-97
10.0μ	97-98

D. MISCELLANEOUS

Paper, white	89-95
Glass pane	87-94
Bricks, red	92
Plaster, white	91
Wood, planed oak	90
Paint, white	91-95
Paint, black	88-95
Paint, aluminum	43-55
Aluminum foil	1-5
Iron, galvanized	13-28
Silver, highly polished	2
Skin, human	95

After Sellers, 1965

4.2.9 Longwave Radiation From the Atmosphere to the Ground

Longwave atmospheric radiation originates from gases in the air, some of which absorb and emit radiation in the far infrared range.

The amount of longwave radiation from the sky, as with short wave radiation is a function of cloud cover. Therefore, initial discussion will deal with clear sky conditions and the effect of cloud cover will be dealt with subsequently.

The temperature of the atmosphere varies within relatively narrow limits of 200 to 300^{o}K and within this range the elementary gases of the atmosphere emit no radiation whatsoever. Therefore, atmospheric longwave radiation originates from water vapour, carbon dioxide and other asymmetrical molecules present in the air (Simpson, 1929).

Carbon dioxide is present in relatively large quantities throughout the atmosphere, but it absorbs only within a very narrow band of the longwave spectrum. Water vapour is therefore the most important radiating gas in the atmosphere.

Water vapour selectively absorbs energy as longwave radiation from the ground, energy from the transport of sensible heat from the ground and energy from the latent heat of condensation of water vapour. It then re-radiates this energy back to earth as longwave radiation. It, therefore, becomes important to understand the absorption characteristics of water vapour.

For certain wave lengths of the spectrum water vapour absorbs (and therefore emits) as a black body, while at other wave lengths it absorbs only a portion, and from 8.5 to 11 μ it is completely transparent (ibid). This range of the spectrum is referred to as the "atmospheric

window (Sellers, 1965). As soon as radiation within this latter band of wave lengths leaves the earth's surface, it is effectively lost as far as the atmosphere is concerned.

The problem has then resolved itself into one of estimating the amount of radiation emitted by a column of gas with varying composition, temperature and pressure. The appropriate equation would take the form of an integral summing the downward radiation from a level z_o near the earth's surface to some level z a few thousand meters above the surface.

Elsasser (1942) has developed a method to determine the contribution of various levels of the atmosphere to the total long-wave radiation received at the earth's surface. This method is quite complex and requires upper air soundings to determine the relevant air parameters. Meyers (1966) has computerized Elsasser's technique which relieves a great deal of the tedium otherwise required in the use of the radiation charts.

The major problem associated with the computation of this term arises in the determination of the emissivity of the atmosphere at various levels. The emissivity of a column of air is a function of:

i) the density-length product (m_v) of the water vapour.

ii) the partial pressure of the water vapour (p_w).

iii) the total pressure of the atmosphere (P).

iv) the temperature of the mixture (T).

However, the emissivity varies only slightly for the range of p_w and T encountered in the atmosphere, and therefore, it may be considered to be essentially independent of these two variables. The effect of

change in total pressure is usually corrected for by increasing or decreasing m_v in the ratio of P/P_o or $\sqrt{P/P_o}$ where P_o is the reference pressure and P is the pressure at whatever level is being considered. The increase in emissivity due to the presence of carbon dioxide can also be considered (Elsasser, 1949, Kondratyev, 1956 and others).

Bliss (1961) has used these approaches and has reduced the required information to that of air temperature near the ground and dew point or relative humidity. The method requires the use of various charts and the reader is referred to the original publication for details.

Since the majority of atmospheric radiation originates within the first few hundred meters above the ground and since it is this region that shows the greatest variability of the factors controlling the amount of radiation, it is, therefore, reasonable to attempt to relate air temperature and vapour pressure near the surface to incoming longwave radiation.

Empirical equations relating longwave radiation from the sky to conditions prevailing near the surface are many and varied. However, for the most part, they take the form of:

$$q_{LD} = \sigma T_a^4 \{\text{fn (vapour pressure)}\} \quad - - - [4.18]$$

where the term in brackets is equivalent to the average emissivity of the atmosphere.

Angstrom (1916) appears to be one of the first researchers to suggest an equation of this form. A reasonably complete listing of these equations is given by Sellers (1965). Brunt (1952) has suggested the ratio:

$$q_{LD}/\sigma T_a^4 = a + b\sqrt{e} \quad - - - [4.19]$$

where a and b are constants and e is the vapour pressure in mb at the corresponding screen air temperature (T_a).

A summary of the range of values of a and b found by various researchers is given by Goss and Brooks (1954). The value of the constant a ranges from 0.34 to 0.71 and the range of b is from 0.023 to 0.110 (Sellers, 1965). Median values are a = 0.605 and b = 0.048. Thus, the equation may be written as:

$$q_{LD} = \sigma T_a^4 (0.605 + 0.048\sqrt{e}) \quad - - - [4.20]$$

and can be used to estimate the quantity of long wave radiation emitted by the atmosphere on a synoptic basis.

Typical values of atmospheric radiation from cloudless skies range from 400 to 600 ly/day (Dines and Dines, 1927) to as little as 320 ly/day in mid-winter in the arctic regions (Vowinckel and Orvig, 1964). The sign of this component of radiation in the heat balance equation is always positive.

The effect of clouds is always to increase long wave atmospheric radiation relative to clear sky conditions. Any cloud which is visually opaque is assumed to radiate as a black body at the temperature of the cloud base. The effect of clouds is to close "the atmospheric window". The absorption spectrum of liquid water is similar to that for water vapour, however, the magnitude of the absorption is much greater. Even relatively thin clouds contain more precipitable water than is required to allow them to radiate as black bodies.

Various equations are put forth to adjust the clear sky values to account for cloud effects (Sellers, 1965). Since the cloud

base is usually at a temperature less than the temperature of the air mass near the ground, the overall effect is to increase the downward radiation by only 15 to 25 per cent (ibid). Dines and Dines (1927) present results to indicate increases of from 20 to 40 per cent of clear sky values due to cloud cover.

Anderson and Baker (1967) provide a convenient and apparently accurate equation for estimating long wave radiation from the sky. It is presented here to illustrate an alternative method of allowing for cloud effect:

$$q_{LD} = \sigma T_a^4 - \{228.0 + 11.16 (\sqrt{e_s} - \sqrt{e_a})\} q_{STHA}/q_{STHC} \quad - - - [4.21]$$

where e_s = saturated vapour pressure at the surface air temperature;

e_a = actual vapour pressure at the surface air temperature;

q_{STHA} = total short wave radiation on a horizontal surface measured at the site;

q_{STHC} = calculated or measured clear sky radiation on a horizontal surface at the site.

Thus q_{STHA}/q_{STHC} is a measure of cloud cover, haze or other impurities in the air.

It would appear that a relationship involving the short wave radiation ratio is a better and much less subjective method of accounting for the effect of clouds on downward long wave radiation.

Long wave radiation from the sky is not entirely isotropic. This is due primarily to the decrease in effective radiating atmospheric temperatures from the horizon to the zenith. It is, therefore, apparent that slopes or areas sheltered by a canopy of trees or similar obstruction will record larger fluxes of downward atmospheric radiation than will areas exposed directly to the zenith.

4.2.10 Net Long Wave Radiation

It has been established that the earth radiates as a grey body with an emissivity (ε_s) of less than one. Since the temperature of the lower atmosphere and earth are not remarkably different, it is valid to assume that the emittance and absorptance of the earth are equal (Kirchhoff's 3rd Law, Wiebelt, 1966). Thus

$$\varepsilon_s = 1-\alpha_L \quad - - - [4.22]$$

where $(1-\alpha_L)$ = absorptance and

α_L = infrared reflectivity or albedo.

The net long wave is, therefore, the difference between that absorbed and that which is emitted. It may be expressed as:

$$q_{LN} = \varepsilon_s q_{LD} - q_{LU} \quad - - - [4.23]$$

Brunt's (1952) empirical equation for q_{LN} is useful in illustrating the sign and magnitude of this component of the heat balance.

$$q_{LN} = \varepsilon_s \sigma \{T_a^4 (a+b\sqrt{e}) - T_s^4\} \quad - - - [4.24]$$

where ε_s = emissivity of the surface,

T_a = air temperature of the surface ^oK (usually measured at screen height),

T_s = surface temperature ^oK,

e = vapour pressure of the air at screen height in mb.

If the air temperature is considered to be approximately equal to the surface temperature, then the equation may be written as:

$$q_{LN} = \varepsilon_s \sigma T_a^4 \, (a + b\sqrt{e} - 1) \qquad - - - [4.25]$$

For average summer conditions in the middle north latitudes, the following conditions are applicable:

$\varepsilon_s = 0.95$

$a = 0.605$

$b = 0.048$

$\sigma = 0.826 \times 10^{-10}$ ly/min $^oK^4$
$(11.9 \times 10^{-8}$ ly/day $^oK^4)$

$T_a \simeq T_s = 20^oC = 293^oK$

For this air temperature and a 5^oC wet bulb depression the vapour pressure (e) = 20 mb. The term $a+b\sqrt{e}$ may be considered to be the average emissivity of the atmosphere (ε_a). Thus

$$\varepsilon_a = a+b\sqrt{e}$$
$$= 0.82$$

Hence, for average conditions

$$q_{LN} = -0.104 \text{ ly/min}$$
$$= -150 \text{ ly/day}$$

Therefore, under these average conditions there is a net loss of approximately 6 ly/hr from the earth to the atmosphere.

Although there is some diurnal and seasonal variation in net long wave radiation losses from clear skies with peaks occurring in the summer months, the average losses are usually tempered to some extent by increased vapour pressure and cloudiness.

A somewhat similar approach (but less fundamental) may be taken for evaluating the net long wave radiation balance using concepts and data provided by London (1957) and Vowinckel and Orvig (1964).

The latter authors suggest that the ratio

$q_{LDa}/q_{LU} = G_s$, where q_{LDa} = the component of atmospheric downward long wave radiation caused by absorption in the atmosphere of radiation from the ground (i.e. "the green house effect").

q_{LU} = long wave radiation from the earth's surface.

$G_a = q_{LDa}/q_{LD}$, where G_a represents the ratio of the component of atmospheric downward long wave radiation caused by absorption in the atmosphere of radiation from the ground to the total downward long wave atmospheric radiation. Combining the two equations produces:

$$G_s/G_a = q_{LD}/q_{LU} \quad - - - [4.26]$$

Substituting in equation [4.23] gives:

$$q_{LN} = -q_{LU} + \varepsilon_s \frac{G_s}{G_a} q_{LU} \quad - - - [4.27]$$

and substituting equation [4.17] results in:

$$q_{LN} = \varepsilon_s \sigma T_s^4 \left(\frac{G_s}{G_a} \varepsilon_s - 1\right) \quad - - - [4.28]$$

If $T_s \simeq T_a$ the equation reverts to [4.25]

and $\frac{G_s}{G_a} \varepsilon_s$ is equivalent to the average emissivity of the atmosphere.

Average summer and winter values of $\frac{G_s}{G_a} \varepsilon_s$ (for $\varepsilon_s = 0.95$) using London's data are 0.86 and 0.83 respectively.

If $T_s \simeq T_a = 20^oC$ as in the previous example, then,

$q_{LN} = -117$ ly/day.

This value is significantly greater than that computed from equation [4.25]. An appropriate synoptic estimate of q_{LN} probably lies somewhere between these two estimates.

Although this latter method appears suitable to evaluate net long wave radiation on a long term or general basis, it gives the inexperienced researcher in radiative heat transfer very little feeling for the fundamentals of the problem. It is for this reason that the author prefers the more basic concepts of emissivity and its variation with changes in atmospheric pressure and water vapour concentration. It is important to review the nature of the above argument. It is the concept rather than actual values of net long wave radiation that are in question. There may be cases when the latter equation provides, what appear to be, better estimates of the magnitude of this component in the heat balance equation.

The so called "green house effect" is a term used by many researchers to describe the phenomenon of water vapour and carbon dioxide absorption and emission characteristics. There is no doubt that a real greenhouse substantially modifies the heat balance in comparison to the natural surroundings. However, the reasons for this serendipitous discovery are only weakly related to long wave radiation. Kondratyev (1965) provides a detailed description and presents field data to show that the glass covering in an average greenhouse has a detrimental or negative effect on the radiation balance during the day and only a slight beneficial effect at night. The real benefit of the covering is that it effectively prevents heat loss by turbulent or convective transfer processes and also heat losses by evaporation are substantially reduced. Obviously the former process is not modified in any way by water vapour, carbon dioxide or cloud cover and

the latter process (evaporation) varies somewhat with changes in relative humidity.

It is for these reasons that the author is opposed to using misleading if not incorrect terminology to describe the fundamental physics of long wave radiation exchange between the earth and the atmosphere.

The foregoing treatment of net long wave radiation is adequate for an assessment of this component of the heat budget on a general basis. However, it is of interest to review the equations with regard to specific situations.

An interesting condition often develops over cold surfaces such as snow packs, glaciers and probably ablating head scarps of bimodal flows in permafrost during the spring and summer months, especially under cloudy conditions.

It has been shown that ε_s of such a surface is essentially equal to unity (O'Neill, 1973). It was previously stated that a cloud mass is assumed to emit black body radiation at the temperature of the cloud base. The net long wave radiation exchange for such a condition is:

$$q_{LN} = \sigma(T_c^4 - T_s^4) \qquad - - - [4.29]$$

where T_c = temperature of the cloud base in ^oK. It, therefore, becomes apparent that the net long wave radiation becomes zero or positive for cloud temperature of 0^oC or greater. This reversal in sign of heat flux has even been noted when ground temperatures are substantially above zero (Muller, 1967). These occurrences would be much more frequent when colder surface temperatures prevail (Streten and Wendler, 1968). Partial cloud cover will obviously contribute

to decreasing the loss of long wave radiation to the sky and various equations have been cited in an attempt to evaluate this effect (Sellers, 1965).

The foregoing treatment illustrates that applying synoptic estimates of net long wave fluxes to specific situations may often cause substantial errors in the estimation of these values. Net long wave radiation fluxes for conditions previously described are likely to be in the order of minus 40 ly/day to plus 6 ly/day (Streten and Wendler, 1968) rather than minus 100 to 150 ly/day as computed from synoptic data.

4.3 Radiative Components on a Sloping Surface

4.3.1 General

Topographic influences on both short and long wave radiation should be considered in evaluating the microclimate of a specific site. These influences are the most significant for the direct beam short wave component.

The equation used to describe the radiation balance on sloping surfaces may be written as follows:

$$q_{NS} = q_{DSS} + q_{dSS} + q_{RSS} + q_{RS} + q_{LDS} + q_{LDR} + q_{LUR} + q_{LUS} \quad \text{- - - [4.30]}$$

where q_{NS} = net radiation balance on a sloping surface.

q_{DSS} = short wave direct beam component (+).

q_{dSS} = short wave diffuse component (+).

q_{RSS} = short wave component of radiation reflected to the surface by surrounding surfaces (+).

q_{RS} = short wave component of radiation reflected by

the slope (-).

q_{LDS} = downward long wave component of radiation falling on the slope (+).

q_{LDR} = downward long wave component reflected to the surface by surrounding surfaces (+).

q_{LUR} = upward component of long wave radiation reflected onto the slope by surrounding surfaces (+).

q_{LUS} = upward component of long wave radiation emitted by the surface (-).

4.3.2 Direct Beam Radiation (q_{DSS})

The ideal method for evaluating the direct beam component of short wave radiation from clear skys on to a sloping surface oriented in any direction appears to have been first formulated by Ohmura (1968) and Garnier and Ohmura (1968). It consists of taking the dot or scalar product of two unit vectors, one parallel to the sun's rays and the other normal to the slope. The result is then combined with the flux density of radiation normal to the sun's ray.

The foregoing may be summarized as follows:

$$q_{DSS} = J_o a^m \, (|\overline{Su}'| \; |\overline{SL}| \cos \Lambda) \qquad - - - [4.31]$$

where q_{DSS} = flux density of direct beam radiation on the slope.

$\overline{SL}$ = unit vector normal to the slope.

$\overline{Su}'$ = unit vector parallel to the sun's rays.

Λ = angle formed between the two vectors.

The remaining terms have been previously defined.

The amount of direct beam radiation upon a slope over a finite period of time equals:

$$Q_{DSS} = J_o \int_{H_1}^{H_2} a^m \, (|\bar{S}u'| \; | \; \bar{S}L| \cos \Lambda) \, dH \quad - - - [4.32]$$

where H = hour angle measured from solar noon.

The equation is evaluated by expressing the unit vectors in terms of their direction cosines. The equation is then evaluated and summed over twenty minute time intervals. The details of this procedure are provided by Ohmura (1968) and Garnier and Ohmura (1968).

The treatment, thus far, has considered conditions involving an unobstructed sky line. In many cases topographic obstructions prevent the sun's rays from falling directly upon the ground and the site remains in shadow for a major part of the day especially during period of time of low sun angles. This aspect of the problem is readily handled by comparing the altitude of the obstruction with the altitude of the sun at the appropriate azimuth during the twenty minute time interval of computation. A variety of equations will determine the azimuth of the sun in terms of the local co-ordinates, the simplest of which is:

$$\sin a = \sin H \cos \delta \csc z \quad \text{(Hosmer \& Robbins, 1958)} \quad - - - [4.33]$$

where a = azimuth of the sun (measured positively through east).

H = hour angle of the sun.

δ = angle of declination of the sun.

z = zenith angle of the sun.

The altitude and azimuth of the obstruction must be determined by physical measurements or estimates at each particular site.

Another and possibly superior alternative is to calculate

the length of the shadow cast by the obstructing object and then to check whether the site lies within that shadow.

The length of shadow cast by an object on a horizontal surface may be easily calculated from the equation:

$$L = H \tan z \sin (A-B) \quad - - - [4.34]$$

where L = length of shadow.

H = height of the obstruction.

z = zenith angle of the sun.

A and B are the azimuths of the sun and obstruction respectively.

No similar simple expression exists for the calculation of shadow length on sloping ground. An equation has been developed to compute this variable. It is contained in Appendix C.

In summary, the amount of direct beam radiation incident upon a sloping surface is a function of:

i) latitude of the site

ii) declination of the sun

iii) strike and dip of the slope

iv) orientation and height of obstruction

v) transmittance of the air

The exact declination of the sun at different times of the year may be determined from one of the common ephemerides used for celestial observations. However, for most meteorological computations it is adequate to calculate the declination of the sun by describing its variation as a function of a sine curve.

$$\delta = A_o \sin \frac{2\pi}{365} t \quad - - - [4.35]$$

where δ = declination of the sun

A_o = amplitude of the sine curve (23.5^o)

$\frac{2\pi}{365}$ = period of the function

t = time in days starting from March 21 (vernal equinox)

The orientation of the slope is given by the azimuth and zenith angle of the normal to the slope. The azimuth is measured positively from the north through east.

The obstruction is described by the height, the azimuth of the beginning and the termination, and the azimuth of a projection along the base.

The transmissivity of the atmosphere may be estimated by vapour pressure data and the direct beam radiation may be corrected for cloud cover as previously outlined. The optical air mass m is adequately described as 1/cos z for zenith angles of 80^o or less. Published values (List, 1968) must be used for zenith angles greater than 80^o.

A simple and acceptable alternative to the procedure outlined above is to relate the actual normal direct short wave radiation on the slope to the actual direct short wave radiation on a horizontal surface.

$$q_{DSHA} = q_{DSNA} \cos z$$

$$q_{DSS} = q_{DSNA} \cos \Lambda$$

$$q_{DSS} = q_{DSHA} \cos \Lambda / \cos z \quad - - - [4.36]$$

where q_{DSS} is the direct short wave radiation on the sloping surface

q_{DSHA} = actual direct beam short wave radiation on a horizontal surface

z = zenith angle of the sun

$\cos \Lambda$ = cos of the angle between the sun's rays and the unit normal to the slope.

This is a complex function of latitude, declination, slope orientation and hour angle. The equation for Λ is listed in Appendix C.

Since the value $\cos \Lambda / \cos z$ is a function of time, it becomes a matter of judgement for each problem as to what time increment is to be used to obtain an average value for this ratio. The problem was handled by evaluating $\cos \Lambda$ and $\cos z$ over 20 min. time periods and plotting these values as ordinates versus time on a daily basis. The ratio of the areas under the curves represents the average daily ratio of $\cos \Lambda / \cos z$. Sky line obstructions and shadows can be handled in the same manner.

4.3.3 Diffuse Radiation (q_{dSS})

The amount of diffuse or scattered short wave radiation from the sky incident upon a sloping surface may be estimated by relating it to the amount falling on a horizontal surface. Kondratyev (1965) has suggested that:

$$q_{dSS} = q_{dSH} \cos^2 a/2 \qquad - - - [4.37]$$

where q_{dSS} = diffuse short wave radiation on the sloping surface

q_{dSH} = diffuse short wave radiation on a horizontal surface

a = inclination of slope from the horizontal

This simple equation assumes that the diffuse component of short

wave radiation is isotropic. Such an assumption is not rigorously correct. The intensity increases with zenith distance for clear sky conditions and decreases with zenith distance for cloudy conditions (Dines and Dines, 1927). The intensity of diffuse radiation is also related to the position of the sun. It increases toward the sun and decreases away from the sun. Thus, the correct equation to describe the flux density of diffuse radiation on a sloping surface would be a function of the direction of the unit normal of the slope relative to the zenith and to the sun.

Stephenson (1965), using data from Threlkeld (1962) formulated an equation to account for the anisotropy of diffuse radiation on vertical surfaces. The empirical relationship is:

$$q_{dSV} = q_{dSH} V_f \quad - - - [4.38]$$

where $V_f = (0.55 \text{ to } 0.437 \cos \theta + 0.313 \cos^2 \theta)$ and

θ = angle formed between the rays of the sun and the unit normal to the wall.

If $102^o < \theta < 259^o$, $V_f = 0.45$; otherwise $V_f = 0.55 + 0.437 \cos \theta + 0.313 \cos^2 \theta$. For the condition of $\theta = 0$, $V_f = 1.3$ and

$$q_{dSV} = q_{dSH} (1.3) \quad - - - [4.39]$$

This expression indicates that at certain periods during the day a vertical surface whose unit normal coincides with the rays of the sun will receive a maximum of 30% more diffuse radiation than a horizontal surface. This observation may be applied to all sloping surfaces at least in a general way. Unfortunately, the equation is derived exclusively on an empirical basis and cannot be utilized

without reservation for any sloping surface.

If the geometrical considerations of short wave diffuse radiation on slopes are compared to those of long wave radiation from the sky incident upon the same slope, without concern for anisotropy, then the similarities should be evident. Kondratyev (1965) presents an equation for net long wave radiation on a sloping surface and then provides measured values in support of the equation. The data can be reasonably well described by:

$$q_{LNS} = q_{LNH} \cos^2 a/2 \quad - - - [4.40]$$

where q_{LNS} and q_{LNH} are the net long wave radiative fluxes on sloping and horizontal surfaces respectively. It follows that the short wave diffuse component may be expressed as:

$$q_{dSS} = q_{dSH} \cos^2 a/_2 \quad - - - [4.41]$$

This equation indicates that a vertical face will receive one-half the diffuse radiation of a horizontal surface.

Although this equation is not rigorously correct, its simplicity makes it attractive for use in the solution of field problems. However, care should be exercised in its use, for it unequivocally indicates that the diffuse radiation falling on a sloping surface is always less than that of a horizontal surface. Garnier and Ohmura (1969) compare values computed from equation [4.41] with those measured on north, east and south facing slopes with a shielded Eppley pyranometer. They indicate that this equation produces overestimates of 56% to underestimates of 26%. Overestimates are more frequent on north facing than on east or south facing slopes. Data for the east facing slope appears to be scattered

equally between over and under estimates, while the data computed for the south facing slope appears to predominantly underestimate the measured values. However, their measurements were restricted to a slope angle of 20^{o} and the correlation between computed and measured values were evaluated solely on that basis. In view of these results, it appears that equation [4.41] may be used to give reasonable estimates of diffuse radiation on sloping surfaces.

4.3.4 Short Wave Component Reflected to the Surface by Surrounding Surfaces (q_{RSS})

Objects or surfaces may reflect diffusely or specularly to the surface of interest. Diffuse reflection occurs from irregular or roughened surfaces and the reflected radiation will be distributed in all directions. On the other hand, specular reflection (from the direct beam) will occur from surfaces such as glass, polished metals or very still water. Real surfaces will exhibit neither purely diffuse nor purely specular reflection and most natural surfaces may be treated as diffuse reflectors (Threlkeld, 1962). Therefore, both direct beam and diffuse radiation will be reflected diffusely by these natural surfaces.

The amount of radiation reflected to a surface by another is a function of the amount of radiation incident upon the first surface and a geometric view factor which relates the size and orientation of the two surfaces. If the adjacent or reflecting surface is designated (1) and the surface receiving the reflected radiation is (2), then the amount of reflected radiation which is incident upon unit surface dA_2 is:

$$q_{RSS(2)} = \alpha_1 \, (q_{DS} + q_{dS})_{(1)} \, V_f/\pi \qquad - - - [4.42]$$

where α_1 = albedo of surface (1)

$(q_{DS} + q_{dS})$ (1) = total short wave radiation incident upon surface (1).

V_f = dimension less geometric view or configuration factor which describes the fraction of energy directly incident on one surface from another surface assumed to be reflecting or emitting energy diffusely (Wiebelt, 1966).

A completely general evaluation for V_f must involve a relationship combining the geometry of the areas and the orientation of the unit normals of the areas in one co-ordinate system. Preliminary investigations suggest that this solution is too complex to be of practical value for most engineering applications. However, useable, but restrictive solutions are available for some problems associated with heating and ventilation system design. Threlkeld (1970) provides an acceptable approach to a number of specific problems. However, care must be exercised regarding the geometry of one surface relative to the other. The choice of the co-ordinate system is dependent upon the orientation of the areas. This aspect does not create problems for situations of windows or walls facing parking lots or large court yards and where hand calculations are used for each problem. In cases of complex geometry, it appears unlikely that the form of this solution is amenable for use with computerized techniques in evaluating radiation on sloping surfaces.

Nonetheless, the procedure taken from Threlkeld (1970) is developed and included in Appendix C. It is left for the reader to decide if his particular problem can be modelled to meet the conditions imposed by this solution.

The solution may be categorized into three general cases (A, B and C) with specific situations arising in each case. For conditions described in Case A, surface dA_2 cannot "see" surface A_1 and thus no radiation is reflected from A_1 to dA_2. In Case C, the surface dA_2 is "facing" A_1. Surface dA_2 is either parallel to or forms an acute angle with surface A_1. This condition would rarely be of significance in nature and would occur only when there was an overhanging bank or canopy of trees.

Case B is the most important and probably the only significant one of the three conditions described in the general solution. If Case $B_{(2)}$ is considered for the condition of a horizontal surface in front of sloping ground, the view factor may be expressed as:

$$V_f = \pi/_2 \, (1 - \cos a) = \pi/_2 \sin^2 a/_2 \qquad - - - [4.43]$$

where a = inclination of the slope.

Then $$q_{RSS} = \alpha_1 \, (q_{DSH} + q_{dSH})_1 \sin^2 a/_2 \qquad - - - [4.44]$$

This equation is also in agreement with Kondratyev (1965).

Threlkeld (1970) performs a sample calculation to show that the reflected radiation intercepted by a vertical south facing window on June 1 at noon, positioned 6 ft. above a 50 x 100 ft. concrete parking lot, represents 26% of the total radiation incident upon the window. This is obviously of significant magnitude and the designer must therefore consider each situation on its own merit and perform at least perfunctory calculations before dismissing this component of radiation as being unimportant.

4.3.5 Short wave Component of Radiation Reflected by the Surface (q_{RS})

The short wave radiation reflected from a sloping surface will be equal to the product of the albedo of the surface and the sum of all short wave radiation incident upon it. The equation to express this value may be written as:

$$q_{RS} = \alpha(q_{DSS} + q_{dSS} + q_{RSS}) \quad - - - [4.45]$$

This equation differs from that of a horizontal surface only in the addition of the last term which represents the short wave radiation that is reflected to the slope by other surfaces.

4.3.6 Downward Longwave Component of Radiation Falling on the Slope (q_{LDS})

Long wave radiative flux from the sky is not isotropic, increasing from the zenith to the horizon. Gardeners and agriculturalists observe this phenomenon in the late stages of the growing season when early morning air temperatures hover near the freezing point. Vegetation on sloping surfaces and regions partially sheltered from the zenith by buildings, trees or canopies will often remain unharmed by otherwise killing frosts. Kondratyev (1965) proposes that the equation to describe the amount of longwave radiation falling on the slope take the form:

$$q_{LDS} = q_{LDH} \cos^2 a/_2 \quad - - - [4.46]$$

The equation suggests that the down ward longwave component decreases as the slope angle increases. This is not strictly correct because anisotropy effects will modify this relationship.

Additional equations and further details concerning anistropy may be found in Sellers (1965). This author suggests that little error will result if equation [4.46] is adopted for use in general

field conditions if it becomes necessary to independently estimate this component of radiation.

4.3.7 Downward Long Wave Component Reflected to the Surface by Surrounding Surfaces (q_{LDR})

This component of radiation will be reflected diffusely to the sloping surface from adjacent surfaces in the same manner that short wave radiation is scattered and reflected. The treatment will, therefore, be identical to that described in section 4.3.4. Equation [4.42] must be rewritten as:

$$q_{LDR(2)} = \alpha_1 (q_{LD})_1 \frac{V_f}{\pi} \quad - - - [4.46]$$

where α_1 = infrared albedo of surface 1.

$(q_{LD})_1$ = long wave radiation falling on surface 1.

The writer suggests that a rigorous treatment of view factors is unwarranted for this relatively small component of radiation. It is, therefore, suggested that equation [4.46] be modified for general use as:

$$q_{LDR} = \alpha_1 (q_{LDH}) \sin^2 a/2 \quad - - - [4.47]$$

where q_{LDH} = long wave radiation falling on a horizontal surface in front of the slope

α_1 = infrared albedo

a = angle of slope with the horizontal

4.3.8 Upward Component of Long wave Radiation Reflected onto the Slope by Surrounding Surfaces (q_{LUR})

Strictly speaking, this radiative component should also be dealt with in the same manner as reflected short wave radiation on

a slope. Again it is the author's opinion that such a rigorous treatment of this radiative component is unjustified in view of its small contribution to the radiation balance at the surface. Kondratyev (1965) suggests:

$$q_{LUR} = q_{LUH} \sin^2 a/2 \quad - - - [4.47]$$

where q_{LUH} = long wave radiation emitted by the surface in front of the slope.

a = angle of slope with horizontal.

4.3.9 Long wave Radiation Emitted by the Surface (q_{LUS})

The theory involved in the computation of this portion of radiation falling on the slope is identical to that outlined in section 4.2.8 dealing with horizontal surfaces. Equation [4.17] may be used to describe this component with slight modifications to the nomenclature.

$$q_{LUS} = \varepsilon_s \sigma T_{ss}^4 \quad - - - [4.48]$$

where T_{ss} = temperature of the sloping surface rather than that of the horizontal adjacent surfaces. The magnitude of this term may experience a substantial diurnal variation as the slope comes into direct contact with the sun during certain periods of the day.

4.3.10 Summary of Components

The following treatment will attempt to briefly summarize the radiation balance on slopes and group the terms into net short wave and net long wave categories.

i) q_{DSS} = complex expression relating the unit normal of the slope to the rays of the sun.

ii) $q_{dSS} = d_{dSH} \cos^2 a/2$

iii) $q_{RSS} = \alpha(q_{DSH} + q_{dSH}) \sin^2 a/2$

iv) $q_{RS} = -\alpha (q_{DSS} + q_{dSH} + q_{RSS})$

v) $q_{LDS} = q_{LDH} \cos^2 a/2$

vi) $q_{LDR} = \alpha_1 (q_{LDH}) \sin^2 a/2$

vii) $q_{LUR} = q_{LUH} \sin^2 a/2$

viii) $q_{LUS} = -\varepsilon_s \sigma T_{ss}^4 \simeq q_{LUH}$

Grouping expression i), ii), iii) and iv)

$$q_{NSS} = \{q_{DSS} + q_{dSH} + \alpha \sin^2 a/2 \, (q_{DSH} + q_{dSH})\}(1-\alpha) - q_{dSH} \sin^2 a/2 \quad - - - [4.49]$$

where q_{NSS} = net short wave radiation on the sloping surface.

This is a suitable form of the equation if all components are to be calculated separately. However, if calculations are based on measured total values then the equation should be recast into the following form:

$$q_{NSS} = \{q_{DSHA} \frac{\cos \Lambda}{\cos z} + q_{dSH} + \alpha \sin^2 a/2 \, (q_{STHA})\} (1-\alpha) - q_{dSH} \sin^2 a/2 \quad - - - [4.50]$$

where q_{DSHA} = actual direct beam short wave radiation on a horizontal surface.

q_{dSH} = diffuse radiation on a horizontal surface.

q_{STHA} = total short wave radiation recorded on a horizontal surface.

α, cos Λ and cos z are as previously defined.

Components v), vi), vii), and viii) may be grouped as follows:

$$q_{LNS} = q_{LDH} (\cos^2 a/2 + \alpha_1 \sin^2 a/2) + q_{LUH} \sin^2 a/2 - q_{LUH}$$

If $\alpha_1 = 1.0$,

$$q_{LNS} = (\varepsilon_s q_{LDH} - q_{LUH}) + \varepsilon_s q_{LUH} \sin^2 a/2$$

$$= q_{LNH} + \varepsilon_s q_{LUH} \sin^2 a/2 \quad - - - \quad 4.51$$

If the value of q_{LN} from equation 4.24 is substituted into equation 4.51, then

$$q_{LNS} = \varepsilon_s \sigma \{T_a^4 (a+b\sqrt{e}) - T_s^4 (1-\varepsilon_s \sin^2 a/2\} \quad - - - \quad 4.52$$

If the value of q_{LN} from equation 4.28 is substituted into equation 4.51, then

$$q_{LNS} = \varepsilon_s \sigma \{T_s^4 \frac{G_s}{G_a} \varepsilon_s - T_s^4 (1-\varepsilon_s \sin^2 a/2\} \quad - - - \quad 4.53$$

Equations 4.52 and 4.53 indicate that in general the net long wave radiation on short slopes facing a horizontal surface will change from negative to positive values at slope angles of 60 degrees or greater. This observation may not be true where slopes are warmed well above the prevailing air temperatures. Under these conditions a very strong negative component may be emitted from the surface of the soil. However, data collected at Fort Simpson, N.W.T. indicate that the net radiometers installed on sloping surfaces rarely recorded negative values of net radiation while those placed over horizontal terrain consistently monitored negative values in the early morning hours of clear days. An example of this data is included in Appen-

dix D.

4.4 Turbulent Transfer Processes

Transfer of water vapour, heat, and momentum within the atmosphere plays a significant role in maintaining the heat balance at the surface of the earth. This transfer process is generally accomplished by turbulent mixing in the atmosphere even when the air mass is very stable. However, this activity cannot extend to the ground surface and a laminar boundary layer of a few millimeters in thickness is present between the surface of the earth and the turbulent activity in the atmosphere above. If the temperature and vapour pressure gradients within this thin layer can be accurately established, then the amount of heat, vapour and momentum in motion could be computed by boundary layer theory (Sellers, 1965). Such measurements are, at worst unobtainable, and at best impractical. The alternative has, therefore, been to measure temperature and vapour pressure gradients at higher levels and to use turbulent transfer theories to estimate the flux of heat or vapour at the surface.

4.5 Evaporation and Condensation

Evaporation occurs when vapour moves from the surface to the atmosphere in response to a gradient, while condensation is simply the reverse of this process. It is, therefore, more reasonable to consider nomenclature that describes heat transfer only, in terms of the latent heat of vaporization or condensation, and to let the sign of the vapour pressure gradient determine whether the net effect is evaporation or condensation.

There are two general procedures utilizing turbulent

theory to estimate this component of the heat balance. The first of these is the eddy flux or eddy correlation technique which assumes that quantities measured at the one meter level will give reliable values of the surface fluxes. Swimbank (1955), Dyer (1961), and Frankenberger (1960) have attempted to use these approaches with varying degrees of success. The equations which describe this process are of the form

$$q_L = L_e \overline{wq} \quad \text{(Sellers, 1965)} \qquad - - - [4.54]$$

where L = latent heat of vaporization

e = density of the air

$\overline{w}$ = mean or average vertical eddy velocity

$\overline{q}$ = mean or average specific humidity

However, Sellars (1965) states, "it is very doubtful that they will ever come into general use".

The second of the turbulent transfer methods is that of aerodynamic or profile techniques. The general form of the equation is

$$q_L = \rho L k^2 \frac{(u_2 - u_1)(q_2 - q_1)}{(fn\ z_2 - fn\ z_1)^2} \quad \text{Ibid} \qquad - - - [4.55]$$

where k = von Karman's coefficient (=0.41).

u_1 and u_2 = wind velocities at levels z_1 and z_2

q_1 and q_2 = specific humidities at levels z_1 and z_2

Various functions are used to model the wind-humidity profiles. Thornthwaite and Holzman (1939) suggest that under adiabatic, fully turbulent conditions with logarithmic wind profiles, the function of z_1 and z_2 is logarithmic and the denominator in

equation [4.55] is $\ln (z_2/z_1)^2$. A variety of specific equations using a combination of empirical and theoretical techniques are available for estimating q_L. O'Neill (1973) provides an excellent review of the background and theory and lists a number of the more popular equations.

In summary, the gain or loss of heat associated with vapour transport can be described as:

$$q_L = fn(u)\ (e_a - e_s) \qquad - - - [4.56]$$

where fn(u) may be a partially empirical and partially theoretical function of the wind profile and where e_a and e_s are the vapour pressures of the air and surface respectively.

It is of interest to note the relative magnitudes of e_a and e_s and to consider their variation over typical weather conditions during the thaw season with specific boundary conditions. The vapour pressure of the surface (e_s) is the saturated vapour pressure at the prevailing surface temperature provided the surface is fully saturated. This relationship is well known and is shown in Figure 4-6. Note that the saturated vapour pressure of water at 0^oC is 6.1 mb. The partial pressure of water vapour in the air (e_a) is related to the air temperature and the amount of water vapour present in the atmosphere. This vapour pressure can be determined by various pyschrometric techniques, which include a variety of humidity sensors and wet and dry bulb temperature relationships. The term relative humidity is used to describe the ratio of the amount of water vapour in the air at a given temperature to the amount of water vapour the air is capable of holding at the same temperature. Table 4-3 shows some typical values of water vapour pressure for various air temp-

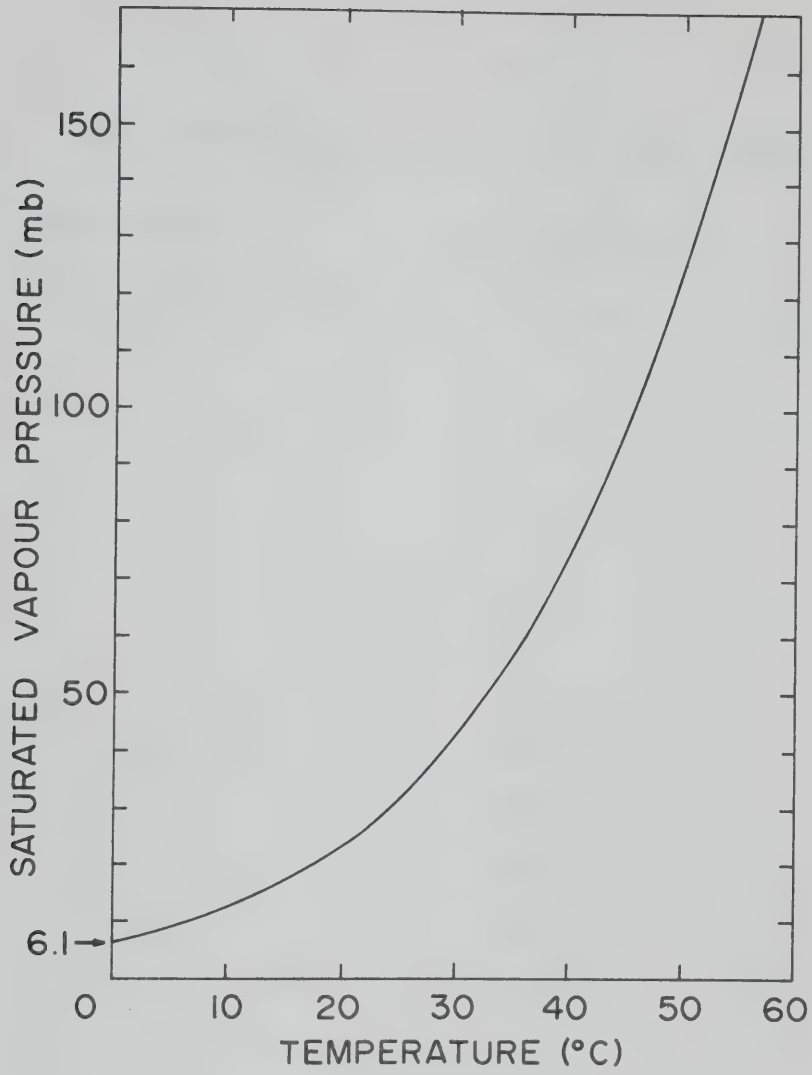

Fig. 4.6 Saturated Vapour Pressure vs Temperature

eratures and relative humidities.

In general the earth's surface is warmer than the air above it so that even with high relative humidities the vapour pressure gradient is from the surface to the air indicating the presence of evaporation. However, there are interesting observations to be made regarding cold surfaces such as glaciers, melting snow packs and exposed permafrost that exist even during the summer months. If the air temperature is $10^{o}C$ then the relative humidity must drop below 50% before the vapour

TABLE 4-3

AIR TEMPERATURE, RELATIVE HUMIDITY AND VAPOUR PRESSURE

AIR TEMPERATURE ^{o}C	RELATIVE HUMIDITY %	VAPOUR PRESSURE mb
5	70	6.1
10	80	9.8
↓	70	8.4
↓	50	6.1
20	80	18.3
↓	70	16.4
↓	60	14.2
↓	40	9.1
↓	30	7.2
↓	26	6.1

pressure gradient becomes negative and at 20°C the relative humidity must drop below 26% before evaporation will occur (Table 4-3). At relative humidities above these values, which are the rule rather than the exception, the gradient is positive and vapour is moving from the air, condensing on the surface resulting in a positive heat flux of 600 $\frac{cal}{cm^2}$ for 1 cm. of condensate.

It is important to realize that all techniques discussed above for estimating q_L are contingent upon the ability to predict, model and maintain a wind and vapour pressure profile over the terrain in question. This is often possible over snow fields, lakes and reservoirs, deserts, and other extensive and reasonably uniform surfaces. However, this is not the case where the area of interest exists as an isolated entity within a totally different environment such as a remaining snowpatch in a bare field, an oasis in a desert or an exposed face of melting permafrost contained with an otherwise warmed surface. Under these conditions, the only alternative is to physically measure the amount of vapour transferred either to or from the surface by a process called lysimetry. The procedure requires that the soil, ice or snow surface be isolated, but remain in contact with the surroundings. Measurements are made at frequent intervals to determine the loss or gain of weight resulting from evaporation or condensation respectively. Countless researchers have employed different techniques for lysimetric measurements with varying degrees of success. The greatest problem associated with this technique appears to be the difficulty associated with installing and maintaining the device without disturbing the heat balance within the lysimeter in comparison to the surrounding terrain. The reader is referred to Technical Note No. 83, WMO (1966), and Nyeburg (1965)

for details regarding various types of lysimeter design and operation.

4.6 Sensible Heat Transfer

The second major activity associated with turbulent motion in the atmosphere is the vertical flux of sensible heat. This term, in the heat balance equation, although usually small and negative, may on some occasions be as large as, and of the same sign as the net radiation (Treidl, 1970). The equations which describe this transfer process are essentially of the same form as those used to describe or predict the transport of water vapour.

The appropriate equation is

$$q_s = \rho C_p \overline{WT} \quad \text{(Sellers, 1965)} \qquad - - - [4.57]$$

where ρ = the density of the air

C_p = the specific heat of the air at constant pressure ($\simeq$ 0.24 cal/gm.^{o}C)

$\overline{T}$ = mean or average temperature

(strictly speaking this is the potential temperature, i.e. the temperature of a body of air brought adabatically to a standard pressure)

$\overline{W}$ = mean or average vertical eddy velocity

The limitations of this equation, discussed in reference to vapour transport, are also true for sensible heat transfer.

A variety of relationships exhibiting minor variations in the form of wind and height functions express the aerodynamic and profile methods for estimating the vertical flux of sensible heat. They take the general form of

$$q_s = \rho C_p k^2 \frac{fn\,(U)\,(T_2 - T_1)}{fn\,(z_2 - z_1)} \qquad - - - [4.58]$$

The reader is again referred to O'Neill (1973), Sellers (1965) or any of the classic texts dealing with climatology and micrometeorology for a complete treatment of the theory and background regarding sensible heat transfer predictions.

The simple semi-empirical approach is again useful in describing the fundamentals and the variation in magnitude and sign that may exist under specific atmospheric and terrain conditions. This relationship is quantified by the equation

$$q_s = fn(u)\ (T_a - T_s) \qquad - - - [4.59]$$

Since the surface temperature is in general somewhat greater than the air temperature, the temperature gradient is negative and the surface of the earth is cooled as heat is transferred to the atmosphere. There are, of course, many exceptions to the above statement one of which occurs at night when temperature inversions are frequent. Other more important exceptions may be noted when the surface temperatures are consistently lower than the air temperatures. These situations are again in evidence during the time of snow melt in the spring and on glaciers and exposed permafrost surfaces in the summer. Under these conditions significant amounts of sensible heat may be utilized in sustaining the melting process (Treidl, 1970; Muller and Keeler, 1969; Streten and Wendler, 1968).

It must be noted, with some emphasis, that the predictive capabilities of these formulae are predicated upon being able to model and maintain the wind and temperature profiles over reasonably uniform surfaces. When the areas of interest are isolated or appear as islands in a substantially different environment, then large amounts of sensible heat will be horizontally advected into this

zone causing an accelerated rate of melting and making prediction almost impossible.

Since the process of evaporation and diffusion of water vapour from any water surface is similar to the conduction or diffusion of specific heat from the same water surface, Bowen (1926) has suggested that it may be represented as a ratio $R = q_S/q_L$, and that

$$R = 0.46 \frac{(T_w - T_a)}{(P_w - P_a)} \frac{P}{760} \quad - - - [4.60]$$

where T_w and T_a = temperatures of the water surface and air respectively in ^oC.

P_w and P_a = vapour pressures of the water and air respectively in mm. of Hg.

P = total pressure of the atmosphere in mm. of Hg.

This equation supposedly reflects the difference in the transfer coefficients associated with the flux of sensible heat and water vapour. However, if the transfer coefficients are considered to be equal the equation takes the form

$$R = 0.501 \frac{(T_w - T_a)}{(P_w - P_a)} \frac{P}{760} \quad - - - [4.61]$$

Obviously the 8% difference in these two equations can hardly be considered significant.

If the ratio is defined simply as $R = q_S/q_L$, and when q_L can be measured and q_S calculated as the residual in the heat balance equation from ablation measurements, then the ratio may be evaluated and compared to the ratios obtained by other researchers. Table 4-4 summarizes the values of R that might be anticipated for the

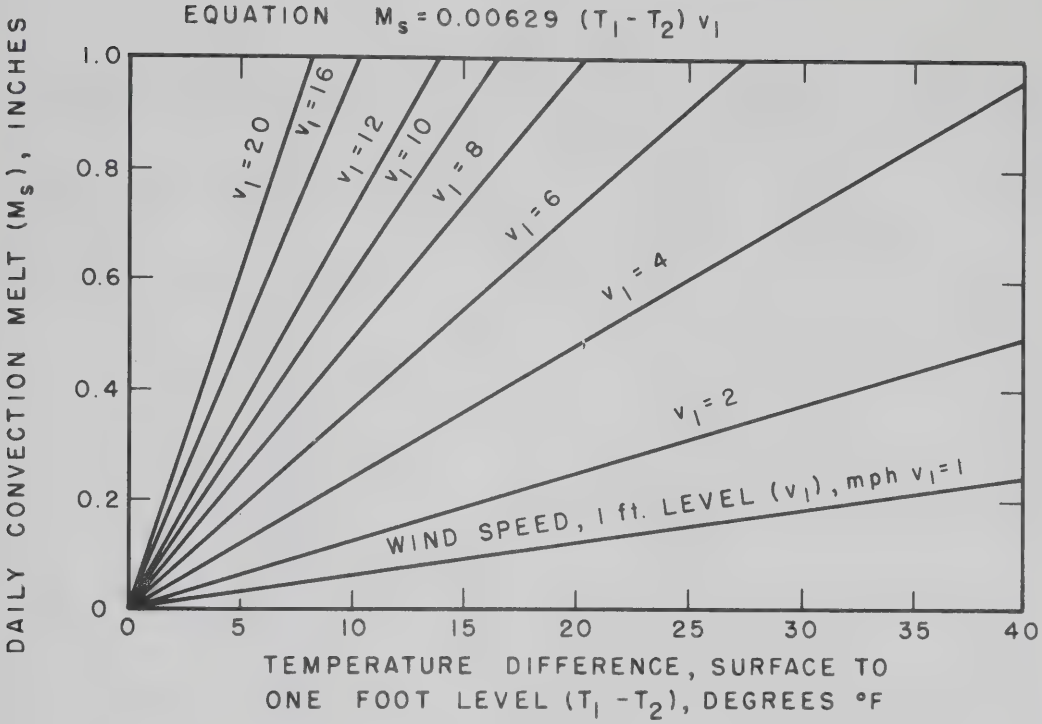

Fig. 4.7 Convection Melt (computed) (After U.S. Army Corps of Eng., 1956)

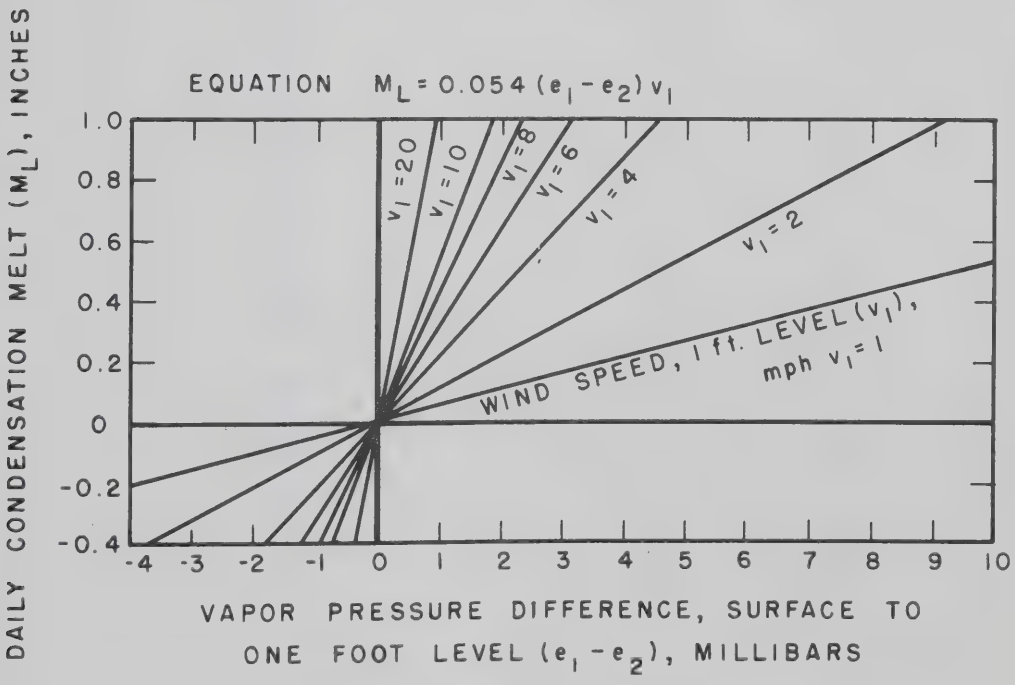

Fig. 4.8 Condensation Melt (computed) (After U.S. Army Corps of Eng., 1956)

TABLE 4-4

SNOW MELT DUE TO SENSIBLE & CONVECTIVE HEAT TRANSFER AND BOWEN'S RATIO
(AFTER U.S. ARMY CORPS OF ENG., 1956)

Temp. Diff. °C	Humidity %	M sensible in/day	M latent in/day	M sensible / M latent	R'	R
5	40	0.05	-0.08	-.63	-0.71	-1.2
	50		-0.05	-1.0	-1.13	-1.8
	60		0	0	0	-3.8
	80		+0.10	0.5	.56	+3.8
	100	0.05	.2	.25	.28	+1.2
10	40	0.11	.05	2.2	2.5	-5.1
	50		.10	1.1	1.13	-460
	60		.20	.55	.62	+4.4
	80		.31	.36	.41	1.7
	100	0.11	.43	.26	.29	1.0
15	40	0.18	.21	.86	.97	8.4
	50		.30	.60	.68	4.0
	60		.40	.45	.51	2.2
	80		.60	.30	.34	1.0
	100	0.18	.78	.23	.26	.85
20	40	0.21	.40	.53	.60	4.2
	50		.54	.39	.44	2.1
	60		.65	.32	.36	1.5
	80	0.21	.90	.23	.26	1.0

* NOTE: Values of M_S and M_L have been established from the accompanying Figures 4-6 and 4-7

equations predicting snow melt supplied by U.S. Army (1956). The snow melt due to sensible and latent heat transfer has been determined partly by theory and partly by empirical procedures (Fig. 4.7 and Fig. 4.8).

$$M_S = 0.00629\ (P/P_o)\ (Z_a/Z_b)^{-1/6}\ (T_a - T_s)\ V_b \quad - - - \quad 4.68$$

$$M_L = 0.054\ (Z_a - Z_b)^{-1/6}\ (e_a - e_s)\ V_b \quad - - - \quad 4.63$$

where M_s and M_L are the magnitudes of snow melts in inches/day due to sensible and latent heat transfer respectively; P and P_o are the actual and reference atmospheric pressures respectively; Z_a and Z_b are the heights of the sensors above the surface; V_b = the wind velocity at level b (mph); T_a and T_s are the air and surface temperatures respectively (^oF); e_a and e_s are the vapour pressures of the air and surface (mb). The magnitudes of heat fluex required to produce M_S and M_L are:

$$q_S = M_S \times 80 \times 2.54 = 203\ M_S \text{ langley/day}$$

$$q_L = M_L \times \frac{600}{8.5} \times 2.54 = 180\ M_L \text{ langley/day and}$$

$$R = q_S/q_L = 1.13\ M_S/M_L$$

It is evident that R calculated from equation 4.60 bears little if any relation to R'. It will subsequently be shown that ratios of q_S to q_L obtained from the Fort Simpson research project agree reasonably well with the ratios calculated from meteorological data.

The author, therefore, concludes that the Bowen Ratio may be a satisfactory means of estimating q_S from measured values of q_L in the general case. However, there appears to be a strong indication that it should not be applied indiscriminantly to specific cases that involve unique or unusual boundary conditions.

4.7 Energy Transfer Due to Precipitation (q_p)

Energy may be transported to or from the surface of the earth by precipitation that is cooler or warmer than the surface. If the precipitation does not change phase as it comes into contact with the surface, the equation describing the heat exchange is:

$$q_p = C_w \rho \, (T_p - T_s) \, P \qquad - - - [4.64]$$

where C_w = specific heat of water $(\frac{cal}{gm\,^oC})$;

ρ = density of water gm/cm^3;

T_p and T_s = temperature of the precipitation and surface respectively;

P = the amount of precipitation received in a given period of time.

Generally speaking the surface of the earth will be cooled by precipitation during the summer. However, many exceptions again exist when the surface temperature remains at or near 0^oC. Under these conditions the heat exchange will be positive. Since the magnitude of this term is small, its sign is of little significance. If, for example, the temperature difference is 5^oC and 10 cm. of rain fall on the surface in a 24-hour period, then only 50 langleys per day are involved in the heat balance equation. Although this is

significant on the day of occurrence, accumulated values are of little importance over the entire thaw season.

4.8 Soil Heat Transfer (q_S)

In many projects dealing with agricultural, biological or engineering studies, the soil heat flux is the term in the heat balance equation that is the major item of interest. It can rarely be calculated as the residual in the equation, with any degree of accuracy, because it represents a relatively small difference of comparatively large numbers. The magnitude of this term varies greatly depending on the type of terrain. Arctic and desert regions will exhibit substantial soil heating while more southerly vegetated regions will show considerably less. Field (1967) suggests that this term is usually not larger than ten percent of the net radiation. However, the limits may range from as little as two percent of the net radiation (Williams, 1967) to values in excess of twenty five percent (Gill, 1971).

Occasionally, attempts are made to measure this component directly by using heat flux plates buried in the soil or below a pavement (Monteith, 1958; Johnston, 1974)*. Problems arise in this procedure due to disturbance and more importantly from the difference in thermal conductivity of the plates and the soil. The equation describing heat flow in a homogeneous, isotropic medium for steady state conditions is:

$$q_G = ks \frac{\partial T}{\partial Z} \quad - - - \quad [4.65]$$

where ks = the thermal conductivity;

T = soil temperature;

Z = depth below the surface.

---

* Johnson, H personal communication

Heat flow is considered negative when it flows into the ground and away from the surface in response to a temperature decrease with depth. Difficulties are encountered when implementing this equation due to the variability of ks, which depends upon soil composition, moisture content and temperature (Chang, 1958). Soil temperature profiles in conjunction with estimates of soil heat capacity (a more stable property) may provide an adequate evaluation of this term.

4.9 Summary of Heat Balance

The terms in the heat balance equation have been defined and quantified for various surface and atmospheric conditions likely to be encountered in practice. The major positive component of the balance appears to be net radiation for most micro-meteorological studies. However, there is a strong indication that a substantial source of heat may be found in the latent heat of condensation and sensible heat transfer terms when cold surfaces and warm atmospheric conditions prevail.

CHAPTER V

HEAT FLUX MEASUREMENTS AT THE HEAD SCARP

5.1 Introduction

The fundamental terms in the heat balance equation have been discussed for both horizontal and sloping surfaces. The magnitude of these quantities described thus far refer primarily to terrain normally encountered throughout the region of interest and therefore synoptic estimates of these terms are generally applicable. In addition, situations involving specific boundary conditions (namely cold surfaces) have been discussed that exist during the summer months. The following deals with the heat balance that exists at a typical head scarp of a bimodal flow slide in the subarctic. A description of the site and equipment used for the data acquisition is also given. The data will be presented and analyzed in relation to the various terms in the heat balance equation. Computed values will be compared to those measured whenever possible.

5.2 Site Location and Description

The field work was performed at a large landslide approximately 18 miles downstream from Fort Simpson, N.W.T. on the Mackenzie River (61^{o} $50'$ N; $121^{o}21'$ W; elev. 432 ft. M.S.L.). The site is shown in Figure 5-1. McRoberts (1973) has provided a preliminary description of this landslide but more recent information introduces two noteable alterations. Measurements made in the course of this study would indicate that the average slope of the profile shown in Figure 5-2 is 13.5^{o} rather than the 19^{o} angle suggested previously. The age of white spruce trees along the head scarp was determined by counting annual rings. They were found to be in excess of 140 years old, which is older than that

Fig. 5-1 Aerial View of Fort Simpson Landslide

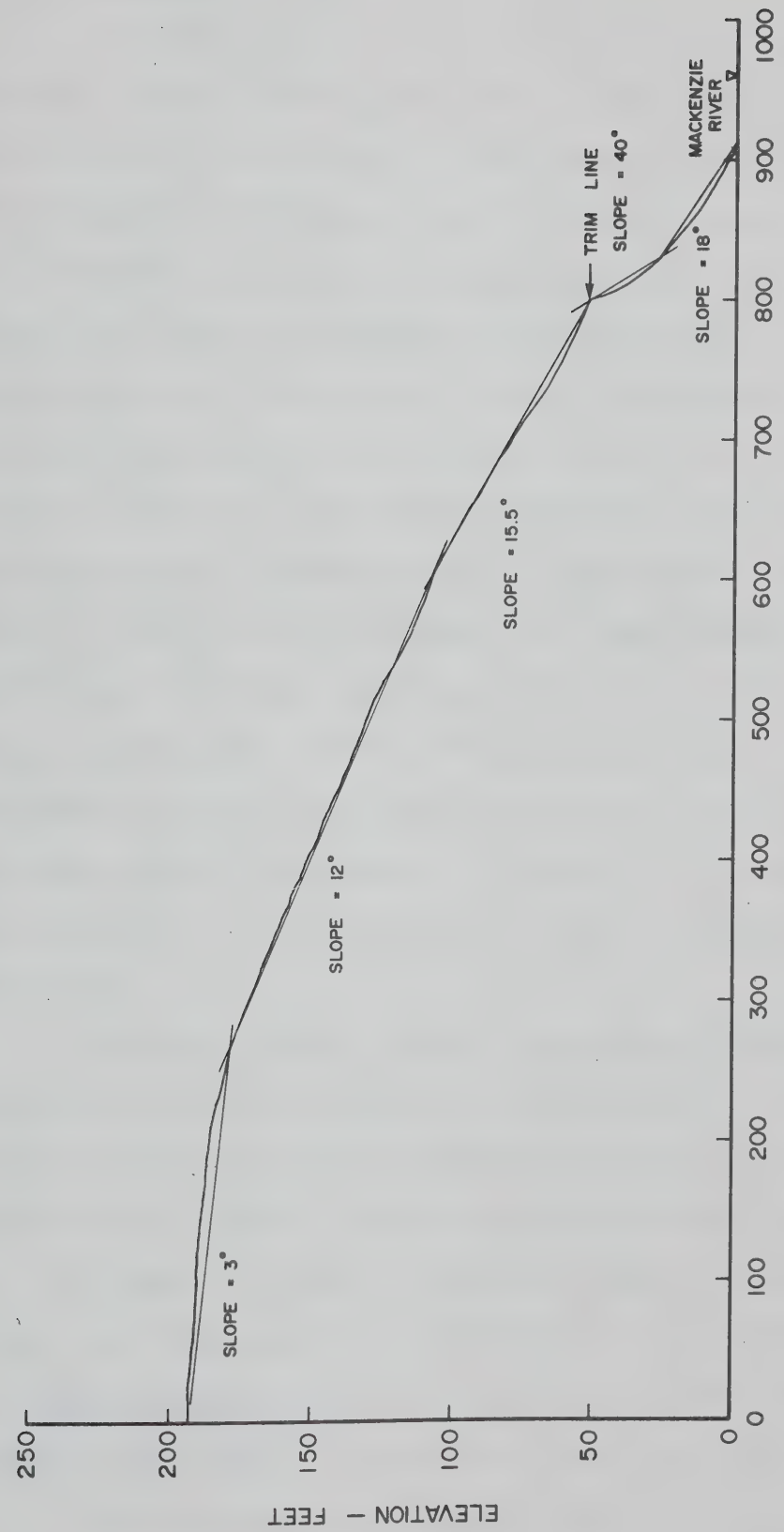

Fig. 5.2 Bank Profile of Mackenzie River Immediately East of Fort Simpson Landslide

reported by McRoberts (1973).

The rotted and charred remains of timber are evident beneath the forest litter, indicating the action of ancient forest fires. The last severe fire apparently occurred approximately 140 years ago and in all probability denuded the area of all trees and shrubs as no fire scars are evident on any of the standing vegetation. The date of the fire has been inferred by determining the age of some of the largest trees on the site. If indeed the fire was hot enough to fell the majority of the trees, then it would logically destroy the insulative quality of the moss cover and precipitate mass movements characteristic of burned over slopes in permafrost regions (Heginbottom, 1971). The action of flow slides does not appear to be consistent with the existing angle of the river bank. Mud flows within the slide area stabilize at angles considerably less than 10^{o} to the horizontal. The question then remains as to why the inferred destruction of the moss cover did not trigger massive flow slides in this region. On the other hand, if flow slides were initiated, why did they stabilize at these relatively steep angles?

The writer makes no attempt to analyse the principal causes of the slide or the different modes of failure that have occurred over the recent period of instability. McRoberts (1973) has described what appear to be the dominant processes involved within the landslide activity. The immediate concern is centered around the southeast portion of the slide. This area is retreating rapidly due to the ablation of the exposed permafrost and forming the classic features characteristic of bimodal flow slides in the Mackenzie River Valley (ibid).

It may be noted from Figures 5-3 and 5-4 that a series of these bowl shaped flow slides have developed, giving the east and

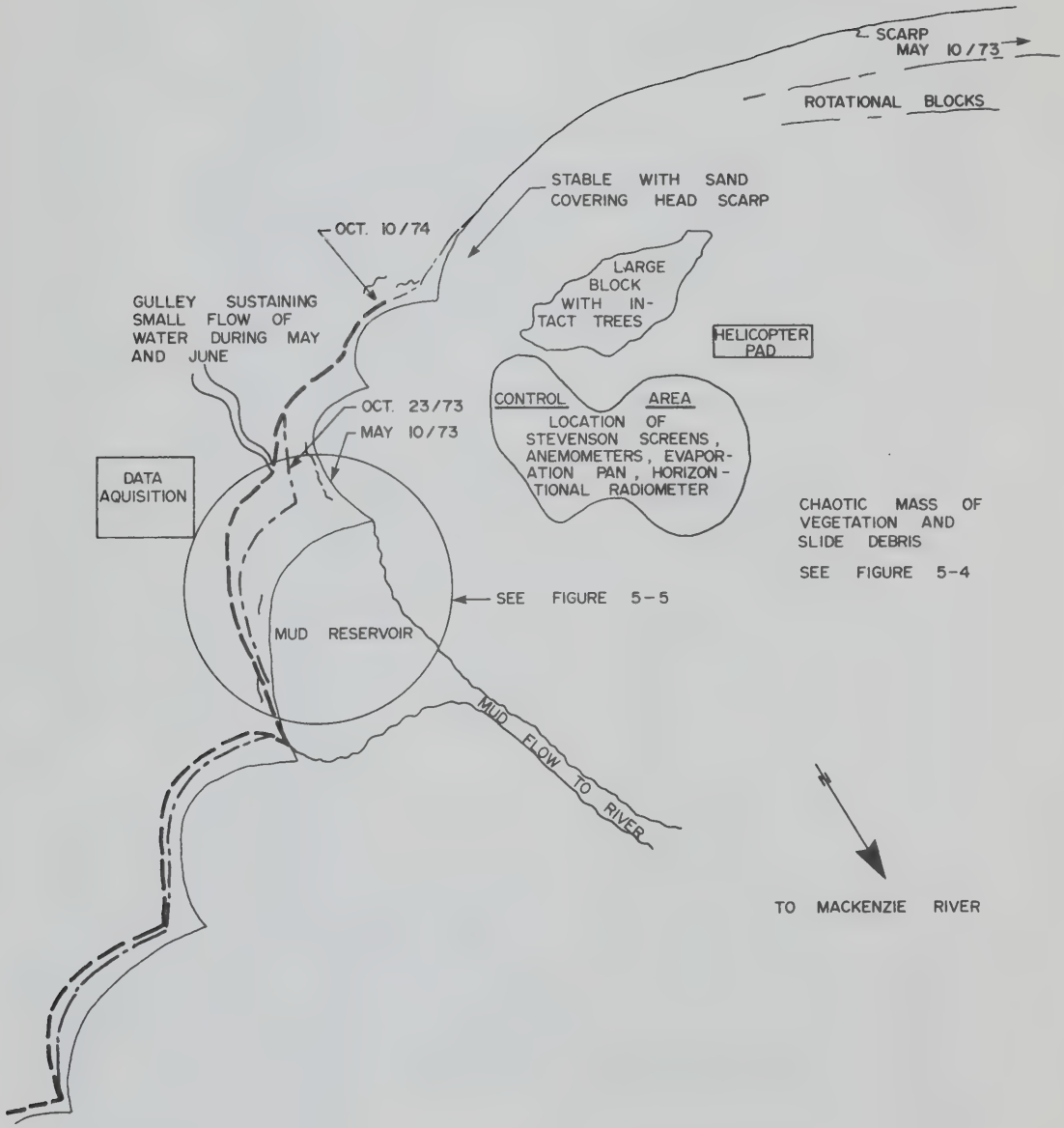

Fig. 5.3 Plan View of Fort Simpson Landslide

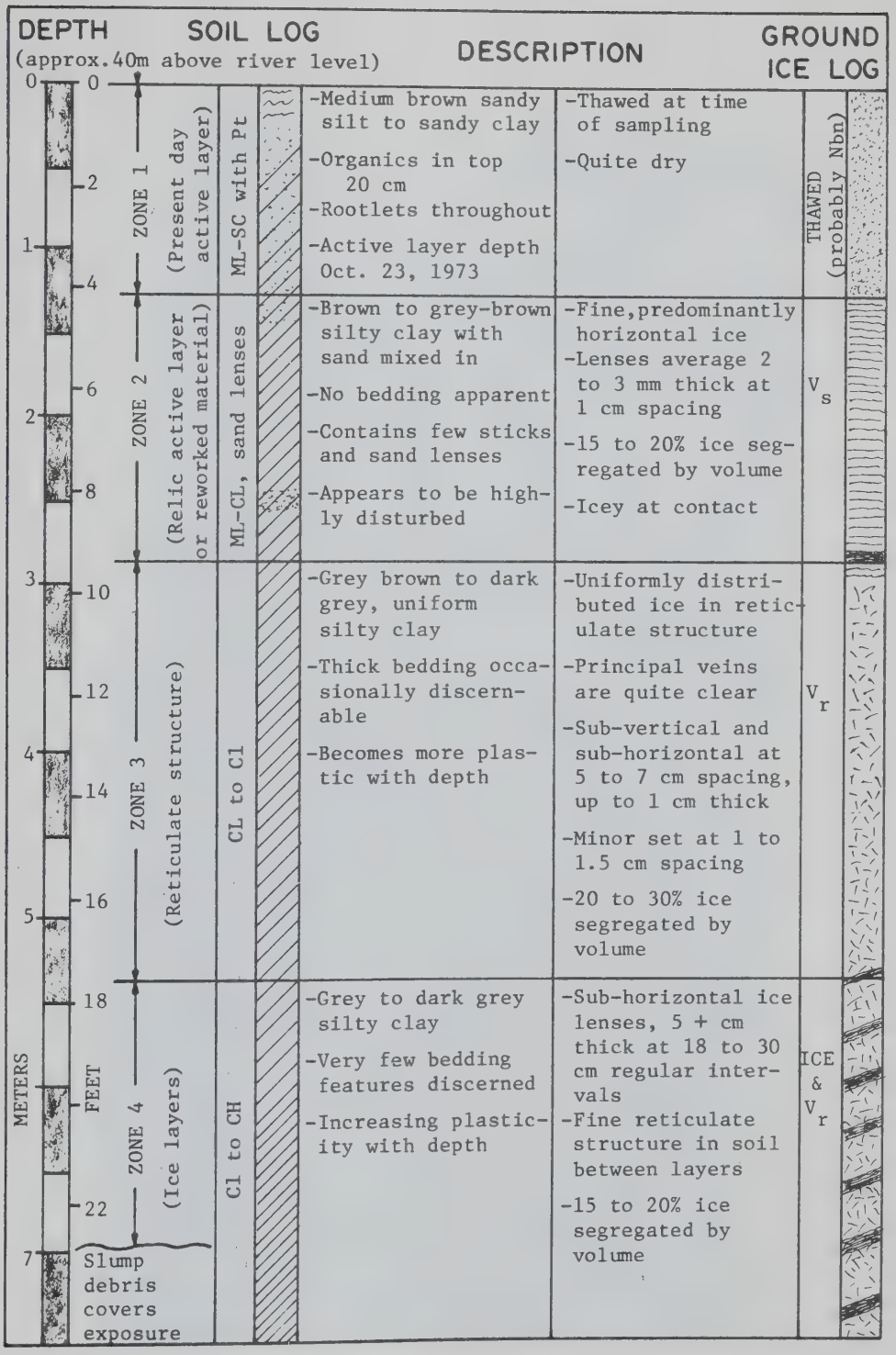

Fig. 5-3(a) Description of Sediments of Fort Simpson Landslide

After Roggensack (1975).

Fig. 5-4 Aerial View of East Flank of Fort Simpson Landslide

southeast flank of the slide a cuspate appearance. It is the area circled "A" in Figure 5-3 and enlarged in Figure 5-5 that was studied in detail in this project.

The shape of this immediate region varies substantially from time to time depending upon the soil-ice stratigraphy and the profile of the bank above the slide. During the summer of 1974 the headscarp varied from 20 to 40 feet in height and sloped at 45^{o} to near vertical. The main part of the ablating face is north facing. However, the flanks of the bowl face east and west and recession of these faces proceeds at a rate comparable to that of the north slope. Figure 5-6 provides a view of the head scarp as it existed in July, 1974. As the permafrost melts, it sloughs off the face and the debris slides down the slope on the frozen surface of the underlying soil. It appears that an exposed face of frozen soil and the pore water pressures that are generated by an advancing thaw front are required to maintain the active retreat of the headscarp. Otherwise, the debris becomes lodged on the face of the headscarp and it will not readily move downslope. A small reservoir of mud, exhibiting a consistency near to that of the liquid limit of the soil forms at the base of the headscarp. When a sufficient volume of this material has accumulated it gradually moves down slope forming a typical mud flow as described by Kerfoot (1969). Figure 5-7 illustrates the mud flow that had developed at the Fort Simpson slide in July, 1974.

The head scarp exposure reveals the presence of an upper layer of sand of varying thickness but generally increasing in thickness with distance from the river. Below this sandy layer lies a silty clay or clayey silt with intrusions of sand pockets. The thickness of the sorted materials appears to be in the order of one hundred

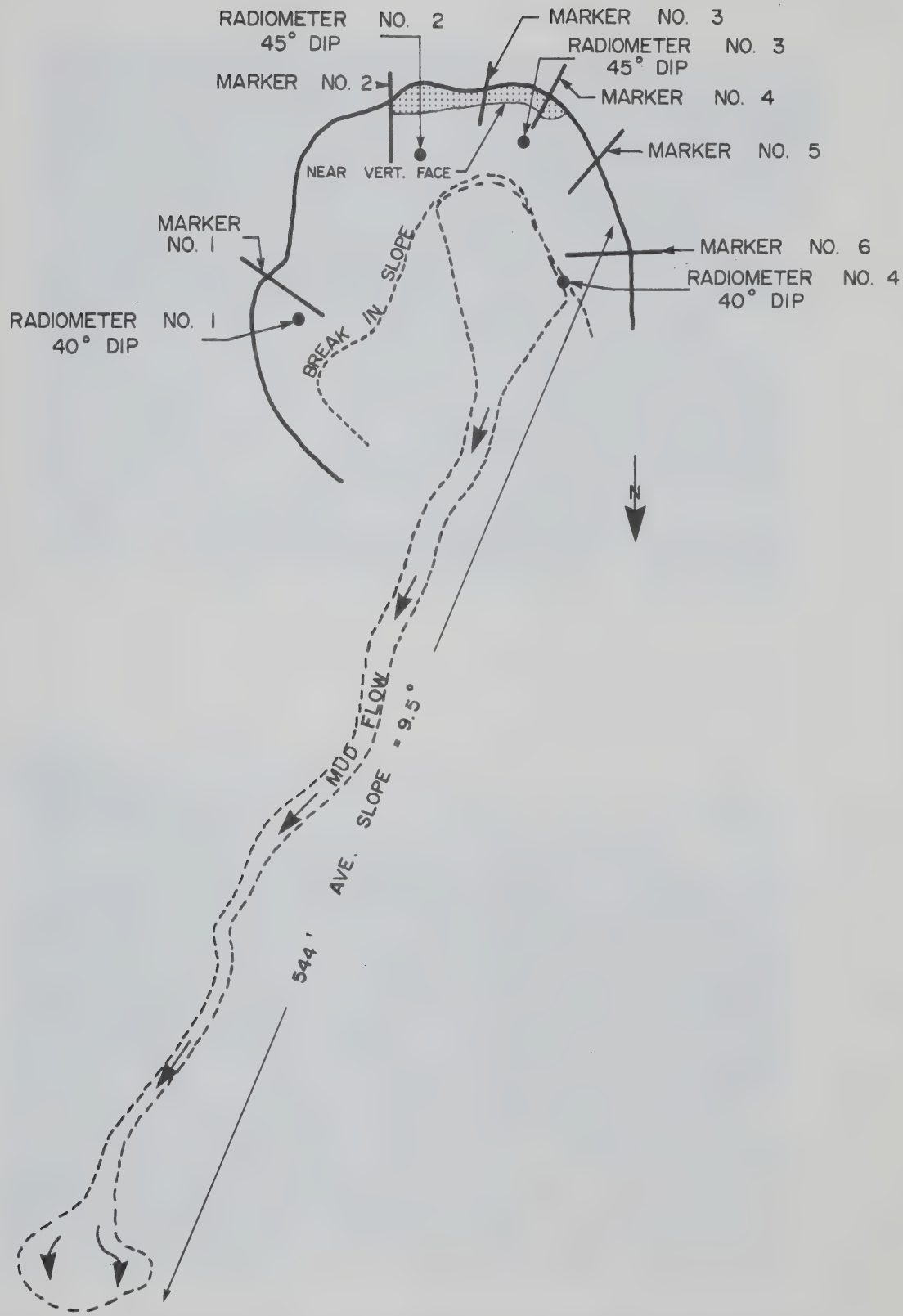

Fig. 5.5 Plan View and Instrumentation of Headscarp of Bimodal Flow at Fort Simpson Landslide

Fig. 5-6 View of Headscarp (July 1974)

Fig. 5-7 Mudflow at the Base of the Headscarp

and fifty feet at a distance one thousand feet back from the shore line. This layer of material appears to pinch out near the shore line of the river.

The upper sand layer is quite variable in thickness throughout its areal extent. It is largely absent in the area where severe ablation is presently in progress. The other areas of the slide are essentially stable because the retreating headscarps have encountered reasonably thick beds of sand. This granular material is thaw stable and as melting occurs it sloughs down over the face of the lower ice rich sediments forming a stable active layer.

The stratigraphic profile shown in Figure 5-3(a) of the head scarp may be most easily described by recognizing four reasonably distinct zones, differentiated on the basis of the amount and type of ground ice. The active layer has been designated as Zone 1 and it is approximately one metre (3 feet) in thickness, as determined from a test pit dug at the top of the head scarp in Oct. of 1973. The thawed soil consisted of clayey sand grading into sandy to silty clay with increasing depth. Zone 2 is considered to be an extended relic active layer. Generally the soil is a silty clay with rhythmically banded ice lenses of from 2 to 5 mm. in thickness. The water contents in this zone are extremely variable, depending on the location and the size of the sample. Occasional lenses of sand and local thick ice lenses are evident in this zone. Water contents as listed in Table 5-1 indicate variations of from 20 to 125%. However, the writer recommends that these high values should not be considered in determining a representative water content for this zone. Zone 3 consists of 4 to 5 meters of medium to highly plastic clay extending across the face of the head scarp. The ground ice is essentially a fine reticulate network occasionally ex-

TABLE 5-1

SUMMARY OF SOIL DATA AT FORT SIMPSON LANDSLIDE

Location	Soil Type	Liquid Limit %	Plastic Limit %	Gross Nat. Water Content %	Specific Gravity	Unit Weight kN/m^3	% Silt	% Clay	Undrained Strength kN/m^2
Zone 1 Active Layer	Clayey sand to sandy clay	-	-	20 to 40	-	-	-	-	-
Zone 2 Relic Active Layer	silty clay with pockets of sand	39 40 46 |42|	23 24 25 |24|	20 - 125 34 - 38 31 - 40 |36|	2.75	17.4-17.8 16.8-18.1 |17.5|	35-40	60-65	
Zone 3	silty clay	41 37 50 |43|	23 24 25 |24|	37 - 72 |60|	2.75	15 - 18 14 - 17 |16.4|	35-45	55-65	variable, may be up to 10 - 15
Zone 4	silty clay	40 33 41 37 |38|	22 22 24 22 |22.5|	28 - 53 |35.5|	2.75	16 - 18 |17.6|	35-45	55-65	19.0 to 48.0

posing repeating horizontal ice lenses of 5 to 10 mm. (2 to 4 in.) in thickness. The unit weight of this material ranges from 14 to 18 kN/m^3 (90 to 115 pcf) with typical water contents of 37 to 72%. This zone is occasionally very ice rich with the lenses ranging from 5 to 25 cm. (2 to 10 in.) in thickness. These lenses appear to dip sub-parallel to the face of the scarp. Bedding planes, although obscure, within the soil mass between the lenses are essentially horizontal. Undrained strength tests performed on this material were extremely variable and generally quite low. Strengths ranged from near zero to as high as 10 to 15 kN/m^2 (200 to 300 psf). Zone 4 is essentially unexposed at the head scarp and exists to an unknown depth below the upper materials. This soil (between the ice lenses) is a high density, medium to highly plastic clay. It has a total unit weight of from 16 to 18 kN/m^3 (102 to 115 pcf) with water contents ranging from 28 to 53%. Undrained strengths of this material range from 5 to 10 kN/m^2 (1000 to 2000 psf), (Roggensack, 1975)*. This layer of competent material may well play an important role in limiting the depth to which the flow slide has developed at this site. The soil is dense enough and of sufficiently low water content to render it reasonably stable when thawed. If this material does not slough and fall away during the ablation process, then it will form the base of the flow slide. The above statements are only speculation and a comprehensive drilling program would be essential to establish the location of this material relative to the base of the mud flow throughout the existing slide. Figures 5-8, 5-9 and 5-10 indicate the different zones described above.

The index properties and soil gradation are given in Table 5-1. It is interesting and of significance to note that the index properties

---

* Personal communication.

Fig. 5-8 Soil Profile Zone 1, 2 & 3 (Oct. 1973)

Fig. 5-9 Soil in Zone 3

Fig. 5-10 Frozen Core Removed From Zone 4

and grain size distribution of the soil within the zones are essentially the same. Only the amount and nature of the ground ice differentiates the visual classification and behavior of the different zones. The numbers set within the boxes are considered to be the most representative of the values recorded for any listed property.

5.3 Ablation Rates

5.3.1 Measurement Techniques

The rate at which the head scarp retreated was determined from physical measurements taken daily around its perimeter at six different stations. A technique was developed that enabled all activity associated with the measurement to be performed from the top of the escarpment. Slender timber rails were extended over the edge and secured in a horizontal position. A plumb bob was permanently fastened to each rail so that it swung freely a few cm. from the face of the soil (Figure 5-11 and 5-12). A light cord was threaded through a hollow conduit and another weight fastened to this cord. At the time of measurement, the conduit was extended along the rail to the point where the plumb bob was fastened. The weight on the cord in the conduit was lowered until it coincided with the level of the plumb bob. The cord was held securely and the conduit was moved back horizontally along the rail until the weight came into contact with the face of the soil. The end of the conduit was marked on the timber rail and thus the movement of the face was established each day at the same level. The weight was lifted an arbitrary amount and a similar measurement taken part way up the slope. All of the stations did not always provide reliable daily ablation rates. Occasionally the melted soil became lodged on the face of the slope indicating that melting was not occurring for

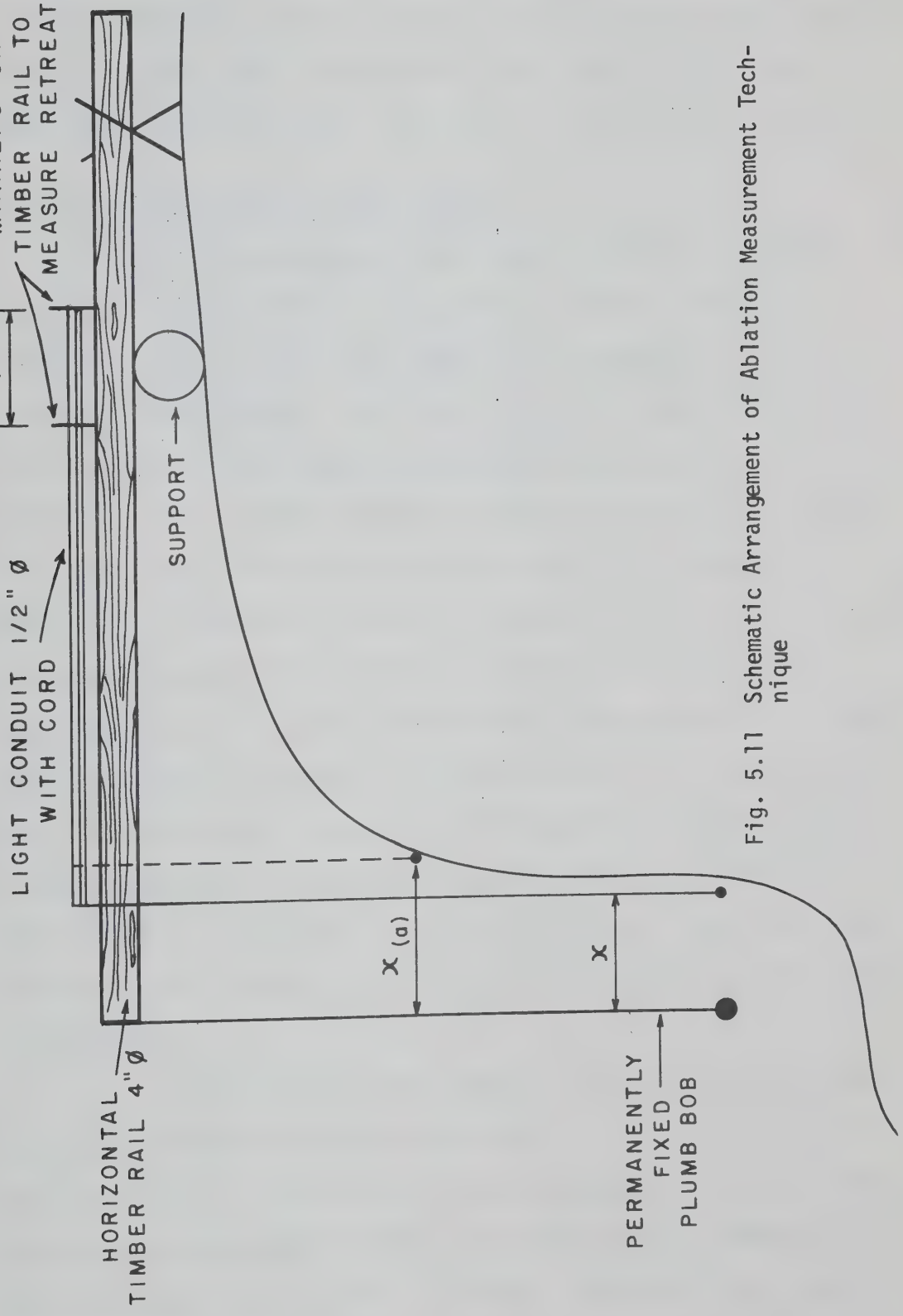

Fig. 5.11 Schematic Arrangement of Ablation Measurement Technique

a number of days. However, when the weight of the melted material became sufficiently large to overcome the shearing strength of the soil at the thaw front, the material would slough off and move down the slope exposing the frozen face to a new cycle of ablation.

5.3.2 Magnitude and Heat Requirements

Ablation measurements were taken from June 21, 1974 to July 21, 1974. The retreat ranged from a minimum of 256 cm. to a maximum of 455 cm. The larger numbers are associated with stations where the ground ice was relatively uniform and rhythmically banded. These soil conditions allowed the material to fall away from the face as quickly as it melted providing a truer indication of the ablation rate than areas that retained the melted soil. The recorded data are presented in Figures 5-13 to 5-18. Figures 5-13, 5-14, 5-16 and 5-17 indicate ablation rates at stations 1 and 1(a), 2 and 2(a), etc. The subscript "a" indicates a measurement taken approximately 1 metre above the break in the slope of the head scarp at the same station. The data presented in Figures 5-15, 5-16, and 5-17 provide the most reliable data and will therefore be used to compute the amount of heat utilized in maintaining this rate of melting. The average rate of retreat for stations 3, 4 and 5 for the time period of measurement was 14 cm/day.

A representative water content of the soil from this body of permafrost is very difficult to determine. This is largely due to the variability of the material and the presence of large ice lenses. Sampling was not attempted during the summer while the remainder of the experimental work was being conducted. Obtaining frozen cores from the face of the melting head scarp was not feasible. Frozen

Fig. 5-12 Ablation Measurement Technique

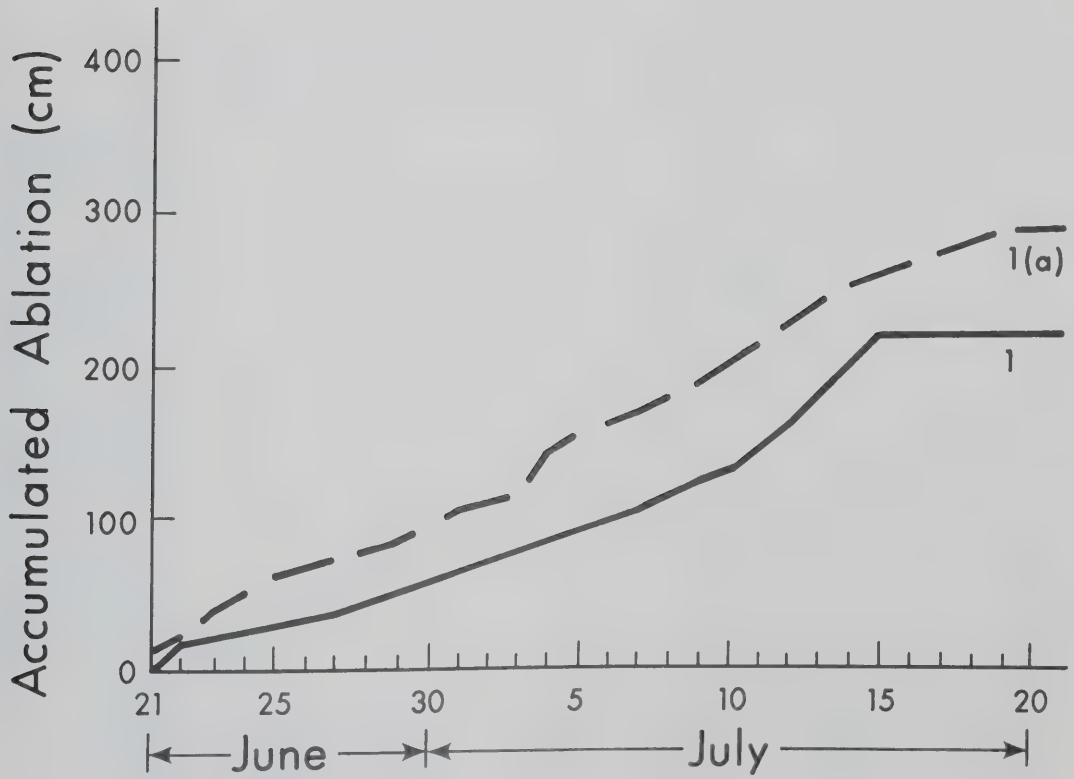

Fig. 5.13 Accumulated Ablation at Sta.1

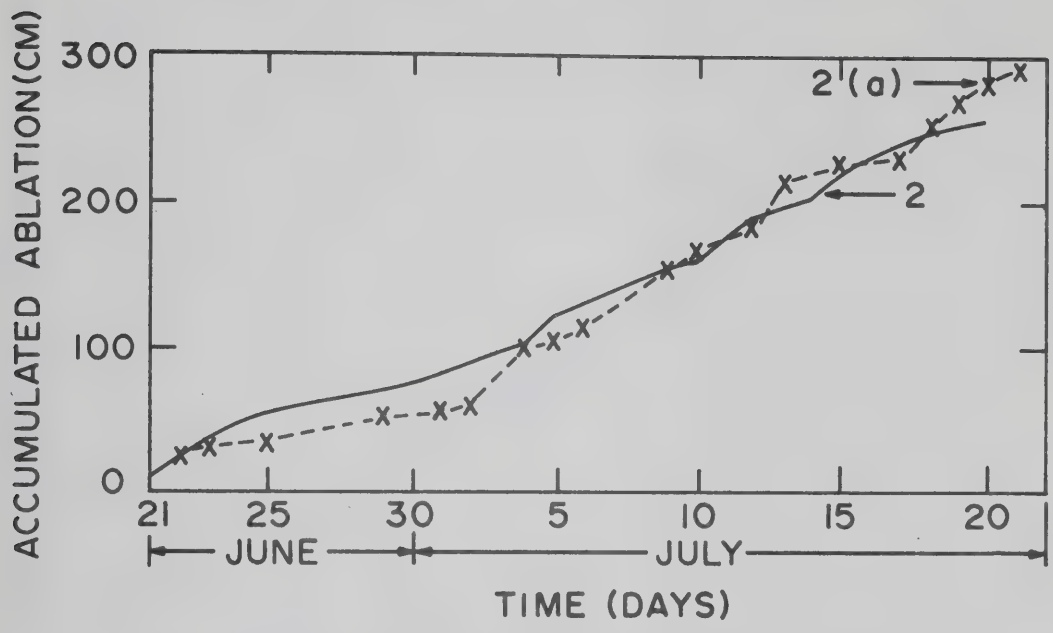

Fig. 5.14 Accumulated Ablation at Sta. 2

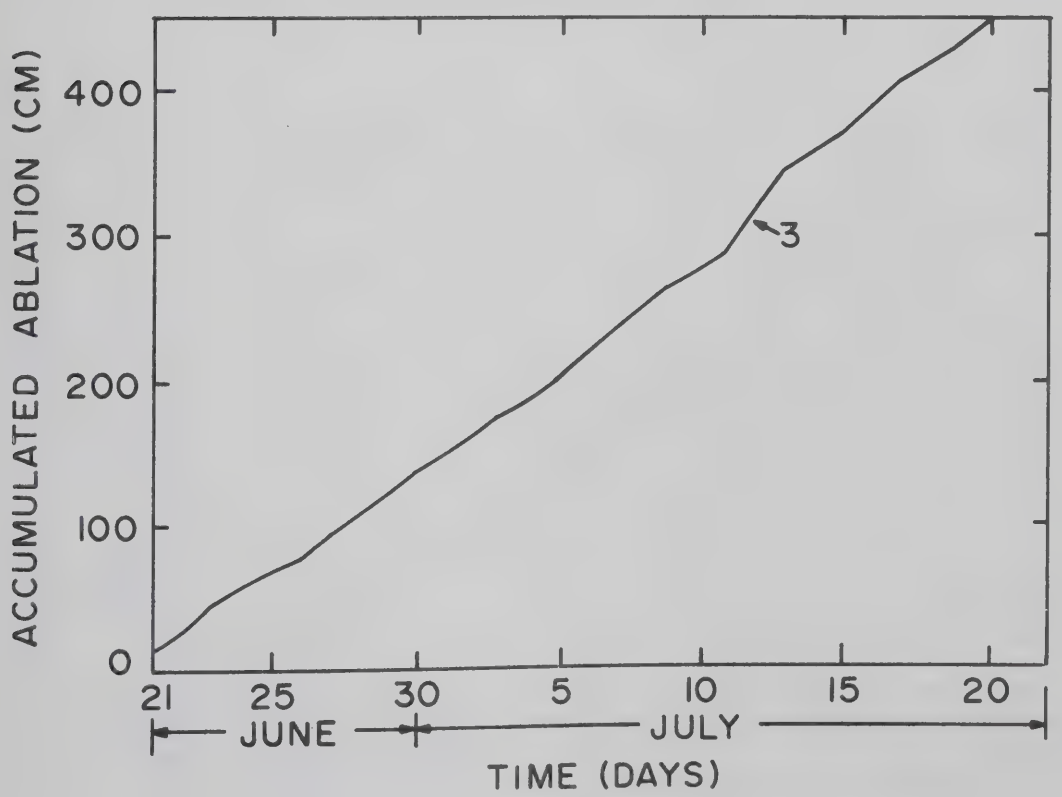

Fig. 5.15 Accumulated Ablation at Sta. 3

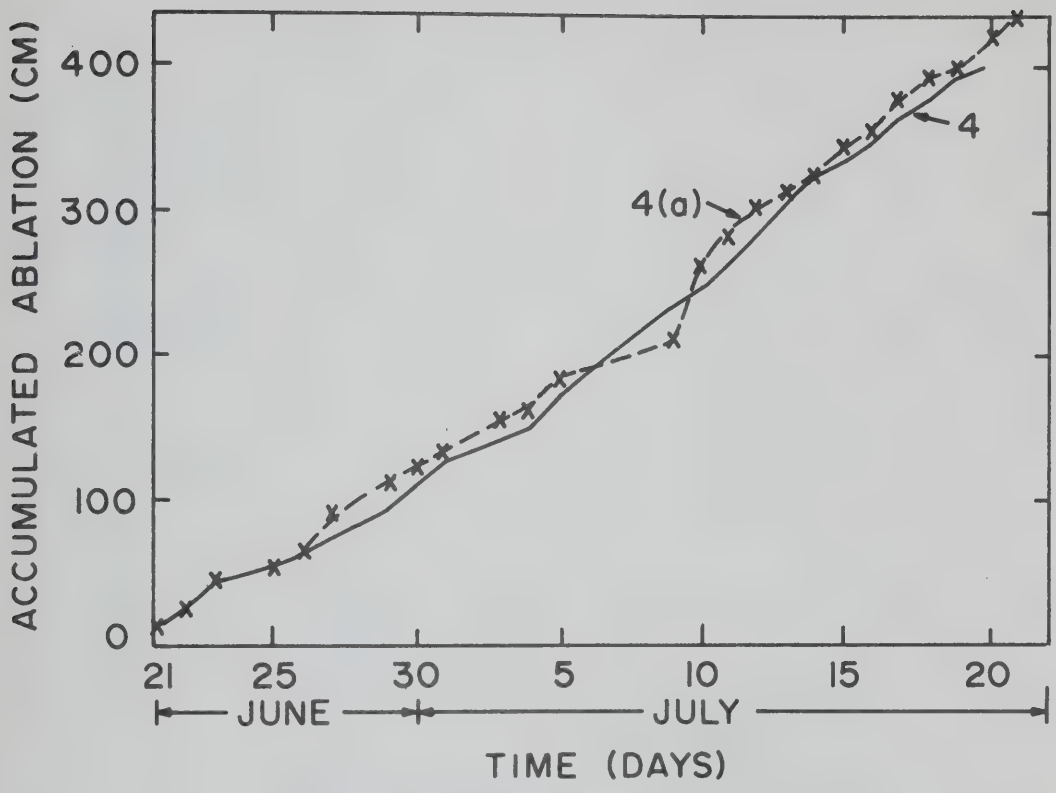

Fig. 5.16 Accumulated Ablation at Sta. 4

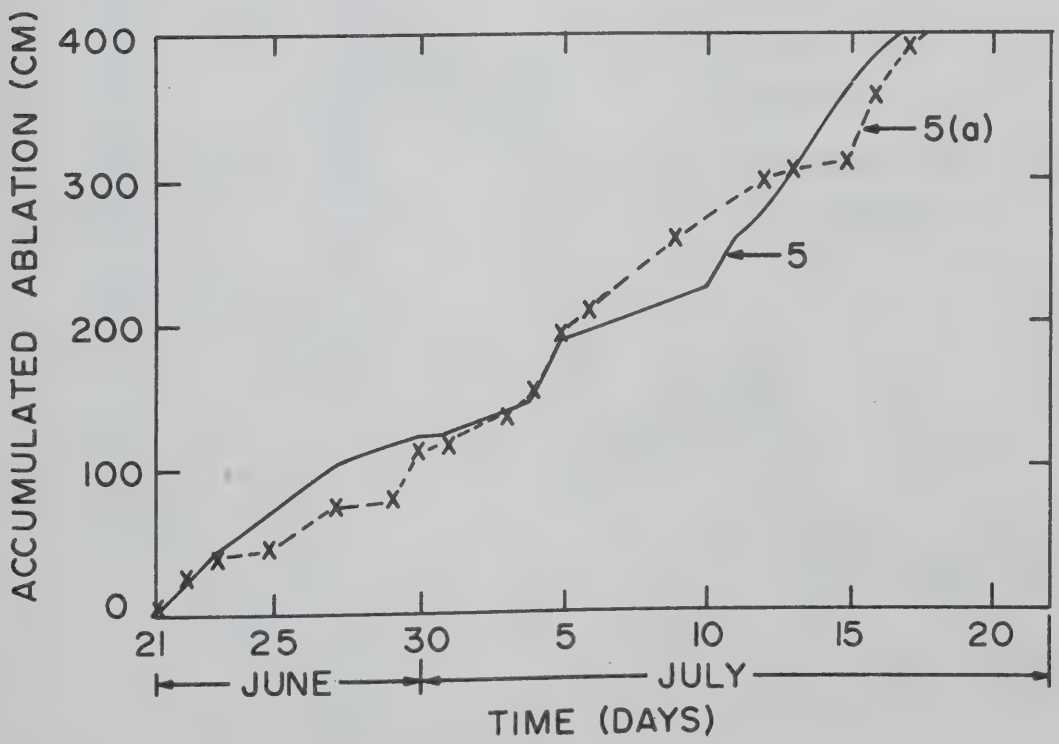

Fig. 5.17 Accumulated Ablation at Sta. 5

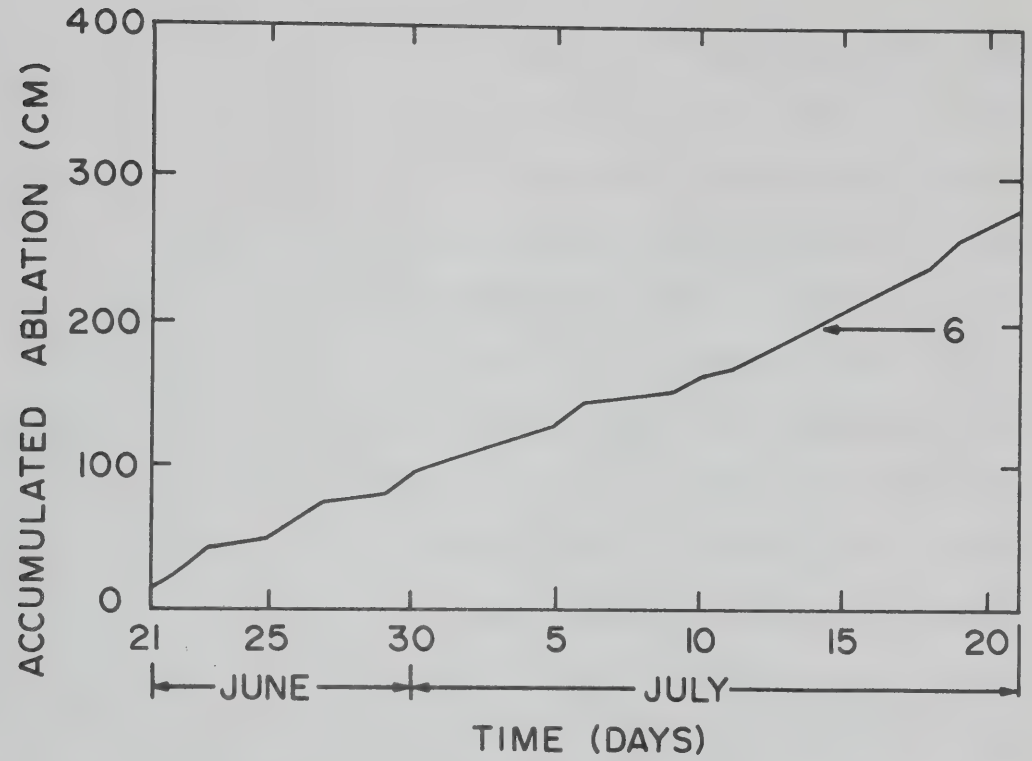

Fig. 5.18 Accumulated Ablation at Sta. 6

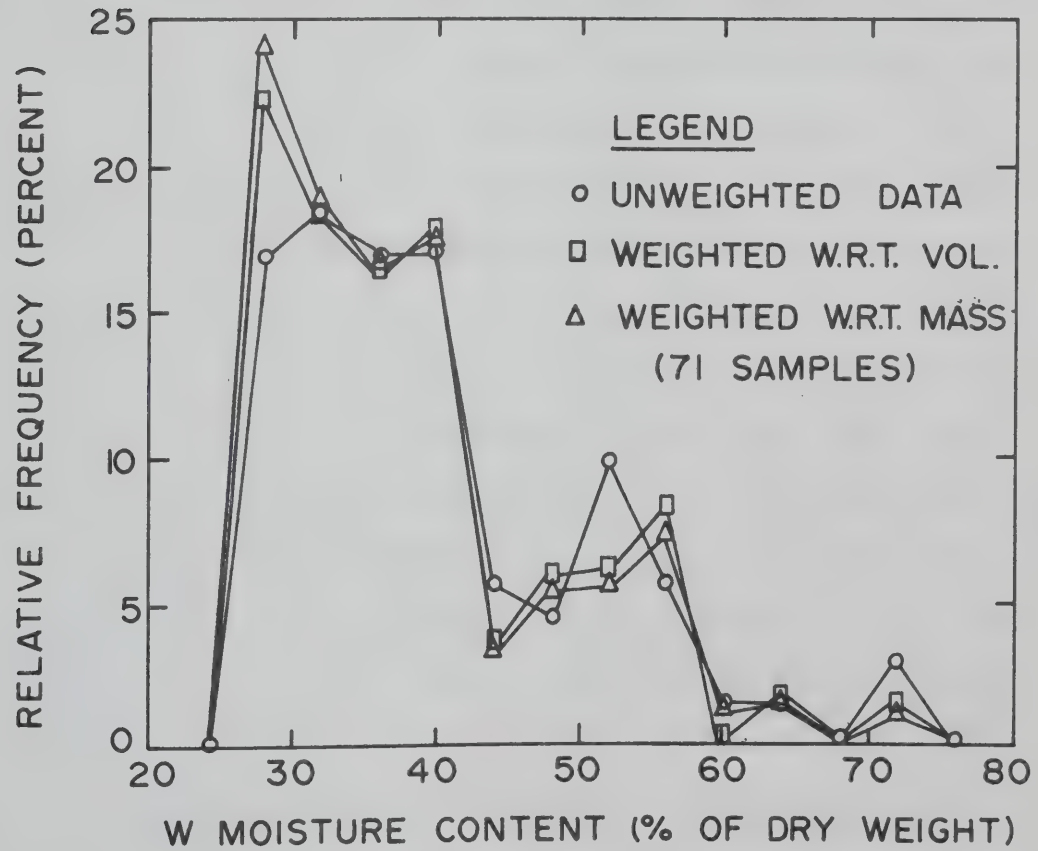

Fig. 5.19 Water Content vs. Relative Frequency Curve
(After Roggensack, 1975)

cores were taken from the face in Oct., 1973 and Oct., 1974. Figures 5-8 and 5-9 indicate the areas in which the major sampling was conducted. Approximately 10 to 15 cores were taken from each zone with the majority obtained from zones 3 and 4. Both three-inch and four-inch diameter samples were obtained that ranged in length from 10 or more cm. to 60 to 70 cm. (4 to 25 in.). A number of these water content determinations are reported in Table 5-1. One possible way of reporting the water contents is to suggest that they embrace a range of 20 to 100% by dry weight of soil. However, this produces an unrealistic range and it becomes necessary to discard the lower and higher values and work toward a more realistic range. The decision to discard the lower and higher values is acknowledged to be somewhat subjective on the part of the author. However, after spending a number of weeks on the site and after examining numerous cores and block samples extracted from the face of the headscarp it was obvious to the observers that these excessively large water contents were not indicative of the average values at the site. Roggensack (1975)* has performed a variety of tests on the material in zones 3 and 4. Part of the information from his work is shown as water content versus relative frequency curves in Figure 5-19. The curve is skewed to the left indicating a subjective bias for testing intact samples of low ice content material. He indicates a mean value of 40% with a standard deviation of approximately 10%. These data, along with that reported in Table 5-1, form the basis for narrowing the range to 30 to 50%.

The value of the volumetric heat in this material may be computed from the equation:

---

* Personal communication.

$$L = \frac{L' (w - w_u) \gamma_t}{1 + w} \qquad - - - [3.7]$$

where L' = (the volumetric latent heat of fusion of ice) = 79.6 cal/gm.

w = the gross water content of the soil.

γ_t = total unit weight of the soil.

If the material is assumed to be saturated and $G_s = 2.75$ then L has values that range from 36 to 46 cal/cm^3. The amount of heat required to sustain the rate of retreat quoted above may be computed from the equation:

$$q = V_L + VC \Delta T \quad \text{(Carslaw and Jaeger, 1947)} \qquad - - - [5.1]$$

where V = the rate of ablation in cm/day

L = the volumetric latent heat of fusion of the soil as computed from equation [5.1]

C = the volumetric heat capacity of the soil in cal/cm^3 ^oC

$\Delta T = (T_g - 0^o)$ where T_g = ground temperature. If the headscarp is considered to be isothermal at 0^o C then the equation reduces to:

$$q = VL \qquad - - - [5.2]$$

The unfrozen water content (w_u) may be neglected since the uncertainty involved in estimating the total water content is substantially greater than the unfrozen water content indicated for this soil. Substituting values of V and L computed above yields a value of q that ranges from a minimum of 504 to a maximum of 645 ly/day.

This is a substantial amount of heat and, as will be shown

subsequently, is well in excess of the amount of net radiation impinging upon the head scarp.

5.4 Radiation Balance

5.4.1 Short Wave Radiation

Total short wave radiation was monitored at Fort Simpson by the Ministry of Transport, Telecommunications Branch with a bimetallic actinograph which recorded daily totals on a horizontal surface for a period of eight years. Collection of data was discontinued on May 11, 1964. The daily mean values for June and July are 534 and 469 ly/day with standard deviations of 29 and 37 ly/day respectively. Daily totals are published in the Monthly Radiation Summary, Canadian Meteorological Branch from 1960 to 1964. The research project activities spanned the time interval from June 15 to July 20, 1974 and it is, therefore, reasonable to average the two values and consider a mean of 500 ly/day with a standard deviation of 33 ly/day.

Since only total values have been recorded it is necessary to separate the direct beam from the diffuse component. This may be accomplished by using Figures 4-3, 4-4 or 4-5. For example, K_T = 500/975 = 0.515 and the total radiation D_r = 0.37 (Fig. 4-4). These data are all the radiation information required to estimate the amount of short wave radiation impinging on the headscarp. The program listed in Appendix C is designed to compute the direct beam and diffuse short wave radiation incident on a sloping surface. The required information is K_T, D_r, the latitude of the site, the angle and orientation of the slope and the time period of interest.

Table 5-2 has been assembled by using 500 ly/day as being representative of the average daily short wave radiation incident upon a horizontal surface at the Fort Simpson site. Four different ratios of diffuse to total radiation have been chosen to cover the possible range likely to be encountered. The slope angle has been varied from 0 to 80^{o} and the orientation has assumed the four principal directions. Column 4 has been computed by evaluating the area under the curve shown in Figure 5-20 and comparing it to the area under the curve in Figure 5-21. The actual magnitudes of the ordinates in the two figures have no meaning and only serve to explain the process. These ratios have been computed on a daily basis and averaged over the period of interest again by using the computer program. Column 5 has been computed from equation 4-37 . All values have been computed without considering the possibility or effect of sky line obstructions.

5.4.2 Net Short Wave Radiation

No direct albedo measurements were attempted at the site. However, the slope may be considered to be a dark wet soil and a value of 13% has been chosen on the basis of values quoted in Table 4-1. Column 7 in Table 5-2 represents the net short wave radiation as computed from equation 4.50 .

5.4.3 Net Long Wave Radiation

The magnitude of the net long wave radiation has been computed for the control area indicated in Figure 5-3. The average ground temperature below the sensor in the control area was generally 2 - 5^{o} C cooler than the air temperature. Equation 4.24

$$q_{LN} = \varepsilon_s \sigma \{T_a^{\,4}(a+b\sqrt{e}) - T_s^{\,4}\}$$ and equation 4.28

$$q_{LN} = \varepsilon_s \sigma_s T_s^{\,4} \left(\frac{G_s}{G_a}\varepsilon_s - 1\right)$$ have been used to compute these values.

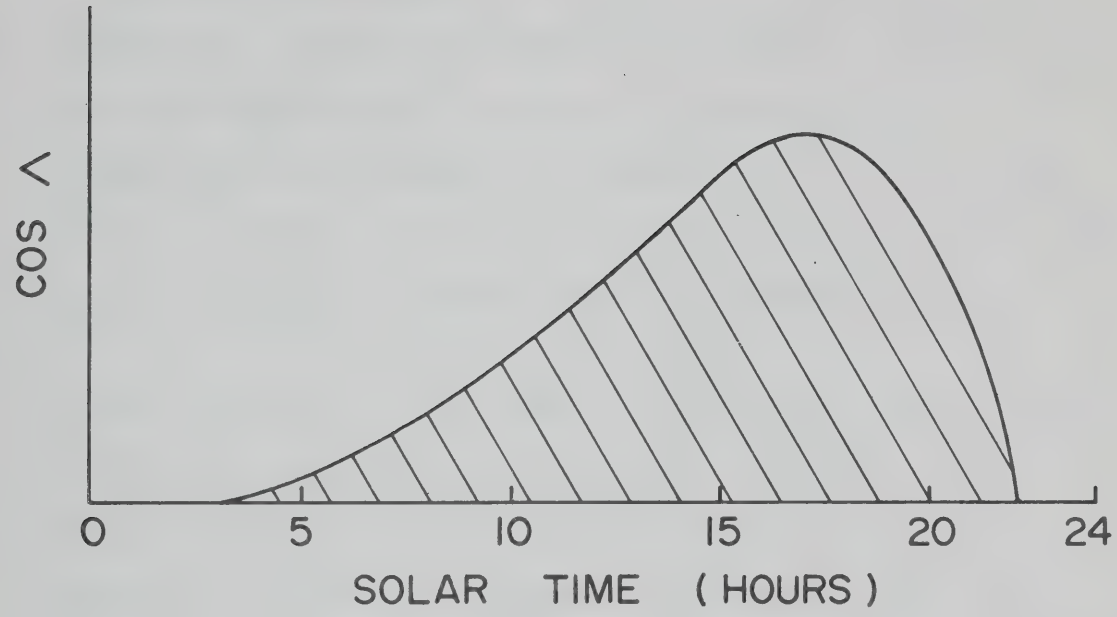

Fig. 5.20 Cos Λ vs. Time for a Sloping Surface

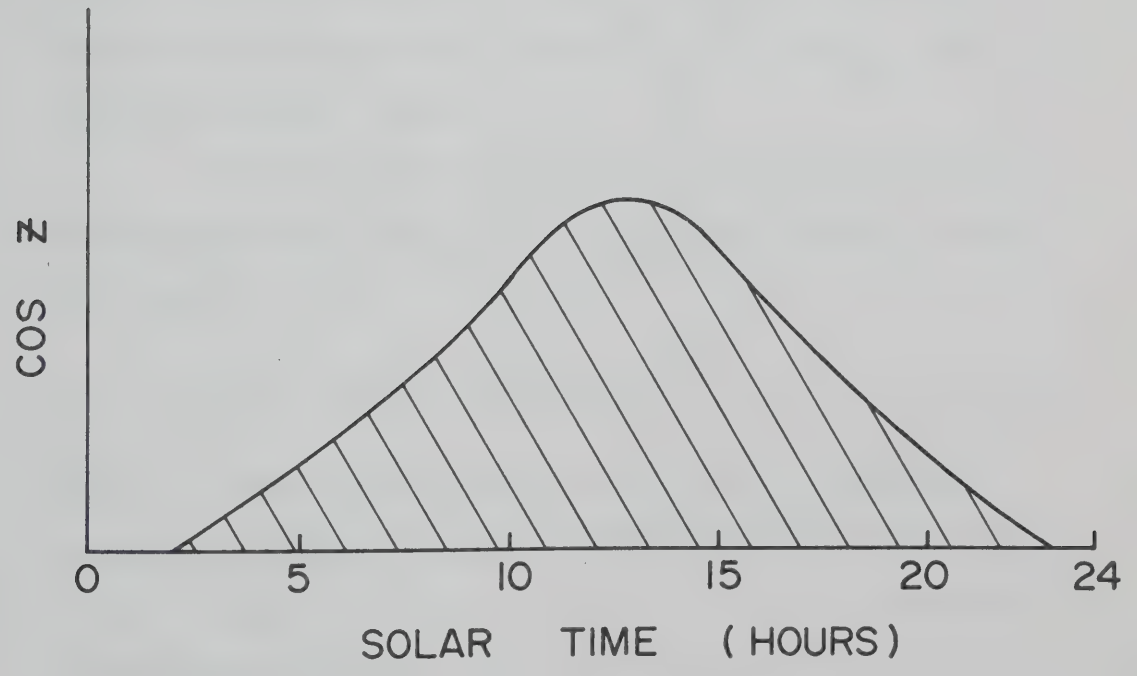

Fig. 5.21 Cos Λ vs. Time for a Horizontal Surface

The average long time air temperature and vapour pressure in Fort Simpson for the period of interest is 15°C and 14.3 mb respectively. These values represent the average of the previous 10 years of measurement (Canada Dept of Transport, 1974). The average ground surface temperature was assumed to be 12°C. If the values a = 0.605, b = 0.048 and ε_s = 0.95 are used in equation [4.24] q_{LN} = -133 ly/day. If equation 4.28 is evaluated using $\frac{G_a}{G_s}$ = 0.87 (London, 1957) and ε_s = 0.95 then q_{LN} = -126 ly/day. The difference between these two values is insignificant. The value computed from equation 4.24 will be accepted because some provision has been allowed for differing air and ground surface temperatures. This daily value of net long wave radiation represents an hourly intensity of approximately -5.5 ly/hr. The maximum negative value recorded at the test site was -6.2 ly/hr. Values of this magnitude have been measured by Wendler and Weller (1974) and are shown to be common by Muller (1967).

Net long wave radiation on sloping surfaces where air temperatures differ from surface temperatures have been computed from equation [4.52]

$$q_{LNS} = \varepsilon_s \sigma \{T_a^4 (a+b)\sqrt{e}) - T_s^4 (1 - \varepsilon_s \sin^2 a/2)\}$$

Table 5.3 summarizes the values for the same air temperature, humidity, soil emissivity, and a and b parameters as used previously. A ground surface temperature of 5°C was considered to be representive of the exposed thawing permafrost (Mackay, 1975)*.

* Personal communication

equation [4-28]

$$q_{LN} = \varepsilon_S \sigma T_a^4 \left(\frac{G_s}{G_a} \varepsilon_S - 1 \right)$$ will be used to compute these values.

The average long time air temperature and vapour pressure in Fort Simpson for the period of interest is 15^{o} C and 14.3 mb respectively. These values represent the average of the previous 10 years of measurement (Canada Dept. of Transport, 1974). If values of a = 0.605, b = 0.048 and ε_S = 0.95 are substituted into equation [4-25], q_{LN} = -174 ly/day. This value appears exceptionally low for an average net loss per day, as there are no known data to support these large negative values. It would, therefore, appear that the parameters a and b have been inappropriately chosen for the particular atmospheric and climatic conditions occurring at this location. If equation [4-28] is evaluated using G_a/G_s = 0.87 (London, 1957) and ε_S = 0.95 then q_{LN} = -135 ly/day. This daily value of net long wave radiation represents an hourly intensity of approximately -5.6 ly/hr. The maximum negative value recorded at the test site was -6.2 ly/day. This occurrence was rare and was noted only once or twice during the period of observation. Therefore, it appears that there is no justification for using average daily values in excess of -135 ly/day. Values of this magnitude have been measured by Wendler and Weller (1974) and are shown to be common by Muller (1967).

Net long wave radiation on sloping surfaces may be computed from equation [4-53]:

$$q_{LNS} = \varepsilon_S \sigma T_a^4 \left(\frac{G_s}{G_a} \varepsilon_S - 1 + \varepsilon_S \sin^2 a/2 \right)$$

Table 5-3 summarizes the values for the same air temperature, humidity

and soil emissivity as listed above.

5.4.4 Net Allwave Radiation

The net Allwave radiation that may be anticipated at the surface of the ground at the test site assuming an albedo of 13% and average air temperature and humidity conditions may be estimated by numerically adding the values of net short wave radiation from column 7 in Table 5-2 with those from column 2 in Table 5-3. The results of this addition appear in Table 5-4. An interesting observation may be made from the former table regarding the computed values of net radiation. The magnitude of the values appear to be essentially independent of the slope angle for slopes up to approximately 50 degrees. The difference in predicted magnitudes for north and east or west facing slopes is only in the order of 80 to 100 ly/day for slopes up to 50 degrees and represents a maximum difference of 25% for the former slope angle.

5.5 Radiation Field Instrumentation

Total short wave radiation was monitored at the site to ensure that unusual discrepancies from the established mean were not occurring over the period of measurement. The instrument used was a standard Eppley Black and White Pyranometer. The pyranometer was mounted according to recommended procedures supplied by the manufacturers. It was located in the region of the slide designated as the control area in Figure 5-3. Data from this sensor were recorded by the data acquisition system and will be presented subsequently.

Net radiation was monitored with five Fretschen Type R422 Net Radiometers. This model simultaneously measures incoming and

outgoing radiation and provides a mV output signal proportional to the sum of the incoming minus the sum of the outgoing radiation. The sensor consists of 2-22 junction thermopiles covered with polyethylene domes. It does not require the continuous flow of dry air across its surfaces as do many other similar models. The domes are sealed and filled with dry air and a desiccant is provided to eliminate internal condensation. The sensor is approximately 5 cm. (2 in.) in diameter and is 55 cm. (22 in.) long. Figure 5-22 provides a view of one of the radiometers used at the site.

One radiometer was mounted in the horizontal position in the control area (Figure 5-3) and placed approximately 4 ft. above a vegetation free surface. The signal from this sensor was recorded on channel 5. The location of the remaining four radiometers is shown in Figure 5-5. Each sensor was fastened to a 3 m. (10 ft.) x 1.25 cm. (1/2 in.) diameter light conduit. The conduit was lashed to a slender, wooden rail and the instrument was carefully placed over the edge of the head scarp and maintained in position 3 or 4 ft. above the surface. The plane of the sensor was placed reasonably parallel to the plane of the head scarp whenever possible. Two of these instruments (No. 2 and No. 3) were placed so that they were facing approximately north while the other two faced east and west respectively. Figure 5-23 indicates the manner in which the sensors were placed and secured around the head scarp. The signals from these four sensors were recorded on channels 1, 2, 3 and 4 of the recording system. The data obtained from these observations will be presented and discussed subsequently.

5.6 Data Acquisition System

Short wave or net radiometers are simply differential thermo-

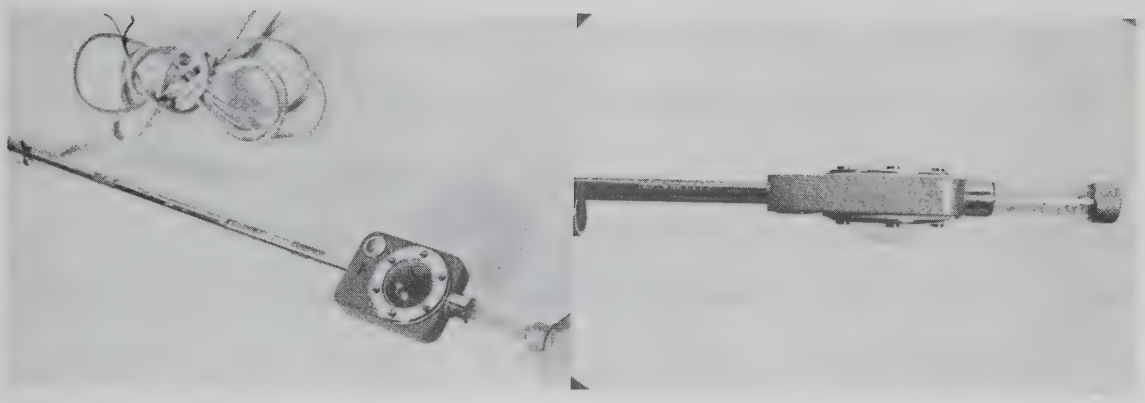

Fig. 5-22 Net Radiometer (Fritchen Model)

Fig. 5-23 Net Radiometers Around Headscarp

piles with hot and cold junctions that generate electromotive forces when exposed to sources of thermal radiation. It is, therefore, necessary to monitor and record the output signal from each sensor by some electronic means. Figure 5-24 indicates that the magnitude of the signal from a radiometer can vary dramatically over a short period of time if cloud cover happens to provide the proper conditions on a typical summer day. It was therefore considered desirable to design a system that would electronically integrate the signal from the sensor over a predetermined period of time. The millivolt signal from the radiometer was carried by a shielded cable to an instrument amplifier* that allowed a very low voltage to be increased to accommodate the requirements of the integrating totalizing circuits**. The amplified signal was then fed to this integrating circuit that changed the D.C. input signal to a square wave pulse signal. These pulses activated decade counters*** that registered the number of pulses per unit of predetermined time. This time unit was chosen to be one hour. The number of pulses which are directly proportional to the original input signal were then printed out on a simple parallel line printer****. The system was somewhat complicated in that it was required to record negative values of net radiation that may occur under clear sky night time conditions (nocturnal radiation). The integrating totalizers were "zero based"

---

* Model 260K Variable Gain Chopper Stabilized Amplifier
Analog Devices Inc.
Cambridge, Massachusetts

** Electronic Integrator-Totalizers Series 200-zero based inputs
Acromag Incorporated
Wixon, Michigan

*** Decade counters: designed and assembled by R. Gitzel,
Electronics Technician, U. of A.

**** Franklin 1200 Digital Printer Model C1220D-11-6B12-SR

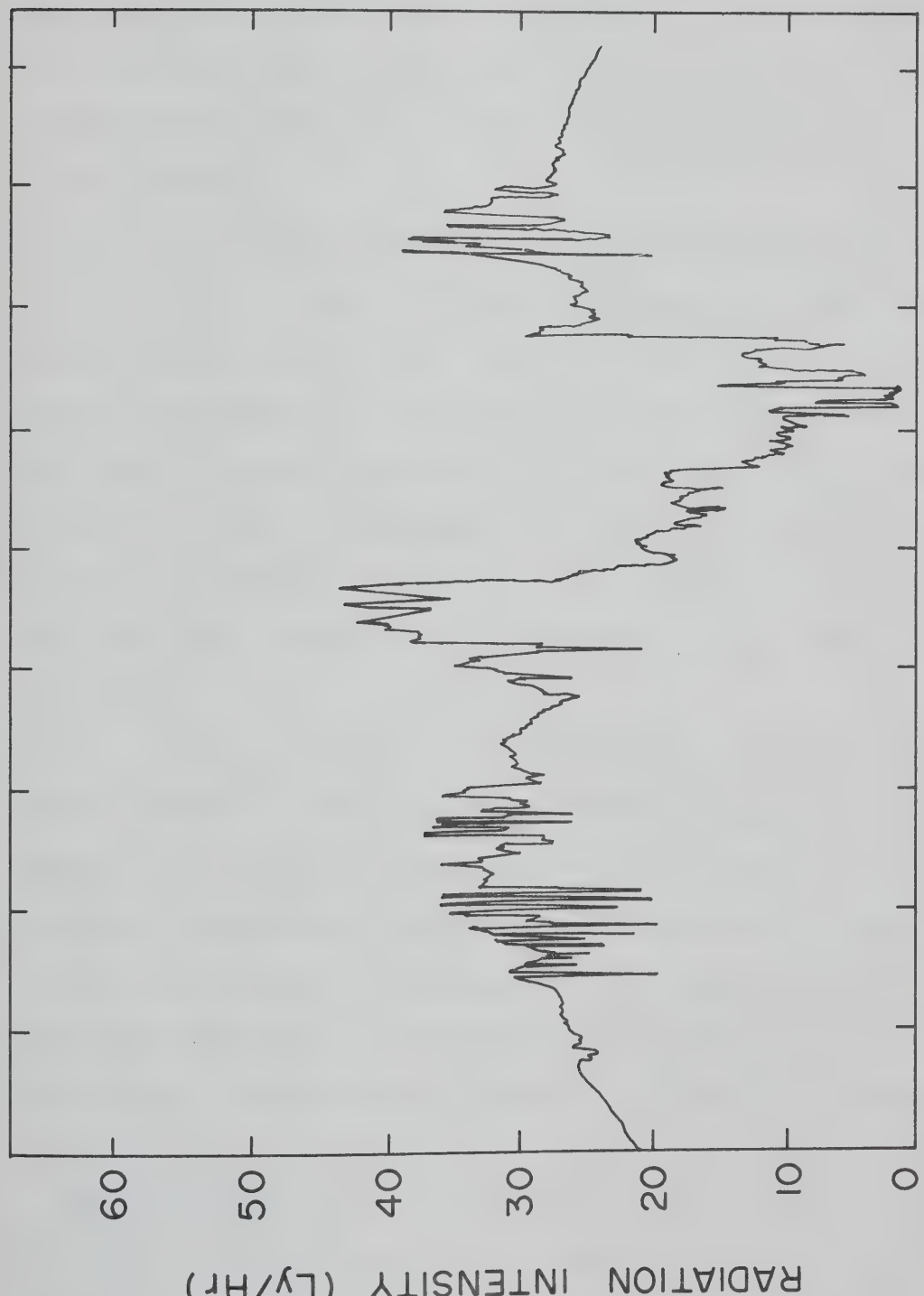

Fig. 5.24 Typical Variation of Radiation Intensity with Time

indicating that they could not accommodate a negative voltage. This problem was solved by placing a summing amplifier* between the instrument amplifier and the integrating totalizers. This feature ensured that the output from the instrument amplifiers would be offset in a positive sense so that negative values would not appear at the integrating totalizers.

The system was capable of handling six channels simultaneously. A control circuit which was activated by a digital clock controlled the counter boards. The control unit sampled each circuit on the hour every hour. The number of pulses accumulated in the previous hour were printed out along with the channel number and the time registered on the digital clock**. The counter was automatically zeroed and monitoring for the following hour continued. All circuits were read, their values printed out and the counters zeroed within six seconds.

The signal from the summing amplifier was also fed to a strip chart recorder***. This latter unit provided a continuous visual presentation of the data and assurance that the system was operating properly. In addition, it acted as a back up system for recording radiation quantities if the integrators or printer ceased to function. Power for the system was provided by 2 - 350 Honda AC 110 volt 60 cycle generators. The power was fed through a regulator**** to eliminate

---

* Operation Amplifier, Cardinal Industrial Electronics, Edmonton, Alta.

** Electronic Research Company Series 2400 Digital Clock

*** Six Channel Honeywell Strip Chart Recorder

**** Silicon Controlled Rectifier AC Regulator Model No. ACR 1000

voltage surges and stabilize the frequency. Figure 5-25 provides a schematic sketch of the radiation instrumentation employed at the site. Figure 5-26 is a pictorial view of the system housed within a nylon tent.

The data acquisition system worked remarkably well as long as the generator supplied uninterrupted power. However, power losses and complete failures were common due to malfunctioning of the generators. These failures caused interruptions in the data accumulation and in some cases precipitated a failure of the power transformer within the control unit of the acquisition system. Parts for repair and replacement units were only available in Edmonton and although only one generating unit was required to operate the system, a number of days often elapsed before power could be restored.

5.7 Measured Total Short Wave Radiation

Monitoring of radiation quantities began at the test site on June 20, 1974 and ended on July 21, 1974. Data collection was not continuous over that period of time due to power failures. A complete record was established for 15 days, partial data for 12 days and the system was completely inoperative for 5 days during the total period of monitoring. The data are presented in Figure 5-27. The solid horizontal bars indicate the days when monitoring was continuous. The dotted lines indicate values that have been determined by partial sampling and correlation with weather conditions existing when sampling was complete. When the above methods could not be used, a value of 467 ly/day was used which represented the average of daily radiation values when sampling was continuous. Table 5-5 lists the values of total radiation as recorded and extrapolated at the test site. The

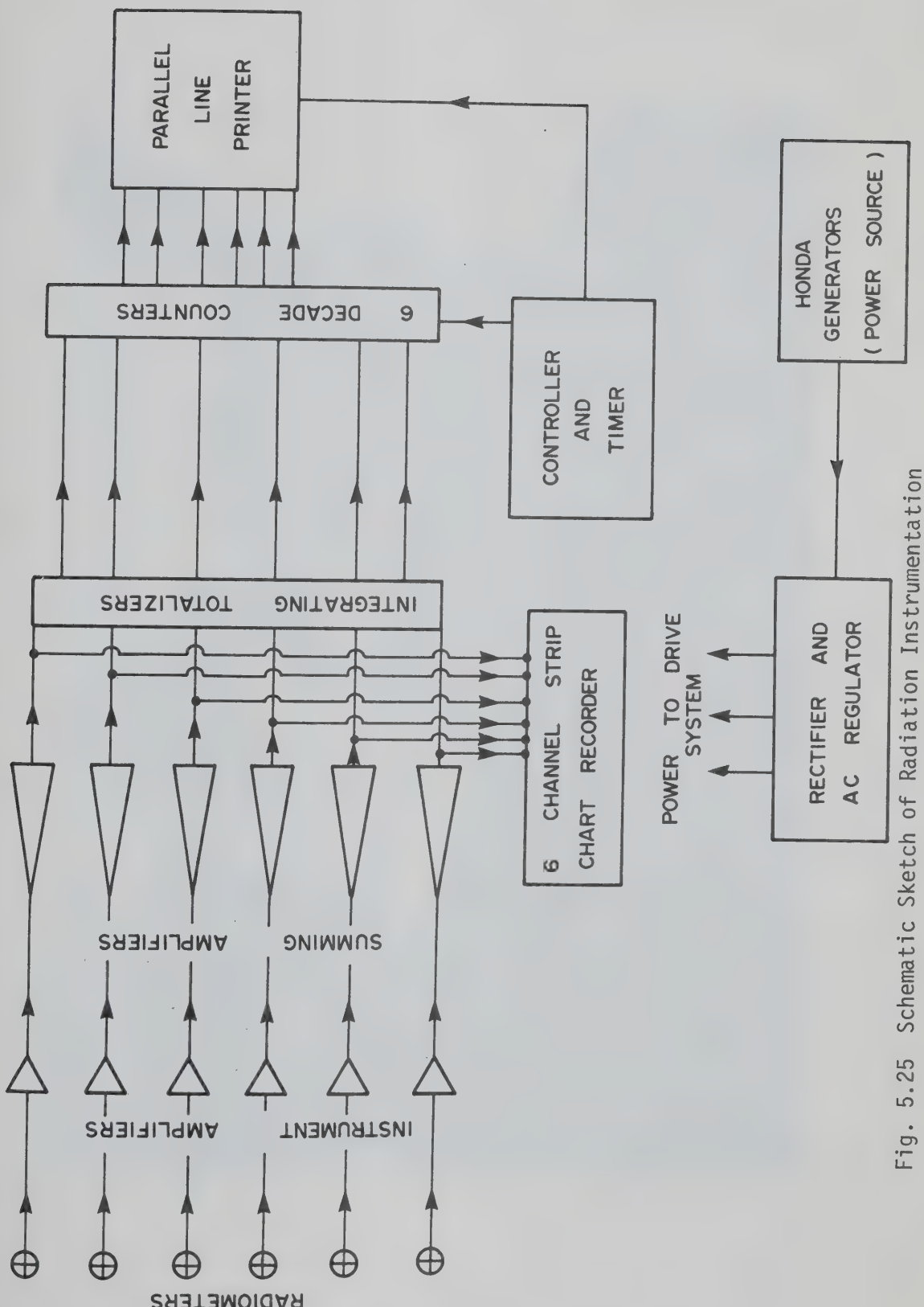

Fig. 5.25 Schematic Sketch of Radiation Instrumentation

Fig. 5-26 Data Acquisition System

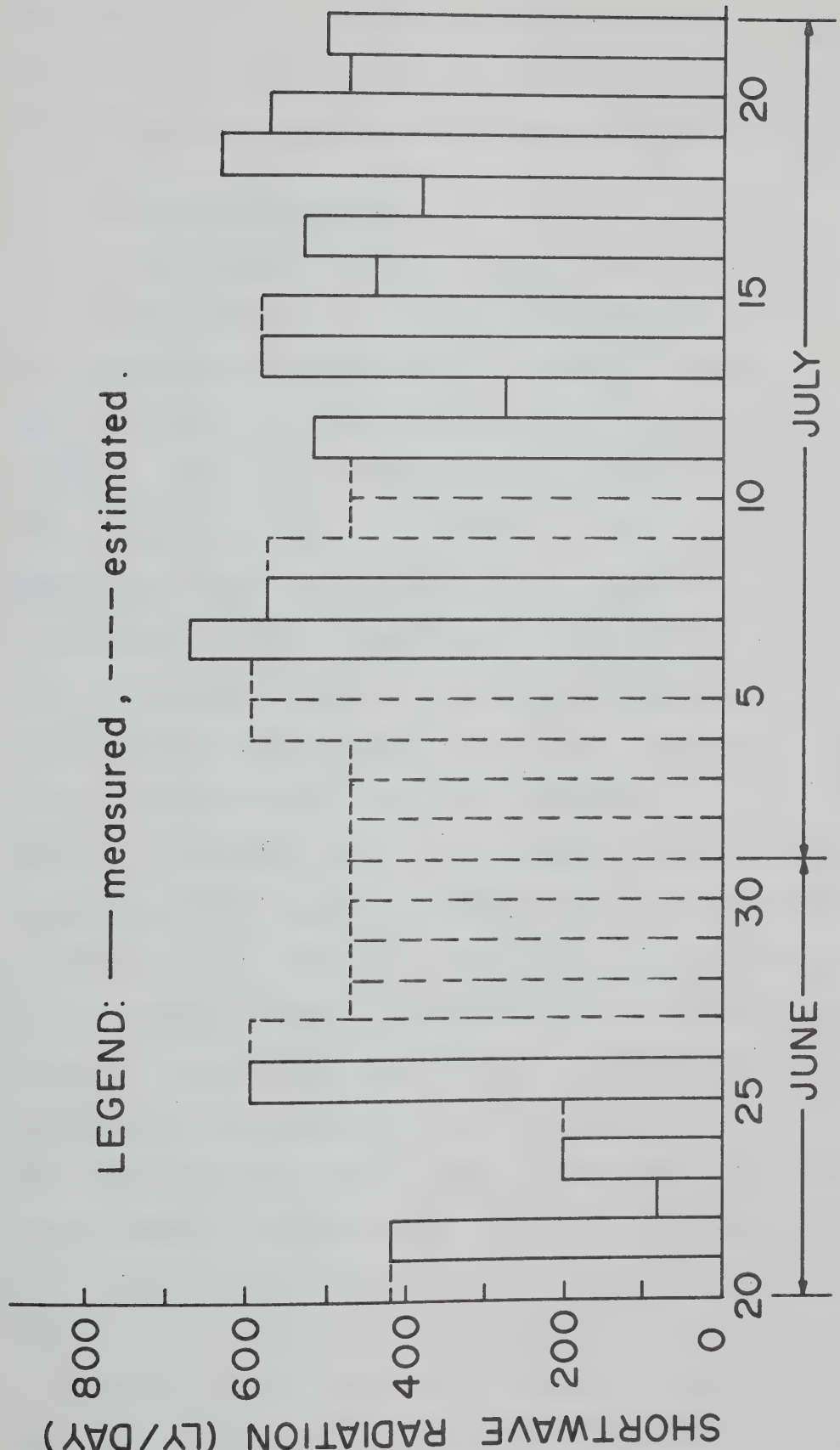

Fig. 5.27 Total Shortwave Radiation on a Horizontal Surface for the Period of Observation

new average using this procedure is 475 ly/day. This value falls within one standard deviation of the long time average for a horizontal surface at Fort Simpson and is therefore considered to be reliable.

5.8 Measured Net Radiation

The problems associated with obtaining a continuous record of net radiation were the same as previously discussed for total short wave radiation and the techniques for filling in the gaps in the record were also similar. The data are presented in Figures 5-28 to 5-32, inclusive. The convention for solid and dotted bars is the same as that presented in Figure 5-27. Table 5-6 summarizes the daily values and also provides the accumulated totals. Figure 5-33 illustrates the accumulated net radiation over the period of observation at the test site. The average accumulated totals have not been plotted in Figure 5-33 because they coincide almost directly with the values from sensors 1 and 3 and the lines become indistinguishable. Table 5-7 compares the measured values of net radiation with those computed using synoptic values of short wave radiation and also using measured values of short wave radiation. The average value of net radiation recorded by the horizontal sensor in the control area using the aforementioned methods of interpolation and extrapolation was 350 ly/day. The computed values, using synoptic estimates and measured values of short wave radiation are 302 and 280 ly/day respectively. The measured value is also greater than the synoptic net radiation estimates of 250 ly/day for this region (Burns, 1973). The latter discrepancy is not unreasonable because the average albedo of the terrain in the Mackenzie Valley is undoubtedly greater than the value assumed for the bare soil beneath the sensor in the control area. Moreover, an average surface temperature that is lower than the average air temperature will contribute

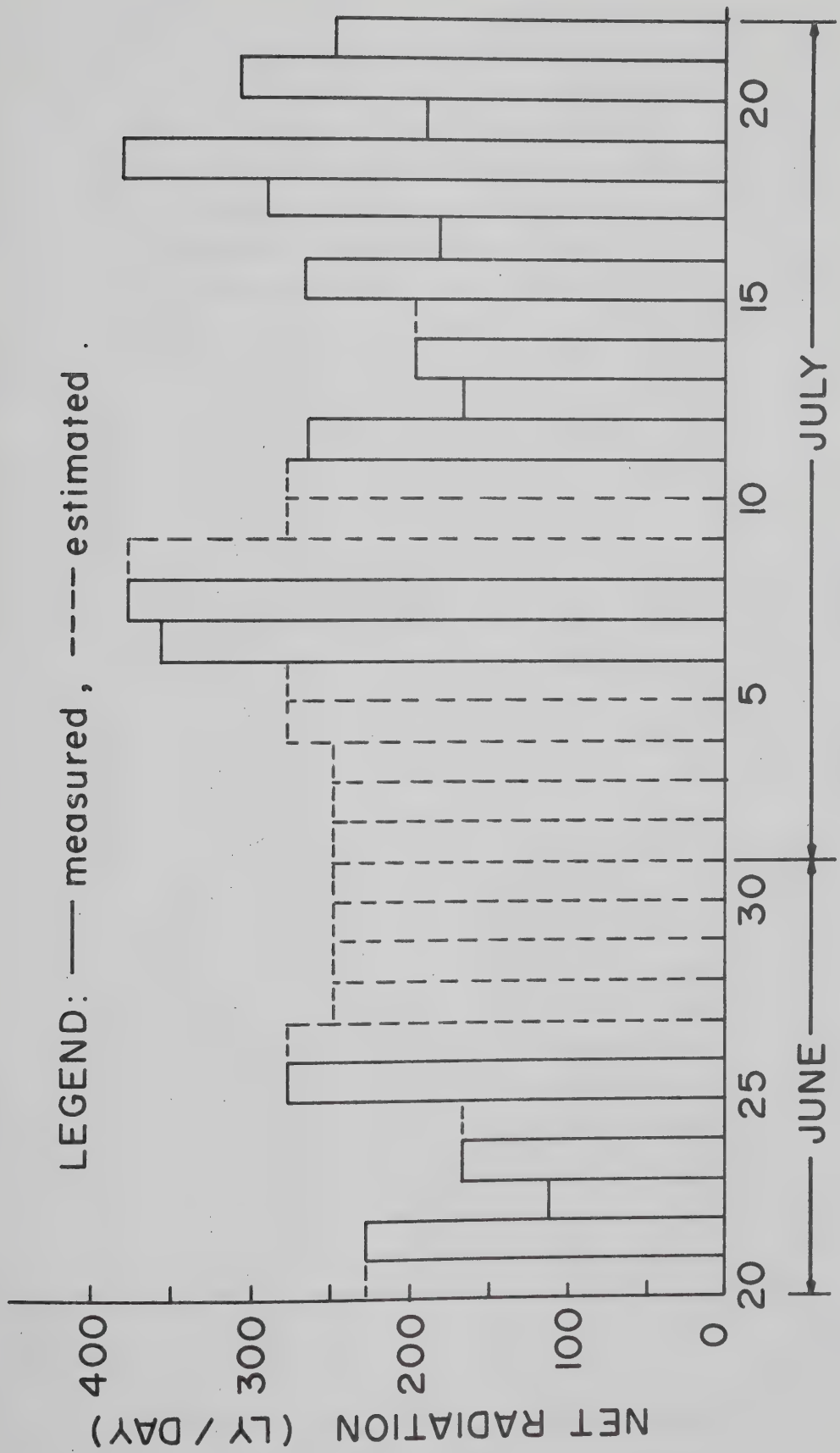

Fig. 5.28 Net Radiation for the Period of Observation (Sta. 1)

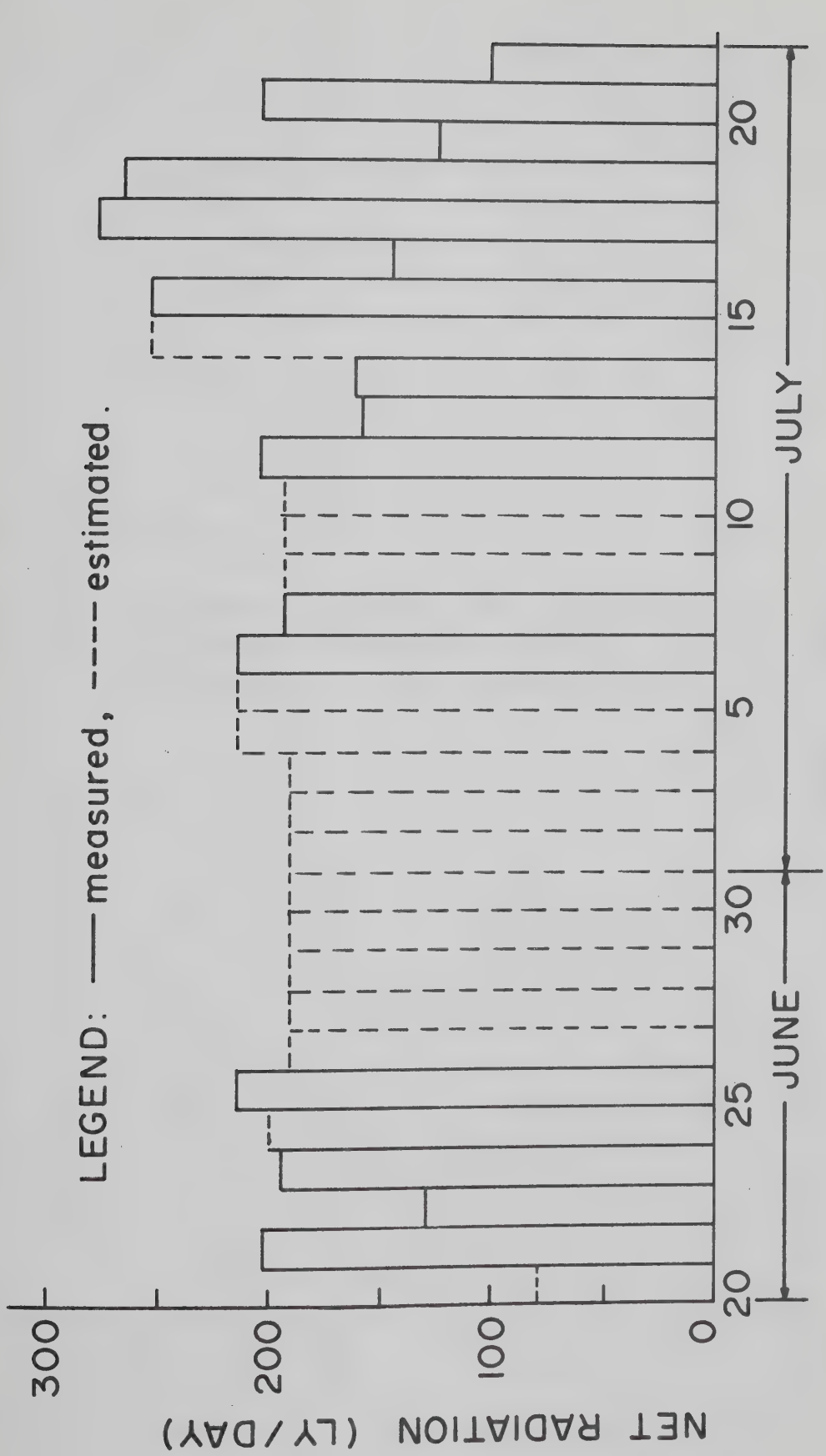

Fig. 5.29 Net Radiation for the Period of Observation (Sta. 2)

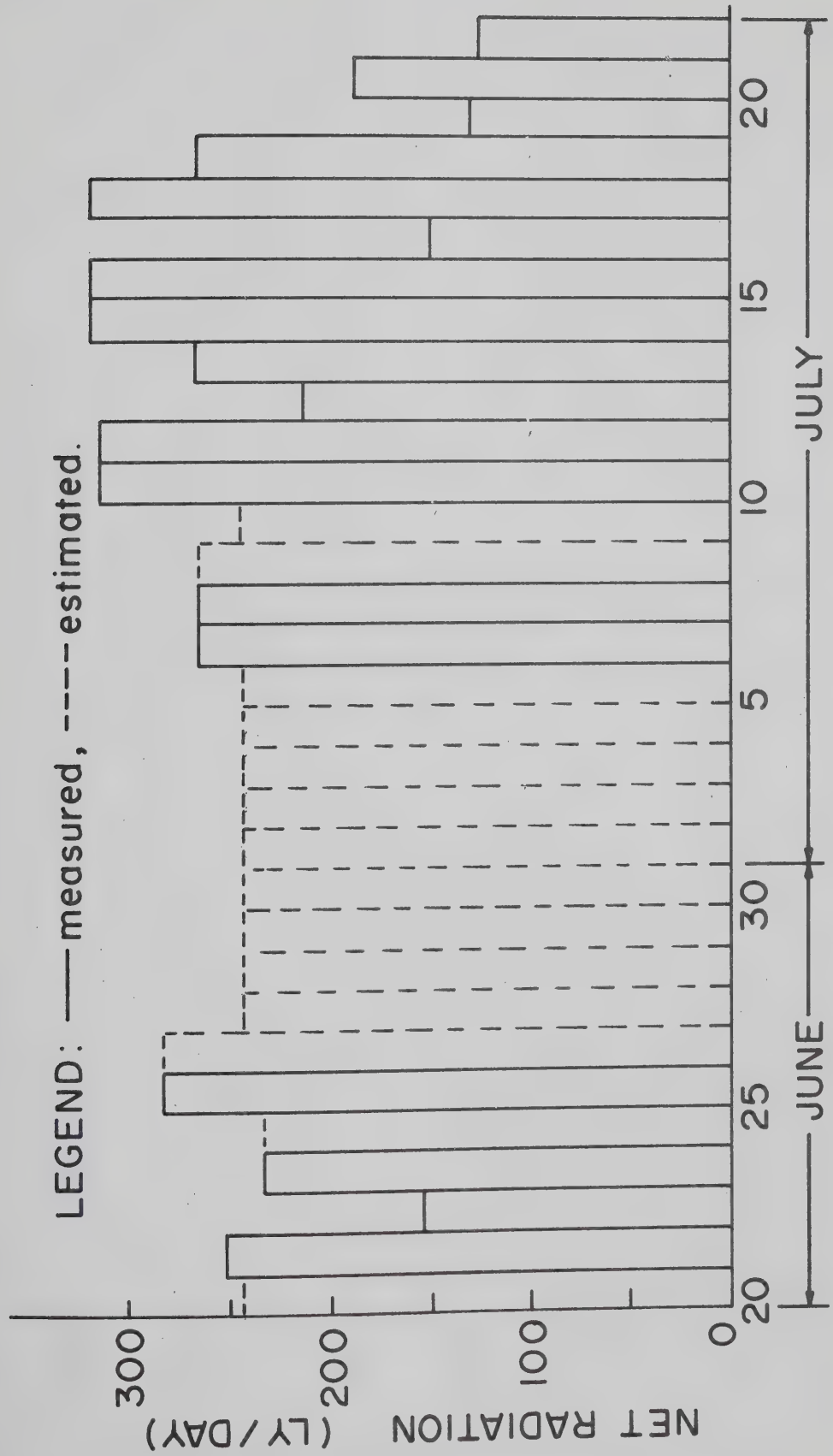

Fig. 5.30 Net Radiation for the Period of Observation (Sta. 3)

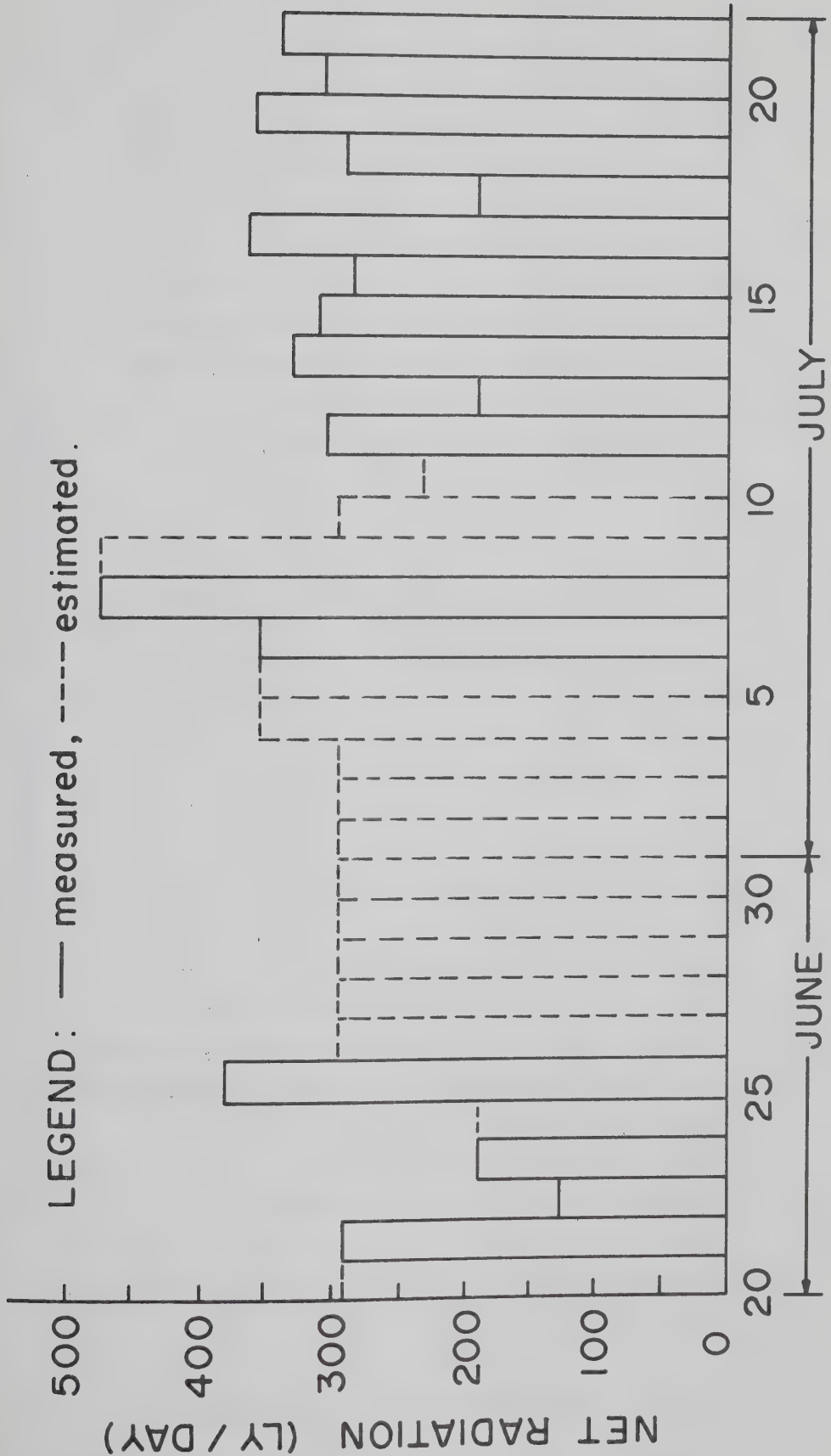

Fig. 5.31 Net Radiation for the Period of Observation (Sta. 4)

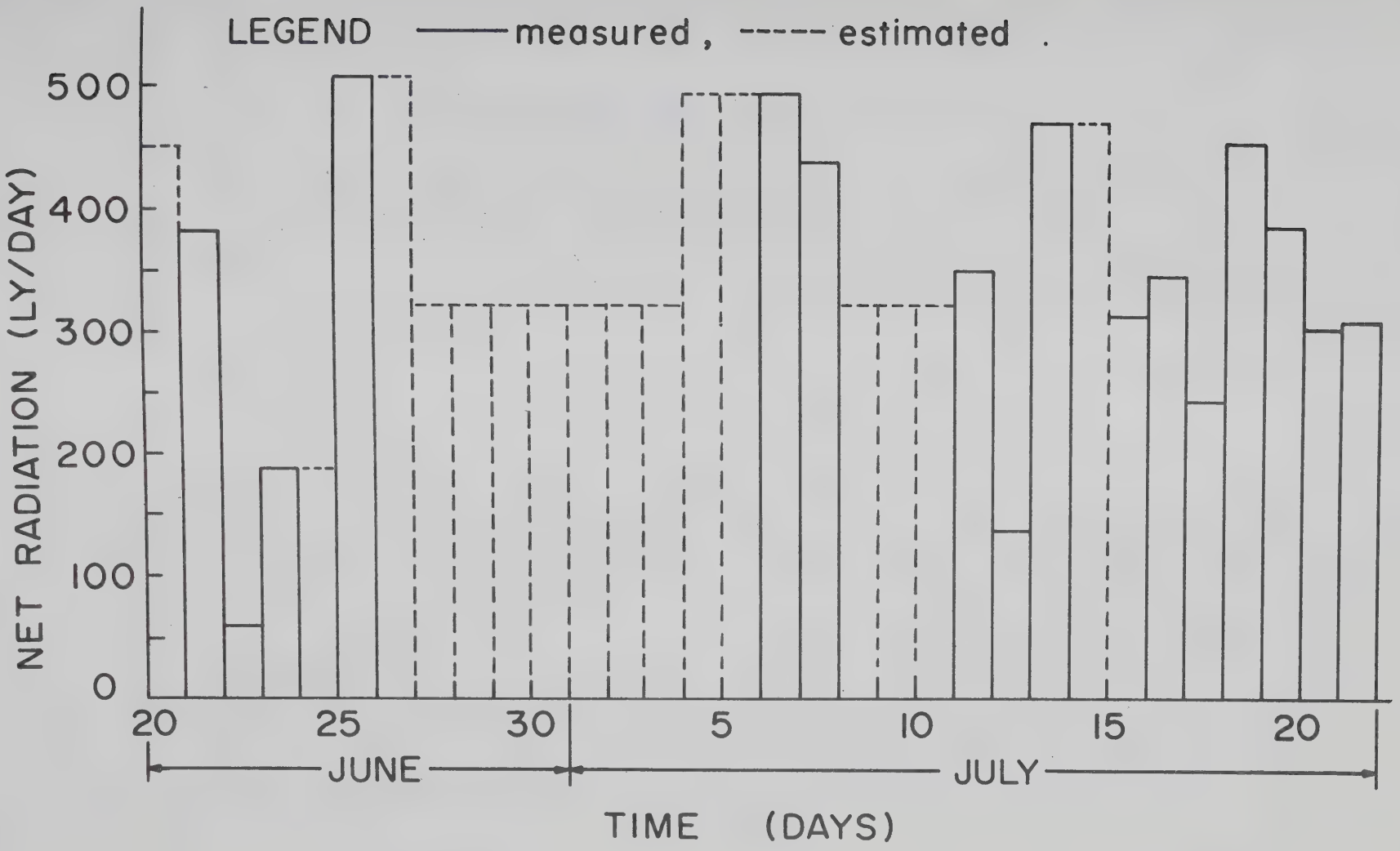

Fig. 5.32 Net Radiation on a Horizontal Surface for the Period of Observation (Sta. 5)

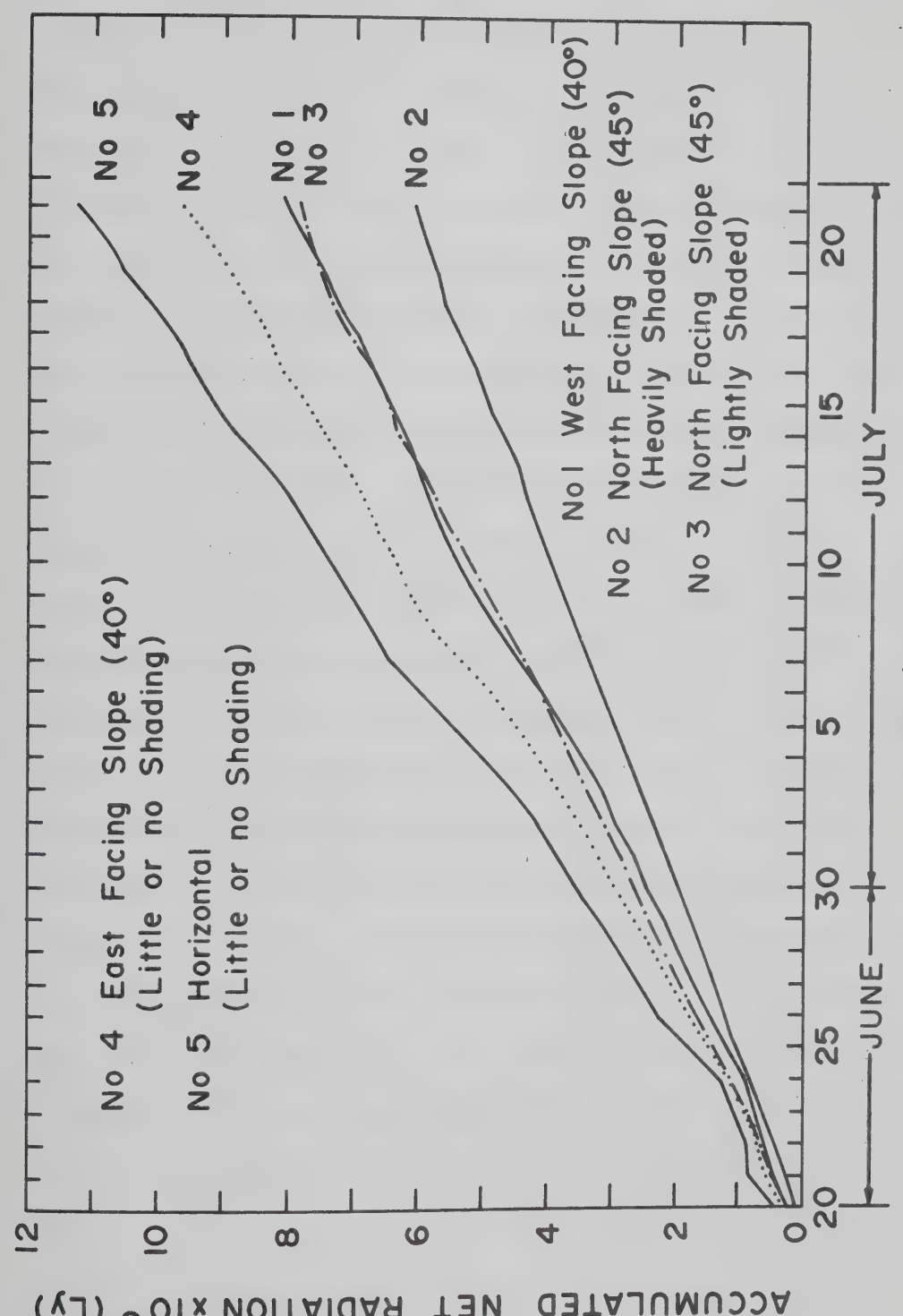

Fig. 5.33 Accumulated Net Radiation for the Period of Observation

to larger measured values of net radiation than those predicted in Table 5-4. A comparison of the predicted values of net radiation with those measured from the net radiometers situated in the bowl of the headscarp indicate that they consistently monitor values that are from 30 to 50% or 26 to 38% lower (depending on which comparison is chosen) than those predicted. This difference is attributed primarily to the shading of the sensors by the 40 to 60 foot trees that surround the south and east portions of the headscarp. Sensors 3 and 4 were exposed to much less shading and the discrepancy between the measured and predicted values is less than 30%. Section 4.3.2 has suggested some methods to account for shading due to sky line obstructions on planar slopes. However, the chaotic and constantly changing geometry of both headscarp and obstructions eliminated the possibility of similar calculations for the test site. The average value of radiation measured in the headscarp is 247 ly/day. This value is 30% lower than that measured on a horizontal surface without shading. The former value is essentially equal to the synoptic estimates for the upper Mackenzie Valley (ibid). This correlation may be somewhat fortuitous in view of the assumptions regarding albedo and the effect of shading. However, the results show that the radiation balance at the headscarp of a bimodal flow slide in the subarctic may be estimated with sufficient accuracy for most engineering applications from published synoptic data.

5.9 Latent Heat Transfer

The two significant remaining terms in the heat balance equation are the latent heat transfer and sensible heat transfer. It is theoretically possible to quantify the former term by physical measurements

involving lysimetric techniques outlined in Chapter 4. A permafrost lysimeter was, therefore, designed and built in an attempt to obtain the magnitude of the latent heat term. Figure 5-34 illustrates the design.

The equipment consisted of a tray to contain the melting soil and a reservoir to retain the melted soil-water mixture (Figure 5-35). Both tray and reservoir were constructed from 1.25 cm. thick polyvinyl-chloride. The tray provided a projected surface area of 2700 cm^2. The lower end of the tray was fitted with a finger type grate that allowed the passage of water and mud, but retained the frozen soil and ice mixture. This end of the tray fitted snugly into a closed reservoir that contained the thawed soil and essentially prevented any loss or gain of water by evaporation or condensation. The reservoir was covered with aluminum foil to minimize radiative heat transfer.

Frozen soil and ice were chipped from the head scarp, placed in the tray and weighed with a load cell to within an accuracy of ± 25 gms. Approximately 18 to 22 kgs. of material were used for each test (Figure 5-36). The tray was then inserted into the mouth of the reservoir and both units were placed in a plywood box designed to contain and transport (at the proper angle) these two latter units. The assembled lysimeter was suspended from a portable hand-operated crane and swung into position over the edge of the escarpment. The unit was carefully lowered to a suitable spot within the melting mass of ice and mud. It was secured in such a way that it rested partly on the slope and was partly suspended by the crane at the same angle as the slope (Figure 5-37).

The exposed ice and soil in the tray were allowed to melt and drain into the reservoir. When melting was reasonably complete the lysimeter was retrieved and the reservoir and tray were again weighed.

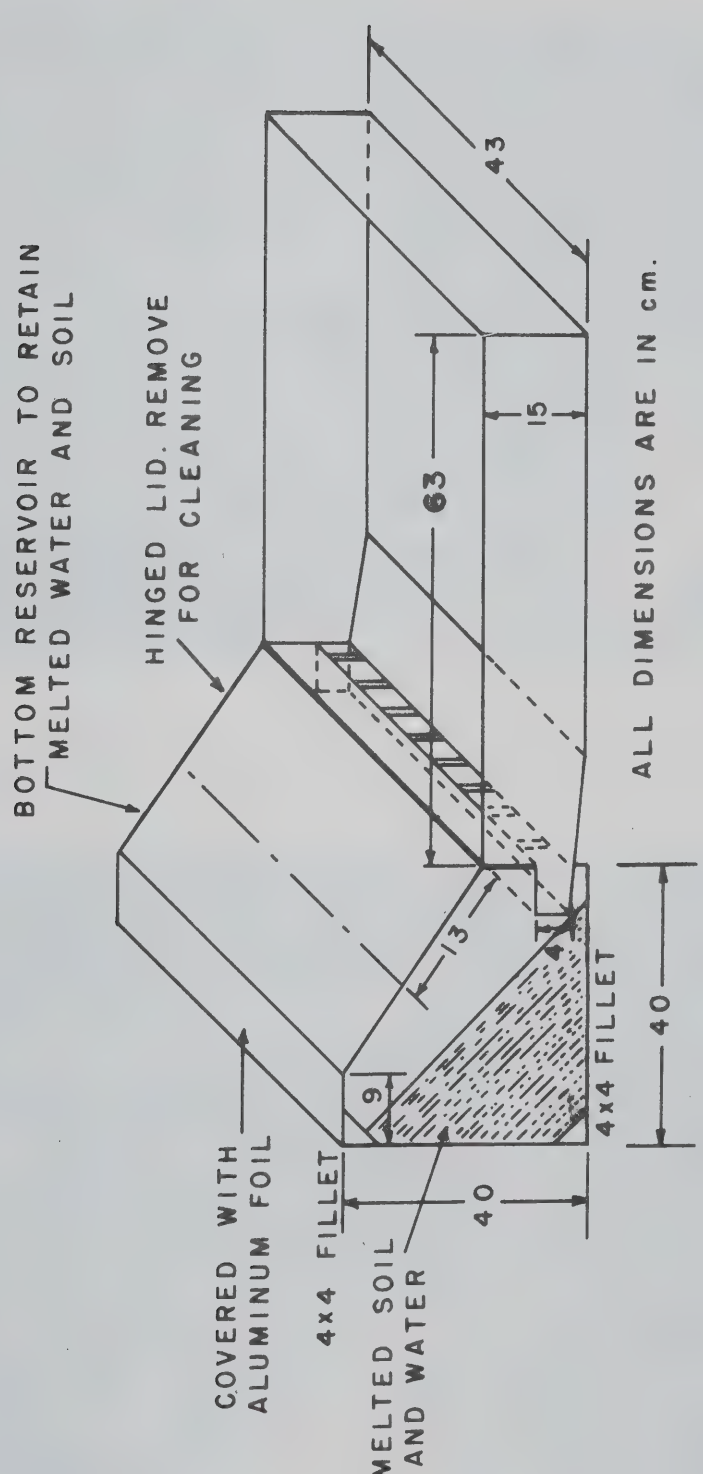

Fig. 5.34 Permafrost Lysimeter

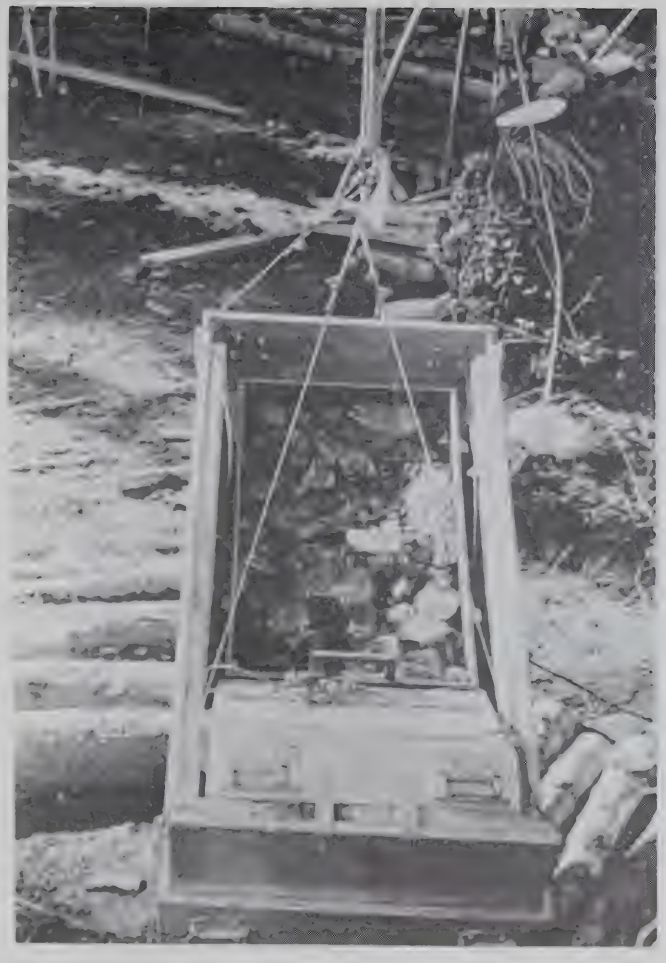

Fig. 5-35 Permafrost Lysimeter

Fig. 5-36 Tray from Permafrost Lysimeter (weighed with standard load cell)

Fig. 5-37 Portable Crane and Permafrost Lysimeter

A gain or loss in weight of the two components could be directly interpreted as either condensation or evaporation respectively. The lysimeter was allowed to remain on the slope for different periods of time, which was usually dictated by the working hours at the test site. Tests were conducted both during the day and night. A measure of the heat gain per day on the exposed slope was estimated from the results of the collected data. The heat gain per hour in the lysimeter was computed by determining the weight gain of the lysimeter, dividing by an estimated exposed surface area of the material in the tray, multiplying by the latent heat of vaporization and finally dividing by the number of hours that melting had occurred. For simplicity an approximate value of of the exposed surface area of the permafrost in the tray may be determined by considering the upper surface to be composed of spherical shaped particles approximately 5 cm in diameter. By adding one half the surface area of the spheres to the remaining exposed area between the spheres a total exposed surface area of 4850 cm^2 is obtained. Table 5-8 provides the presentation and interpretation of the data collected at the test site.

A wide variation in the weight change of the lysimeter was noted during the period of time that the tests were conducted. However, it is interesting to note that the lysimeter gained a substantial amount of weight for all the tests conducted at the site. It is also significant to note that the amount of heat supplied to the slope by the heat of condensation was always significantly greater during the day than at night. This observation is to be expected because the transfer of vapour is a function of air turbulence which is invariably greater during the daylight hours than at night. Day time values indicate an average of 8.9 ly/hr. and night time values of 3.4 ly/hr. If these values are to be extended to daily averages

and ultimately to accumulated totals, it is necessary to decide over which hours they are applicable. A reasonable division during this season is suggested to be 10 hours of daytime and 14 hours of nighttime atmospheric conditions. The heat flux due to condensation of vapour on the slope using these numbers is, therefore, approximately 137 ly/day.

The data in Table 5-8 indicate that there is a general but not rigorous correlation between wind speed,* relative humidity and magnitude of heat flux due to the heat of condensation. The higher wind speeds and relative humidities are often but not always associated with the larger magnitudes of vapour transfer. The technique of measurement and computation inadvertently incorporate averaging mechanisms that tend to obscure the direct interrelationship of atmospheric conditions and vapour transport to the surface. The theoretical equations referred to in the previous chapter used to predict vapour transport use the general relationship of vapour pressure differences combined with some functional relationship involving the product of wind speed. Figure 5-38 shows the relationship derived by plotting the product of the average wind speed and relative humidity versus the measured heat of condensation. Although the scatter is substantial the trend is evident and follows the form that would be anticipated. The dotted curve indicates that maximum rates of condensation will occur under appropriate combinations of wind speed and humidity. This phenomenon is also typical of measured evaporation rates and wind speeds (W.M.O., 1966).

---

* wind speeds were recorded with a standard Monroe (Mark II) Totalizing 3 cup counter anemometer.

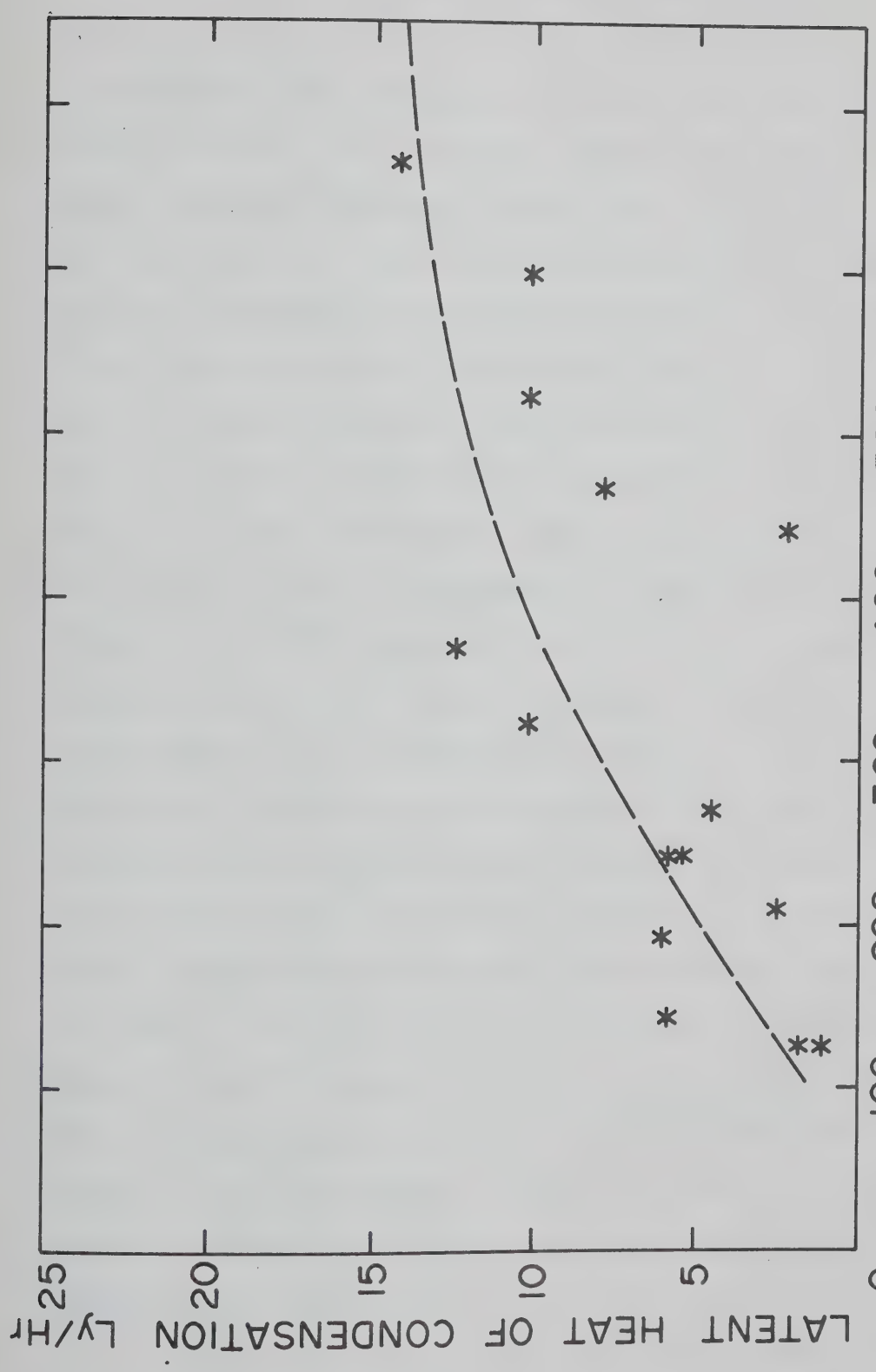

Fig. 5.38 Product of Average Wind Speed and Relative Humidity vs. Latent Heat of Condensation

An attempt was made to establish the vapour pressure gradient above the headscarp. The wet bulb-dry bulb technique was employed to determine the vapour pressure at different levels above the exposed permafrost. The temperature sensors consisted of 24 gauge copper constantan thermocouples housed inside a 2.5 cm. diameter by 1.5 cm. lucite tube. The tube was covered with Virginia Foam Insulation tape and wrapped in aluminum foil. Since the foil has a high albedo and correspondingly high emissivity and since the insulation tape is a poor heat conductor, radiant heating was minimized. The wet bulb sensor was encased within a cotton muslin sheath approximately 15 cm. long. Distilled water was fed by gravity to the cotton sheath from a plastic bottle suspended above the sensor. The water flowed through a small plastic tube and into a 11 cm. long 20 gauge steel hypodermic needle tube. The steel tubing was encased within the cotton sheath so that the water was precooled by the evaporating wick. The mouth of the radiation shield was covered with mosquito netting and aspirated with a domestic vacuum cleaner. The response of the wet bulb sensor seemed to be relatively insensitive to the volume of air flowing through the tube and it was found that a vacuum cleaner was capable of supplying sufficient air velocities to completely depress the wet bulb sensor. The dry bulb sensor was placed within the shield approximately 2.5 cm. in front of the saturated wet bulb sheath. Figure 5-39 provides a schematic illustration of the components. The complete system was comprised of 3 units placed approximately 1 meter, 3 meters and 6 meters above the headscarp.

The wet and dry bulb temperatures were recorded on a 12 channel Honeywell Electronik 15 Strip Chart Multipoint Recorder that sampled the signal from each sensor once every two minutes. The

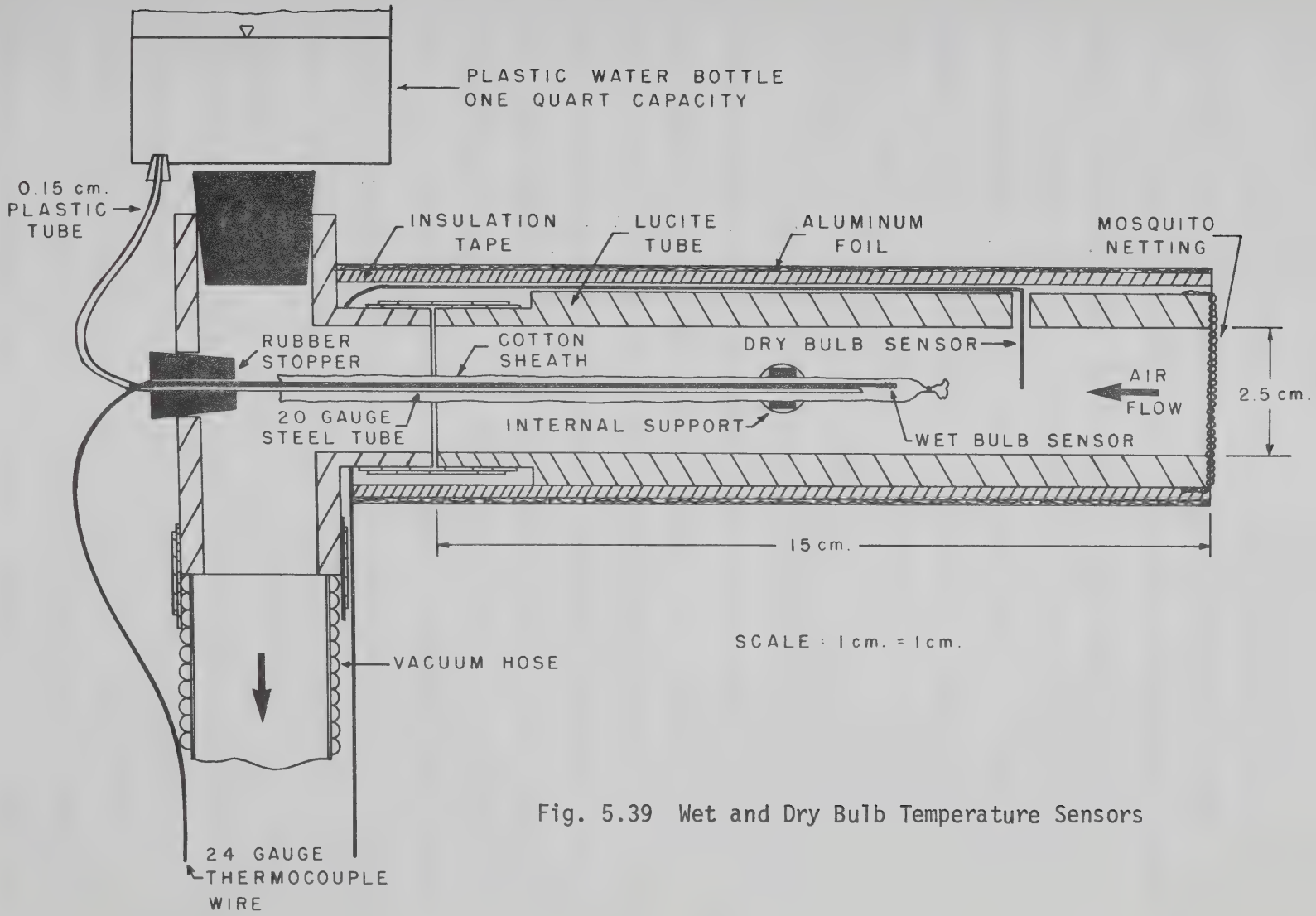

Fig. 5.39 Wet and Dry Bulb Temperature Sensors

sensors were calibrated in the laboratory using a constant temperature bath and a precision thermometer that was accurate to better than ± 0.1° C over the range of 8 to 25° C.

The whole system could be rated as moderately satisfactory. The major problem encountered was that of maintaining a constant rate of water flow to the cooling wicks. If the water reservoirs had been operated under pressure and the rate of flow controlled with a needle valve, perhaps a higher level of performance could have been realized. It was necessary to inspect the wicks once every 2 or 3 hours to ensure the flow was maintained at a reasonably uniform rate. As a result, excess water as well as insufficient water often caused spurious readings in the magnitude of the wet bulb depression.

Considerable data have been collected to indicate the magnitude and direction of the vapour pressure gradients existing above the headscarp. Again the data are sporadic due to power failures. Obvious errors were often evident in the wet bulb readings, and therefore, a measure of data selection was employed in assembling the values that are presented in Appendix D. The gradients have been computed between the surface and the 1 meter level, 1 meter and 3 meters, and 3 meters and 6 meters. The vapour pressure of the surface was assumed to be the saturation vapor pressure over ice or water at 5° C (8.7 mb). The results indicate that a sharp positive gradient exists from the air to the surface at the lowest level. The profile of this gradient is highly non linear because sporadic checks of the vapour pressure at 0.3 meters indicated pressures only slightly lower than those recorded at the 1 meter level. Figure 5-40 presents some selected data from Appendix D to show the sign and magnitude of the gradients above the headscarp and how they vary with time. Reversals in sign often occur

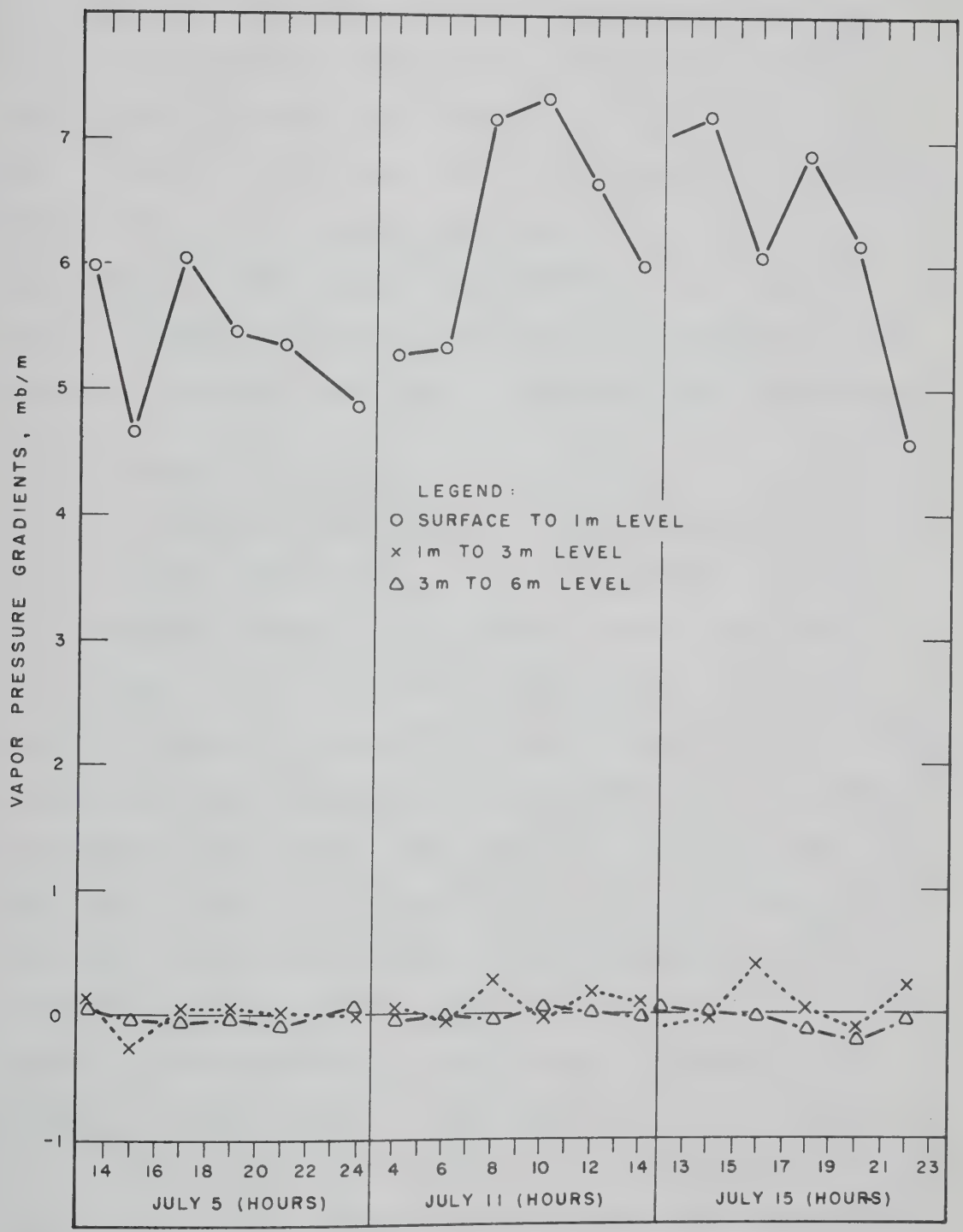

Fig. 5.40 Typical Vapor Pressure Gradients Above the Headscarp

at the 3 meter level indicating the unpredictability of the stability of the air mass in the region of the landslide. This type of instability was anticipated because of the non uniformity of the terrain.

All the vapour pressure data substantiate the results from the lysimeter in general terms. However, it appears unlikely that this information could be used effectively in an analytical approach for computing the amount of energy transferred to or from the surface. It was stated in Chapter IV and is again reaffirmed that these methods require a degree of atmospheric predictability and uniformity. Such atmospheric conditions were absent in the region above the headscarp.

5.10 Evaporation Quantities

Evaporation quantities were monitored in the control area by using a Class A evaporation pan. The pan was mounted in accordance with recommended practices (W.M.O., 1966). Readings were taken on a daily basis. Figure 5-41 indicates the magnitude of the daily evaporation values. A pan coefficient must be applied to these values if they are to be interpreted as being representative of the potential evaporation in this region. These coefficients may range from 0.67 to values in excess of 0.90, depending upon the time of year (ibid). The lower values are usually associated with evaporation quantities recorded in the summer months. It is suggested that a value of 0.70 applied to the pan data would provide reasonable estimates of the potential or lake evaporation in the area.

The average daily corrected value of 0.45 cm/day is somewhat greater than 0.32 cm/day recorded by Brown (1965). The former value is equivalent to 270 ly/day which indicates that the major part of the net radiation available at the surface is utilized in evaporating water.

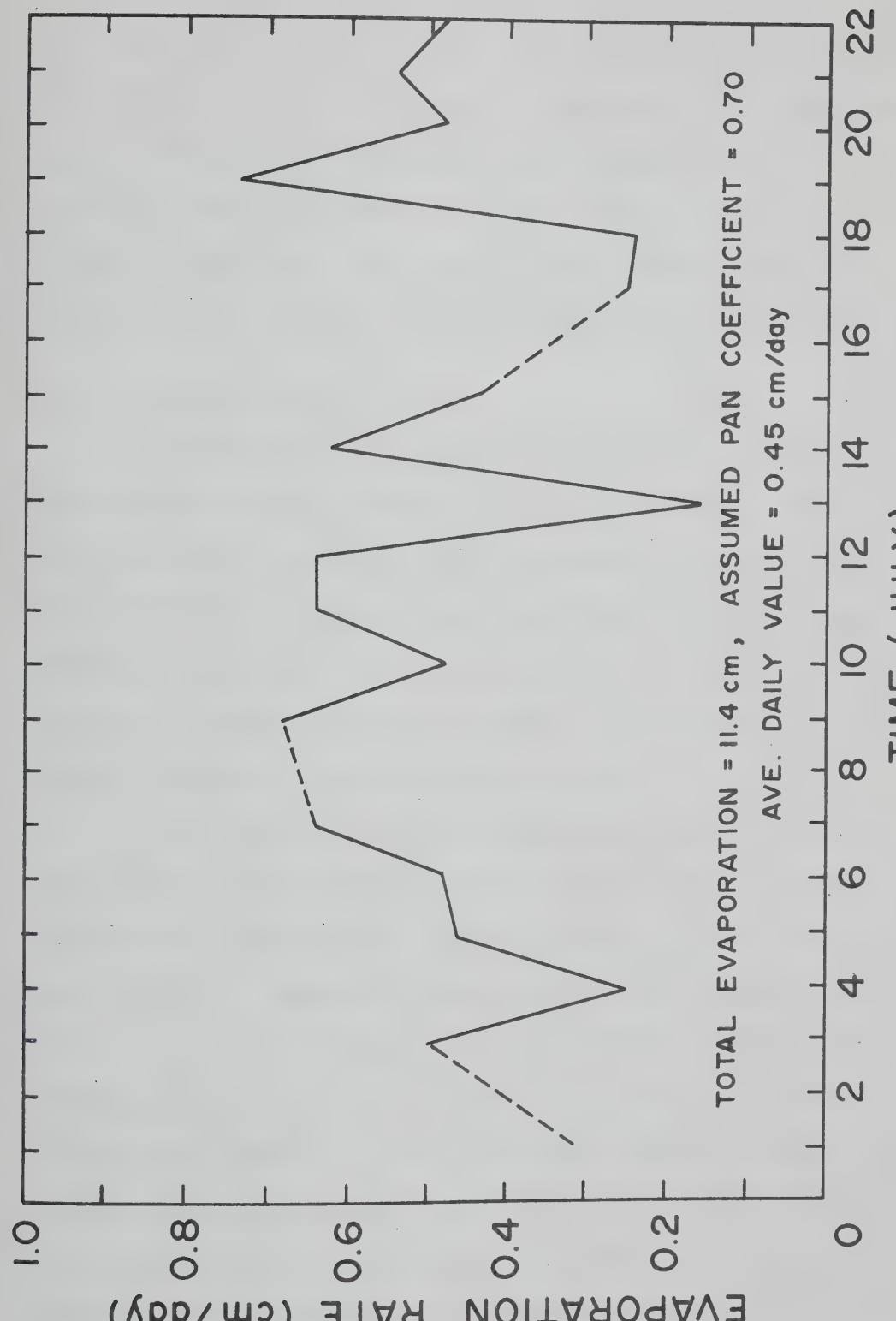

Fig. 5.41 Daily Evaporation Rates at Test Site

It is interesting to point out the very significant changes that occur in the heat balance at the surface of the exposed permafrost and the bare soil which is warmed to approximately air temperatures and is within a few hundred feet of the exposed permafrost. The amount of latent heat transfer is approximately double but opposite in sign, indicating a strong cooling effect where evaporation is occurring and a strong heating effect over the cool permafrost surface.

5.11 Sensible Heat Transfer

The discussion in Chapter 4 suggests that attempts to compute the transfer of heat to or from the surface are largely futile. Moreover, techniques involving direct measurement are very costly, require uniform terrain, and are generally unreliable. Therefore, under the conditions imposed by the character of the local terrain, the magnitude of this term may only be determined by computing it as the residual quantity in the heat balance equation.

Dry bulb temperature readings were taken (as previously described) in order to establish the existence of a temperature profile above the headscarp. Again the data is sporadic due to power failures. Temperature gradients have been computed from these results and appear in Appendix D. The gradients have been computed between the surface and the 1 meter level, 1 meter and 3 meters, and 3 meters and 6 meters. A strong non-linear positive gradient exists between the surface and the 1 meter level with a general decrease noted with height. Figure 5-42 indicates the sign and magnitude of some temperature gradients selected from Appendix D. The occasional reversal in sign will be noted at the 3 meter level, again suggesting instability of the air mass. However, the data firmly substantiate the claim of a strong positive temperature gradient and thus a sub-

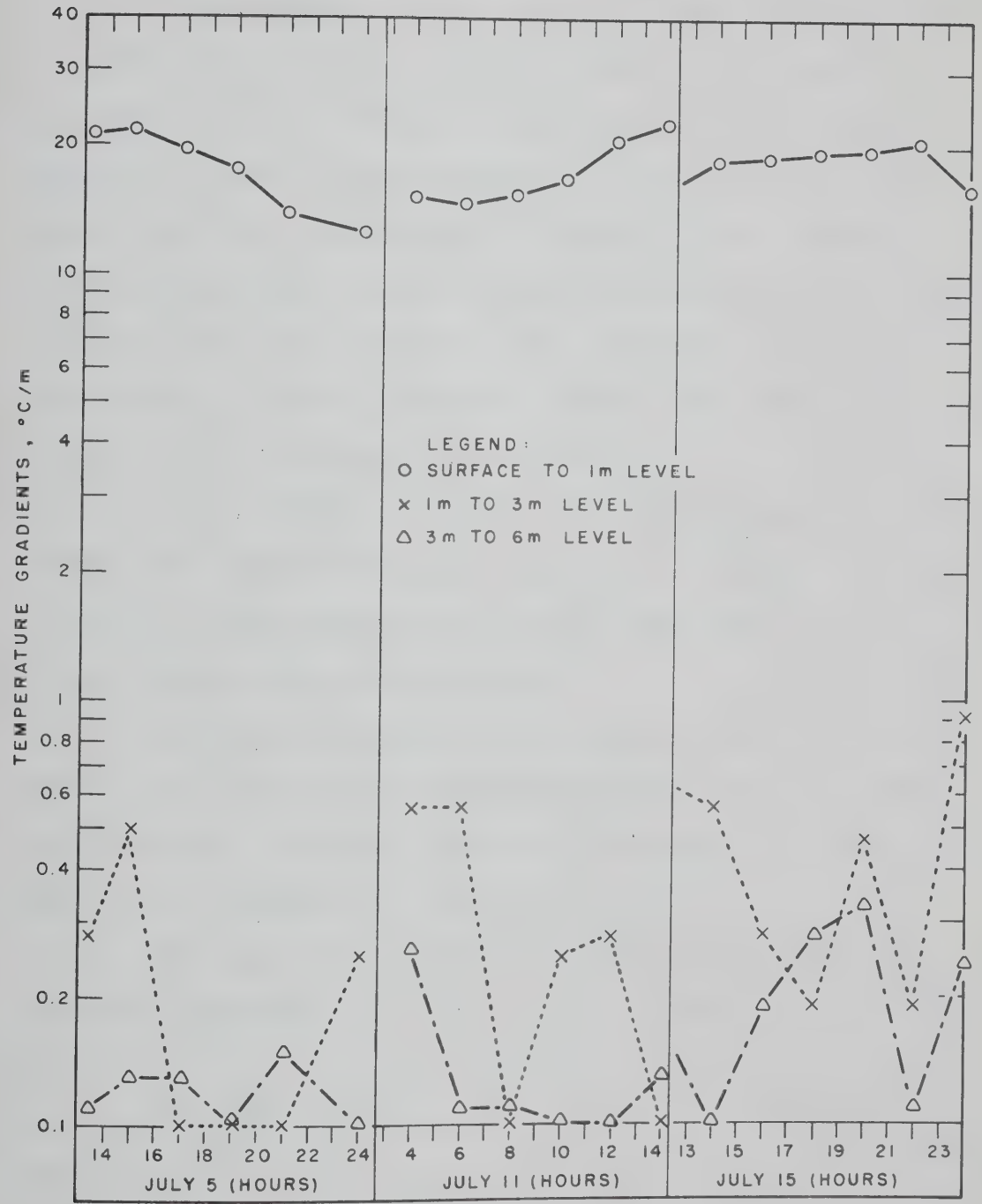

Fig. 5.42 Typical Temperature Gradients Above the Headscarp

stantial flux of sensible heat toward the surface of the head scarp.

5.12 Ablation and the Heat Balance

The accumulated ablation rates have been established and are illustrated in Figure 5-13 to 5-18. Stations 3, 4 and 5 which correspond to Figures 5-15, 5-16 and 5-17 respectively have been selected as supplying the most representative values and a comparison of the curves will indicate the similarity in the measured values at these three stations. These data have been used to establish an average rate of retreat of 14 cm/day. The heat requirements computed for this rate allowing for a range in water contents of 30 to 50% are 504 to 645 ly/day respectively.

The net radiation available at the head scarp is shown in Figure 5-33. The writer suggests that the average values listed in Table 5-6 be used to represent the accumulated average totals in further computations of the heat balance.

Section 5.9 has described the method of quantifying the magnitude of the latent heat of condensation at the surface of exposed permafrost and a reasonable average daily value over the period of observation is suggested to be 137 ly/day.

The heat balance equation at a head scarp existing under isothermal conditions of 5^{o} can be simply described as:

$$q_A = q_{NR} + q_L + q_H \quad - - - \quad 5.3$$

where q_A = the heat required for ablation

q_{NR} = the net radiation

q_L = the latent heat of condensation

q_H = the sensible heat

Since q_A, q_{NR} and q_L have been quantified it is now possible to evaluate q_H by treating it as the residual quantity in equation 5.3 . Figure 5-43 provides a graphical solution for equation [5.4] in terms of accumulated values. If the lower value of q_A = 504 ly/day is chosen then q_H = 120 ly/day and if the largest values of q_A is used, q_H = 261 ly/day. The appropriate value will fall somewhere within these limits. Part of this heat flux may have arrived at the head scarp by advection from warm adjacent areas. However, there is no way of separating the total sensible heat flux into horizontal and vertical components. Moreover, it is unlikely that such a separation would provide information that was of significant engineering value.

Since the value of q_H has been determined as a residual quantity in the heat balance equation without verification by computation or measurement, there is need to establish its credibility. If the value of q_H is assumed to have an average value of 191 ly/day, then the relative contributions of energy can be described as a percentage of the total energy required for the measured ablation rate.

$$q_{NR} = 43\%;\ q_H = 33\%;\ q_L = 24\%.$$

Numerous glaciologists determining the heat balance of glaciers and hydrologists dealing with the heat balance of melting snow packs have shown somewhat similar results. However, they have generally found that the contribution of q_H relative to q_L to be somewhat greater and that q_L may occasionally be negative. This is to be expected because they are generally dealing with environments when atmospheric conditions lend themselves to lower vapour pressures and thus smaller contributions of q_L relative to q_H (Muller and Keeler, 1969; Treidl, 1970; O'Neill, 1973). Other reasons for the apparently large con-

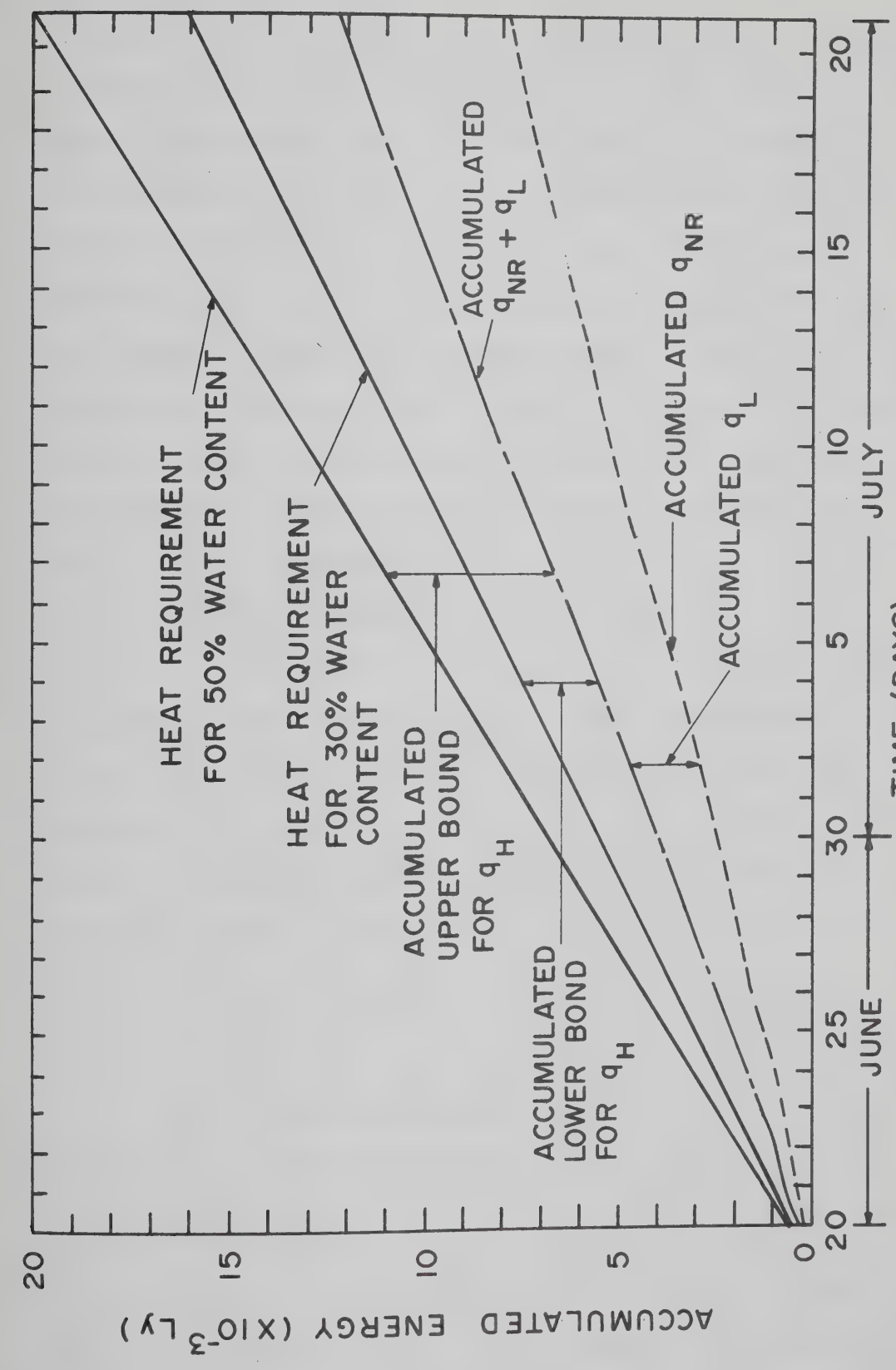

Fig. 5.43 Heat Balance at the Headscarp of the Fort Simpson Landslide

tribution of the latent heat term in the ablation process is that the lysimeter is cooler than the slope and thus attracts more condensation, and also the procedure used to estimate the total exposed surface area of the material in the tray may have provided somewhat lower values than those actually existing in the tray over the period of measurement. Continued observations at the Fort Simpson site would undoubtedly show changes in these relative contributions. In fact, a set of wet bulb-dry bulb readings on June 30 show that very low vapour pressure gradients exist between the surface and the 1 meter level and that a reversal in the direction of vapour transport may have temporarily occurred (data in Appendix D).

It is of interest to compute the Bowen ratio from the results of q_H and q_L. The ratio q_H/q_L = 1.4. This value may then be compared to that computed from the average temperature and vapour pressure data that were recorded at the 6 meter level above the head scarp. The values at this level were chosen as they probably compare most favourably with any synoptic estimates that may be utilized for similar computations.

T_a (ave) = 17.4° C

T_w = 5° C

P_a = 11.89 mb (8.94 mm Hg)

P_w = 8.7 mb (6.54 mm Hg)

P = 744 mm Hg

If these values are substituted into equation [4.60] the Bowen ratio (R) = 2.3. If the ratio q_H/q_L = 1.4 is somewhat low due to overestimates of q_L then it appears that the Bowen ratio (R) computed from meteorological data may provide reasonable relationships between q_L

and q_H in ablation estimates.

Another possibility of utilizing the data obtained for q_H and q_L is to normalize these values relative to the net radiation, which may be predicted from monthly synoptic estimates.

Thus $q_{NR}/q_{NR} = 1$; $q_L/q_{NR} = 0.55$; $q_H/q_{NR} = 0.77$.

Unfortunately, these ratios undoubtedly change dramatically through the spring, summer and fall seasons. Atmospheric conditions in the early part of the thaw season could change not only the magnitude of q_L, but also the direction of heat flow. The magnitude of q_H will also change over the period of thaw; however, its sign should almost always remain positive. It is unfortunate that it will be difficult if not impossible to estimate the amount of heat flux utilized in melting the permafrost over the thaw season from radiation data alone. This technique would only be viable if q_{NR}, q_L and the ablation rates were continuously monitored at a number of sites in the Mackenzie Valley. It would then be possible to evaluate q_L/q_{NR} and q_H/q_{NR} over the entire thaw season and to establish the anticipated ablation rate of permafrost from soil moisture contents and synoptic estimates of net radiation.

In view of the foregoing presentation, it may be concluded that the terms in the energy balance at the head scarp of a bimodal flow slide have been measured to reasonable accuracy for the period of observation. The measured and deduced values are consistent with those anticipated and compare favourably with data provided by other researchers who are involved with problems having similar temperature boundary conditions. It must also be recognized that the relative contributions of the various components may vary over the thaw season. This will, however, rarely be of concern or of interest to the geo-

technical engineer.

The following chapter is intended to show that the energy balance of exposed melting permafrost is unique to that temperature boundary condition. In general, any attempt to retard or halt the ablation process will change the surface temperature and will completely alter the heat flux boundary conditions.

TABLE 5-2

SHORT WAVE RADIATION QUANTITIES FOR SLOPES AT DIFFERENT ORIENTATIONS AND INCLINATIONS FOR FORT SIMPSON REGION (LAT = 61°52'N)

Slope Orientation	Slope Angle°	Ratio Diffuse / Total	Direct Beam (Ly/Day)	Diffuse (Ly/Day)	Total (Ly/Day)	Net Short Wave Radiation Albedo = 13% (Ly/Day)
	0	0.35	325	175	500	435
N	10		316	174	490	427
E & W	10		323	174	497	433
S	10		330	174	504	439
N	20		298	170	468	408
E & W	20		321	170	491	429
S	20		334	170	504	439
N	30		271	163	434	380
E & W	30		321	163	484	423
S	30		331	163	494	432
N	40		235	155	390	343
E & W	40		318	155	473	415
S	40		320	155	475	417
N	50		193	144	337	300
E & W	50		313	144	457	403
S	50		302	144	446	394
N	60		171	131	302	271
E & W	60		303	131	434	386
S	60		276	131	407	363
N	70		160	118	278	253
E & W	70		286	118	404	363
S	70		243	118	361	325
N	80		151	103	254	235
E & W	80		266	103	369	335
S	80	0.35	204	103	307	281
	0	0.40	300	200	500	435
N	10		292	199	491	427
E & W	10		298	199	497	433
S	10		305	199	504	438
N	20		275	194	469	409
E & W	20		297	194	491	428
S	20		308	194	502	438
N	30		250	187	437	382
E & W	30		296	187	483	422
S	30		305	187	492	430
N	40		217	177	394	346
E & W	40		294	177	471	413
S	40		296	177	473	415
N	50		178	164	342	303
E & W	50		289	164	453	400
S	50		279	164	443	391
N	60		157	150	307	275
E & W	60		279	150	429	381

TABLE 5-2 (CONTINUED)

Slope Orientation	Slope Angle ^{o}	Ratio $\frac{\text{Diffuse}}{\text{Total}}$	Direct Beam (Ly/Day)	Diffuse (Ly/Day)	Total (Ly/Day)	Net Short Wave Radiation Albedo = 13% (Ly/Day)
S	60	0.40	255	150	405	360
N	70	0.40	148	134	282	256
E & W	70		265	134	399	357
S	70		225	134	359	322
N	80		139	118	257	234
E & W	80		245	118	363	328
S	80	0.40	189	118	307	279
	0	0.45	275	225	500	435
N	10		268	223	491	427
E & W	10		274	223	497	433
S	10		280	223	503	438
N	20		252	219	471	410
E & W	20		272	219	491	428
S	20		282	219	501	437
N	30		229	210	439	384
E & W	30		271	210	481	421
S	30		280	210	490	428
N	40		199	199	398	349
E & W	40		269	199	468	410
S	40		271	199	470	412
N	50		163	185	348	308
E & W	50		264	185	449	396
S	50		255	185	440	388
N	60		144	169	313	279
E & W	60		256	169	425	376
S	60		233	169	402	357
N	70		136	151	287	258
E & W	70		243	151	394	352
S	70		206	151	357	320
N	80		128	132	260	237
E & W	80		225	132	357	322
S	80	0.45	173	132	305	277
	0	0.50	250	250	500	435
N	10		244	248	492	428
E & W	10		249	248	497	433
S	10		254	248	502	437
N	20		229	243	472	411
E & W	20		247	243	490	427
S	20		257	243	500	435
N	30		208	233	443	386
E & W	30		247	233	480	419
S	30		255	233	488	426
N	40		181	221	402	353
E & W	40		245	221	466	408
S	40		246	221	467	410

TABLE 5-2 (CONTINUED)

Slope Orientation	Slope Angle ^{o}	Ratio $\frac{\text{Diffuse}}{\text{Total}}$	Direct Beam (Ly/Day)	Diffuse (Ly/Day)	Total (Ly/Day)	Net Short Wave Radiation Albedo = 13% (Ly/Day)
N	50	0.50	149	205	354	312
E & W	50	↓	241	205	446	392
S	50	0.50	233	205	438	385
N	60	0.50	131	187	318	283
E & W	60	|	233	187	420	372
S	60	|	213	187	400	354
N	70	|	123	168	291	261
E & W	70	|	221	168	389	346
S	70	|	187	168	355	317
N	80	|	116	147	263	239
E & W	80	↓	204	147	351	316
S	80	0.50	157	147	304	275

TABLE 5-3

NET LONGWAVE RADIATION FOR DIFFERENT SLOPES
COMPUTED FROM EQUATION 4-52

$$q_{LNS} = \varepsilon_s \sigma T_a^4 (a+b\sqrt{e}) - T_s^4 (1-\varepsilon_s \sin^2 a/2)$$

Slope Angle ^{o}	Ground Temp ^{o}C	Radiation Quantity ly/day
0	12 (control area)	-133
10	5	-58
20	5	-43
30	5	-18
40	5	+16
45	5	35
50	5	57
60	5	105

TABLE 5-4

NET RADIATION FOR SLOPES AT DIFFERENT ORIENTATIONS AND INCLINATIONS FOR FORT SIMPSON REGION (LAT 61°52'N)

Slope Orientation	Slope Angle °	Ground Temp °C	Ratio Diffuse/Total	Net Radiation (Ly/Day)
	0	12	0.35	302
N	10	5		369
E & W	10			375
S	10			381
N	20			365
E & W	20			386
S	20			396
N	30			362
E & W	30			405
S	30			414
N	40			359
E & W	40			431
S	40			433
N	50			357
E & W	50			460
S	50			451
N	60			376
E & W	60			491
S	60	5	0.35	468
	0	12	0.40	302
N	10	5		369
E & W	10			375
S	10			380
N	20			366
E & W	20			385
S	20			395
N	30			364
E & W	30			404
S	30			412
N	40			362
E & W	40			429
S	40			431
N	50			360
E & W	50			457
S	50			448
N	60	5	0.40	380
E & W	60			486
S	60	5	0.40	465

TABLE 5-4 (CONTINUED)

Slope Orientation	Slope Angle ^{o}	Ground Temp ^{o}C	Ratio Diffuse/Total	Net Radiation (Ly/Day)
	0	12	0.45	302
N	10	5		369
E & W	10			375
S	10			380
N	20			367
E & W	20			385
S	20			394
N	30			366
E & W	30			403
S	30			410
N	40			365
E & W	40			426
S	40			428
N	50			365
E & W	50			453
S	50			445
N	60			384
E & W	60			481
S	60	5	0.45	462
	0	12	0.50	302
N	10	5		370
E & W	10			375
S	10			379
N	20			368
E & W	20			384
S	20			392
N	30			368
E & W	30			401
S	30			408
N	40			369
E & W	40			424
S	40			426
N	50			369
E & W	50			449
S	50			442
N	60			388
E & W	60			477
S	60	5	0.50	459

TABLE 5-5

DAILY AND ACCUMULATED TOTAL RADIATION ON A HORIZONTAL SURFACE AT THE FORT SIMPSON TEST SITE

Date	Daily Radiation Ly/Day	Accumulated Radiation Ly
June 20 *	420	420
21	420	840
22	82	922
23	202	1124
24 *	202	1326
25	595	1921
26 *	595	2561
27 *	467	2983
28 *	467	3450
29 *	467	3917
30 *	467	4384
July 1 *	467	4851
2 *	467	5318
3 *	467	5785
4 *	595	6380
5 *	595	6975
6	667	7642
7	574	8216
8 *	574	8790
9 *	467	9257
10 *	467	9724
11	518	10,242
12	274	10,516
13	581	11,097
14	581	11,678
15	439	12,117
16	528	12,645
17	380	13,025
18	634	13,659
19	570	14,229
20	470	14,699
21	500	15,199
Ave	475	

* Indicates days when values were estimated from partial records, weather conditions, and average values when data was complete.

TABLE 5-6

NET RADIATION AT THE FORT SIMPSON TEST SITE

DATE	STA 1 (ly/day)	STA 1 ACCUM-ULATED VALUE (ly)	STA 2 (ly/day)	STA 2 ACCUM-ULATED VALUE (ly)	STA 3 (ly/day)	STA 3 ACCUM-ULATED VALUE (ly)	STA 4 (ly/day)	STA 4 ACCUM-ULATED VALUE (ly)	STA 5 (ly/day)	STA 5 ACCUM-ULATED VALUE (ly)	AVE DAILY VALUE (ly/day)	AVE ACCUM-ULATED VALUE (ly)
June 20 *	228	228	80	80	243	243	290	290	420	420	210	210
21	228	456	202	282	252	495	290	580	384	804	243	453
22	111	567	127	409	154	649	118	698	60	864	128	581
23	166	733	194	603	233	882	192	890	187	1051	196	777
24 *	166	899	200	803	233	1115	192	1082	187	1238	198	975
25	276	1175	214	1017	283	1398	381	1463	506	1744	288	1263
26 *	276	1451	191	1208	283	1681	294	1757	506	2250	261	1524
27 *	248	1699	191	1399	243	1924	294	2051	323	2573	244	1768
28 *	248	1947	191	1590	243	2167	294	2345	323	2896	244	2012
29 *	248	2195	191	1781	243	2410	294	2639	323	3219	244	2256
30 *	248	2443	191	1972	243	2653	294	2933	323	3542	244	2500
July 1 *	248	2691	191	2163	243	2896	294	3227	323	3865	244	2744
2 *	248	2939	191	2354	243	3139	294	3521	323	4188	244	2988
3 *	248	3187	191	2545	243	3382	294	3815	323	4511	244	3232
4 *	276	3463	214	2759	243	3625	355	4170	492	5003	272	3504
5 *	276	3739	214	2973	243	3868	355	4525	492	5495	272	3776

* Indicates days when values were estimated from partial records, weather conditions, and average values when data was complete.

TABLE 5-6 (CONTINUED)

NET RADIATION AT THE FORT SIMPSON TEST SITE

DATE	STA 1 (ly/day)	STA 1 ACCUM-ULATED VALUE (ly)	STA 2 (ly/day)	STA 2 ACCUM-ULATED VALUE (ly)	STA 3 (ly/day)	STA 3 ACCUM-ULATED VALUE (ly)	STA 4 (ly/day)	STA 4 ACCUM-ULATED VALUE (ly)	STA 5 (ly/day)	STA 5 ACCUM-ULATED VALUE (ly)	AVE DAILY VALUE (ly/day)	AVE ACCUM-ULATED VALUE (ly)
July 6	355	4094	214	3187	264	4132	355	4880	492	5987	297	4073
7	377	4471	194	3381	266	4398	473	5353	437	6424	328	4401
8 *	377	4848	194	3575	266	4664	473	5826	323	6747	328	4729
9 *	276	5124	194	3769	243	4907	294	6120	323	7070	252	4981
10 *	276	5400	194	3963	314	5221	230	6350	323	7393	253	5234
11	262	5662	204	4167	314	5535	302	6652	350	7743	271	5505
12	166	5828	158	4325	214	5749	190	6842	137	7880	182	5687
13	197	6025	162	4487	264	6013	330	7172	470	8350	238	5925
14	197	6222	252	4739	319	6332	310	7482	470	8820	270	6195
15	266	6488	252	4991	319	6651	281	7763	312	9132	280	6475
16	180	6668	115	5106	151	6802	362	8125	346	9478	202	6677
17	288	6956	276	5382	319	7121	191	8316	245	9723	269	6946
18	350	7306	230	5612	265	7386	291	8607	454	10,177	284	7230
19	189	7495	125	5737	139	7525	341	8948	386	10,563	199	7429
20	306	7801	203	5940	190	7715	305	9253	303	10,866	251	7680
21	248	8049	101	6041	126	7841	389	9642	370	11,236	216	7896
Ave	252		189		245		301		351		247	

* Indicates days when values were estimated from partial records, weather conditions, and average values when data was complete.

TABLE 5-7

COMPARISON OF PREDICTED VALUES AND MEASURED VALUES OF NET RADIATION

SENSOR NO.	SLOPE ORIENTATION *	SLOPE ANGLE (DEGREES)	RATIO DIFFUSE/TOTAL	PREDICTED FROM SYNOPTIC ESTIMATES OF SHORT WAVE RADIATION & USING TABLE 5-3 FOR NET LONG WAVE RADIATION LY/DAY	AVE. OF PREVIOUS COLUMN	PREDICTED FROM MEASURED VALUES OF SHORT WAVE RADIATION & USING TABLE 5-3 FOR NET LONG WAVE RADIATION LY/DAY	AVE. OF PREVIOUS COLUMN	MEASURED NET RADIATION LY/DAY	$\frac{(\text{COL 9} - \text{COL 6})}{\text{COL 6}}$ %	$\frac{(\text{COL 9} - \text{COL 8})}{\text{COL 8}}$ %
5	horizontal	0	-	302	302	280	280	350	+16	+25
1	270°	40	.35	431	427	409	405	252	-41	-38
			.40	429		407				
			.45	426		404				
			.50	424		402				
2	0°	45	.35	358	364	336	342	189	-48	-45
			.40	363		341				
			.45	365		343				
			.50	369		347				
3	0°	45	0.35	358	364	336	342	245	-33	-28
			0.40	363		341				
			0.45	365		343				
			0.50	369		347				
4	90°	40	0.35	431	427	409	405	301	-30	-26
			0.40	429		407				
			0.45	426		404				
			0.50	424		402				

*Azimuth of normal to slope measured positively from north through east.

TABLE 5-8

LYSIMETRIC DATA

DATE	TIME OF DAY	ELAPSED TIME FOR TEST (HRS)	HEAT GAIN CAL/CM^2	LANGLEYS PER HR.	AVE WIND SPEED M.P.H.	RELATIVE HUMIDITY %
July 5	10:00 17:00	7	40	5.6	5.1	53
9	10:00 15:00	5	62	12.3	4.8	68
10	10:30 15:10	4.7	31	6.7	4.2	58
11	11:00 15:40	4.7	71	15	7.1	52
12	10:25 16:55	6.5	115	17	8.5	78
13	10:26 17:15	6.8	66	9.5	7.0	67
*	18:00 11:28	17.3	40	2.2	3.0	41
*14	16:15 9:21	17	13	0.8	2.0	59
*15	17:18 9:35	16.3	36	1.7	2.1	-
16	10:25 15:17	4.9	13	2.8	11.0	40
*	16:40 9:19	16.7	75	4.5	2.5	-
17	10:12 16:45	6.3	44	7.0	2.6	93
*	17:14 10:41	17.5	124	7.0	2.1	69
18	12:45 17:30	4.8	13	2.8	4.0	52
*	17:45 9:30	15.8	49	3.1	1.6	-
19	10:16 16:10	5.9	44	7.3	4.2	46
*	16:45 11:30	18.8	62	3.4	4.5	-
20	12:10 16:10	4.0	49	12.3	8.7	60
*	16:37 7:55	15.3	81	4.5	11.0	-
21	11:36 17:30	6.0	49	8.1	9.5	63

* Night time test

CHAPTER VI

CONTROL OF THAWING IN EXPOSED PERMAFROST

6.1 Head Scarp Geometry of Bimodal Flows

The characteristic shapes of the head scarp of bimodal flow slides in periglacial regions have been of interest to observers for a number of years and have prompted a variety of descriptions. Capps (1940) refers to them as "an expanded spatulate-like bowl"; Washburn (1947), as "a horseshoe like shape"; Bird (1967), as "a semi-circular hollow" and Kerfoot (1969), as "an amphitheatre". McRoberts (1973) has speculated on the possibility that this characteristic shape is a self-perpetuating phenomenon associated with the concentration or focussing of radiation within the parabolic shaped bowl. Kerfoot (1969) made a very significant comment in his observation that active flows on Garry Island assumed multi-directional aspects. He reported,

> "It may seem easy to conclude that slope aspect is a dominant factor influencing scarp retreat...however...comparisons made between stakes located around the same mudslumps revealed that the maximum retreat did not always occur on the slopes with the most southerly aspect."

McRoberts and Morgenstern (1974) attempted to rationalize this statement by noting,

> "--the sun will not set during these summer months and solar radiation, especially on steep slopes, will be received on all slopes."

Both the bowl-like shape and the apparent lack of preference

in terms of direction of head scarp retreat may be readily explained by examining the nature of the heat source causing the ablation. The combined latent and sensible heat flux represent 58% of the total heat flux required to maintain the observed melting rate at the Fort Simpson test site. Admittedly net radiation is somewhat directional at this latitude, but this is not of significance on slopes less than 30^{o} (Table 5-4). A typical value from this table suggests that a difference of less than 80 ly/day may exist at a slope of 45^{o}. This differential accounts for less than 14% of the total heat flux at the surface of the permafrost at the test site. These conditions represent an essentially isotropic heat source causing a relatively uniform rate of melting in all principal directions of the compass.

It therefore seems entirely reasonable to expect that a bowl-like shape would develop in reasonably homogeneous material. A suitable comparison would be to consider a standard incandescent light bulb placed and maintained in contact with the sloping surface of an ice sheet. The rate of melting would be expected to proceed equally in all directions with the water running forward out of the lip of the depression. The resulting crater formed under these conditions of heat transfer would be very similar to the profile of the bowl shaped headscarp of natural bimodal flow slides encountered in the Arctic.

6.2 Basis for Control

It is apparent that an exposed body of permafrost combined with favorable summertime atmospheric conditions creates temperature, vapor pressure and possibly turbulent air conditions to allow a positive influx of sensible and latent heat. Thus net

radiation, the latent heat of condensation and the sensible heat flux all combine to provide the heat source for the melting of the frozen soil. Under these boundary conditions ablation proceeds at an unusually rapid pace. The most favorable conditions occur when the melting material is able to slough off of the face and is removed immediately. The rate of melting may be affected by the presence of water discharging from the active layer or from gullies above the headscarp. This water flushes the melted soil off of the slope, increases the mobility of the melted material and is responsible for some thermal erosion. The overall effect may cause differential melting and the formation of gullies in the face of the scarp. The action of this surface water has been noted and well documented by Kerfoot (1969).

If the ablation process is to be retarded or controlled, then the boundary conditions must be altered. As the exposed face becomes covered with accumulating debris, overhanging organic mat or artificial cover the temperature boundary conditions will have changed completely. As soon as the surface begins to dry it will warm to near air temperature. When this occurs the temperature and vapor pressure gradients will have been substantially reduced and ultimately reversed. They will then provide a cooling rather than a heating effect. Under these conditions, net radiation will become the governing heat source and the rate of melting beneath the covering will decrease dramatically.

McRoberts and Morgenstern (1974) have suggested that the average heat flux computed from measured ablation rates may be used as an upper bound in the design of remedial measures for

bimodal flow slides. It appears that conditions are not nearly that severe and that such a value is unrealistically high. If the remedial measures are intended to completely stabilize the retreating slope, then it becomes a matter of creating a surface cover that will eventually form a stable active layer. If heat flux boundary conditions are employed in such a design then the two important variables in the heat balance equation are net radiation and sensible heat transfer. Evaporation or condensation can be ignored because the surface will be essentially dry and the energy added by condensation will be lost when the condensate evaporates. Sensible heat transfer will be negative as energy is transferred from the warm surface to the cooler air. The difference between the net radiation term and the sensible heat loss will represent the amount of heat that is used to warm the surface cover and to melt the frozen material below.

Attempts to evaluate the sensible heat component under similar conditions by any analytical means have met with marginal success. However, rough estimates of the magnitude may be attempted by referring to the work of Budyko (1958), Scott (1969), (1970 a,b) and Berg (1974). They all follow the general theme of adopting a simple equation in the form of:

$$q_H = H\,(T_a - T_s)^n \qquad - - - [6.1]$$

where H = a convection coefficient of varying complexity.

T_a = the temperature of the air.

T_s = the surface temperature.

n = arbitrary exponent varying between 1.0 and 1.2.

Berg (1974) evaluated the energy balance for a paved road surface in New Hampshire. His conclusions were not optimistic:

> "Heat loss by the combined fluxes of convection, evaporation and sublimation is nearly 225% different from measured values and causes the greatest portion of error between calculated and measured heat fluxes (into) out of the ground".

Furthermore, the computed values of the energy balance were inaccurate and more complex relationships were required. These complex relationships required too many parameters to be of practical use in design. He recommended the continued use of surface index factors for most design studies. The alternative to using heat flux boundary conditions is to use an equivalent step temperature or ground surface thawing index as described in Chapter III.

The problem is then reduced to one of computing the required thickness of insulating materials to either prevent melting or to retard the thaw rate to some acceptable value.

6.3 Suggested Methods of Control

The choice of methods and the cost of retarding or controlling the rate of melting of exposed permafrost will depend primarily on:

i) the amount and type of ground ice present in the formation,

ii) the latitude of the site (surface thawing index).

If massive ice is encountered in the exposure, then the lack of soil

particles will seriously limit the use of concepts presented in Chapter III. That technique was based on the assumption that sufficient soil was available in the permafrost to form a stable active layer without serious settlement and destruction of the insulative covering. The presence of massive ice will require a design that will prevent any thaw from occurring or that will allow the exposure to retreat at an acceptably slow rate. The rate of retreat for these latter ground ice conditions may be estimated at different latitudes for varying thicknesses of sand/gravel cover in the following manner.

The depth of thaw is a constant value under these conditions and is equal to the thickness of the gravel cover. The temperature distribution in the gravel will be approximately linear varying from some value T_s at the surface to 0^o C at the thaw front. The heat balance at the thaw front may be described by the equation:

$$-K_1 \frac{\partial \theta}{\partial h} = L(ice) \frac{dx}{dt} \qquad - - - [6.2]$$

where K_1 = the thermal conductivity of the sand/gravel cover.

$\frac{\partial \theta}{\partial h}$ = the temperature gradient in the gravel with h being measured positively downward.

$\frac{dx}{dt}$ = the rate of advance of the thaw front into the ice.

$L(ice)$ = the volumetric latent heat of fusion of ice.

The temperature gradient through the gravel layer is:

$$\frac{\partial \theta}{\partial h} = - \frac{T_s}{H} \qquad - - - [6.3]$$

where H = the thickness of the gravel layer.

The rate of retreat of the head scarp may be computed as:

$$\frac{dx}{dt} = \frac{K_1 T_s}{L(ice)H} \quad - - - [6.4]$$

The total amount of retreat over the thaw season is:

$$X = \frac{K_1 T_s \ (t - t_o)}{L \ (ice) \ H} \quad - - - [6.5]$$

t_o = the time required to thaw through the gravel layer.

$$t_o = \frac{H^2 L_1}{2K_1 T_s} \quad - - - [6.6]$$

Equation [6.6] is the classical Neumannsolution used in Chapter III.

L_1 = the volumetric latent heat of the gravel layer and may be computed from the equation.

$$L' = \frac{\gamma_t \ (w - w_u) \ L'}{1 + w} \quad - - - [3.7]$$

The unfrozen water content w_u is assumed to be zero. The time to thaw through the gravel layer will be small for shallow gravel pads in comparison to the total length of the thaw season. However, this term will become significant when thick gravel covers are used and should not be ignored. Figure 6-1 illustrates the manner in which a sand/gravel cover controls the rate of melting or the amount of retreat over the thaw season. The volumetric latent heat of fusion (L_1) as described by equation [3.7] was computed for:

γ_t = 19.6 kN/m^3 (125 pcf)

w = 10%

K_1 = 0.0065 cal/^{o}C cm. sec.

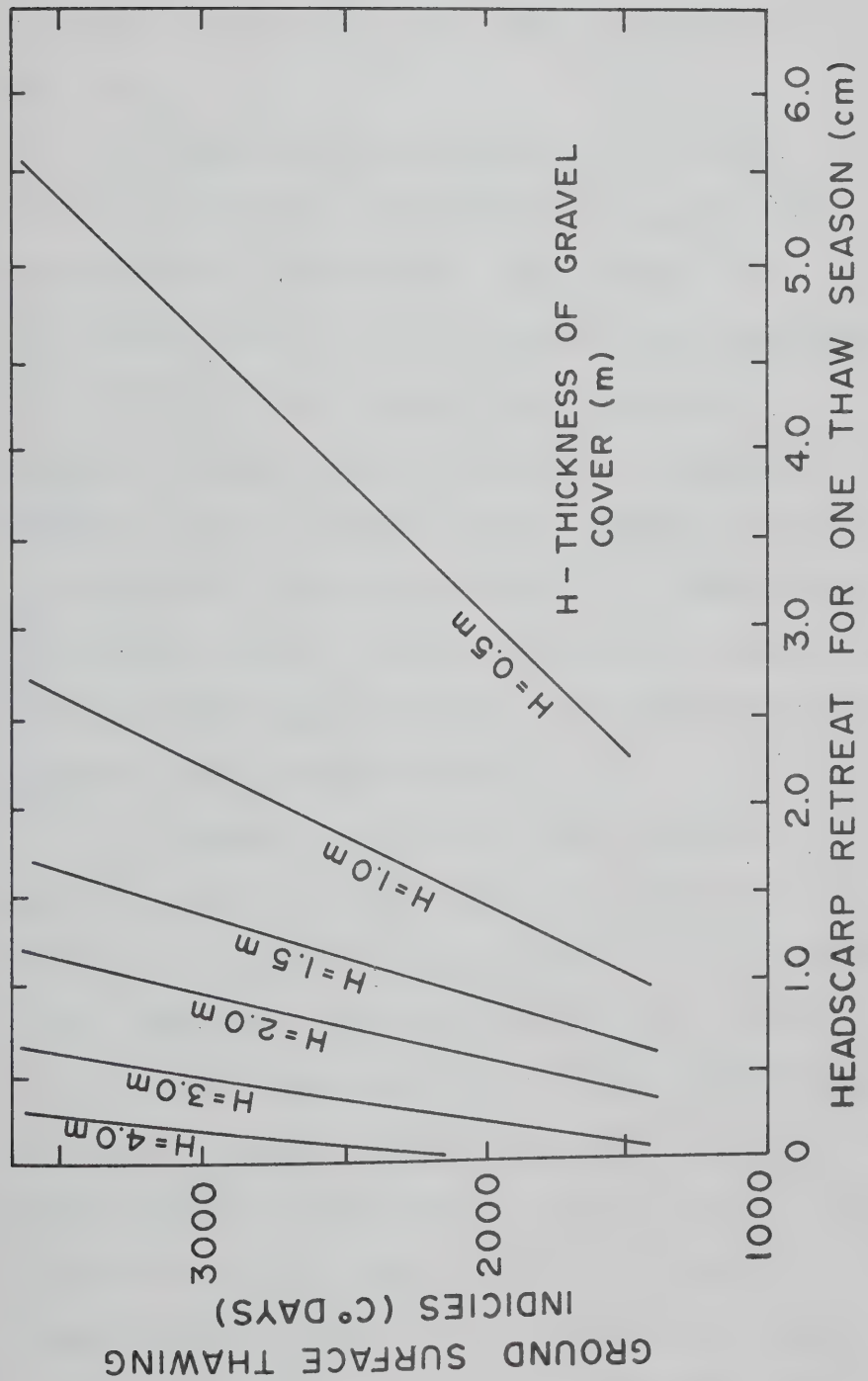

Fig. 6.1 Gravel Thickness, Ground Surface Thawing Index, and Headscarp Retreat for Ice

It is apparent that approximately 4 m. (13 ft.) of sand/gravel cover are required in the subarctic (62^{o}N latitude) to reduce the retreat to less than 0.5 m. (1.6 ft.) per thaw season. At latitudes of 68^{o}N or greater (Inuvik) the thickness of gravel required to maintain the same amount of thawing is only 2.5 m. (8.2 ft).

Other insulating materials may be used in conjunction with sand and gravel. The requirements may be estimated by comparing the ratio of the thermal conductivities. Table III-1 provides the thermal properties of some suitable insulating materials. The ratio of the thermal conductivity of sand/gravel to styrofoam is approximately 100. Therefore, 1 cm. of styrofoam is roughly equivalent to 1 meter of gravel. Thus the use of high quality insulation is attractive in areas where gravel is in short supply. The reader is reminded, however, that the use of a semi-ridgid insulation on well developed bimodal flows may prove to be rather difficult because of their steep biangular profiles.

Exposures that do not contain appreciable quantities of massive ice will be somewhat easier to stabilize because the parent material will generally contain enough soil to form a stable active layer. When these conditions prevail it will generally be sufficient to control the rate of melting until a stable active layer has developed. It would seem that encounters with massive ground ice become less frequent with decreasing latitude. This factor will allow the use of the concepts outlined in Chapter III to be used extensively in the zones of discontinuous permafrost.

In general, any successful design must meet three criteria.

i) it must satisfy the thermal requirements of establishing a favorable heat balance at the surface.

ii) it must provide free drainage.

iii) it must meet the structural requirements of strength and durability.

Although sand/gravel is scarce and therefore costly in many regions of the Arctic, its strength and flexibility combined with high permeability and ease of placement make it the most attractive component for any stabilizing scheme applied to degrading permafrost that might be considered.

6.4 Recommended Practice for Cut Slope Design

The need for stabilizing cut slopes in frozen soils will depend primarily on the amount and type of ground ice exposed in the cut, the soil type, and the depth of the cut. Other considerations involving the potential environmental impact and general aesthetics may also dictate the need for backslope preservation.

6.4.1 Self-Healing Cut Slopes

Many cut slopes will be self-stabilizing over the period of one or more thaw seasons. If the maximum retreat is in the order of 2 to 4 meters and the results of the degradation do not seriously interfere with the functional aspects of the transportation facility, then there appears to be little basis for serious concern.

This class of cuts will be common to land forms that are composed of till, colluvial or alluvial silt and sands and other

combinations of rock and soil that are relatively free draining and stabilize at reasonably steep angles. Ground ice forms are predominantly wedges or lenses of limited extent. The soil in between these ice concentrations is often of low water content and relatively thaw stable. The reader is reminded, however, that many of these soil and ice characteristics will not become evident until construction is in progress. It is often difficult, if not impossible, to obtain a true picture of subsurface conditions by existing site investigation techniques.

Nevertheless, if the soil and ground ice conditions that are encountered possess the stated characteristics a number of helpful design and construction procedures may be cited.

1) Steep, short slopes are recommended because they will intersect fewer ice wedges than will long flat slopes.
2) Reasonably wide ditches will provide space for accumulating debris and will allow the placement of rock revetments.
3) Rock revetments placed at the toe of the slope will retain the soil and allow the water released from the melting permafrost to drain into the ditch. These structures will be machine placed and will, therefore, be approximately 2 m. (6 ft.) wide and 1 to 1.5 meters (3 to 5 ft.) high. The material may be crushed rock or gravel.
4) Hand clearing of the trees above the back slope is recommended. The presence of large trees at the top of the slope will cause a substantial increase

in the load on the organic mat as it drapes over the exposed permafrost and will lead to undue tearing. General aesthetics are also improved by eliminating the unpleasant appearance of leaning and fallen trees.

5) The tensile strength of the organic mat may be increased appreciably by fastening a competent wire mesh to the remaining tree stumps.

6) Diversion of surface runoff above the back slope is imperative. This must be accomplished by the use of dykes rather than ditches. Special care should be given to preventing disturbance of the organic cover above the slope during all construction activity.

7) Revegetation measures are desirable as they reduce the erosion potential by mechanically binding the soil particles together and also help to improve the heat balance at the surface. The use of rapidly growing nurse crops are encouraged along with the establishment of slower growing shrubs and grasses.

8) The depth of cut should be limited to 4 to 5 meters (12 to 15 ft.) whenever possible if these self-healing techniques are to be successful.

9) Rapid excavation and subcutting with immediate replacement of granular subgrade materials is essential if construction is occurring during the summer months. Otherwise melting of permafrost often causes impossible working conditions for men

and equipment.

10) Some care should be exercised if explosives are used to loosen the permafrost prior to excavation. Overbreak may cause cracking of the material in the backslope. These cracks will provide access for surface water. Increased rates of thawing along these fracture planes may result in the failure of large chunks of otherwise intact material.

6.4.2 Non Self-Healing Cut Slopes

When transportation facilities encounter terrain units that possess less favorable geotechnical properties related to soil and ground ice conditions, a more positive form of cut slope preservation must be employed. The land forms most likely to cause the greatest concern regarding cut slope degradation are the proglacial lake bed sediments and fluvial reworked tills common to the Mackenzie Valley and the ice cored topography in the regions north of Inuvik. The methods employed in these areas will also find application as remedial measures at locations where self-healing techniques proved unsuccessful.

Construction of steep slopes in these locations may initially appear to be appealing due to the reduced quantity of excavation. However, excessively steep slopes may require large quantities of excavation if a stabilizing or preserving technique such as that shown in Figure 6-2 is employed. Slope protection techniques will vary with angle of the slope and the relative abundance of insulating materials.

Figure 6-2 illustrates a suitable stabilizing technique for steep slopes or exposed head scarps with established biangular

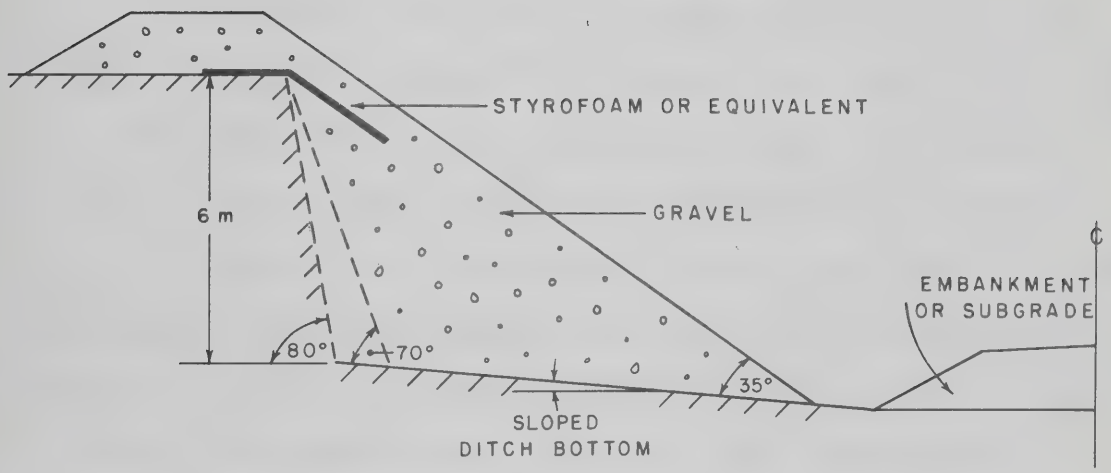

Fig. 6.2 Gravel and Artificial Insulation Configuration for Steep Slopes

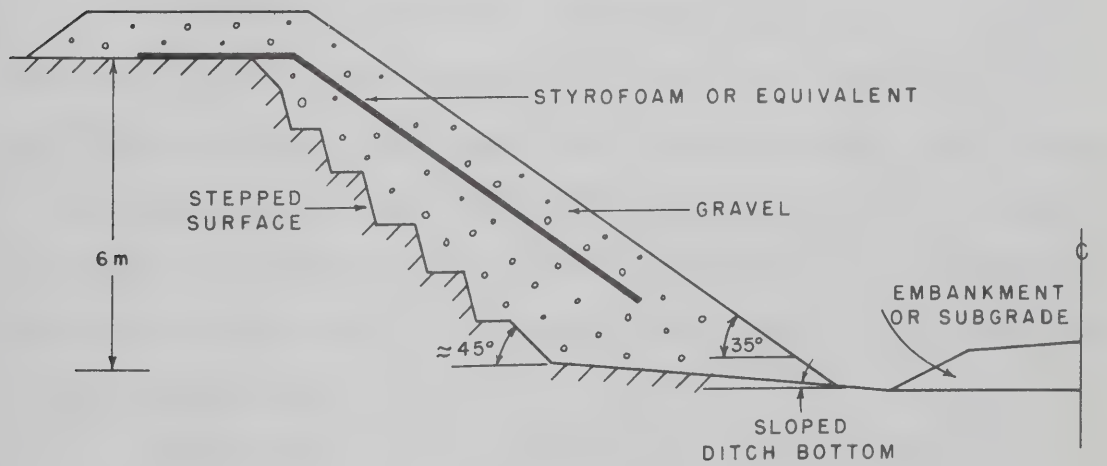

Fig. 6.3 Gravel and Artificial Insulation Configuration for Moderately Steep Slopes

profiles. A large quantity of gravel is required in this instance. Styrofoam insulation (or its equivalent) may be used near the top to reduce the thickness of gravel in that part of the exposure. This configuration will not likely receive serious consideration in right of way cuts because of the excessive quantities of excavation required to provide adequate space for the gravel cover.

Figure 6-3 illustrates a plausible design for steep cut slopes. This configuration would be suitable for slopes of (15 to 20^{o}) to (50^{o}). The choice of the lower bound was based on an assumed friction angle of gravel on permafrost containing significant quantities of massive ice. This aspect of the design may require further consideration by some simple model and field tests of sand/gravel on melting ice. The cut surface is stepped to provide mechanical interlocking of the permafrost and the gravel cover. The inclusion of artificial insulation is an optional feature in this design and will again depend on the abundance of sand/gravel materials.

Figure 6-4 is an example of slope preservation in areas where the slope is steep, gravel is scarce and where erosion may be particularly severe. The design shows styrofoam (or equivalent) sandwiched between gravel and/or rock filled gabions. The inner gabions are required for drainage. A free draining gravel or rock revetment should be placed at the toe to increase the stability of the cover and to preserve the base.

A variation of this configuration would be a combination of Figure 6-3 and 6-4. Drainage would be provided at the cut face by loose gravel placed at a stable angle of approximatley 35^{o}. Insulation would be placed over the loose gravel and then secured with rock/gravel

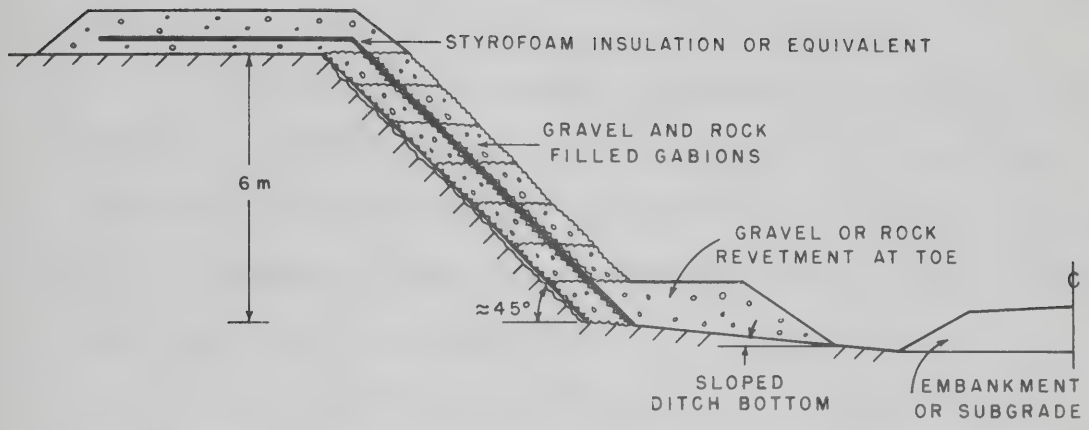

Fig. 6.4 Gravel and Rock Filled Gabions with Artificial Insulation on Moderately Steep Slope

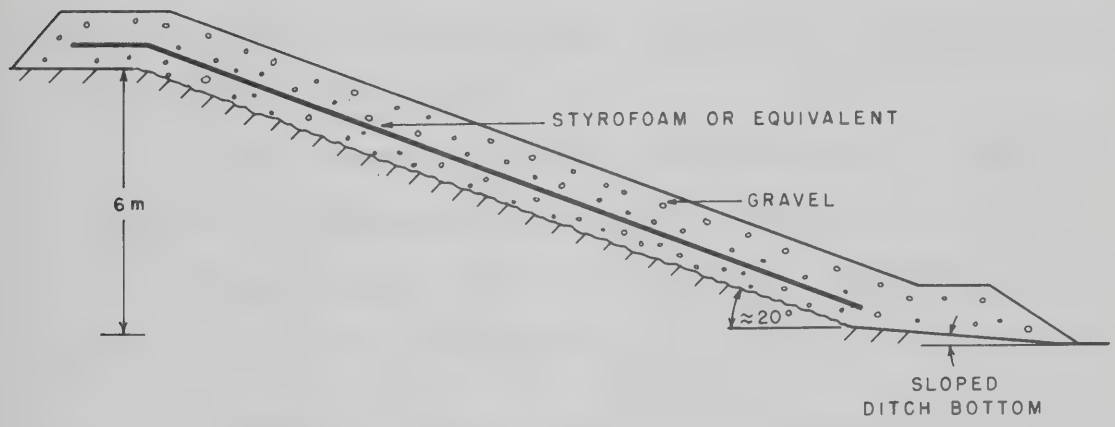

Fig. 6.5 Gravel and Artificial Insulation on Low Angle Slope

filled gabions. In this case the gabions would be used for erosion control only, as loose gravel placed over the insulation would be stable at this angle.

Figure 6-5 is an example of a stabilizing technique for slopes of 15 to 20^{o} or less. Again styrofoam (or its equivalent) is optional in this design. The surface of the cut should be deliberately roughened to ensure some degree of mechanical interlocking between the gravel and permafrost.

It is important to emphasize that all construction and stabilization or preservation measures should be undertaken during the months of the year when freezing air temperatures prevail. It will be difficult if not impossible to perform the required operations while melting is in progress.

The foregoing section has provided a series of possible combinations of sand/gravel and insulation that may be used to preserve slopes and prevent excessive degradation. The essential requirements in any of these combinations are to provide:

1) drainage at the surface of the permafrost.
2) sufficient flexibility, strength, durability and stability of the covering.
3) sufficient insulation to retard to melt rate to some acceptable value.

Other combinations of materials may be considered and various types of insulation may be used. These factors will be left to the imagination of the designers who will be responsible for providing the details of a working design for a field installation.

CHAPTER VII

CONCLUDING REMARKS

The field reconnaissance has shown that limited instability of highway back slopes may be encountered in almost all regions of permafrost. It has also defined the factors which appear to control the performance of cuts in these regions. Emphasis has been placed on the knowledge of the geological history and the recognition of associated land forms over which transportation routes are to be located. There appears to be substantial evidence to suggest that soil types, amounts of ground ice and ground ice patterns are all closely associated for any given land form.

The evidence of natural instability in any given region continues to be one of the most reliable indicators regarding the anticipated behavior of cuts in frozen soils. A variety of methods have been used by highway designers to prevent continued degradation of thawing back slopes. It was, however, clear that none of the existing roads had encountered extensive deposits of glacio lacustrine deposits of ice rich material which are common in the Mackenzie Valley and adjacent areas. The present methods of stabilization occurred in areas where the soil was identified as silt or till and the ground ice was present in the form of wedges. The heterogeneous distribution of this ground ice form and the relatively free draining nature of these soils resulted in only limited degradation in most cases. Rock revetments at the toe of the slope and revegetation programs also contributed to the control of slope retreat. Good construction practices involving rapid excavation and subcutting with the immed-

iate replacement of granular subgrade material are essential to any successful road building technique exercised during the summer months. Cuts made with near vertical back slopes will occasionally perform better than those made with sloping surfaces. However, this technique should be used with caution for it will not always provide the desired effect that has been witnessed in areas such as the TAPS Haul Road in Alaska.

A more thorough understanding of ground ice quantities, patterns, and genesis associated with identifiable land forms would assist in both the route selection and the requirements of subsurface investigation. These endeavours logically follow the initial identification of the geological history and the associated land forms.

The reconnaissance concluded that the experience with cut slopes in permafrost should not greatly inhibit the location and construction arteries across the subarctic and arctic regions.

The need, however, remained to find a suitable and more rational approach to prevent the initiation of potentially serious flow slides on planar surfaces. These remedial or preventive techniques could be used on natural as well as cut slopes. It was recognized from the work of earlier researchers that the excess pore pressures generated during thaw consolidation and the resulting decrease in effective stress was fundamental to any stabilizing technique. As a result, an effective means of stabilizing planar landslides in thawing soils was developed. The technique utilizes an insulative material to control the rate of melting and thus the generation of excess pore water pressures and a surcharge load con-

sisting of sand/gravel or other suitable material. The free-draining surcharge produces an increase in the normal effective stress disproportionate to any increase in the shearing stress. Numerical procedures were used to provide data for design charts that incorporate all the variables and allow the designer to rapidly determine a suitable combination of insulation and surcharge for most practical problems.

The most latitude for engineering judgement regarding the solution lies in the determination of a representative soil moisture content and the choice of a representative value of the coefficient of consolidation (C_v). The solution requires the use of a surface thawing index factor (N) to determine the surface thawing index. The range of the N parameter for gravel surfaces has limits of 1.5 to 2.0 and therefore any choice within this range will not drastically affect the results.

A field installation using different types of insulation and different combinations of insulation and surcharge would be of great benefit in assessing the effectiveness of the proposal.

A thorough understanding of the energetics of exposed melting permafrost was required to fully explain the ablation process for both cut slopes and naturally occurring bimodal flow slides common to the subarctic and arctic regions. The terms in the heat balance at the head scarp of a typical flow slide were reviewed and a field program was employed to confirm or deny the developed theory. The results indicated that all the terms in the heat balance were positive. Net radiation, latent heat flux, and sensible heat flux

all combine under the temperature boundary conditions imposed by the cold surface and the warm atmosphere above the head scarp. The components provided an uncommonly large heat source which produced the high rates of ablation that had been previously noted and monitored at the test site.

The absolute values of the components will generally not be of interest to the geotechnical engineer, for any attempt to control or retard the rate of thawing will alter the temperature boundary conditions and, therefore, change the heat flux boundary conditions.

Methods of control must provide adequate cover to the exposed melting surface. These covers will allow the surface to warm sufficiently and therefore reverse the direction of sensible and latent heat transfer. The problem is, therefore, resolved into one of computing the required thickness of gravel and/or insulation to reduce the rate of thaw to some acceptable value. The heat flux boundary conditions imposed by an effective surface cover are very similar to those encountered for gravel pads or airstrips in arctic regions. It is recognized that a heat flux boundary condition is the most ideal method of design. However, the problems of evaluating the sensible heat flux term essentially remain unresolved and it appears that temperature boundary conditions provide an adequate basis for design.

Simple computations have provided a means of estimating the thickness of gravel covers required to retard the rate of retreat of head scarps containing massive ground ice to some acceptable level. It is anticipated that the thickness of gravel and/or insulation may be reduced in the lower latitudes of the subarctic (for a given

surface thawing index) where ground ice conditions are less severe. The occurrence of massive ground ice becomes less frequent in these regions and the permafrost contains sufficient soil to form a stable active layer if the rate of thaw is properly controlled.

Recommendations regarding the design and construction of cut slopes were reviewed. They have been divided into two broad categories, those that are self-healing and those that required substantial covers of insulating materials. The basis for differentiation hinges principally on the soil type, and the amount and type of ground ice present in the land form.

Future research should be directed to verifying the effectiveness of the proposed stabilizing techniques for planar landslides, cut slopes and bimodal flows. A field station established in the subarctic or arctic region could provide this information. This station should be located in an area where access is possible by conventional wheeled vehicles.

A variety of insulating materials should be considered as well as different combinations of surcharge and insulation thickness. Instrumentation would be a major consideration in such a project and would include the monitoring of ground temperatures, pore water pressures and slope movements.

Such endeavours will be well received and will provide a measure of further confidence in the development of arctic regions.

REFERENCES

Anderson, E.A. and Baker, D.R. 1967. Estimating incident terrestrial radiation under all atmospheric conditions. Water Resources Research, vol. 3, no. 4, pp. 975-988.

Anderson, D.M. and Tice, A.R. 1972. Predicting unfrozen water contents in frozen soil from surface area measurements. Highway Research Record No. 393, pp. 12-18.

Angstrom, A. 1916. Über die gegenstrahlung der atmospäre. Meteorology Z.33, pp. 529-538.

Ashrae 1963. American Society of Heating, Refrigeration and Air Conditioning Engineers. Guide and Data Book.

Ashrae 1967. American Society of Heating, Refrigeration and Air Conditioning Engineers Guide and Handbook Systems and Equipment, by ASHRAE.

Berg, R.L. 1974. Energy balance on a paved surface. U.S.A. CRREL Technical Report 226.

Bird, J.B. 1967. The physiography of Arctic Canada. The John Hopkins Press, Maryland.

Bliss, R.W. 1961. Atmospheric radiation near the surface of the ground. A summary for engineers. Solar Energy vol. 5, #3, pp. 103-120.

Bostock, H.S. 1957. Yukon Territory, Selected field reports of geological survey of Canada 1898 to 1933. Geological Survey of Canada, Memorandum 284, 650 pp.

Bostock, H.S. 1961. Physiography and resources of the Northern Yukon. Canadian Geographical Journal, vol. 63, no. 4, Oct., pp. 112-119.

Bostock, H.S. 1964. A provisional physiographic map of Canada, Geological Survey of Canada Paper 64-35, 24 pp.

Bowen, I.S. 1926. The ratio of heat losses by conduction and by evaporation from any water surface. Physical Review, vol. 27, pp. 779-787.

Brooks, F.A. 1959. An introduction to physical microclimatology. Davis University of California.

Brown, R.J.E. 1965. Some observations on the influence of climatic and terrain features on permafrost at Norman Wells, N.W.T., Canada. Canadian Journal of Earth Sciences, vol. 2, no. 1, pp. 15-31.

Brown, R.J.E. 1967. Permafrost in Canada. Map published by Division of Bldg. Research, National Research Council Canada (NRC 9769) and Geol. Survey of Can., Map 1246A.

Brown, R.J.E. 1967b. Permafrost investigations in British Columbia and the Yukon Territory. Division of Building Research, National Research Council Canada Technical Paper no. 253.

Brunt, D. 1952. Physical and Dynamical Meteorology. Cambridge University Press.

Budyko, M.I. 1956. The heat balance of the earth's surface. Translation from Russian Office of Technical Services U.S. Dept. of Commerce, Washington.

Budyko, M.I. 1958. The heat balance of the earth surface. U.S. Depth. of Commerce, translation by N.A. Stepanova.

Burns, B.M. 1973. The climate of the Mackenzie Valley - Beaufort Sea. Vol. 1, Climatological Studies no. 24, Environment Canada, Toronto.

Campbell, W.G. 1961. The search for oil in the Yukon Territory. Canadian Geographical Journal vol. 63, no. 4, pp. 120-129.

Capps, S.R. 1919. The Kantishna Region, Alaska, U.S. Geological Survey Bulletin 687, pp. 7 - 112.

Capps, S.R. 1940. Geology of the Alaska Railroad. U.S. Geological Survey Bulletin 907, 197 pp.

Carslaw, H.S. and Jaeger, J.C. 1947. Conduction of heat in solids. Clarendon Press, Oxford, England.

Chang, J. 1958. Ground Temperature. Vol. 1, Harvard University, Blue Hill Meteorological Observatory, Milton, Mass.

Department of the U.S. Army and Air Force 1966. Calculation methods for determination of depths of freeze and thaw in soils. TM5-852-6 and AFM88-19, chap. 6, 90 pp.

Dines, W.H. and Dines. L.H.G. 1927. Monthly mean values of radiation from various parts of the sky at Benson, Oxfordshire. Memoirs of the Royal Meteorological Society, vol. 2, no. 11, pp. 1-9.

Dow Chemical of Canada Ltd. 1972. Application and product manual.

Dyer, A.J. 1961. Measurements of evaporation and heat transfer in the lower atmosphere by an automatic eddy correlation technique. Quarterly Journal Royal Meteorological Society, vol. 87, pp. 401-412

Eakin, H. 1919. The Cosna Nowitna region, Alaska, U.S. Geological Survey Bulletin 667, pp. 5 - 53.

Elsasser, W.M. 1942. Heat transfer by infrared radiation in the atmosphere. Harvard meteorological studies no. 6, Harvard University printing office.

Environmental Impact Statement, proposed Trans-Alaska pipeline system (EISPTAPS) 1972, vol. 2.

Ferrians, O.J. Jr., Kachadoorian, R. and Greene, G.W. 1969. Permafrost and related engineering problems in Alaska. U.S. Geological Survey Professional Paper 678, 37 pp.

Field, R.T. 1967. Measurement of factors of the energy balance of natural surfaces. Factors of the heat and water balance of different surfaces. John Mather et al, C.W. Thornthwaite Associates, Elmer, N.J., Oct. 1967.

Frankenberger, E. 1960. Beitrage internationalen geophysikalischen Jahr 1957/58. Berechte Deutschen Wellerdrenstes no. 73 Bad Kissingen.

Fritz, S. and MacDonald T.H. 1949. Average solar radiation in the United States. Heating and Ventilating, vol. 46, July, 1949, pp. 61-64

Garnier, B.J. and Ohmura, A. 1968. A method of calculating the direct short wave radiation income of slopes. Journal of Applied Meteorology, Oct. 1968, vol. 7, no. 5, pp. 796-800

Garnier, B.J. and Ohmura, A. 1969. The evaluation of surface variations in solar radiation income. Solar Energy, vol. 13, 1970, Pergamon Press, pp. 21-34

Geiger, R. 1965. Climate near the ground. Havard University Press, Cambridge.

Gill, D. 1971. Vegetation and environment in the Mackenzie River delta. Unpublished Ph.D. thesis, Dept. of Geography, U.B.C, Vancouver, B.C.

Goss, J.R. and Brooks, F.A. 1954. New constants for the empirical expression for downcoming atmospheric radiation under cloudless skies. Paper presented at 134th national Dec. 54 meeting AMS Berkeley, Cal. (Also see: U.S. Army Corps. of Engineers, 1956).

Green, L.H. 1972. Geology of Nash Creek, Larsen Creek and Dawson Map-Areas, Yukon Territory. Geological Survey of Canada Memorandum 364, 157 pp.

Haag, R.W. and Bliss, L.C. 1974. Energy budget changes following surface disturbance to upland tundra. Journal of Applied Ecology II, pp. 355-374.

Hamon, R.W., Weiss, L.L. and Wilson, W.T. 1954. Insolation as an empirical function of daily sunshine duration. Monthly Weather Review. Vol. 82, no. 6, pp. 141-146.

Hardy, R.M. and Morrison, H.A. 1972. Slope stability and drainage considerations for Arctic pipelines. Proceedings Canadian North Pipeline Research Conference, Ottawa, Canada NRCC Tech. memo 104, pp. 249-266.

Haurwitz, B. 1948. Insolation in relation to cloud type. Journal of Meteorology, no. 5, pp. 110-130.

Heginbottom, J.A. 1971. Some effects of a forest fire on a permafrost active layer at Inuvik, N.W.T. Conference on Permafrost active layer Tech. memo 103, N.R.C. of Ottawa, pp. 31-36.

Hosmer, G.L. and Robbins, J.M. 1958. Practical Astronomy. 4th Edition, John Wiley & Sons Inc., N.Y.

Hughes, O.L. 1972. Surficial geology of Northern Yukon Territory and Northwestern District of Mackenzie, Northwest Territories. Geological Survey of Canada, Department of Energy, Mines and Resources, paper 69 - 36, 11 pp.

Hughes, O.L. 1974. Geology and permafrost in relation to hydrology and geophysics. Permafrost hydrology proceedings of work shop seminar, 1974, Calgary Can. Nat. Committee, The Int. Hydrological Decade, Environment Can., pp. 21-30.

Hume, G.S. 1954. The lower Mackenzie River area, Northwest Territories and Yukon. Geological Survey of Canada, Memorandum 273, 118 pp.

Isaacs, R.M. and Code, J.A. 1972. Problems in engineering geology related to pipeline construction. Proceedings Canadian North Pipeline Research Conf. Ottawa, Canada NRCC tech. memo 104, pp. 147 - 178.

Kachadoorian, R. 1971. Preliminary engineering geologic maps of the proposed Trans-Alaska pipeline route, Livengood and Tanana Quadrangles. U.S. Geological Survey open file.

Kerfoot, D.E. 1969. The geomorphology and permafrost conditions of Garry Island, N.W.T. Unpublished Ph.D. thesis, Dept. of Geography, University of British Columbia.

Kersten, M.S. 1949. The thermal properties of soils. Bulletin 28, Engineering Experimental Station, University of Minn., 1949.

Kimball, H.H. 1928. Amount of solar radiation that reaches the surface of the earth on land and sea and the methods by which it is measured. Monthly Weather Review, vol. 56 U.S. Weather Bureau, pp. 393-398.

Kimball, H.H. 1935. Intensity of solar radiation at the surface of the earth and its variations with latitude, altitude, season and time of day. Monthly Weather Review, Jan. 1935, U.S. Dept. of Agriculture, U.S. Weather Bureau, pp. 1-4.

Klein, W.H. 1948. Calculation of solar radiation and the solar heat load on man. Journal of Meteorology, vol. 5, #4, 1948, pp. 119-129.

Kondratyev, K.Y. 1956. Radiative heat exchange in the atmosphere. Translation from Russian Pergammon Press.

Lachenbruch, A.H. 1959. Periodic heat flow in a stratified medium with application to permafrost problems. U.S. Geological Survey Bulletin No. 1083-A, 36 pp.

Lambe, T.W. and Whitman, R.V. 1969. Soil mechanics. Series in Soil Engineering, John Wiley and Sons Inc., Toronto.

List, R.J. 1968. Smithsonian meteorological tables. Smithsonian Institute Press, Washington, D.C. 6th edition.

Lui, Y.H. and Jordan, R.C. 1960. The interrelationship and characteristic distribution of direct, diffuse and total solar radiation. Solar Energy, vol. 5, #3, July, 1960, pp. 1-19.

London, J. 1957. A study of the atmospheric heat balance. Dept. of Meteorology and Oceanography, N.Y. University. Report AFCRC-TR-57-287 (1957).

Mackay, J.R. and Black, R.F. 1973. Origin, composition and structure of perennially frozen ground and ground ice: a review. North American Contribution to 2nd Int Conf. on Permafrost, Yakutsk USSR NAS Washington, D.C. pp. 185-192.

Mackay, J.R. and Mathews, W.H. 1973. Geomorphology and quaternary history of the Mackenzie River valley near Fort Good Hope. N.W.T. Canada Can. Journal Earth Science 10, pp. 26 - 41.

Mateer, C.L. 1955. Average insolation in Canada during cloudless days. Canadian Journal of Technology, no. 33, pp. 12-32.

Meyers, V.A. 1966. Infrared radiation from air to underlying surface. Technical note 44, Hydro 1, U.S. Dept. of Commerce, Environmental Science Service Administration, Weather Bureau, Washington.

McRoberts, E.C. 1972. Discussion Proceedings Canadian North Pipeline Research Conf., Ottawa, Can. NRCC tech. memo 104, pp. 291-295.

McRoberts, E.C. 1973. Stability of slopes in permafrost. Unpublished Ph.D. thesis, U of A.

McRoberts, E.C. and Morgenstern, N.R. 1973. A study of landslides in the vicinity of the Mackenzie River, Mile 205 to 660. Environmental-Social Committee, Northern Pipelines, Task Force on Northern Oil Development.

McRoberts, E.C. and Morgenstern, N.R. 1974. Stability of thawing slopes. Canadian Geotechnical Journal, vol. 11, no. 4, pp. 447-469.

Mollard, J.D. 1971. Dempster Highway air photo materials search mile 166 - 275. Unpublished report.

Monteith, J.L. 1958. The heat balance of soil beneath crops. UNESCO arid zone research climatology & microclimatology, Proceedings, Canberra Symposium #11.

Monthly Radiation Summary, 1960 - 1964. Canadian Meteorological Branch, Dept. of Transport, Ottawa.

Morgenstern, N.R. and Nixon, J.R. 1971. One dimensional consolidation of thawing soils. Canadian Geotechnical Journal 8, pp. 558-565.

Muller, R.A. 1967. A critical review of energy and water balance analyses of various land cover types. Factors of the heat and water balance of different surfaces, John Mather et al, C.W. Thornwaite Assoc., Elmer, N.J. Oct., 1967.

Muller, F. and Keeler, C.M. 1969. Errors in short-term ablation measurements on melting ice surfaces. Journal of Glaciology, vol. 8, no. 52, pp. 91-105.

Newman, U. 1954. Insolation in relation to cloud amount. Monthly Weather Review, vol. 82, no. 11, Nov., 1954, pp. 317-319.

Nixon, J.F. and McRoberts, E.C. 1973. A study of some factors affecting the thawing of frozen soils. Canadian Geotechnical Journal 10, pp. 439-452.

Nixon, J.F. and Morgenstern, J.R. 1973. Practical extensions to a theory of consolidation for thawing soils. Permafrost: the North American Contribution to the Second Int. Conference, pp. 368-377.

Nyeburg, A. 1965. A study of evaporation and condensation at a snow surface. Arkiv for Geofysik band 4, no. 30, pp. 577-590.

Ohmura, A. 1968. The computation of direct insolation on a slope. Climatological Bulletin no. 3, Jan. 1968, McGill University, Dept. of Geog., Montreal. pp. 42-53.

O'Neill, A.D.J. 1973. The energetics of shallow prairie snowpacks. Unpublished Ph.D. thesis, University of Saskatchewan, Saskatoon, Sask. University microfilm no. 713-18, 664.

Pelletier, B.R. and Stott, D.F. 1963. Trutch map-area British Columbia. Geological Survey of Canada Paper 63-10, 12 pp.

Planck, M. 1959. The theory of heat radiation. New York Dover Publications 1959.

Reitan, C.H. 1963. Surface dew point and water vapor aloft. Journal of applied meteorology, vol. 2, pp. 776-779.

Roggensack, W.D. 1975. Deals with - Geotechnical properties of frozen and thawing soils, Ph.D. Thesis, - In preparation University of Alberta, Edmonton, Alberta.

Sadler, G. W. 1970. Measurement of apparent solar constant and apparent extinction coefficient at Edmonton. Solar Energy, vol. 13, 1970, Pergamon Press, pp. 35-41.

Scott, R.F. 1969. Predicted depths of freeze or thaw in soils by climatological analysis of cumulative heat flow. U.S.A. CRREL Technical Report 195 (AD 696414).

----- 1970a. Validation of the cumulative heat flow technique. U.S.A. CRREL Technical Report 200.

----- 1970b. Study of cumulative heat flow. U.S.A. CRREL Technical Report 201.

Sellers, W.D. 1965. Physical climatology. University of Chicago Press, Chicago.

Sigafoos, R.S. and Hopkins, D.M. 1952. Soil instability on slopes in regions of perenially frozen ground. Frost action in soils, Highway Research Board Report no. 2, pp. 176-192.

Simpson, G.C. 1929. Further studies in terrestrial radiation. Memoirs of the Royal Meteorological Society, vol. 3, no. 21, 26 pp.

Smith, N. and Berg, R. 1972. Observations along the pipeline construction haul road between Livengood and the Yukon River, April 1970 - August 1971. U.S. Army CRREL, Hanover, New Hampshire, unpublished report.

Smith, N., Berg R. and Muller, L. 1973. The use of polyurethane foam plastics in the construction of exedient roads in permafrost in Central Alaska. Permafrost North American Contribution 2nd Int. Conf., Yakutsk, U.S.S.R., pp. 736-745.

Smith, N. and Berg, R. 1973. Encountering massive ground ice during road construction in Central Alaska. North American Contribution Second International Conference on Permafrost, Yakutsk, U.S.S.R., pp. 730-736.

Stefan, 1891. Annual physics and chemistry (Wiedemann) N.F. 42 - See Carslaw, H.S. and Jaeger, J.C., 1960 "Heat Conduction in Solids", Oxford University Press, 1959.

Stephenson, D.G. 1965. Equations for solar heat gain through windows. Solar Energy vol. 9, #2, April - June, 1965, pp. 81-86.

Stephenson, D.G. 1967. Tables of solar altitude, azimuth intensity and heat gain factors for latitudes from 43 to 55^{0} north. N.R.C. - DBR Technical Paper 243.

Streten, N.A. and Wendler, G. 1968. The midsummer heat balance of an Alaskan maritime glacier. Journal of Glaciology, vol. 7, no. 51, pp. 431-440.

Swimbank, W.C. 1955. An experimental study of eddy transports in the lower atmosphere. Technical paper no. 2 CSIRO Division Meteorological Physics, Melbourne.

Sverdrup, H.U. 1942. Oceanography for meteorologists. Prentice Hall, Inc., N.Y.

Taber, S. 1943. Perenially frozen ground in Alaska. Geological Society of America Bulletin 54, pp. 1435-1548.

Thompson, H.A. 1963. Air temperatures in northern Canada with emphasis on freezing and thawing indicies. Proceedings of the First International Permafrost Conference, Perdue University.

Thornthwaite, C.W. and Holzman, B. 1939. The determination of evaporation from land and water surfaces. Monthly Weather Review, vol. 67, 1939, pp. 4-11.

Threlkeld, J.L. 1963. Solar irradiation of surfaces on clear days. Transactions ASHRAE, no. 69, 1963, pp. 24-36.

Threlkeld, J.L. 1970. Thermal environmental engineering. 2nd Edition, Prentice Hall, Toronto.

Threlkeld, J.L. and Jordan, R.C. 1958. Direct solar radiation on clear days. Transactions American Society of Heating and Air Conditioning Engineers. Vol. 64, 1958, pp. 45

Treidl, R.A. 1970. A case study of warm air advection over a melting snow surface. Boundary-Layer Meteorology, vol. 1, pp. 155-168.

U.S. Army Corps of Engineers 1956. Snow hydrology. Summary report of the snow investigations, North Pacific Division, Corps. of Engineers, Portland, Oregon.

Vernon, P. and Hughes, O.L. 1966. Surficial geology, Dawson, Larsen Creek, and Nash Creek map-areas, Yukon Territory. Geological Survey of Canada Bulletin 136, 25 pp.

Vowinckel, E. and Orvig, S. 1962. Relation between solar radiation income & cloud type in the Arctic. Arctic Meteorological Research Group, Dept. of Meteorology, McGill Univeristy, Montreal.

Vowinckel, E. and Orvig, S. 1964. The green house effect of the Arctic atmosphere. Arctic Meteorological Research Group, Dept. of Meteorology, McGill University, Montreal.

Washburn, A.L. 1947. Reconnaissance geology of portions of Victoria Island and adjacent regions. Geological Soc. Americ. Mem. 22.

Wiebelt, J.A. 1966. Engineering radiation heat transfer. New York, Holt, Rinehart and Winston

Wien, W. 1894. Temperature und entiopie der strahlung. Ann Physik series 2 vol. 52 See Sergel, R. and Howell, J., 1972. Thermal radiation heat transfer, McGraw Hill Book Company.

Williams, G.P. 1967. Heat balance over saturated sphagnum moss. Proceedings of the 1st Canadian Conference on Micrometeorology, part 1, Dept. of Transport, Met Branch.

World Meteorological Organization 1966. Measurement and estimation of evaporation and evapotranspiration. Technical note no. 83.

Zoltai, S.C. and Tarnocai, C. 1974. Soils and vegetation of hummocky terrain. Environmental-Social Committee, Task Force on Northern Oil Development, Government of Canada, report no. 74-5.

APPENDIX A

The following Appendix provides the background, observations and detailed descriptions of the road cuts encountered during the field reconnaissance as outlined and summarized in Chapter II.

A.1 Alaska Highway (Mile 222 (from Dawson Creek, B.C.) 57°58N Latitude; 122°46'W Longitude)

A.1.1 Physiography

This section of highway lies within the Interior Plains physiographic province. It is bordered on the west by the Foothills and the Front Ranges of the Rocky Mountains. The region of specific interest is characterized by high buttes and mesas of Cretaceous sandstone (Pelletier and Stott, 1963). The area is drained by several rivers, the nearest of which is the Prophet, lying to the east and roughly paralleling the Alaska Highway. The drainage patterns vary from dendritic in the softer sediments to local trellis patterns where control is established by bedrock structure in the harder sandstone sediments.

A.1.2 Climate

The climate is essentially continental with long cold winters and short generally mild to cool summers. The mean annual air temperature of this area is slightly greater than thirty degrees F and the mean freezing and thawing indices are approximately forty-five hundred and four thousand F degree days respectively. The mean January daily temperature is approximately minus seven degrees F and the mean July daily temperature is approximately sixty degrees F. The average yearly precipitation is approximately seventeen inches with a rainfall of ten inches and a snowfall of seventy inches. Maximum rainfall takes place during June and July. Uniform snowfall occurs during the months of October through March with the amount ranging from ten to thirteen inches per month. The average monthly depth of snow cover for the area is approximately fifteen inches (Brown, 1967(b)).

A.1.3 Permafrost

The location of this section of highway places it just within the southern limit of permafrost (Brown, 1967(a)). Permafrost can exist only in localized areas where unique types of terrain have

maintained its existence. It is found on north facing slopes supporting heavy moss cover, black spruce, alder, and other flora which provide effective ground cover. Flat-lying poorly drained areas supporting sphagnum and feather mosses, Labrador tea, marsh sedge, as well as tree growth consisting of tamarack, black spruce, willow, alder, and birch will harbour remnants of fossil permafrost (Figure 2-2).

At this latitude permafrost is in delicate thermal equilibrium, existing at or near thirty-two degrees F. Construction techniques make no attempt to preserve the ground in its frozen condition.

A.1.4 Bedrock Geology

According to Pelletier and Stott (1963) all formations in the area are of sedimentary origin with the exception of mildly metamorphosed lower Paleozoic rocks some thirty-five miles west of the highway. Upper Cretaceous coarse-grained sandstones, conglomerates, and carbonaceous shales, mainly non-marine in origin, are found to the east with Lower Cretaceous sandstones and shales lying in the Foothills and Rocky Mountain region to the west.

A.1.5 Surficial Geology

This area of study is very near the western limit of the Wisconsin-Laurentide ice sheet and the region adjacent to and east of the highway is largely unaffected by glacial activity.

A thin layer of unsorted drift covers the uplands but may exceed sixty feet in thickness in river valleys. Landforms associated with ice contact sorted drift are largely absent.

The area to the west has been subjected to continental and/or Cordilleran ice. The drift is both sorted and unsorted and appears as tills and bedded clays up to twenty feet in thickness. Similar deposits in the mountains further west may be up to one hundred feet in thickness.

Gravel deposits are found in the form of bars in the bed or the Prophet River as well as terraces along the flanks of the valley wall. Occasional deposits have been noted to the north of Mile 222. These gravel deposits are used as subgrade construction materials and as select borrow for surfacing depending on their abundance, proximity to the road, and general quality.

Small hills or knolls with relief in the order of thirty to fifty feet are evident in the vicinity. They appear to be dead ice or ablation moraine features. Although no comprehensive study has been made of these surficial deposits (to the author's knowledge), the material appears to be a water modified drift. These soft unconsolidated deposits of till are inter-fingered or occasionally covered with fine-grained, sorted material consisting of silts and silty clays.

A.1.6 Highway Details (Mile 222)

Concern for unstable backslope cuts caused by permafrost degradation in this area is slight due to the sporadic occurrence of permafrost conditions.

North facing slopes hosting suspicious vegetation are avoided as are low lying poorly drained areas. Encounters with permafrost in this immediate area are therefore often unanticipated and as a result may lead to some particularly troublesome situations.

A construction project is presently under way on this section of the Alaska Highway. The project consists of realignment, grading, and asphaltic concrete surfacing of a twenty mile section of road.

At Mile 222 the road parallels a small air strip and due to Ministry of Transport regulations a minor relocation was required to maintain specified clearance between the highway right-of-way and the air strip. To accomodate this relocation a twenty to twenty-five foot deep cut with a 2:1 backslope intersecting an eleven degree natural north-facing slope was made into one of the small knolls or hills previously described.

Very wet, partially frozen till with lenses or inclusions of silt and silty clay was encountered. The nature and amount of ice has not been well established. Verbal descriptions by construction personnel suggest that it is of the thin lense variety exhibiting a sirloin type of ice texture. Soil properties are shown in Table 2-1.

Excavation was commenced in the fall of 1972. Problems were encountered with construction equipment due to the wetness of the soil. Rather than face the problems of excessively wet material, frozen ground, and cold weather, excavation was discontinued when the backslope was developed to the design ditch grade. It was felt that melting and/or drainage would occur during the following spring and early summer and the remaining four to six feet of excavation along the centerline of the highway could then be completed.

Effective drainage did not occur. The backslope began to thaw and degrade, blocking the ditch and contributing additional water to an already saturated subgrade.

The degradation beyond the top of the backslope had not been particularly severe at the time of inspection and amounted to approximately fifteen feet in a localized area directly above the silt run. A small vertical backscarp was formed in this immediate area. The repose angle of the silt run is six degrees.

Fig. A-1 provides a pictorial view of the site.

A.2 Dempster Highway

Dawson City, Yukon Territory $64^{o}04'$N latitude, $139^{o}26'$W

longitude; to Fort McPherson 67°26'N latitude, 135°58'W longitude; to Arctic Red River 67°27'N latitude, 134°44'W longitude (Plate II-1).

The Dempster Highway follows an old overland route between the water drainage system of the Yukon and MacKenzie Rivers.

Construction of this highway began in 1959 and consisted largely of improving, grading, and maintaining an existing tote road. Subsequently more money was appropriated to the project with the aim of connecting Dawson City on the Yukon River to Fort McPherson on the Peel River and from this point to Arctic Red on the MacKenzie River and onto Inuvik via the MacKenzie Highway.

The highway lies primarily within the Northern Plateau and mountain area of the Interior System of the Canadian Cordillera. It traverses at least nine different physiographic units (Bostock, 1961). These are in order from south to north: Southern Ogilvie Ranges, Taiga Valley, Central Ogilvie Ranges, Ogilvie Valley, Eagle Plain, Richardson Mountains, and the Peel Plateau (Fig. 2-4).

A.2.1 Dempster Highway (Mile 0 to Mile 80)

Physiography

The Dempster Highway begins approximately 26 miles east of Dawson City and follows the North Klondike River to its source in the Central Ogilvie Mountains. It then parallels the East Blackstone River to approximately Mile 95.

This section of the highway lies almost completely within the Southern Ogilvie Ranges and the Taiga Valley (Bostock, 1961). According to Green (1972), the Ogilvie Mountains consist of compact forms of peaks and ridges separated by intricate networks of valleys and swales. These rise to the east with summits reaching eighty five hundred feet in elevation. Peaks greater than seven thousand feet in altitude are rare in the western part of the Southern Ogilvie Ranges.

The Taiga Valley is an east-west trending valley approximately one hundred and twenty miles in length and forty miles wide. Its surface is formed from long undulating, northward draining valleys, and hills covered by tundra, brush, small spruce, and birch. The Blackstone and Hart Rivers flow across it and into the Northern Ogilvie Ranges.

These rivers provide a natural corridor of travel into the Central and Northern Yukon.

A.2.2 Climate

The climate of this region is not unlike that described in the previous section. It is essentially continental with long cold winters

and short warm summers. The mean annual air temperature is 23.6 degrees F. The mean freezing and thawing indices for this region are sixty-five hundred and three thousand degree days respectively. Yearly precipitation is approximately thirteen inches at Dawson City of which eight inches is rainfall and the remainder is derived from fifty inches of snowfall. The normal monthly depth of snow cover is approximately eighteen inches in the Dawson area (Brown, 1967(b)).

A.2.3 Permafrost

The entire Dempster Highway lies within the upper half of the discontinuous permafrost region, except for that portion between Fort McPherson and Arctic Red River which lies in the continuous zone (Brown, 1967(a)).

A.2.4 Bedrock Geology

The Southern Ogilvie Ranges are developed from or on Precambrian, Paleozoic, Mesozoic, and Cretaceous rocks (Green, 1972). The mountains to the east of the highway are formed from Precambrian, Ordovician, and Silurian sedimentary rocks consisting of quartzite, sandstone, shale, and slate. The mountains to the west, on the other hand, are Cretaceous sedimentary massive quartzite and shales. The entire area contains intrusive igneous rocks that cap the mountain peaks. These porphyry-syenite rocks weather into ruinous peaks and jagged spines often with vertical joint controlled faces that prompted early prospectors to refer to this area as "tombstone country."

A.2.5 Surficial Geology

The region containing the lower portion of the Dempster Highway has been glaciated by a large transection glacier moving from the southeast to northwest and by locally originating valley glaciers (Vernon and Hughes, 1966). The area exhibits evidence of three glaciations. The limits of the intermediate and last glaciations are marked by distinctive moraines. The limit or extent of the oldest glaciation is marked by erratics beyond the limits of the moraines of the two latter glaciations. The upland terrain west of the Klondike River has not been glaciated at least in recent times.

In general there is an abundance of glacial sediments along the lower portion of the highway forming recognizable landforms.

A.2.6 Highway Details

Material for the subgrade consisting of dirty gravels was obtained from terrace formations along the west flank of the North

Klondike Valley. Unfrozen material of suitable moisture content was found to a depth of 3 or 4 feet. Below this depth permafrost existed and no attempt was made to use this material until it had thawed and drained. Consequently, borrow pits in this area tend to be rather large and shallow.

Weathered shales and sandstones occasionally outcrop along the route and are used extensively as surfacing material.

Beyond North Fork Pass the highway follows the East Blackstone River. This section of road was built in 1961-62 at design standards somewhat below the previous forty-five miles.

The subgrade embankment was constructed from bouldery till, ice contact sands and gravels, occasional terraces flanking the valley and alluvial sands and gravels from the Blackstone River (Fig. A-2).

The grade line was originally three feet above the surrounding terrain. Thermal subsidence of the road bed has been estimated to be in the order of from one to two feet and substantial maintenance has been required.

Road cuts along this eighty mile section of road were not considered significant. They were small (less than ten feet high) and were stable in all cases.

A.3 Dempster Highway (Mile 80 to Mile 154)

A.3.1 Physiography

The highway departs from the Blackstone River and parallels Big Creek, a tributary of the Ogilvie River to Mile 123 and then follows the Ogilvie River to Mile 154 (Fig. 2-5). The road traverses the following physiographic units as indentified by Bostock (1961): the Central Ogilvie Ranges, the Ogilvie Valley and the Peel Valley.

According to Bostock (1961) the Central Ogilvie Ranges lie between the Taiga and Peel Valleys and trend from east to west. They are composed of long, narrow, single, and paired ridges separated by wide sweeping valleys.

The Ogilvie Valley is similar to the Taiga Valley in that they are both low areas with subdued topography developed on late Paleozoic rocks. These rocks seldom outcrop and the region is covered with organic deposits supporting a growth of stunted spruce (Fig. A-3). Occasional ridges of more resistant rock outcrop due to fold or fault structures (Green, 1972).

The Ogilvie and Blackstone Rivers unite to form the Peel River in the western part of a trough known as the Peel Valley. The

Peel River gathers the Hart, Wind, Bonnet Plume and Snake Rivers and then flows around the south end of the Richardson Mountains and north to the MacKenzie.

A.3.2 Climate

The climate in this section maintains its severe continental nature with mean annual air temperatures of approximately twenty degrees F and mean freezing and thawing indices of approximately seventy-five hundred and twenty-five hundred degree days respectively. Although precipitation records are not available for this area, extrapolation from existing records would suggest amounts to be slightly less than at Dawson City and in the order of ten inches per year.

A.3.3 Permafrost

Permafrost is essentially continuous in this region except for areas immediatley adjacent to major streams and rivers consisting of active flood plain deposits. The depth of permafrost is unknown.

A.3.4 Bedrock Geology

The Ogilvie Ranges are founded on or formed from Precambrian rocks in this region. They consist mainly of dark grey or black argillite, slate, and phyllite, minor grey quartzite and grey weathering, thinly laminated siliceous limestone. Many slopes are shrouded in talus due to severe periglacial weathering.

The Peel and Ogilvie, east-west trending, valleys are developed on relatively soft, late Paleozoic rocks as previously indicated. Outcrops of the more resistant rocks occasionally occur throughout the region.

A.3.5 Surficial Geology

This section of the Yukon Territory lies beyond the limits of either the Laurentide or Cordilleran ice sheet and apparently, precipitation quantities were inadequate to form valley glaciers during the Pleistocene.

Surficial deposits, therefore, consist of talus covered slopes, alluvial fan deposits, active and inactive flood plain deposits. Muskeg is prevalent in this area and unusually thick deposits of reworked fluvial organic matter often cover the coarse gravel of the inactive flood plains.

Pediment slopes consisting of frozen colluvium and alluvial silts interspersed with rock detritus and organic matter are frequent along the flanks of the valleys.

A.3.6 Highway Details

A.3.6.1 Highway Details (Mile 80 - 96)

This section of road was constructed in 1969-70. Reference to Fig. A-4 will show a substantial improvement of the alignment and design standards. Experience gained from the previous sections had indicated that three to four feet of fill was inadequate. Five to six feet of embankment consisting primarily of fairly clean gravel was obtained from the river and stream beds.

Backslope cuts were rare, as the major portion of the road was constructed as a fill section. A minor cut was encountered at Mile 96. The cut varies in depth from eight to ten feet and has a 2:1 backslope. Three to five feet of retreat have occurred in three years and it is apparent that the slope is completely stable.

The genesis of the material at this location is uncertain, but it appears till-like in composition and texture with a relatively low ice content.

A.3.6.2 Highway Details (Mile 96 - 123)

The road enters Big Creek Valley, a tributary of the Ogilvie River and follows it to its confluence with the Ogilvie River.

The highway subgrade is formed from five to six feet of fill consisting primarily of active flood plain gravels from Big Creek.

Maintenance personnel have placed weathered shale bedrock over the subgrade to provide a suitable binder and a smoother wearing surface.

The proximity of Big Creek occasionally forced the location into the flank of the valley wall. At one of these locations (Mile 107.6) a thirty foot cut with 1.5:1 backslopes was made into a side hill. The material is a colluvial silt and weathered shale with organic inclusions. The organic mat is tearing loose and is sliding down the slope; the backslope is, however, completely stable.

Mile 108.9 exhibits a similar situation. The problem is slightly more acute in this instance as the material has a higher silt content, less angular weathered rock and a higher ice content. In this region the cuts were made in the fall of 1969 with no particular problem. Ice lenses and/or wedges up to eight feet in thickness (with an average of two to three feet) were exposed. The ice was described as "tear shaped" and the soil had relatively few small inclusions of ice (Davies, 1973)* suggesting that the ice was of the wedge variety. The slope subsequently stabilized with modest amounts of ditch maintenance. The tongue or frontal lobe is stable at approximately twelve degrees with the upper or back scarp slope at approximately thirty-five degrees (Fig. A-5).

---

* Personal communication.

A.3.6.3 Highway Details (Mile 114)

At Mile 114 the highway still parallels Big Creek and the road, in its present location, is completely stable. However, some disturbance has taken place on the hillside across the valley. This is the location of an old tote road. Disturbance of the terrain has caused thermal subsidence due to the melting of what apparently must have been massive tabular ice. (Fig A-6).

The tote road was located on a natural five to six degree north facing slope. The landform appears to consist of alluvial silt or slope wash derived from the sedimentary bedrock in the adjacent Ogilvie Mountains. The material is a non-plastic silt with only ten to fifteen per cent clay size particles. Atterberg Limits are given in Table 2-1.

The frontal lobe of these ablation features appears to stabilize at approximately nine to eleven degrees. It is of interest to note that this is roughly twice the angle of the natural slope. This is probably the reason that substantial and lengthy flows have not occurred downslope beyond the immediate region of disturbance.

The original activity and disturbance is approximately eight to ten years old as indicated by the largest willows growing on the site.

A.3.6.4 Highway Details (Mile 120.7)

A series of relatively shallow cuts (approximately ten feet or less) were required in this section of road. The backslopes were cut at 2:1 into a terrain sloping at twelve degrees and consisting of ice-rich organic alluvial and/or colluvial silts. Sloughing of the backslopes upon melting has resulted in the material attaining a stable angle similar to that of the original terrain. Some ditch clearing has been required to maintain effective drainage (Fig. A-7).

A.3.6.5 Highway Details (Mile 123 to Mile 154)

The Jackfell Bridge, built by the Canadian Army in 1971, provides the crossing of the Ogilvie River at Mile 122.6. The highway follows the Ogilvie River throughout this section.

The subgrade is constructed from unfrozen sands and gravels obtained from old stream channels and gravel bars in the Ogilvie River.

A number of rock cuts were required where the river was immediately adjacent to the valley wall. These cuts are, of course, completely stable.

A cut sloped at 2:1 was made into a hillside at Mile 139. The material is a frozen organic silt-shale detrital mixture. Some melting has occurred and minor sloughing has resulted. The slope is performing satisfactorily with a minimum of maintenance required to date.

The proximity of the Ogilvie River at Mile 152 required that a cut be made into a southeast facing hillside sloping at twenty-six degrees.

The soil encountered was approximately 80% silt, 20% weathered shale, and was reasonably free of interstitial ice. The excavated material taken from this cut was used as fill in the section beyond so that it is safe to conclude that the material has a gross water content of less than about 15%.

The initial excavation was made in the autumn of 1971 and no problem was evident until the following spring when surface runoff above the cut began eroding gulleys into the face of the 1:1 backslope. The material was deposited below the slope, blocking the ditches and preventing drainage. This material was removed as it collected and the backslope continued to retreat until a thirty foot vertical face developed exposing ice lenses or wedges eight to twelve feet thick and continuous for a distance of forty feet in length (Fig. A-8).

This condition prevailed for the entire 1972 summer season. The following spring gravel from the Ogilvie River was placed over the face of the cut to act as an inverted filter and/or to provide insulation to prevent further melting (Fig. A-9). These remedial procedures appeared to have been effective at the time of inspection.

A.3.7 Summary

Subgrade materials in this section of highway consist primarily of select borrow materials from gravel bars in the adjacent streams and rivers. The usual maintenance problems associated with melting of ice and ice wedges were encountered in the first year or two after the road was constructed, but maintenance crews have comfortably coped with the task of maintaining a highly acceptable riding surface. This seventy-four mile section of road was the highest quality of recently constructed gravel road encountered in the entire field reconnaissance program.

The performance of cuts constructed along this section have been excellent and nothing more than ditch clearing was required to maintain effective drainage except for the single problem located at Mile 153.

It appears that remedial measures employed to cope with this latter problem have been entirely adequate.

A.4 Dempster Highway (Mile 154 to Mile 178)

A.4.1 Physiography

The Dempster Highway departs from the Ogilvie River and ascends the flank of the valley up to the Eagle Plains which are part of the Porcupine Plateau.

According to Bostock (1961), the Eagle Plain is like a "tray with low rounded ridges". It extends north for one hundred and ten miles and is approximately sixty miles wide.

The drainage pattern is dendritic with the streams entrenching their valleys back from the northward flowing Porcupine and Eagle Rivers. The drainage divides between the streams are long even topped connecting ridges with broad gently rounded summits exhibiting three hundred to five hundred feet of relief. Many of these ridges are twenty-five hundred feet or more in elevation.

A.4.2 Climate

The climate continues to become more severe with the northern progress of the road. Scanty climatic records indicate the mean annual air temperatures to be approximately fifteen degrees F. The mean freezing and thawing indices are eighty-five hundred and twenty-two hundred degree days respectively (Thompson, 1963). Precipitation in this region of the Yukon Territory is in the order of nine to eleven inches per year.

A.4.3 Permafrost

Permafrost is continuous in this zone outside of areas immediately adjacent to streams and rivers. Depths vary from a few feet below the surface to over one thousand feet (Campbell, 1961).

A.4.4 Bedrock Geology

The bedrock geology of this area has not been mapped in detail (to the knowledge of the author). According to Mollard (1971), the sedimentary bedrock strata consist primarily of Cretaceous interbedded shales and sandstones. They vary from steeply dipping to essentially flat lying with only slight evidence of some local folding and faulting.

A.4.5 Surficial Geology

This region is unmarked by recent glaciation. The surficial deposits consist of discontinuous felsenmere and/or colluvium over bedrock with extensive cover of organic deposits. The sandstone is more resistant to weathering and therefore forms the tops of ridges and escarpments. The shales on the other hand, are softer and weaker and form smoother more gentle slopes.

The shales can vary from clayey to sandy in composition. The sandstones vary from arenaceous to clayey in composition as they grade into the shales.

Borrow material for the highway subgrade embankment is comprised almost exclusively of weathered sandstone and sandy shales. Cut and fill construction is used extensively on this section of the road.

A.5 Highway Details

The ascent from the Ogilvie River valley represents a change in elevation of some fifteen hundred feet in the space of ten miles. Large side hill cuts were required in combination with reasonably steep grades (eight percent) to maintain reasonable horizontal and vertical alignment. Since these cuts were made into sandstone and shale bedrock deposits, no problems were encountered with stability.

The road location follows the sandstone ridges with the engineering design and construction aspects in complete accord with landscape aesthetics.

A.5.1 Highway Details (Mile 168)

A small cut was made into a side hill sloping at approximately six degrees. The backslope was cut at 1.5:1.

The material is a sandy silt with angular weathered rock inclusions. The soil is obviously ice-rich, (estimated to be approximately 20% excess by volume) but appears to be draining freely.

The melted material is stabilizing at an angle of eleven degrees. The slope has retreated twenty to twenty-five feet during the first thaw season. The slope appears to be stabilizing without total destruction of pre-existing vegetation or without creating an excessively displeasing appearance.

A.5.2 Highway Details (Mile 175)

An eight to ten foot cut was made into a soil formed from weathered shale and sandstone. The material has 25% clay size particles, 45% silt size particles, 20% sand size particles, and 10% gravel size particles and a natural water content equaling or exceeding the liquid limit (35 - 45%). (Table 2-1).

The 1.5:1 backslope is presently retreating and material is sloughing into the ditch. Subsidence is also occurring on the shoulder of the road and in the ditch. This activity is apparently due to the melting of a large tabular body of ice some two to four feet in thickness and fifteen to twenty feet in areal extent (estimated by D.P.W. personnel).

The slope had retreated approximately twenty-five feet at the time of inspection in mid-July (Fig. A-10).

This section of road was built in the Spring of 1973. At this time of year the maximum depth of the active layer had not yet been developed. When subgrade construction material is placed directly on the active layer without stripping, the subgrade tends to undergo substantial differential settlement and cracking as melting proceeds into the active layer during the remaining summer. On the other hand, subgrades that are constructed in late summer and fall tend to be more stable and exhibit less differential settlement. This behavior is attributed to the fact that much of the settlement occurs during the construction period and not after the grading has been completed.

Serious cracking of the subgrade has occurred in this last section of the Dempster Highway. Constant maintenance with heavy motor graders is required to fill the cracks and seal the surface, preventing moisture from entering the subgrade and contributing to its softening and thermal degradation (Fig. A-11).

A.5.3 Summary

The subgrade of this highway segment is built almost exclusively from weathered sandstone, which is obtained from broad shallow borrow pits along the right-of-way.

Excavation of a number of small cuts was performed without major difficulty by maintaining the permafrost in an essentially frozen state. Minor problems of backslope instability are evident but it is felt that stability will be essentially re-established by the end of the 1974 summer season. Some ditch maintenance will be required to sustain drainage requirements in this region.

This represents the present extent of construction of the Dempster Highway in the Yukon Territory.

A section of this highway between Fort McPherson and Arctic Red River in the North West Territories is completed and will be discussed subsequently.

A new contract is presently underway to construct 56.5 miles of road from Mile 178.3 to Mile 236.8 at the Eagle River. This section of road is similar in almost all aspects to the previous twelve miles.

The location follows the summits of the ridges whenever possible and borrow material will consist almost exclusively of weathered sandstone and shale bedrock except where limited quantities of sand and gravel are available from the Eagle River or other lesser streams adjacent to the right-of-way.

A.6 Dempster Highway (Fort McPherson to Arctic Red River, Mile 330 to Mile 365

A.6.1 Physiography

The location is shown in Fig. 2-3 and Fig. 2-5. This region lies within the Peel Plateau, a subdivision of the Interior Plains Province (Bostock, 1964). Hills and ridges in the northeast section rise to an elevation of fifteen hundred feet about mean sea level. The remaining area is relatively flat with many small lakes. Local relief along the right-of-way is usually less than one hundred feet. The major rivers are the Peel in the western part and the Arctic Red running the full length of the region.

A.6.2 Climate

The climate of this area is again continental in character with long cold winters, short warm summers, and low annual precipitation.

The mean annual air temperature is approximately fifteen to sixteen degrees F with a mean annual precipitation of nine inches consisting of forty inches of snow and five inches of rain.

The mean annual freezing index is eight thousand degree days F and the mean thawing index is approximately twenty-one hundred degree days.

A.6.3 Permafrost

This area is well within the zone of continuous permafrost (Brown, 1967). The depth of the active layer is of course related to the soil type, slope, aspect and ground cover. Probings conducted in conjunction with geotechnical investigations for the highway suggest that two feet is an average value.

Vegetation is limited to scrubby spruce, birch, willow, alder, and tamarack, with low ground cover consisting of reindeer and sphagnum mosses, Labrador tea, alder, and berry plants.

A.6.4 Bedrock Geology

Bedrock geology studies indicate interbedded sedimentary Cretaceous shales and sandstones at Fort McPherson and Upper Devonian interbedded shales and sandstones at Arctic Red River.

A.6.5 Surficial Geology

This area has been glaciated by Laurentide ice and the pre-

dominant landform is a hummocky or dead ice moraine. Large areas are covered with silt and organic materials.

Surface drainage is not well developed on the relatively flat terrain and many small lakes dot the surface.

The soil is essentially unsorted drift with thin deposits of fine-grained, ice-rich material draped over and/or filling depressions in the landscape.

A.6.6 Highway Details

The main engineering design problems concerned the stability of various available construction materials, embankment design, and design of drainage structures.

An attempt was made to use the till as embankment material but excessive moisture contents rendered this material generally unsuitable. Consequently the subgrade material consisted almost exclusively of ripped sandy shales.

The feature of special interest to this study is a large cut at Mile 343 (Fig. A-13).

The soil at this location consists of a silty clayey till with a natural water content of twelve to twenty-eight per cent and containing ice lenses or inclusions up to four feet in thickness. Some soil samples contained thirty per cent excess water.

Initial soil investigations did not indicate such large ice contents and plans have been made to use this material excavated from this area as fill for adjacent sections. The use of this material for fill resulted in a substantial saving in haul costs. As a result some of the excavated material was utilized as fill. However, the soil proved to be quite unstable when thawed. A substantial amount of time was required to allow this soil to drain and stabilize before a crushed shale capping could be placed upon it. Much of the material that was removed from the cut was subsequently wasted in adjacent spoil areas.

The resulting cut is approximately one half mile long, thirty-five feet deep, and two hundred and fifty to three hundred feet wide. The backslopes were constructed at 1.5:1 and the minimum stable angle in localized areas was found to be seventeen degrees. The road bed is formed from four to five feet of borrow material consisting of compacted broken shale bedrock.

After the cut had been made (with some difficulty) the ice began melting and the backslopes exhibited fairly serious degradation in various areas of the cut. The amount of retreat was apparently limited to the areal extent of the ice. It appears that retreat of the slope ceased when the excess ice had melted and the water had drained away.

Small amounts of maintenance have been performed on this cut in an attempt to re-establish a more or less planar backslope surface where degradation was most severe. Organic material and small trees, serving as insulation, were placed in one area in an attempt to reduce permafrost degradation. Some ditch maintenance has been performed to sustain effective drainage (Fig. A-13).

At the time of inspection the backslopes appeared to have completely stabilized without serious detrimental results.

This is the most substantial cut on all of the Dempster Highway that has been constructed to date. It is the width and length of the cut rather than the depth or backslope instability that makes it an outstanding feature on the landscape.

A.7 Dempster Highway (Mile 178 to Mile 330)

A brief helicopter reconnaissance was made of the proposed location of the section of Dempster Highway between Fort McPherson and south to Mile 178 of the constructed portion. It was hoped to collect some information regarding the possibility of potential problems regarding slope instability along the proposed route.

A.7.1 Physiography

The Richardson Mountains develop almost imperceptibly from the rolling hills and valleys of the western part of the Peel Plateau. Their highest summits reach fifty-five hundred feet in elevation. South of McDougall Pass (the lowest point in the mountains) they become lower and narrower and are about thirty-five hundred feet in elevation (Bostock, 1961).

A.7.2 Climate

Climatic records are sparse for this region. Mean annual air temperatures are probably somewhat less than at Fort McPherson due to the increased altitude. The freezing and thawing indices are eighty-five hundred and twenty-one hundred F days respectively.

A.7.3 Permafrost

Permafrost is essentially continuous in this region.

A.7.4 Bedrock Geology

Bedrock geology is not well known for this particular region. It can be inferred from Hume (1954) and Bostock (1957) that the area is underlain by, and the mountains are formed from, interbedded sedimentary rocks of Devonian to Cretaceous Age.

A.7.5 Surficial Geology

This region lies east of the western limits of the Wisconsin and Pre-Wisconsin glaciation (Hughes, 1972). This history provides a basis for the occurrence of glacial moraines, glacio-fluvial, and fluvio-lacustrine deposits that may be ice-rich and exhibit total instability when thawed.

Beaded drainage, patterned ground and solifluction slopes are common in this area.

A.7.6 Observations

Several naturally occurring bi-modal flow slides were noted in the Richardson Mountains near the Yukon-North West Territories border. Some of these flows have run their course or have become dormant, while others are presently very active. None of these flows were in close proximity to the proposed right-of-way.

An excellent example of one of these active flow slides is shown in Fig. A-14. The light colored material on the left is definitely a till with twenty-five percent gravel size particles, ten per cent sand size particles, thirty-five per cent silt size particles, and thirty per cent clay size particles. This soil has a liquid limit of thirty-three per cent and a plastic limit of twenty-three per cent. The dark area is a very ice-rich silty clay or clayey silt with fifteen per cent sand size particles, fifty per cent silt size particles, and thirty-five per cent clay size particles. This latter soil has a liquid limit of forty per cent and a plastic limit of twenty-one per cent. It was not possible to establish the nature of the ice in the headscarp but it was, however, evident that the material below the upper two feet was almost pure ice.

This flow slide is occurring on a southeast facing natural slope of seven degrees. The headscarp angle varies in slope from near vertical to approximately fifty degrees in the lower section just above the flat-lying seven degree lobe. The land form appears to be an alluvial fan. However, the uniform surface of the undisturbed terrain may be slide debris deposited from an old flow.

A.7.7 Summary

The Dempster Highway between Fort McPherson and Arctic Red River is an excellent gravel highway. Although the observers did not travel the road by surface transport, it is reported to be comfortably negotiable at speeds in excess of fifty miles per hour (Aspden, 1973).*

Only one cut was encountered along the route. Although it had caused the designers and builders considerable concern in the initial stages, it has subsequently stabilized without serious consequences.

It would appear that cuts made in regions where the landform is a ground moraine should not create major problems under normal circumstances.

---

* Personal communication

Flow slides as encountered in the eastern reaches of the Richardson Mountains and along the Mackenzie River have been observed to occur primarily in regions that have been subject to either continental or valley glaciation. Sediments encountered at these sites consist of significant quantities of ice-rich fine-grained lacustrine deposits.

A.8 Mackenzie Highway (Inuvik to Arctic Red River)

A section of the Mackenzie Highway is being constructed south from Inuvik and another section north from Arctic Red River. Helicopter reconnaissance was made of these sections of road. No cuts of significance were encountered on the Inuvik section.

A large cut was being constructed on the north approach to the Mackenzie River crossing at Arctic Red River. The maximum depth of the cut is approximately forty-five feet. The section exposed from fifteen to twenty-five feet of ice-rich fine-grained sediments over interbedded shale and sandstone bedrock. The cut was designed with 1.5:1 backslopes but they were increased to 1:1 in the bedrock portion in order to obtain more borrow material. The thickest part of the overburden occurred on the south or southwest facing bluff of the Mackenzie River. This material was quite low in water content and it was assumed that this portion of the cut would be thaw stable. As excavation proceeded away from the river bank, the overburden soils increased in ice content. Unfortunately no accurate soils data exist for these fine-grained sediments. The engineering personnel, however, decided that excessive ice contents would result in unstable backslopes when thawing began. To prevent such an occurrence, the slope was benched at the bedrock level and the ice-rich fine-grained sediments in the upper portion of the slope were dressed with ten feet of crushed shale.

The slope has been exposed during the 1973 summer season and it appears to be performing satisfactorily (Fig. A-15).

A.9 Alaska Reconnaissance

A.9.1 General

The roads in Alaska, to date, have been built in the discontinuous permafrost zone except for minor activity on the Arctic Coast. The designers for the most part have been able to choose their locations judiciously and thus avoid cuts where ice-rich fine-grained soils were suspected. Even so, demands from the oil industry have created a need for road locations that do not allow the designer as much latitude in choice of route. The Trans-Alaska Pipeline System (TAPS) Haul Road is an example of this type of problem.

The TAPS Haul Road begins some sixty miles northwest of Fairbanks and presently extends fifty-five miles beyond to the Yukon River (1973). This road will eventually extend north to Prudhoe Bay on the Arctic Coast and will provide facilities for ground surface transport

of all supplies and personnel required for the construction of the proposed Trans-Alaska Pipeline System.

The great difficulty associated with the routing of this road is that it crosses the "grain" of the country. Its origin and destination require the route to climb south-facing slopes and descend north-facing slopes (Fig. 2.6).

A.9.2 Physiography

The TAPS Haul Road originates at 65°39'N latitude; 148°39'W longitude and terminates at 65°52'N latitude; 149°37'W longitude.

The road crosses two physiographic regions: the Yukon-Tanana Upland in the southern portion and the Rampart Trough in the northern section.

The climate, permafrost conditions and surficial geology of the two physiographic regions are very similar and only the physiography and bedrock geology are significantly different.

The Yukon-Tanana Upland is part of the Northern Plateau physiographic province of the Intermontane Plateau system (Environmental Impact Statement Proposed Trans-Alaska Pipelines System (EISPTAPS) Volume 2, 1972). Broad undulating divides and flat-topped spurs characterize this section of even topped ridges. These rounded ridges trend northeast to east with elevations of fifteen hundred to three thousand feet and rise five hundred to fifteen hundred feet above adjacent valley floors. Occasional mountain peaks rise from four thousand to five thousand feet in elevation. The valleys in the western section (adjacent to the TAPS right-of-way) are from one quarter to one half mile in width. They are flat and are generally filled with alluvium.

The entire section is in the Yukon drainage basin with streams flowing south to the Tanana River and north to the Yukon River. The drainage pattern is controlled by the bedrock structure and the streams trend northeast-southwest so that no opportunity is created to cross the "grain" of the country by following natural drainage channels.

The Rampart Trough lying directly north of the Yukon-Tanana Upland is a large depression eroded five hundred to twenty-five hundred feet into sedimentary rocks. This lowland exhibits gently rolling topography five hundred to fifteen hundred feet in elevation.

This trough contains the broad and sometimes meandering Yukon River. The only two significant tributaries traversed by the road are Hess Creek and Isom Creek.

Occasional thermokarst lakes dot the broad Yukon flood plain and may be found in the surrounding terrain.

A.9.3 Climate

The climate of this region is dominated by continental climatic conditions characterized as usual with long cold winters and relatively short warm summers. The mean maximum and mean minimum temperatures for January are minus four to minus six degrees F and minus sixteen degrees F respectively. The mean maximum and mean minimum temperatures in July are seventy-four degrees F and forty-six degrees F respectively. The mean freezing and thawing indices are sixty-five hundred and three thousand degree days respectively.

A.9.4 Permafrost and Vegetation

The entire fifty-five mile section of the TAPS haul road lies within a zone that is underlain by discontinuous permafrost (Ferrians et al, 1969). The active layer varies in depth along the route depending on landform, exposure, aspect, and vegetation. Probings suggest it to be eighteen inches to ten feet below the surface.

Most of the area is covered by dense forest. The well-drained areas support white spruce, white birch, aspen, and balsam poplars. Upland areas where drainage is poor support heavy stands of black spruce.

The lower slopes and valleys are often covered with black spruce heath and small birch shrubs. Ground cover consists of the usual sub-arctic mosses and shrubs.

Abrupt changes in vegetative cover are characteristic of this region (Fig A-16). These changes are related to terrain aspect, moisture and soil nutrient levels, and depth of active layer.

The vegetation patterns were quite confusing to the route locaters and designers. Areas supporting healthy stands of white spruce and birch with occasional aspen were considered to be preferred routes. However these sites often contained extremely ice-rich sediments and caused the designers and builders as much trouble as did the sites with more easily recognized vegetation types normally associated with difficult terrain.

A.9.5 Bedrock Geology

The Yukon Tanana Upland is formed from a zone of highly deformed Paleozoic sedimentary and volcanic rocks containing limestone deposits along the north side of the Upland (Kachadoorian, 1971). The remainder of the region is primarily Precambrian schists and gneisses with small scattered granitic intrusions in the northwestern part.

The bedrock geology of the Rampart Trough consists of tightly folded soft continental coal bearing sedimentary rocks of Tertiary age. The surrounding uplands and hard rock hills of Mississippian age are

partly metamorphosed with volcanic rocks and occasional granitic intrusions (ibid).

A.9.6 Surficial Geology

Kachadoorian (1971) states that this segment of Alaska is unglaciated and surficial deposits are composed of reworked wind blown silt, colluvial and alluvial silt, sand and rock fragments, dune sand and alluvial sand and gravel. These sediments are unconsolidated, usually frozen and often very rich in ice. Ice forms include wedges, lenses, and interstitial ice.

A.9.7 Highway Details

The TAPS Haul Road was built in 1969 and 1970 so that sufficient time has elapsed to allow a critical evaluation of the behaviour of the backslopes and subgrade.

The road had many substantial cuts on north-facing slopes that exposed what was termed as "massive ice". Certainly the ice did appear massive, in that cuts in the order of twenty feet had twelve feet of ice exposed in the section. However, the tabular extent of these ice exposures was not and has not been established.

Many of the cuts were excavated with vertical or near vertical faces with the thought that prior to any self-healing, the cuts would have to melt back into a vertical position. The upper covering of soil and organic mat would then slough down over the melting ice and thus provide sufficient insulation to re-establish a stable ground thermal regime. Vegetative cover would then establish itself on the sloughed material, thus preventing erosion and any further fouling of the ditches.

Inspection of these cuts in the summer of 1973 indicated that the backslopes had essentially stabilized. Many slope angles are very steep (thirty-five to forty degrees) and the present conditions probably do not represent long term stable slope angles for most of the colluvial silt encountered along the route. It is therefore conceivable that adverse pore water pressure conditions developing in the backslope could initiate instability, re-expose ice wedges, and re-initiate the cycle of melting, sloughing, draining, and self-healing.

A.9.7.1 Highway Details (Mile 14)

Massive ice was encountered in a series of cuts along this section of road (Wellman, 1973).* The cuts varied in depth from ten to

---

* Wellman (1973) Personal communication.

twenty-five feet with ice conditions being the most serious on the poorly drained tops rather than the slopes. These cuts were excavated with 2:1 backslopes and the photographs indicate that reasonably serious but limited degradation has occurred in many locations. The tree cover was removed by hand to prevent rupture of the moss cover and it has draped itself over the retreating slope (Fig. A-17).

Beaded drainage is developing in the ditches along this section of road.

A.9.7.2 Highway Details (Mile 19.6)

Cuts, typically fifteen to twenty feet deep with 1.5:1 backslopes were constructed along this section of road.

Crushed rock revetments have occasionally been placed at the toe of some of these slopes to retain the soil and allow the water to filter through into the ditch bottom.

Revegetation of the slopes has developed remarkably well. This is due primarily to extensive hydroseeding programs that were preformed subsequently to construction.

Although no borehole data is available for this specific section it is felt that Fig. A-18 is representative of this area. The borehole location is approximately one mile northwest of Mile 20 and adjacent to the proposed TAPS route.

Photos dating from May, 1971 to June, 1972 are available for comparison for this section of road (Smith and Berg, 1973). The conditions of the backslope are illustrated in Fig. A-19 (1973).

A.9.7.3 Highway Details (Mile 20.3 to Mile 20.5)

A long cut varying from twenty to forty feet in depth with 1/4:1 backslopes was made into a north-facing slope with essentially the same or similar ground profile as described in the previous section.

This section of road was referred to as the "ice tunnel", due to the massive ice exposed on either side of the road. The backslopes have since become essentially stable at slopes of thirty-five to forty degrees. The vegetation is becoming well established and the slopes are not aesthetically objectionable to the road user.

A series of photographs dating from June, 1970 to Aug., 1971 illustrate the genesis of this section (Smith and Berg, 1973). Fig. A-19 illustrates the conditions of the backslope (July, 1973).

A.9.7.4 Highway Details (Mile 22.9)

A fifteen to twenty foot cut with backslopes of 1/4:1 was

required at this location.

Shallow boreholes (fourteen feet in depth) were made prior to construction. They indicated four to six feet of organic matter with silt with ice, or ice with silt extending to the bottom of the borehole. Boreholes subsequently drilled along the right-of-way and within one half mile of this location indicate in excess of thirty-two feet of massive ice.

The slope has degraded approximately seventy-five feet in localized areas. The frontal lobes are stable at seventeen to twenty-three degrees. The slopes are being revegetated and appear to be functioning satisfactorily. Some ditch blockage has occurred in this region.

Fig. A-21 provides a view of the cut shortly after construction was completed in April, 1970. Fig. A-22 illustrates the condition of the backslope in July, 1973.

A.9.7.5 Highway Details (Mile 23.4)

The approach to Hess Creek required a thirty foot cut to maintain suitable horizontal alignment. The backslopes were constructed at 1/4:1 and exposed fifteen to twenty feet of massive ice.

Special concern was expressed about the future stability of the backslopes of this particular section because of disturbance of the terrain above the slope associated with the contractor's activity. The tree cover had been removed and the moss cover damaged by equipment using a temporary access road.

Rock revetments have been placed at the toe of the slope to retain the sloughing soil. Insulation was placed on the disturbed terrain above the cut to prevent excessive degradation.

Results from limited probing data indicate that the thaw depth on the face of the slope in July, 1973 was approximately three feet, two to eighteen inches under the insulation, and eighteen inches in the undisturbed forest cover.

The thawed slope has become essentially stable at angles varying from twenty-five to thirty-five degrees. A scalloped pattern has developed subsequent to the melting of the ice. This pattern may have resulted from the melting of ice wedges rather than tabular ice bodies of significant extent.

It is difficult to confirm or deny such an assertion without an extensive drilling program or visual logging of ground ice patterns during excavation.

Fig. A-23 illustrates the cut shortly after construction was

completed. Fig. A-24 illustrates the condition of the backslope in July, 1973.

A.9.7.6 Highway Details (Mile 33.0 to Mile 33.4)

A series of cuts varying from fifteen to sixty feet were required in this short section approaching an unnamed tributary to Hess Creek.

Part of this large cut was benched in bedrock. The bedrock surface is irregular and the swales and smaller rises are covered with ice-rich colluvial and/or alluvial silts. Cuts made in this latter material exhibited extensive instability after construction. Some of these smaller cuts developed a bi-modal flow profile with five to six foot near vertical headscarps and lobe angles of fifteen degrees.

The backslopes, originally cut at 1.5 to 1 are essentially stable after retreating seventy-five to one hundred feet from their original position.

Revegetation procedures have again produced backslopes which are satisfactory to even a critical viewer. Hand clearing that was apparently done during the winter, has left four foot stumps protruding above the moss cover, a particular feature that does nothing to enhance the aesthetics of this section. Fig. A-25 illustrates the backslope of one of the smaller cuts in this section.

A.9.7.7 Highway Details (Mile 42.8)

A twelve to fifteen foot cut at 1/4 to 1 backslopes was made in relatively dry but frozen silt. A minor amount of thaw-flow occurred here, but a stable appearance precluded further serious examination.

A.9.7.8 Highway Details (Mile 53.5)

A relatively dry silt overlies shale bedrock at this location. The cut was made into fifteen feet of silt, benched, and the remaining ten feet cut into the bedrock. The silt has melted and sloughed onto the bench. The backslope appears quite attractive and is completely stable.

A.9.7.9 Highway Details (Mile 54.4)

This location represents the approach to the Yukon River and the end of the haul road.

Cuts in the order of twenty to twenty-five feet were made at 1/4 to 1 into frozen silts, but no significant excess ice was encountered. When the material thawed it was essentially dry and now the silt is

sloughing off the near vertical banks to form a more stable slope configuration. Fig. A-26 illustrates the backslope in July, 1973.

A.9.8 Summary

Although the surficial geology of both physiographic regions appears to be essentially the same, there does seem to be at least a subtle difference in the ground ice content and conditions between the two regions. This change was evidenced beyond Hess Creek and to a greater extent beyond Isom Creek (Mile 23.5 and Mile 43, respectively). The soil that was exposed in the cuts in the latter section was substantially drier. This observation was made by the designers and it has been well substantiated by noting the improved behavior of the backslopes in this latter section of haul road.

The TAPS Haul Road has provided the first real opportunity to observe and record the performance of a significant number of substantial road cuts in ice-rich fine-grained soils in areas of discontinuous permafrost. It appears that the performance of these cuts is entirely satisfactory.

However, with the limited information available on the exact nature of ground ice conditions it is difficult to draw absolute conclusions as to why these cut slopes (through what appears to be massive ice) have stabilized without excessive degradation and retreat.

Certainly the relatively free draining nature of the silt deposits, the massive revegetation program, and probably the initial vertical cross-sections have all contributed to rapid stabilization. More important, however, may be that the ground ice occurs in the form of wedges of limited extent and that the backslopes stabilized when the exposed ice wedges melted and allowed the remaining soil to slough down forming a quasi stable slope of relatively low moisture content material. Summaries of soil classifications for the TAPS Haul Road appear in Table 2-1.

A.10 Copper River Basin

A general reconnaissance of backslope highway cuts was made from Anchorage to the Copper River Basin.

A.10.1 Physiography

The Copper River Basin lies in southeastern Alaska. It is a structural and topographic basin enclosed by diverging and converging mountain ranges. The Basin is drained by the Copper River and its tributaries which have steep walls one hundred to five hundred feet high. Thaw lakes are common in the eastern part of this region. Salt springs and mud volcanoes are formed from highly saline ground water.

A.10.2 Climate

The climate of the Copper River Basin is somewhat less severe than the Fairbanks region. The mean maximum temperatures for January are minus two degrees F and minus twelve degrees F respectively. The mean maximum and mean minimum temperatures for July are sixty-eight degrees F and forty-six degrees F respectively. The mean freezing and thawing indices are approximately twenty-three hundred degree F days and three thousand degree F days respectively. The mean annual precipitation is approximately ten inches. Snow fall is approximately forty-six inches per year.

A.10.3 Permafrost

The region lies within the discontinuous permafrost zone and permafrost is essentially continuous except in the valleys of major rivers (Ferrians, 1965). The permafrost table is as much as thirty feet below the surface in the southern part of this basin.

A.10.4 Bedrock Geology

The northern region is underlain by erosion resistant late Paleozoic and Mesozoic metamorphosed volcanic rocks with granitic intrusions. The southern part is underlain by soft interbedded sedimentary sandstones and shales of Mesozoic age. Tertiary gravels are found on many of the hills in the southwestern part of the basin (EISPTAPS).

A.10.5 Surficial Geology

This region has been subjected to extensive glaciation during the Pleistocene. Extensive pro-glacial lakes were formed when the drainage routes were blocked by these ice sheets. In one of the early glaciations ice filled the basin and flowed out in several outlets.

The area contains major deposits of glacial and pro-glacial materials up to five hundred feet in thickness. They include glacio-lacustrine clay, silt and sand, fluvial silt, sand and gravel, colluvium, and organic deposits. The glacio-lacustrine soils are plastic and dense with ground ice prevalent in the form of veins. Some massive ice is found in this region (EISPTAPS).

A.10.6 Highway Details

Highway designers are plagued with instability of large cuts and fills in this region of Alaska. Soil and ground ice conditions are extremely variable. Natural moisture contents may be as high as the liquid limit. Ground ice is found in the form of lenses and interstitial ice. In some cases the lenses may be of substantial thickness.

Slopes in this region are cut at appropriate angles to ensure stability in the thawed but essentially undrained case. No excess pore pressures due to thaw are considered in the analyses.

Several significant cuts were investigated in this region but the ice contents are apparently low enough to prevent appreciable degradation or slope retreat upon melting.

Instability of the natural slopes is common but most are rotational or block-type failures and are not necessarily related to the degradation of permafrost.

A.11 Conclusions

General conclusions obtained from the reconnaissance are contained in the body of the thesis (Chapter II) and consequently, will not appear in this Appendix.

Fig. A.1 Mile 222 Alaska Highway (Backslope instability during construction, July 1973).

Fig. A.2 Mile 50 Dempster Highway (Headwaters of the East Blackstone River. Road built at very modest geometric design standards).

Fig. A.3 Mile 124 Dempster Highway (Typical view of the Ogilvie physiographic unit).

Fig. A.4 Mile 80 Dempster Highway
(Improved geometric design standards).

Fig. A.5 Mile 109 Dempster Highway (Biangular profile of backslope due to permafrost degradation).

Fig. A.6 Mile 114 Dempster Highway (Large thermal degradation scar - 150 ft. wide and 15 to 20 ft. deep).

Fig. A .7 Mile 120.7 Dempster Highway (Ten ft. cut with 2:1 backslopes made into ice rich organic silt.

Fig. A .8 Mile 153 Dempster Highway (Melting of large ice wedges caused slope degradation).

Fig. A.9 Mile 153 Dempster Highway
(View from top dressed backslope).

Fig. A.10 Mile 175 Dempster Highway (Backslope and shoulder failure due to melting of a large ice lense).

Fig. A.11 Mile 175 Dempster Highway (Severe cracking of shoulder due to differential thermal subsidence caused by construction).

Fig. A.12 Mile 343 Dempster Highway- Large cut between Arctic Red River and Fort McPherson (Looking west).

Fig. A.13 Mile 343 Dempster Highway - Stabilized backslope. (Hand placed vegetation to control rate of thaw).

Fig. A.14 Bimodal flow in the Richardson Mountains.

Fig. A15 Approach cut to Mackenzie River crossing at Arctic Red River.

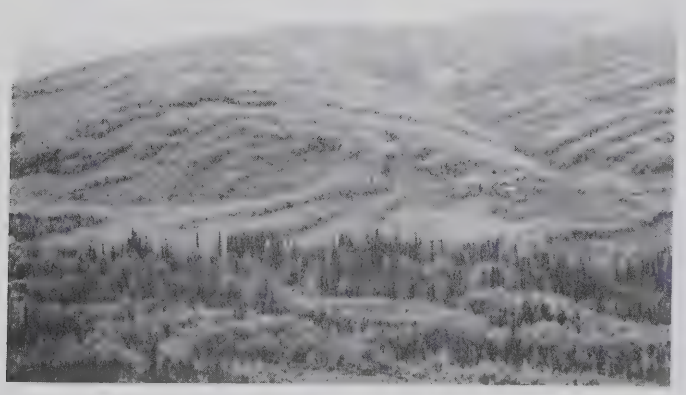

Fig. A.16 Typical vegetation patterns at southern end of TAPS Haul Road.

Fig. A.17 Mile 14 TAPS Haul Road (July 1973).

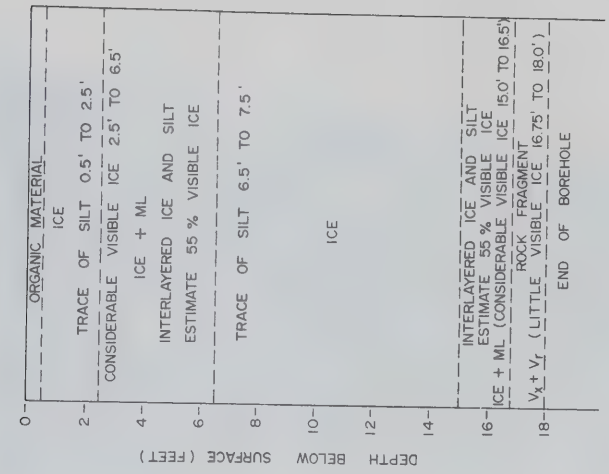

Fig. A.18 Mile 20 TAPS Haul Road - Typical Bore Hole Log (After Smith & Berg 1972).

Fig. A.19 Mile 19.6 (31.6 km) TAPS Haul Road (July 1973).

Fig. A.20 Mile 20.3 (32.6 km) TAPS Haul Road (July 1973).

Fig. A.21 Mile 22.9 TAPS Haul Road (April 1970) (After Smith & Berg 1972).

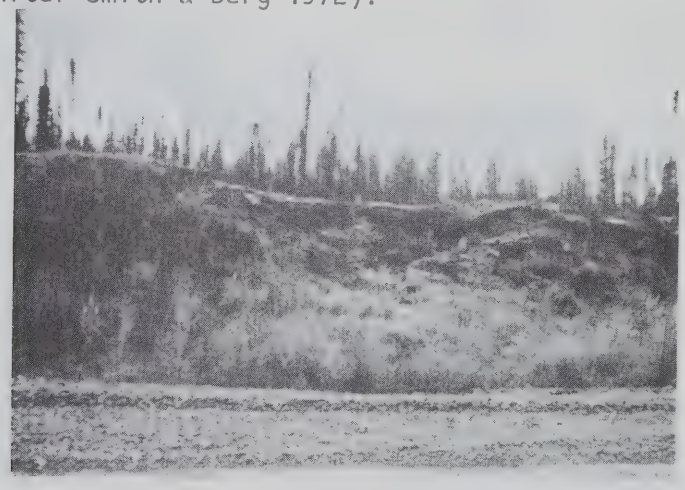

Fig. A.22 Mile 22.9 TAPS Haul Road (July 1973).

Fig. A.23 Mile 23.4 TAPS Haul Road. Approach to Hess Creek (April 1970).

Fig. A.24 Mile 23.4 TAPS Haul Road. Approach to Hess Creek (July 1973).

Fig. A.25 Mile 33 TAPS Haul Road (July 1973).

Fig. A.26 Mile 54.4 TAPS Haul Road (July 1973).

APPENDIX B

The following appendix contains a computer program that was used in Chapter III of this thesis.

This program may be utilized in the design of insulation thickness and surcharge loading for the stabilization of planar landslides in thawing soils. The insulation used in this example is woodchips. The input for trial one is:

Thermal conductivity of gravel	(K1)	= 0.0065 cal/deg C cm s
Thermal conductivity of woodchips	(K2)	= 0.00030 cal/deg C cm s
Thermal conductivity of thawed soil	(K3)	= 0.0030 cal/deg C cm s
Insulation thickness	(H)	= 0.15 m
Surface temperature	(TS)	= 16.9° C
Length of thaw season	(TF)	= 130 days
Coeff. of consolidation	(Cv)	= 0.002 cm^2/sec
Grid spacing	(Dx)	= 0.040 m
Depth of surcharge	(DEP)	= 0.91 m
Unit wt. of G amt 1		= 19.65 kN/m^3
Specific gravity of parent material	(GS)	= 2.70
Water content of parent material	(W)	= 35%
Unfrozen water content of parent material		= 0%
Friction angle of parent material	(Ø)	= 22
Slope angle (beta)		= 12%
Number of times output is produced	(IO)	= 5

Trial number two has increased insulation thickness and decreased surcharge load. All other parameters remain constant.

Insulation thickness	(H)	= 0.23 m
Depth of surcharge	(DEP)	= 0.61 m

The elapsed time, the thaw depth, the number of depth increments, the pore pressure-depth increment profile, the pore pressure at the thaw front, the effective normal stress at the thaw front, the shearing stress at the thaw front and the factor of safety are listed in the output.

```
C---- PROGRAM TO CALCULATE THE PORE PRESSURES AND THE FACTOR OF SAFETY
C-----OF A THAWING SLOPE WITH INSULATION AND SURCHARGE LOADING
C-----THE PROGRAM USES THE CRANK-NICHOLSON FINITE DIFFERENCE METHOD..
C-----IT IS A FIXED GRID, MOVING BOUNDARY SITUATION. AND THE SOIL IS
C-----ASSUMED HOMOGENEOUS... ONE DIMENSIONAL FLOW IS PERMITTED. AND
C-----THE PROGRAM CAN INCORPERATE ANY SPECIFIED RATE OF THAW....
C-----*****************************************************************
C-----KN/SQ M MAY BE CONVERTED TO PSF BY MULTIPLYING BY 20.89
C-----KN/CU M ( KN/M3 ) MAY BE CONVERTED TO PCF BY MULTIPLING BY 6.37
C-----*****************************************************************
0001        COMMON U(500),A(500),B(500),C(500),D(500),UOUT(500),DX,P0,N1,V1,X
0002        COMMON GAMSUB,GAMT1,GAMT3,CV,TIME,PHR,BETR,DEPIV,CB,CN,DEP,CB1
0003        REAL K1,K2,K3,L
C-------ENTER THE PARAMETERS NECESSARY FOR SOLUTION
0004     99 READ(5,101)K1,K2,K3,H,TS,TF,CV3,DX,DEP,GAMT1,GS,W,WU,PHI,BETA,IO
0005    101 FORMAT(8F10.0,/,7F10.0,I3)
0006        IF(H.LE.0.0) K2=K3
0007        WRITE(6,102)K1,K2,K3,H,TS,TF,CV3,DX,DEP,GAMT1,GS,W,WU,PHI,BETA,IO
0008    102 FORMAT('1','   DATA INPUT:'/'-','   THE RATE OF THAW IS GIVEN BY:
           1X(T)=SQRT(K3/K2*H+2*K3*TS/L*TIME)-K3/K2*H'/'    THE THERMAL COND.O
           2F THE SURCHARGE=',F7.5,'CAL/DEG C CM S'/'    THE THERMAL COND. OF
           3THE INSULATION=',F7.5,'CAL/DEG C CM S'/'    THE THERMAL COND. OF T
           4HE LOWER SOIL =',F7.5,'CAL/DEG C CM S'/'    THE THICKNESS OF INSUL
           5ATION=',F7.2,' M. '/'    THE AVE AIR TEMP=',F7.2,'DEG C'/'    THE
           6SOLN WILL TERMINATE AT TIME=',F7.1,'DAYS'/'    THE COEFF OF CONSOI
           7=',F9.4,'CM SQ/SEC'/'    THE GRID SPACING IN THE X-DIRECTION =',F7
           8.3,' M. '/'    THE DEPTH OF SURCHARGE =',F7.2,' M. '/'    THE TOTA
           9L UNIT WT.OF THE SURCHARGE MATRL=',F7.2,'KN/M3'/'    THE SPECIFIC
           1GRAVITY OF THE SOIL=',F7.2/'    THE WATER CONTENT OF THE LOWER SOI
           2L=',F7.2/'    THE UNFROZEN WATER CONTENT OF THE LOWER SOIL=',F7.2/
           3'    THE FRICTION ANGLE OF THE SOIL=',F7.2,' DEGREES'/'    THE SLO
           4PE ANGLE=',F7.2,' DEGREES'/'    THE DESIRED NO. OF TIMES  OUTPUT
           5WILL BE PRODUCED OVER THE THAW PERIOD=',I4/'0','----------------
           6---------------------------------------------------------- ')
0009        HE=H+K2/K1*DEP
0010        GAMTCG=GS*(1.+W)/(1.+GS*W)
0011        GAMDF=GAMTCG/(1.+W)
0012        L=GAMDF*(W-WU)*79.6
0013        CB=K3/K2*HE
0014        CB1=K3/K1*DEP
0015        CN=2.*K3*TS/L*8.64
0016        GAMSUB=(GAMTCG-1.0)*9.8066
0017        GAMT3=GAMTCG *9.8066
C-----CHANGE DEGREES TO RADIANS FOR COMPUTATIONS
0018        BETR=BETA*3.1415927/180.
0019        PHR=PHI*3.1415927/180.
C-----CHANGE CV UNITS FROM CM SQ/SEC TO M SQ/DAY
0020        CV=CV3*8.64
0021        P0=DEP*GAMT1
C-----THE DENOMINATOR OF THE FOLLOWING STATEMENT INDICATES NUMBER OF TIMES
C-----OUTPUT WILL BE GENERATED FOR THE TOTAL TIME OF THAW
0022        TOUT=TF/IO
0023        TOUTP=TOUT
0024        X0=2.1*DX
C-----CALCULATE TIME TO THAW THROUGH 2.1 DEPTH INCREMENTS
```

```
0025              IF(H)  60,60,70
0026           60 TO=((XO+CB1)*(XO+CB1)-CB1*CB1)/CN
0027              GOTO 71
0028           70 TO=((XO+CB)*(XO+CB)-CB*CB)/CN
0029           71 TIME=TO
                C-----ESTIMATE OF PORE PRESSURES FOR THIS THAW DEPTH
0030              U(1)=0.2*P(PO,GAMSUB,XO,BETR)
0031              U(2)=U(1)
0032              DT=TO/20.
0033              X=XO
0034              DERIV=X/TIME
0035              CALL POSIT(N,V,NP)
0036              N1=NP
0037              V1=V
0038              N=N1+1
0039              U(N)=U(1)
0040              CALL OUTPUT
                C-----THIS PROGRAM DOES NOT RETURN ABOVE THIS STATEMENT UNTIL A NEW SET
                C-----OF DATA IS READ
0041           25 IF(TIME.GT.TF)   GO TO 99
0042              TIME=TIME+DT
0043              BT=CV*DT/(DX*DX)
                C-----  STORE  X AND DX/DT AT THE JTH TIME STEP.....
0044              XJ=X
0045              DERJ=DERIV
                C-----CALCULATE X AND DX/DT AT THE (J+1)TH TIME STEP.....
0046              IF(H) 65,65,75
0047           65 CALL THAW1
0048              GOTO 85
0049           75 CALL THAW
0050           85 XJ1=X
0051              DERJ1=DERIV
0052              CALL POSIT(N2,V2,NP)
0053              MARK=0
0054              N2=NP
0055              IREM=0
0056              IF(N2.EQ.N1)   GO TO 1
0057              IREM=N2-N1
0058              V2=V2+IREM
0059              MARK=1
0060           1  D(1)=2.*(1.-BT)*U(1)+BT*U(2)
0061              N=N1+1
0062              NL2=N-2
0063              IF(NL2.LE.1)   GO TO 4
0064              DO 2 I=2,NL2
0065           2  D(I)=BT*(U(I+1)+U(I-1))  +2.*(1.-BT)*U(I)
0066           4  D(N-1)=BT*V1*U(N-2)/(1.+V1)  +(1.-BT)*U(N-1) + BT*U(N)/(1.+V1)
0067              DO 3 I=1,NL2
0068              A(I)=2.*(1.+BT)
0069              B(I)=-BT
0070           3  C(I)=-BT
0071              C(1)=0.
0072              A(N-1)=1.+BT
0073              C(N-1)=-BT*V2/(1.+V2)
0074              B(N-1)=-BT/(1.+V2)
```

```
                C-----CALCULATE THE COEFFICIENTS FOR THE FINITE DIFFERENCE EQUATION
                C-----AT THE BOUNDARY(NTH) NODE ......
0075                  BJ=CV*DT/(V1*V1*DX*DX)
0076                  BJ1=CV*DT/(V2*V2*DX*DX)
0077                  PJ=P(PO,GAMSUB,XJ,BETR)
0078                  PJ1=P(PO,GAMSUB,XJ1,BETR)
0079                  CJ=V1*DX*DEPJ/CV
0080                  CJ1=V2*DX*DERJ1/CV
0081                  A(N)=1.+PJ1*(1.+CJ1)
0082                  C(N)=-BJ1
0083                  B(N)=0.
0084                  D(N)=(1.-BJ-BJ*CJ)*U(N)+BJ*U(N-1) +BJ1*CJ1*PJ1 +BJ*CJ*PJ
                C-----SOLVE THE ESTABLISHED FINITE DIFFERENCE EQUATIONS
0085                  CALL GAUSEL(N)
0086                  DO 8 I=1,N
0087                8 U(I)=C(I)
0088                  IF(MARK.EQ.0)   GO TO 10
0089                  DIST=V2*DX
0090                  GRAD=(U(N)-U(N1))/DIST
0091                  UX=U(N)
0092                  DO 5 I=N,N2
0093                5 U(I)=U(N1)+GRAD*(I-N1)*DX
0094                  U(N2+1)=UX
0095               10 N1=N2
0096                  V1=V2-IREM
0097                  IF(V1.LE.0.0) V1=0.0000000001
0098                  MARK=0
                C-----ESTABLISH APPROPIATE TIME STEP
0099                  NG=300
0100                  DT=DX/(NG*DERIV)
0101                  TIME2=TIME/2.
0102                  IF(DT.LT.TIME2)   GO TO 30
0103                  DT=TIME2
0104               30 IF (TIME.LT.TOUTP)   GO TO 25
0105                  TOUTP=TOUTP+TOUT
0106                  CALL OUTPUT
0107                  WRITE(6,108)
0108              108 FORMAT('0','-------------------------------------------------------
                     1---------------------------------------------------------- ')
0109                  GO TO 25
0110                  END
```

```
0001              SUBROUTINE GAUSEL(N)
0002              COMMON U(500),A(500),B(500),C(500),D(500),UOUT(500),DX,PC,N1,V1,X
0003              COMMON GAMSUR,GAMT1,GAMT3,CV,TIME,PHR,BETR,DERIV,CB,CN,DEP,CB1
                 C-----**************************************************************
                 C-----THIS SUBROUTINE SOLVES 'N' LINEAR SIMULTANEOUS TRIDIAGONAL
                 C-----EQUATIONS, AND STORES THE RESULT IN THE ARRAY C(I).......
                 C-----**************************************************************
0004              IF(N.GT.1)GO TO 8
0005              C(N)=D(N)/A(N)
0006              GO TO 6
                 C----- TO CHANGE TO UPPER TRIANGULAR FORM.
0007            8 DO 5 I=2,N
0008              A(I)=A(I)-B(I-1)*C(I)/A(I-1)
0009              D(I)=D(I)-D(I-1)*C(I)/A(I-1)
0010            5 C(I)=0.
                 C----- BACK SUBSTITUTION..
0011              C(N+1)=0.
0012              I=N
0013            4 C(I)=(D(I)-B(I)*C(I+1))/A(I)
0014              IF(I.LE.1)GO TO 6
0015            7 I=I-1
0016              GO TO 4
0017            6 RETURN
0018              END
```

```
0001              SUBROUTINE OUTPUT
0002              COMMON U(500),A(500),B(500),C(500),D(500),UOUT(500),DX,PC,N1,V1,X
0003              COMMON GAMSUB,GAMT1,GAMT3,CV,TIME,PHR,BETR,DEPIV,CB,CN,DEP,CB1
0004              NL1=N1-1
0005              TIMDAY=TIME
0006              V1N1=N1+V1
0007              WRITE(6,8)TIMDAY,X,V1N1
0008            8 FORMAT('0',' THE ELAPSED TIME FOR THIS CALCULATION =',F9.2,' DA
                 1YS'/'0',' THE THAW DEPTH =',F7.2,' M. '/'0',' THE NUMBER OF
                 1DEPTH INCREMENTS =',F10.2)
0009              IF(NL1.LE.1)WRITE(6,10)
0010             10 FORMAT('0',' PORE PRESSURES ARE NOT VALID FOR THIS THAW DEPTH
                 1AND FACTOR OF SAFETY WILL NOT BE CALCULATED'/' ******************
                 2**********************************************************
                 3*****************')
0011              N=N1+1
0012              IF(NL1.LE.1)GOTO12
0013              WRITE(6,105)
0014            105 FORMAT('0',' THE PORE PRESSURE-DEPTH INCREMENT PROFILE IS AS FOL
                 1LOWS:  UNITS ARE IN KN/SQ M ')
0015              WRITE(6,3)(U(I),I=1,N)
0016            3 FORMAT('0',10F10.2)
0017              IF(BETR.LE.0) GOTO 12
0018              CALL SSAN(N)
0019             12 RETURN
0020              END
```

```
0001              SUBROUTINE THAW1
0002              COMMON U(500),A(500),B(500),C(500),D(500),UOUT(500),DX,PC,N1,V1,X
0003              COMMON GAMSUB,GAMT1,GAMT3,CV,TIME,PHR,BETR,DERIV,CB,CN,DEP,CB1
                C---  THIS SUBROUTINE CALCULATES THE DEPTH OF THAW FROM THE EQUATION
                C-----X=SQRT(CB1**CB1+CN*TIME)-CB1
                C---  THE ROUTINE ALSO CALCULATES THE DERIVITIVE DX/DT...
                C---- ***************************************************************************
0004              X=SQRT(CB1*CB1+CN*TIME)-CB1
0005              DERIV=CN/(2.*SQRT(CB1*CB1+CN*TIME))
0006              RETURN
0007              END
```

```
0001              SUBROUTINE THAW
0002              COMMON U(500),A(500),B(500),C(500),D(500),UOUT(500),DX,P0,N1,V1,X
0003              COMMON GAMSUB,GAMT1,GAMT3,CV,TIME,PHR,BETR,DEPIV,CB,CN,DEP,CB1
                C---- THIS SUBROUTINE CALCULATES THE DEPTH OF THAW FROM THE EQUATION
                C---  X=SQRT(CB*CB+CN*TIME)-CB
                C---- THE ROUTINE ALSO CALCULATES THE DERIVITIVE DX/DT...
                C---- ********************************************************************************
0004              X=SQRT(CB*CB+CN*TIME)-CB
0005              DERIV=CN/(2.*SQRT(CB*CB+CN*TIME))
0006              RETURN
0007              END
```

```
0001              SUBROUTINE POSIT(N,V,NP)
0002              COMMON U(500),A(500),B(500),C(500),D(500),UOUT(500),DX,P0,N1,V1,X
0003              COMMON GAMSUB,GAMT1,GAMT3,CV,TIME,PHR,BETP,DERIV,CB,CN,DEP,CB1
                C-----THIS POUTINE GIVES THE POSITION OF THE FREEZE-THAW INTERFACE
0004              NP=X/DX
0005              V=X/DX-NP
0006              N=NP+1
0007              RETURN
0008              END
```

```
MTS  FORTRAN IV G COMPILER (C/S REL 21.7)              SSAN        12-27-75    08:45:03        PAGE 0001

0001                  SUBROUTINE SSAN(N)
                C     ************************************************************************
                C-----THIS SUBROUTINE CALCULATES THE FACTOR OF SAFETY OF A THAWING SLOPE
                C     ************************************************************************
0002                  COMMON U(500),A(500),B(500),C(500),D(500),UOUT(500),DX,P0,N1,V1,X
0003                  COMMON GAMSUB,GAMT1,GAMT3,CV,TIME,PHF,BETR,DERIV,CB,CN,DEP,CB1
0004                  ENS=(DEP*GAMT1+X*GAMSUB)*COS(BETR) U(N)
0005                  SS=(DEP*GAMT1+GAMT3*X)*SIN(BETR)
0006                  FS=TAN(PHR)/TAN(BETR)*(GAMT1*DEP+GAMSUB*X-(U(N)/COS(BETR)))/(GAMT1
                     1*DEP+GAMT3*X)
0007                  WRITE(6,105)U(N),ENS,SS,FS
0008            105   FORMAT('0','   THE PORE PRESSURE ACTING AT THE BASE OF THE THAW DE
                     1PTH =',F10.2,'KN /SQ M '/'0','   THE EFFECTIVE NORMAL STRESS AT TH
                     2E BASE OF THE THAW DEPTH =',F10.2,'KN/SQ M '/'0','   THE SHEARING
                     3STRESS AT THE BASE OF THE THAW DEPTH =',F10.2,'KN/SQ M '/'0','   T
                     4HE FACTOR OF SAFETY =',F10.2)
0009                  RETURN
0010                  END
```

```
0001            REAL FUNCTION P(PO,GAMSUB,X,BETR)
               C-----THIS FUNCTION CALCULATES THE NORMAL EFFECTIVE OVERBURDEN STRESS
               C-----AT THE FREEZE-THAW INTERFACE....
0002            P=(PC+GAMSUB*X)*COS(BETR)
0003            RETURN
0004            END
```

```
 DATA INPUT:

 THE RATE OF THAW IS GIVEN BY: X(T)=SQRT(K3/K2*H+2*K3*TS/L*TIME)-K3/K2*H
 THE THERMAL COND.OF THE SURCHARGE=0.00650CAL/DEG C CM S
 THE THERMAL COND. OF THE INSULATION=0.00030CAL/DEG C CM S
 THE THERMAL COND. OF THE LOWER SOIL =0.00300CAL/DEG C CM S
 THE THICKNESS OF INSULATION=   0.15 M.
 THE AVE AIR TEMP=  16.90DEG C
 THE SOLN WILL TERMINATE AT TIME=  130.0DAYS
 THE COEFF OF CONSOL=   0.0020CM SQ/SEC
 THE GRID SPACING IN THE X-DIRECTION =  0.040 M.
 THE DEPTH OF SURCHARGE =   0.91 M.
 THE TOTAL UNIT WT.OF THE SURCHARGE MATRL=  19.65KN/M3
 THE SPECIFIC GRAVITY OF THE SOIL=  2.70
 THE WATER CONTENT OF THE LOWER SOIL=   0.35
 THE UNFROZEN WATER CONTENT OF THE LOWER SOIL=   0.0
 THE FRICTION ANGLE OF THE SOIL=  22.00 DEGREES
 THE SLOPE ANGLE=  12.00 DEGREES
 THE DESIRED NO. OF TIMES  OUTPUT  WILL BE PRODUCED OVER THE THAW PERIOD=   5

-------------------------------------------------------------------------------

  THE ELAPSED TIME FOR THIS CALCULATION =    14.70  DAYS

  THE THAW DEPTH =   0.08  M.

  THE NUMBER OF DEPTH INCREMENTS =      2.10

    PORE PRESSURES ARE NOT VALID FOR THIS THAW DEPTH AND FACTOR OF SAFETY WILL NOT BE CALCULATED
*******************************************************************************************************

  THE ELAPSED TIME FOR THIS CALCULATION =    26.01  DAYS

  THE THAW DEPTH =   0.15  M.

  THE NUMBER OF DEPTH INCREMENTS =      3.66

  THE PORE PRESSURE-DEPTH INCREMENT PROFILE IS AS FOLLOWS:   UNITS ARE IN KN/SQ M

     0.22      0.45      0.67      0.82

  THE PORE PRESSURE ACTING AT THE BASE OF THE THAW DEPTH =      0.82KN /SQ M

  THE EFFECTIVE NORMAL STRESS AT THE BASE OF THE THAW DEPTH =     17.90KN/SQ M

  THE SHEARING STRESS AT THE BASE OF THE THAW DEPTH =     4.28KN/SQ M

  THE FACTOR OF SAFETY =      1.69

-------------------------------------------------------------------------------

  THE ELAPSED TIME FOR THIS CALCULATION =    52.00  DAYS

  THE THAW DEPTH =   0.28  M.

  THE NUMBER OF DEPTH INCREMENTS =      7.07

  THE PORE PRESSURE-DEPTH INCREMENT PROFILE IS AS FOLLOWS:   UNITS ARE IN KN/SQ M
```

0.22 0.43 0.65 0.86 1.08 1.30 1.51 1.52

THE PORE PRESSURE ACTING AT THE BASE OF THE THAW DEPTH = 1.52KN /SQ M

THE EFFECTIVE NORMAL STRESS AT THE BASE OF THE THAW DEPTH = 18.34KN/SQ M

THE SHEARING STRESS AT THE BASE OF THE THAW DEPTH = 4.80KN/SQ M

THE FACTOR OF SAFETY = 1.54

THE ELAPSED TIME FOR THIS CALCULATION = 78.01 DAYS

THE THAW DEPTH = 0.41 M.

THE NUMBER OF DEPTH INCREMENTS = 10.29

THE PORE PRESSURE-DEPTH INCREMENT PROFILE IS AS FOLLOWS: UNITS ARE IN KN/SQ M

0.21 0.42 0.63 0.84 1.05 1.26 1.47 1.68 1.89 2.10

2.16

THE PORE PRESSURE ACTING AT THE BASE OF THE THAW DEPTH = 2.16KN /SQ M

THE EFFECTIVE NORMAL STRESS AT THE BASE OF THE THAW DEPTH = 18.78KN/SQ M

THE SHEARING STRESS AT THE BASE OF THE THAW DEPTH = 5.29KN/SQ M

THE FACTOR OF SAFETY = 1.43

THE ELAPSED TIME FOR THIS CALCULATION = 104.01 DAYS

THE THAW DEPTH = 0.53 M.

THE NUMBER OF DEPTH INCREMENTS = 13.35

THE PORE PRESSURE-DEPTH INCREMENT PROFILE IS AS FOLLOWS: UNITS ARE IN KN/SQ M

0.20 0.41 0.61 0.82 1.02 1.23 1.43 1.64 1.84 2.05

2.25 2.46 2.66 2.73

THE PORE PRESSURE ACTING AT THE BASE OF THE THAW DEPTH = 2.73KN /SQ M

THE EFFECTIVE NORMAL STRESS AT THE BASE OF THE THAW DEPTH = 19.24KN/SQ M

THE SHEARING STRESS AT THE BASE OF THE THAW DEPTH = 5.76KN/SQ M

THE FACTOR OF SAFETY = 1.35

THE ELAPSED TIME FOR THIS CALCULATION = 130.03 DAYS

THE THAW DEPTH = 0.65 M.

THE NUMBER OF DEPTH INCREMENTS = 16.26

THE PORE PRESSURE-DEPTH INCREMENT PROFILE IS AS FOLLOWS: UNITS ARE IN KN/SQ M

0.20 0.40 0.60 0.80 1.00 1.20 1.40 1.60 1.80 2.00

2.20 2.40 2.60 2.80 3.00 3.20 3.25

THE PORE PRESSURF ACTING AT THF BASE OF THE THAW DEPTH = 3.25KN /SQ M

THE EFFECTIVF NORMAL STRESS AT THE BASE OF THE THAW DEPTH = 19.69KN/SQ M

THE SHEARING STRFSS AT THE BASE OF THE THAW DEPTH = 6.20KN/SQ M

THE FACTOR OF SAFETY = 1.28

```
DATA INPUT:


THE RATE OF THAW IS GIVEN BY: X(T)=SQRT(K3/K2*H+2*K3*TS/L*TIME)-K3/K2*H
THE THERMAL COND.OF THE SURCHARGF=0.00650CAL/DEG C CM S
THE THERMAL COND. OF THE INSULATION=0.00030CAL/DEG C CM S
THE THERMAL COND. OF THE LOWER SOIL =0.00300CAL/DEG C CM S
THE THICKNESS OF INSULATION=   0.23 M.
THE AVE AIR TEMP=  16.90DEG C
THE SOLN WILL TERMINATE AT TIME=  130.0DAYS
THE COEFF OF CONSOL=   0.0020CM SQ/SEC
THE GRID SPACING IN THE X-DIRECTION =  0.040 M.
THE DEPTH OF SURCHARGE =   0.61 M.
THE TOTAL UNIT WT.OF THE SURCHARGE MATRL=  19.65KN/M3
THE SPECIFIC GRAVITY OF THE SOIL=   2.70
THE WATER CONTENT OF THE LOWER SOIL=   0.35
THE UNFROZEN WATER CONTENT OF THE LOWER SOIL=   0.0
THE FRICTION ANGLE OF THE SOIL=  22.00 DEGREES
THE SLOPE ANGLE=  12.00 DEGREES
THE DESIRED NO. OF TIMES  OUTPUT  WILL BE PRODUCED OVER THE THAW PERIOD=   5

--------------------------------------------------------------------------------

   THE ELAPSED TIME FOR THIS CALCULATION =    19.46  DAYS

   THE THAW DEPTH =   0.08  M.

   THE NUMBER OF DEPTH INCREMENTS =      2.10

     PORE PRESSURES ARE NOT VALID FOR THIS THAW DEPTH AND FACTOR OF SAFETY WILL NOT BE CALCULATED
**********************************************************************************************

   THE ELAPSED TIME FOR THIS CALCULATION =    26.02  DAYS

   THE THAW DEPTH =   0.11  M.

   THE NUMBER OF DEPTH INCREMENTS =      2.79

     PORE PRESSURES ARE NOT VALID FOR THIS THAW DEPTH AND FACTOR OF SAFETY WILL NOT BE CALCULATED
**********************************************************************************************

--------------------------------------------------------------------------------

   THE ELAPSED TIME FOR THIS CALCULATION =    52.01  DAYS

   THE THAW DEPTH =   0.22  M.

   THE NUMBER OF DEPTH INCREMENTS =      5.47

   THE PORE PRESSURE-DEPTH INCREMENT PROFILE IS AS FOLLOWS:   UNITS ARE IN KN/SQ M

      0.12      0.24      0.36      0.48      0.60      0.66

   THE PORE PRESSURE ACTING AT THE BASE OF THE THAW DEPTH =      0.66KN /SQ M

   THE EFFECTIVE NORMAL STRESS AT THE BASE OF THE THAW DEPTH =     12.90KN/SQ M

   THE SHEARING STRESS AT THE BASE OF THE THAW DEPTH =      3.33KN/SQ M

   THE FACTOR OF SAFETY =      1.57
```

THE ELAPSED TIME FOR THIS CALCULATION = 78.02 DAYS

THE THAW DEPTH = 0.32 M.

THE NUMBER OF DEPTH INCREMENTS = 8.06

THE PORE PRESSURE-DEPTH INCREMENT PROFILE IS AS FOLLOWS: UNITS ARE IN KN/SQ M

0.12 0.24 0.36 0.48 0.60 0.73 0.85 0.97 0.97

THE PORE PRESSURE ACTING AT THE BASE OF THE THAW DEPTH = 0.97KN /SQ M

THE EFFECTIVE NORMAL STRESS AT THE BASE OF THE THAW DEPTH = 13.45KN/SQ M

THE SHEARING STRESS AT THE BASE OF THE THAW DEPTH = 3.72KN/SQ M

THE FACTOR OF SAFETY = 1.46

THE ELAPSED TIME FOR THIS CALCULATION = 104.02 DAYS

THE THAW DEPTH = 0.42 M.

THE NUMBER OF DEPTH INCREMENTS = 10.55

THE PORE PRESSURE-DEPTH INCREMENT PROFILE IS AS FOLLOWS: UNITS ARE IN KN/SQ M

0.12 0.24 0.36 0.49 0.61 0.73 0.85 0.97 1.09 1.22

1.28

THE PORE PRESSURE ACTING AT THE BASE OF THE THAW DEPTH = 1.28KN /SQ M

THE EFFECTIVE NORMAL STRESS AT THE BASE OF THE THAW DEPTH = 13.98KN/SQ M

THE SHEARING STRESS AT THE BASE OF THE THAW DEPTH = 4.10KN/SQ M

THE FACTOR OF SAFETY = 1.38

THE ELAPSED TIME FOR THIS CALCULATION = 130.02 DAYS

THE THAW DEPTH = 0.52 M.

THE NUMBER OF DEPTH INCREMENTS = 12.96

THE PORE PRESSURE-DEPTH INCREMENT PROFILE IS AS FOLLOWS: UNITS ARE IN KN/SQ M

0.12 0.24 0.37 0.49 0.61 0.73 0.85 0.98 1.10 1.22

1.34 1.46 1.58

THE PORE PRESSURE ACTING AT THE BASE OF THE THAW DEPTH = 1.58KN /SQ M

THE EFFECTIVE NORMAL STRESS AT THE BASE OF THE THAW DEPTH = 14.49KN/SQ M

THE SHEARING STRESS AT THE BASE OF THE THAW DEPTH = 4.47KN/SQ M

THE FACTOR OF SAFETY = 1.31

APPENDIX C

This appendix contains two computer programs that may be utilized in computing the amount of solar radiation encountered by a sloping surface. It also contains the details for computing the amount of radiation reflected from one surface to another.

C.1 Program 1:

This program computes the length of a shadow cast by a sky line obstruction on a sloping surface. Figure C-1 illustrates the configuration. The symbols in the figure are defined as:

$\hat{S}_u$ = a unit vector along the rays of the sun.

$\hat{S}_L$ = a unit vector normal to the slope.

$\hat{O}_b$ = a unit vector along the base line of the obstruction.

$\overline{S_H}$ = the length of the shadow measured on the slope along the azimuth of the sun.

$\overline{P}$ = the length of the shadow measured perpendicular to the obstruction on the slope.

$\overline{H}$ = height of the obstruction.

Direction cosines for the sun and the normal to the slope are:

	Sun ($\hat{S}_u$)	Slope $\hat{S}_l$
x axis	$\sin Z \cos a_{su}$	$-\cos a_{sl} \sin b$
y axis	$-\sin Z \sin a_{su}$	$\sin a_{sl} \sin b$
z axis	$-\cos Z$	$\cos b$

where a_{su} = azimuth of the sun

a_{sl} = azimuth of the normal to the slope

Z = zenith angle of the sun

b = zenith angle of the normal to the slope or the slope angle measured from the horizontal

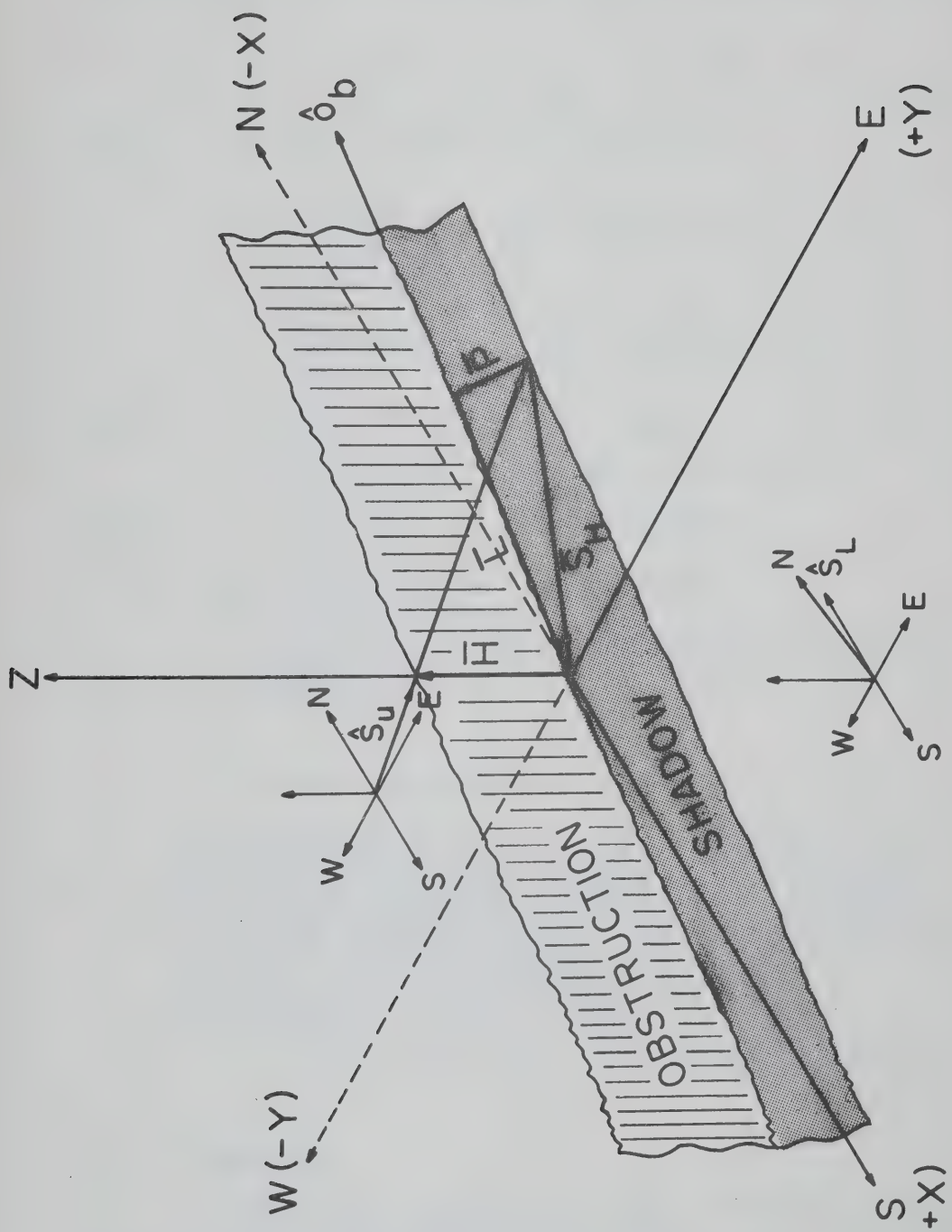

C.1 Shadow Cast by Obstruction On Sloping Ground

Let $\overline{E}$ be a vector in the plane of the slope along the base of the obstruction and, therefore, perpendicular to the unit normal of the slope.

$$\overline{E} = \{1 + \tan^2 b\,[\cos^2 (a_{ob} - a_{sl})]\}^{1/2} \quad - - - [C.1]$$

where a_{ob} = the azimuth of the obstruction

$$\overline{N} = \{ \frac{H^2 \tan^2 z}{[\overline{E}\,(1+c)]^2} \quad [2.0 \tan^2 b \cos^2 (a_{sl} - a_{su})$$

$$(1 - \cos(a_{su} - a_{ob}))] + \sin^2 (a_{su} - a_{ob})\}^{1/2} \quad - - - [C.2]$$

where $c = \tan Z \tan b[(\cos (a_{sl} - a_{su})]$ - - - [C.3]

$Z = \text{arc cos } [\cos \delta \cos \phi \cos w + \sin \delta \sin \phi]$

where δ = declination of the sun (degrees)

ϕ = latitude of the site (degrees)

w = hour angle of the sun measured positively to the west of the solar noon or negatively to the east (degrees)

The input parameters for the program are:

i) Declination of the sun in degrees (DECLIN) (F6.2 format)
ii) Latitude of the site in degrees (ALAT) (F6.2 format)
iii) Height of obstruction in meters (H) (F5.1 format)
iv) Azimuth of obstruction in degrees (AOB) (F7.2 format)
v) Azimuth of slope in degrees (ASL) (F7.2 format)
vi) Slope angle in degrees (B) (F7.2 format)
vii) Hour angle in degrees (HRANGL) (F7.2 format)

The listing and a sample of the output are included.

C.2 Program 2:

This program computes the daily direct beam radiation and the total solar daily radiation on a slope. It also computes the average daily direct beam radiation and the average total solar daily radiation on a slope for the time period of interest.

The expression for the angle between the rays of the sun and the normal to the slope:

$$\cos \Lambda = \cos \delta(-\cos w \sin \phi \cos a \sin b - \sin w \sin a \sin b + \cos b \cos w \cos \phi) + \sin \delta\,(\cos \phi \cos a \sin b + \sin \phi \cos b) \quad - - - [C.4]$$

δ = declination of the sun
w = hour angle of sun (measured positively to the west of solar noon)
ϕ = latitude of the site
a = azimuth of a unit normal to the slope
b = angle of slope to the horizontal

The input parameters for the program are contained on two cards.

Card 1: number of cards (N) (I10 format)
Card 2: i) latitude of the site (Alat) (F10.2 format)
ii) azimuth of the normal to the slope (Azsl) (F10.2 format)
iii) slope angle in degrees (Sla) (F10.2 format)
iv) time to begin calculations; measured from Mar 21 in days (T1) (I10 format)
v) final time of calculations in days (T2) (I10 format)
vi) total solar radiation on a horizontal surface at the site (QHT) (F10.0 format)

A sample of the output follows the computer listing.

C.3 Reflected Radiation from Surface 1 to Surface 2 (After Threlkeld 1970)

The following provides a basis for computing the amount of radiation diffusely reflected from one surface to another.

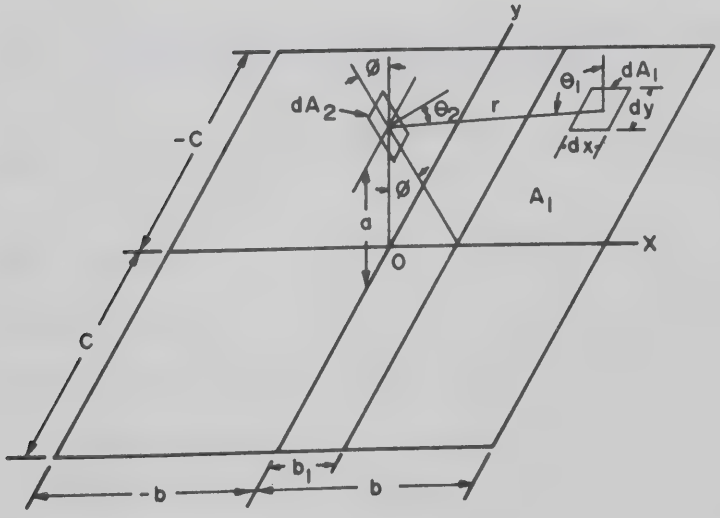

C.2 Relation of a Small Surface dA_2 to a Diffusely Reflecting Large Surface A_1 (After Threlkeld, 1963).

Figure C.2 illustrates a small surface dA_2 whose plane is inclined by an angle $\emptyset$ to a perpendicular position with respect to surface A_1. The distance between the two surfaces is a. The surface A_1 is rectangular and reflects radiation diffusely. The albedo of this surface is α_1. The amount of radiation reflected by surface A_1 is given by:

$$dq = \alpha_1 I_1 dA_1 \qquad - - - [C.5]$$

where dq = the radiation in ly/hr diffusely reflected by dA_1 upon a hemisphere of radius r

I_1 = the intensity of solar radiation on surface A_1

Since A_1 is assumed to be a pure diffuse reflector,

$$dq = \pi r^2 \; I_{rn} \qquad - - - [C.6]$$

where I_{rn} is the intensity of reflected radiation along the normal to dA_1 and at a distance r away.

$$dI_r = I_{rn} \cos \theta_1 \cos \theta_2 \qquad - - - [C.7]$$

where dI_r = the intensity of radiation incident upon dA_2 due to radiation diffusely reflected by dA_1.

$$dI_r = \frac{\alpha_1 \; I_1 \; dA_1 \cos \theta_1 \cos \theta_2}{\pi r^2} \qquad - - - [C.8]$$

$$dA_1 = dx \; dy$$

$$\cos \theta_1 = a/r$$

$$\cos \theta_2 = x/r \cos \emptyset - a/r \sin \emptyset$$

$$r = \sqrt{x^2 + y^2 + a^2}$$

Integration of equation [C.8] gives

$$I_r = \frac{\alpha_1 I_1 a}{\pi} \int_{-c}^{c} \int_{b_1}^{b} \frac{(x \cos \emptyset - a \sin \emptyset)}{(x^2 + y^2 + a^2)^2} \, dxdy \qquad - - [C.9]$$

$$I_r = \frac{\alpha_1 I_1}{\pi} F \qquad - - - [C.10]$$

where $$F = a \int_{-c}^{c} \int_{b_1}^{b} \frac{(x \cos \phi - a \sin \phi)}{(x^2 + y^2 + a^2)^2} \, dx \, dy \qquad - - - [C.11]$$

The soltuion for F for several special cases is contained in Table C-1.

TABLE C-1

FACTOR F IN EQ. (C.10) FOR SEVERAL SPECIAL CASES

CASE	F
A. $\tan\phi \geq b/a$, $b_1 = b$	$F = 0$
B. $-b/a \leq \tan\phi \leq b/a$, $b_1 = a\tan\phi$	$F = \tan^{-1}\frac{c\cos\phi}{a} - \frac{(a\cos\phi + b\sin\phi)}{\sqrt{a^2+b^2}}\tan^{-1}\frac{c}{\sqrt{a^2+b^2}}$
1. General case	$+\frac{c\sin\phi}{\sqrt{a^2+c^2}}\left(\tan^{-1}\frac{a\tan\phi}{\sqrt{a^2+c^2}} - \tan^{-1}\frac{b}{\sqrt{a^2+c^2}}\right)$
2. Same as Case B-1 with b and c infinitely large and a finite	$F = \frac{\pi}{2}(1 - \sin\phi)$
3. $\phi = 0$, $b_1 = 0$ (Plane of dA_2 perpendicular to A_1)	$F = \tan^{-1}\frac{c}{a} - \frac{a}{\sqrt{a^2+b^2}}\tan^{-1}\frac{c}{\sqrt{a^2+b^2}}$
4. Same as Case B-3 but with b and c infinitely large and a finite	$F = \frac{\pi}{2}$
C. $\tan\phi \leq -b/a$, $b_1 = -b$	$F = -2\sin\phi\left(\frac{b}{\sqrt{a^2+b^2}}\tan^{-1}\frac{c}{\sqrt{a^2+b^2}}\right.$
1. General case	$\left.+\frac{c}{\sqrt{a^2+c^2}}\tan^{-1}\frac{b}{\sqrt{a^2+c^2}}\right)$
2. $\phi = -\pi/2$ (dA_2 parallel to and facing A_1)	$F = \frac{2b}{\sqrt{a^2+b^2}}\tan^{-1}\frac{c}{\sqrt{a^2+b^2}}$
	$+\frac{2c}{\sqrt{a^2+c^2}}\tan^{-1}\frac{b}{\sqrt{a^2+c^2}}$
3. Same as Case C-2 but with b and c infinitely large and a finite	$F = \pi$

```
                C**** PROGAM TO COMPUTE SHADOW LENGTH ON SLOPING GROUND
0001                1 READ(5,2)DECLIN,ALAT,H,AOB,ASL,B,HRANGL
0002                2 FORMAT(2F6.2,F5.1,4F7.2)
0003                  WRITE(6,3)DECLIN,ALAT,H,AOB,ASL,B,HRANGL
0004                3 FORMAT('0', '    DECLINATION OF THE SUN  =',F7.2,'DEG'/'     LATIT
                     1UDE OF THE SITE =',F7.2,'DEG'/'     HEIGHT OF OBSTRUCTION =',F7.2,
                     2'M'/'     AZIMUTH OF OBSTRUCTION =',F7.2,'DEG'/'     AZIMUTH OF SL
                     3OPE =',F7.2,'DEG'/'     SLOPE ANGLE =',F7.2,'DEG'/'     HRANGL =',
                     4F7.2)
0005                  CONV=3.1415927/180.0
0006                  DECLIN=DECLIN*CONV
0007                  ALAT=ALAT*CONV
0008                  AOB=AOB*CONV
0009                  ASL=ASL*CONV
0010                  B=B*CONV
0011                  HRANGL=HRANGL*CONV
0012                  Z=ARCOS(COS(DECLIN)*COS(ALAT)*COS(HRANGL)+SIN(DECLIN)*SIN(ALAT))
0013                  ASU=ARSIN(SIN(HRANGL)*COS(DECLIN)*1.0/SIN(Z))
0014                  SUX=SIN(Z)*COS(ASU)
0015                  SUY=-SIN(Z)*SIN(ASU)
0016                  SUZ=-COS(Z)
0017                  SLX=-COS(ASL)*SIN(B)
0018                  SLY=SIN(ASL)*SIN(B)
0019                  SLZ=COS(B)
0020                  EX=-COS(AOB)
0021                  EY=SIN(AOB)
0022                  EZ=(COS(AOB)*SLX-SIN(AOB)*SLY)/SLZ
0023                  E=SQRT(EX**2+EY**2+EZ**2)
0024                  OBX=-COS(AOB)/E
0025                  OBY=SIN(AOB)/E
0026                  OBZ=(-TAN(B)*COS(AOB-ASL))/E
0027                  C=TAN(Z)*TAN(B)*COS(ASL-ASU)
0028                  SHZ=(-H*C)/(1+C)
0029                  SHY=(H/(1+C))*TAN(Z)*SIN(ASU)
0030                  SHX=(H/(1+C))*COS(ASU)*TAN(Z)
0031                  ANX=SHY*OBZ-SHZ*OBY
0032                  ANY=SHZ*OBX-SHX*OBZ
0033                  ANZ=SHX*OBY-SHY*OBX
0034                  AN=SQRT(ANX**2+ANY**2+ANZ**2)
0035                  WRITE(6,20)ANX,ANY,ANZ,AN
0036               20 FORMAT('0',10X,'  NX=',F7.2,3X,'  NY=',F7.2,3X,'  NZ=',F7.2,3X,'
                     1N=',F7.2)
0037                  GO TO 1
0038                  END
```

```
$RUN -LOAD#
08:44:33

     DECLINATION OF THE SUN  =  23.50DEG
     LATITUDE OF THE SITE =  60.00DEG
     HEIGHT OF OBSTRUCTION =  30.00M
     AZIMUTH OF OBSTRUCTION =   0.0 DEG
     AZIMUTH OF SLOPE = 180.00DEG
     SLOPE ANGLE =  20.00DEG
     HRANGL =  75.34

            NX=  19.76     NY=  -0.07     NZ=  54.28     N=  57.77

     DECLINATION OF THE SUN  =  23.50DEG
     LATITUDE OF THE SITE =  60.00DEG
     HEIGHT OF OBSTRUCTION =  30.00M
     AZIMUTH OF OBSTRUCTION =   0.0 DEG
     AZIMUTH OF SLOPE = 270.00DEG
     SLOPE ANGLE =  20.00DEG
     HRANGL =  75.34

           NX=   0.00     NY= -69.97     NZ= 192.23     N= 204.57
   * * *
```

```
C-----PROGRAM TO DETERMINE SHORT WAVE RADIATION ON A SLOPE FROM VALUES ON
C-----A HORIZONTAL SURFACE
0001        DIMENSION COPR(365)
0002        INTEGER T1,T2
0003        CONV=3.1415927/180.
0004     80 READ(5,100)ALAT,AZSL,SLA,T1,T2,QHT,R,AL
0005    100 FORMAT(3F10.0,2I10,3F10.0)
0006        AZSL=-90.0
0007        DO 30 N=1,3
0008        AZSL=AZSL+90.0
0009        R=0.30
0010        DO 30 L=1,4
0011        R=R+0.05
0012        SLA=-10.0
0013        DO 20 M=1,9
0014        SLA=SLA+10.0
0015        WRITE(6,101)ALAT,AZSL,SLA,T1,T2,QHT,R,AL
0016    101 FORMAT('1','   DATA INPUT :'/'-','   THE LATITUDE OF THE SITE IS',
           1F7.2,'DEGREES'/'    THE AZIMUTH OF THE SLOPE IS',F7.2,'DEGREES'/'
           2   THE ANGLE OF THE SLOPE IS',F7.2,'DEGREES'/'    TIME TO BEGIN CA
           3LCULATIONS (COUNTED IN DAYS FROM MAR.21) IS',I10,' DAYS'/'    FINA
           4L TIME OF CALCULATIONS',I10,' DAYS'/'    AVERAGE TOTAL RADIATION O
           5N A HORIZONTAL SURFACE FOR THIS PERIOD OF TIME',F7.2,'LANGLEYS PER
           6 DAY'/'    THE RATIO OF DIFFUSE SKY RADIATION TO TOTAL RADIATION =
           7',F7.2/'    THE ALBEDO OF THE TERRAIN IS  ',F7.2)
C-----ESTABLISH SINES AND COSINES
0017        SLAT=SIN(ALAT*CONV)
0018        SAZSL=SIN(AZSL*CONV)
0019        SSLA=SIN(SLA*CONV)
0020        CLAT=COS(ALAT*CONV)
0021        CAZSL=COS(AZSL*CONV)
0022        CSLA=COS(SLA*CONV)
0023        CSQSLA=COS(SLA/2.0*CONV)**2.0
0024        SSQSLA=SIN(SLA/2.0*CONV)**2.0
0025        SUM=0
0026        QDH=QHT*(1.-R)
C-----BEGIN CALCULATIONS
0027        DO 93 I=T1,T2
0028        WRITE(6,102)I
0029    102 FORMAT('0',7X,'DAY',I4,' '/'       ********')
0030        DECL=23.5*CONV*SIN(2.*CONV*180./365.*I)
0031        SDECL=SIN(DECL)
0032        CDECL=COS(DECL)
0033        SCOSZT=0
0034        SCOSST=0
0035        ICOUNT=0
0036        X= CAZSL*SSLA
0037        Y=SSLA*SAZSL
0038        Z=CSLA
0039        TT1=(X*SIAT+Z*CLAT)*CDECL
0040        TT2=(-X*CLAT+Z*SLAT)*SDECL
C-----SET HOUR ANGIE TO 00:00 HOURS
0041        W=-CONV*180.
0042        ITIME=0100
C-----INCREMENT HOUR ANGLE BY 20 MINUTES
```

```
0043          97   W=W+0.087265
0044               ICOUNT=ICOUNT+1
              C-----DETERMINE COSINE OF SUN'S ZENITH ANGLE
0045               COSZ=CDECL*CLAT*COS(W)+SDECL*SLAT
              C-----TEST WHETHER SUN IS ABOVE HORIZON
0046               IF(COSZ.LE.0.0) GOTO 96
              C-----CALCULATE AREA UNDER COSZ VS TIME PLOT
0047               SCOSZT=SCOSZT+COSZ*0.087265
              C-----DETERMINE COSINE OF ANGLE BETWEEN SOLAR BEAM AND THE NORMAL TO THE SLOPE
0048               Q2=-Y*SIN(W)*CDECL+TT1*COS(W)
0049               COSSS=Q2+TT2
              C-----CHECK THAT SLOPE IS NOT IN SHADOW
0050               IF(COSSS.LE.0.0) COSSS=0.0
              C-----CALCULATE AREA UNDER COSSS VS TIME PLOT
0051               SCOSST=SCOSST+COSSS*0.087265
0052          96   IF(ICOUNT.NE.3)GOTO 97
0053               ICOUNT=0
0054               ITIME=ITIME+100
0055               IF(ITIME.LE.2400)GOTO 97
0056               CORR(I)=SCOSST/SCOSZT
0057               WRITE(6,104)CORR(I)
0058          104  FORMAT('-',24X,' THE DAILY CORRECTION =',F7.2)
0059               QDS=QDH*CORR(I)
0060               WRITE(6,105)QDS
0061          105  FORMAT('-',24X,' THE DAILY DIRECT BEAM RADIATION =',F7.2,'LY/DAY')
0062               QTS=QDS+QHT*R*CSQSLA
0063               WRITE(6,106)QTS
0064          106  FORMAT('-',24X,' THE TOTAL RADIATION ON THE SLOPE =',F7.2,'LY/DAY'
                  1)
0065          93   SUM=SUM+CORR(I)
0066               AVCORR=SUM/(T2-T1+1)
0067               WRITE(6,107)AVCORR
0068          107  FORMAT('-',24X,' THE AVE. CORR. FOR TIME PERIOD T2-T1=',F7.2)
0069               QDSAV=QDH*AVCORR
0070               WRITE(6,108)QDSAV
0071          108  FORMAT('-',24X,' THE AVE DAILY DIPECT BEAM RADIATION FOR TIME PERI
                  1OD T2-T1 =',F7.2,'LY/DAY')
0072               QTSAV=QDSAV+QHT*R*CSQSLA
0073               WRITE(6,109)QTSAV
0074          109  FORMAT('-',24X,' THE AVE TOTAL RADIATION ON THE SLOPE FOR THE TIME
                  1 PERIOD T2-T1=',F7.2,'LY/DAY')
0075               QNSS=(QDSAV+SSQSLA*AL*QHT+QHT*P)*(1.0-AL)-QHT*R*SSQSLA
0076               WRITE(6,113)QNSS
0077          113  FORMAT('-',24X,' THE AVE. NET SHORT WAVE RADIATION FOR TIME PERIOD
                  1 T2-T1=',F7.2,'LY/DAY')
0078            20 WRITE(6,112)
0079          112  FORMAT('-',10X,' ************************************************
                  1**********************')
0080            30 CONTINUE
0081               GO TO 80
0082               END
```

DATA INPUT :

THE LATITUDE OF THE SITE IS 68.30DEGREES
THE AZIMUTH OF THE SLOPE IS   0.0 DEGREES
THE ANGLE OF THE SLOPE IS 20.00DEGREES
TIME TO BEGIN CALCULATIONS (COUNTED IN DAYS FROM MAR.21) IS   86 DAYS
FINAL TIME OF CALCULATIONS   121 DAYS
AVERAGE TOTAL RADIATION ON A HORIZONTAL SURFACE FOR THIS PERIOD OF TIME 473.00LANGLEYS PER DAY
THE RATIO OF DIFFUSE SKY RADIATION TO TOTAL RADIATION =   0.35
THE ALBEDO OF THE TERRAIN IS   0.13

DAY 86
****

THE DAILY CORRECTION =   1.08

THE DAILY DIRECT BEAM RADIATION = 330.75LY/DAY

THE TOTAL RADIATION ON THE SLOPE = 491.31LY/DAY

DAY 87
****

THE DAILY CORRECTION =   1.08

THE DAILY DIPECT BEAM RADIATION = 330.75LY/DAY

THE TOTAL RADIATION ON THE SLOPE = 491.31LY/DAY

DAY 88
****

THE DAILY CORRECTION =   1.08

THE DAILY DIRECT BEAM RADIATION = 330.75LY/DAY

THE TOTAL RADIATION ON THE SLOPE = 491.31LY/DAY

DAY 89
****

THE DAILY CORRECTION =   1.08

THE DAILY DIRECT BEAM RADIATION = 330.75LY/DAY

THE TOTAL RADIATION ON THE SLOPE = 491.31LY/DAY

DAY 90
****

THE DAILY CORRECTION = 1.08

THE DAILY DIRECT BEAM RADIATION = 330.75LY/DAY

THE TOTAL RADIATION ON THE SLOPE = 491.31LY/DAY

DAY 91
****

THE DAILY CORRECTION = 1.08

THE DAILY DIRECT BEAM RADIATION = 330.75LY/DAY

THE TOTAL RADIATION ON THE SLOPE = 491.31LY/DAY

DAY 92
****

THE DAILY CORRECTION = 1.08

THE DAILY DIRECT BEAM RADIATION = 330.75LY/DAY

THE TOTAL RADIATION ON THE SLOPE = 491.31LY/DAY

DAY 93
****

THE DAILY CORRECTION = 1.08

THE DAILY DIRECT BEAM RADIATION = 330.75LY/DAY

THE TOTAL RADIATION ON THE SLOPE = 491.31LY/DAY

DAY 94
****

THE DAILY CORRECTION = 1.08

THE DAILY DIRECT BEAM RADIATION = 330.75LY/DAY

THE TOTAL RADIATION ON THE SLOPE = 491.31LY/DAY

DAY 95
****

THE DAILY CORRECTION = 1.08

THE DAILY DIRECT BEAM RADIATION = 330.75LY/DAY

THE TOTAL RADIATION ON THE SLOPE = 491.31LY/DAY

DAY 96
****

THE DAILY CORRECTION = 1.08

THE DAILY DIRECT BEAM RADIATION = 330.75LY/DAY

THE TOTAL RADIATION ON THE SLOPE = 491.31LY/DAY

DAY 97
****

THE DAILY CORRECTION = 1.08

THE DAILY DIRECT BEAM RADIATION = 330.75LY/DAY

THE TOTAL RADIATION ON THE SLOPE = 491.31LY/DAY

DAY 98
****

THE DAILY CORRECTION = 1.08

THE DAILY DIRECT BEAM RADIATION = 330.75LY/DAY

THE TOTAL RADIATION ON THE SLOPE = 491.31LY/DAY

DAY 99
****

THE DAILY CORRECTION = 1.08

THE DAILY DIRECT BEAM RADIATION = 330.75LY/DAY

THE TOTAL RADIATION ON THE SLOPE = 491.31LY/DAY

DAY 100
****

THE DAILY CORRECTION = 1.08

THE DAILY DIRECT BEAM RADIATION = 330.75LY/DAY

THE TOTAL RADIATION ON THE SLOPE = 491.31LY/DAY

DAY 101
****

THE DAILY CORRECTION = 1.08

THE DAILY DIRECT BEAM RADIATION = 330.75LY/DAY

THE TOTAL RADIATION ON THE SLOPE = 491.31LY/DAY

DAY 102
****

THE DAILY CORRECTION = 1.08

THE DAILY DIRECT BEAM RADIATION = 330.75LY/DAY

THE TOTAL RADIATION ON THE SLOPE = 491.31LY/DAY

DAY 103
****

THE DAILY CORRECTION = 1.08

THE DAILY DIRECT BEAM RADIATION = 330.75LY/DAY

THE TOTAL RADIATION ON THE SLOPE = 491.31LY/DAY

DAY 104
****

THE DAILY CORRECTION = 1.08

THE DAILY DIRECT BEAM RADIATION = 330.75LY/DAY

THE TOTAL RADIATION ON THE SLOPE = 491.31LY/DAY

DAY 105
****

THE DAILY CORRECTION = 1.08

THE DAILY DIRECT BEAM RADIATION = 330.75LY/DAY

THE TOTAL RADIATION ON THE SLOPE = 491.31LY/DAY

DAY 106
****

THE DAILY CORRECTION = 1.08

THE DAILY DIRECT BEAM RADIATION = 330.75LY/DAY

THE TOTAL RADIATION ON THE SLOPE = 491.31LY/DAY

DAY 107
****

THE DAILY CORRECTION = 1.08

THE DAILY DIRECT BEAM RADIATION = 330.75LY/DAY

THE TOTAL RADIATION ON THE SLOPE = 491.31LY/DAY

DAY 108
****

THE DAILY CORRECTION = 1.08

THE DAILY DIRECT BEAM RADIATION = 330.75LY/DAY

THE TOTAL RADIATION ON THE SLOPE = 491.31LY/DAY

DAY 109
****

THE DAILY CORRECTION = 1.08

THE DAILY DIRECT BEAM RADIATION = 330.75LY/DAY

THE TOTAL RADIATION ON THE SLOPE = 491.31LY/DAY

DAY 110
****

THE DAILY CORRECTION = 1.08

THE DAILY DIRECT BEAM RADIATION = 330.75LY/DAY

THE TOTAL RADIATION ON THE SLOPE = 491.31LY/DAY

DAY 111
****

THE DAILY COPRECTION = 1.08

THE DAILY DIRECT BEAM RADIATION = 330.75LY/DAY

THE TOTAL RADIATION ON THE SLOPE = 491.31LY/DAY

DAY 112
****

THE DAILY CORRECTION = 1.08

THE DAILY DIRECT BEAM RADIATION = 330.75LY/DAY

THE TOTAL RADIATION ON THE SLOPE = 491.31LY/DAY

DAY 113
****

THE DAILY CORRECTION = 1.08

THE DAILY DIRECT BEAM RADIATION = 330.75LY/DAY

THE TOTAL RADIATION ON THE SLOPE = 491.31LY/DAY

DAY 114
****

THE DAILY CORRECTION = 1.08

THE DAILY DIRECT BEAM RADIATION = 330.75LY/DAY

THE TOTAL RADIATION ON THE SLOPE = 491.31LY/DAY

DAY 115
****

THE DAILY CORRECTION = 1.03

THE DAILY DIRECT BEAM RADIATION = 317.94LY/DAY

THE TOTAL RADIATION ON THE SLOPE = 478.50LY/DAY

DAY 116
****

THE DAILY CORRECTION = 1.01

THE DAILY DIRECT BEAM RADIATION = 309.34LY/DAY

THE TOTAL RADIATION ON THE SLOPE = 469.90LY/DAY

DAY 117
****

THE DAILY CORRECTION = 1.01

THE DAILY DIRECT BEAM RADIATION = 309.16LY/DAY

THE TOTAL RADIATION ON THE SLOPE = 469.72LY/DAY

DAY 118
****

THE DAILY CORRECTION = 1.00

THE DAILY DIRECT BEAM RADIATION = 308.98LY/DAY

THE TOTAL RADIATION ON THE SLOPE = 469.54LY/DAY

DAY 119
****

THE DAILY CORRECTION = 0.98

THE DAILY DIRECT BEAM RADIATION = 300.24LY/DAY

THE TOTAL RADIATION ON THE SLOPE = 460.80LY/DAY

DAY 120
****

THE DAILY CORRECTION = 0.98

THE DAILY DIPECT BEAM RADIATION = 299.97LY/DAY

THE TOTAL RADIATION ON THE SLOPF = 460.52LY/DAY

DAY 121
****

THE DAILY CORRECTION = 0.95

THE DAILY DIRECT BEAM RADIATION = 291.21LY/DAY

THE TOTAL RADIATION ON THE SLOPE = 451.77LY/DAY

THE AVE. CORR. FOR TIME PERIOD T2-T1= 1.06

THE AVE DAILY DIRECT BEAM RADIATION FOR TIME PERIOD T2-T1 = 325.79LY/DAY

THE AVE TOTAL RADIATION ON THE SLOPE FOR THE TIME PERIOD T2-T1= 486.35LY/DAY

THE AVE. NET SHORT WAVE RADIATION FOR TIME PERIOD T2-T1= 424.09LY/DAY

****

APPENDIX D

Appendix D contains a computer program for the computation of vapor pressures, vapor pressure gradients and temperature gradients above the headscarp at the Fort Simpson landslide. Typical values of wet and dry bulb temperatures are included. Some selected values of net radiation are also listed in this Appendix. They indicate typical hourly intensities during the day and at night for both horizontal and sloped surfaces. They are listed in Table D-1.

D.1 This program computes vapor pressure, vapor pressure gradients and temperature gradients.

The vapor pressure is computed using the equations listed in lines 18, 19, and 20 of the program.

The variables in these equations are the wet bulb temperature (WBT), the dry bulb temperature (DBT), and the barometric pressure (BP). The steam point temperature (STMPT) = 373.16^{o} K.

The data cards are assembled in groups of three. The first card provides the data at the 1 m level, the second at the 3 m level and the third at the 6 m level. The variables on each card are the same.

i) Date (MDATE1, MDATE2) (A2,A4 format)
ii) Time (ITIME 1, ITIME 2) (A4, A3 format)
iii) Level (L(I) (F6.2 format)
iv) Dry bulb temperature (DBT(I) (F6.2 format)
v) Wet bulb temperature (WBT) (F6.2 format)
vi) Barometric pressure (BP) (F8.2 format)
vii) Temperature scale (ISCALE) (C or F, A2 format)

The listing and output are contained in the following pages.

```
                C**** PROGRAM TO COMPUTE VAPOR PRESSURES,VAPOR PRESSUPE GRADIENTS AND
                C**** TEMP. GRADIENTS
                C**** VP GRAD1=VAPOR PRESSURE GRAD. FROM SURFACE TO 1 METER LEVEL
                C**** VP GRAD2=VAPOR PRESSURE GRAD. FROM 1 METER LEVEL TO 3 METER LEVEL
                C**** VP GRAD3=VAPOR PRESSURE GRAD. FROM 3 METER LEVEL TO 6 METER LEVEL
                C**** T GRAD1=TEMP GRAD. FROM SURFACE TO 1 METER LEVEL
                C**** T GRAD2=TEMP GRAD. FROM 1 METER LEVEL TO 3 METER LEVEL
                C**** T GRAD3=TEMP GRAD. FROM 3 METER LEVEL TO 6 METER LEVEL
                C**** VAPOR PRESSURE GRADS. ARE IN MB/METER
                C**** TEMP. GRADS. ARE IN DEG C/METER
                C**** WRITE HEADINGS
0001                 IMPLICIT REAL*8(A-H,O-Z)
0002                 DIMENSION VP(10),L(10),DBT(10)
0003                 INTEGER C/'C'/, ISCALE/'  '/
0004                 REAL L
0005                 WRITE(6,22)
0006                 WRITE(6,12)
0007              12 FORMAT(' ',' *****  *****  ******  *******  *******  *******
                    1 *******  ********  ********  *******  *******  *******  ********
                    2')
0008              22 FORMAT('1',4X,'DATE',4X,'TIME',4X,'LEVEL',3X,'DB TEMP',2X,'WB TEMP
                    1',2X,'B.PRES.',2X,'VP PRES',2X,'VP GRAD1',2X,'VP GRAD2',2X,'VP GRA
                    2D3',2X,'T GRAD1',2X,'T GRAD2',2X,'T GRAD3')
0009              32 DO 30 I=1,3
0010                 READ(5,23)MDATE1,MDATE2,ITIME1,ITIME2,L(I),DBT(I),WBT,BP,ISCALE
0011              23 FORMAT(A2,A4,A4,A3,3F6.2,F8.2,A2)
0012                 IF(ISCALE.EQ.C)GOTO 36
0013                 DBT(I)=(DBT(I)-32.0)*5.0/9.0
0014                 WBT=(WBT-32.0)*5.0/9.0
0015              36 STMPT=373.16
0016                 IF(BP.NE.0.0) GOTO 5
0017                 BP=1000.0
0018               5 EPRIME=7.95357242D10*DEXP(-18.1972839*(STMPT/(WBT+273.16))+5.02808
                    1*DLOG(STMPT/(WBT+273.16))-70242.1852*DEXP(-26.1205253/(STMPT/(WBT+
                    2273.16)))+58.0691913*DEXP(-8.03945282*(STMPT/(WBT+273.16))))
0019                 DELTAE=(0.00066*(1.0+0.00115*WBT))*BP*(DBT(I)-WBT)
0020                 VP(I)=EPRIME-DELTAE
0021                 WRITE(6,25)MDATE1,MDATE2,ITIME1,ITIME2,L(I),DBT(I),WBT,BP,VP(I)
0022                 IF(I.EQ.3) GOTO31
0023              30 CONTINUE
                C     COMPUTE GRADIENTS
0024              31 VPG1=(VP(1)-8.7)/(L(1)-0.0)
0025                 VPG2=(VP(2)-VP(1))/(L(2)-L(1))
0026                 VPG3=(VP(3)-VP(2))/(L(3)-L(2))
0027                 TEG1=(DBT(1)-5.0)/(L(1)-0.0)
0028                 TEG2=(DBT(2)-DBT(1))/(L(2)-L(1))
0029                 TEG3=(DBT(3)-DBT(2))/(L(3)-L(2))
0030                 WRITE(6,24)VPG1,VPG2,VPG3,TEG1,TEG2,TEG3
0031                 GOTO 32
0032              24 FORMAT('0',64X,F6.2,5X,F6.2,4X,F6.2,4X,F6.2,3X,F6.2,3X,F6.2)
0033              25 FORMAT('0',3X,A2,A4,2X,A4,A3,1X,F5.2,3X,F6.2,3X,F6.2,3X,F7.2,4X,F6
                    1.2)
0034                 END
```

DATE	TIME	LEVEL	DB TEMP	WB TEMP	B.PRES.	VP PRES	VP GRAD1	VP GRAD2	VP GRAD3	T GRAD1	T GRAD2	T GRAD3
JUN19	18:00	1.00	16.25	12.78	996.18	12.44						
JUN19	18:00	3.00	16.83	13.11	996.18	12.59						
JUN19	18:00	6.00	17.19	13.22	996.18	12.54						
							3.74	0.08	-0.02	11.25	0.20	0.12
JUN21	08:20	1.00	12.17	10.69	996.18	11.88						
JUN21	08:20	3.00	13.22	11.31	996.18	12.11						
JUN21	08:20	6.00	13.31	11.50	996.18	12.36						
							3.18	0.12	0.08	7.17	0.53	0.03
JUN21	10:00	1.00	16.11	12.78	996.18	12.53						
JUN21	10:00	3.00	16.72	13.39	996.18	13.13						
JUN21	10:00	6.00	17.11	13.61	996.18	13.24						
							3.83	0.30	0.04	11.11	0.31	0.13
JUN21	12:00	1.00	18.06	13.61	996.18	12.61						
JUN21	12:00	3.00	18.61	14.03	996.18	12.94						
JUN21	12:00	6.00	19.08	14.28	996.18	13.06						
							3.91	0.17	0.04	13.06	0.28	0.16
JUN21	14:00	1.00	20.56	14.28	996.18	12.07						
JUN21	14:00	3.00	20.94	14.44	996.18	12.10						
JUN21	14:00	6.00	22.06	14.61	996.18	11.64						
							3.37	0.01	-0.15	15.56	0.19	0.37
JUN21	16:00	1.00	20.22	14.28	996.18	12.29						
JUN21	16:00	3.00	21.44	14.44	996.18	11.76						
JUN21	16:00	6.00	21.67	14.67	996.18	12.00						
							3.59	-0.26	0.08	15.22	0.61	0.07
JUN22	04:00	1.00	14.44	12.39	996.59	13.01						
JUN22	04:00	3.00	14.44	13.44	996.59	14.74						
JUN22	04:00	6.00	15.00	13.72	996.59	14.84						
							4.31	0.87	0.03	9.44	0.0	0.19
JUN22	09:40	1.00	11.72	11.53	996.59	13.46						
JUN22	09:40	3.00	11.89	11.89	996.59	13.91						

JUN22	09:40	6.00	12.28	11.94	996.59	13.74						
							4.76	0.23	-0.06	6.72	0.08	0.13
JUN22	12:00	1.00	10.44	10.28	996.59	12.39						
JUN22	12:00	3.00	10.83	10.81	996.59	12.93						
JUN22	12:00	6.00	10.92	10.86	996.59	12.96						
							3.69	0.27	0.01	5.44	0.19	0.03
JUN24	10:20	1.00	10.78	9.17	983.39	10.55						
JUN24	10:20	3.00	10.89	9.33	983.39	10.71						
JUN24	10:20	6.00	10.97	9.39	983.39	10.74						
							1.85	0.08	0.01	5.78	0.06	0.03
JUN24	12:00	1.00	11.94	10.56	983.39	11.82						
JUN24	12:00	3.00	12.11	10.81	983.39	12.09						
JUN24	12:00	6.00	11.78	10.89	983.39	12.44						
							3.12	0.13	0.12	6.94	0.08	-0.11
JUN27	09:20	1.00	13.56	8.72	983.25	8.09						
JUN27	09:20	3.00	14.00	9.00	983.25	8.20						
JUN27	09:20	6.00	14.39	9.39	983.25	8.50						
							-0.61	0.05	0.10	8.56	0.22	0.13
JUN27	15:20	1.00	17.56	11.11	983.25	8.98						
JUN27	15:20	3.00	18.33	11.39	983.25	8.90						
JUN27	15:20	6.00	19.03	11.56	983.25	8.70						
							0.28	-0.04	-0.07	12.56	0.39	0.23
JUN27	16:00	1.00	18.42	12.00	983.25	9.80						
JUN27	16:00	3.00	19.17	12.56	983.25	10.19						
JUN27	16:00	6.00	19.56	12.72	983.25	10.20						
							1.10	0.20	0.00	13.42	0.38	0.13
JUN28	05:00	1.00	9.22	9.06	986.59	11.41						
JUN28	05:00	3.00	10.94	10.39	986.59	12.23						
JUN28	05:00	6.00	11.94	10.44	986.59	11.65						
							2.71	0.41	-0.19	4.22	0.86	0.33
JUN28	07:00	1.00	11.78	11.00	986.59	12.61						

JUN28	07:00	3.00	12.50	11.83	986.59	13.42						
JUN28	07:00	6.00	13.17	12.39	986.59	13.87						
							3.91	0.41	0.15	6.78	0.36	0.22
JUN29	15:00	1.00	11.39	10.44	990.59	12.02						
JUN29	15:00	3.00	11.22	10.67	990.59	12.46						
JUN29	15:00	6.00	11.94	11.22	990.59	12.84						
							3.32	0.22	0.12	6.39	-0.08	0.24
JUN30	12:20	1.00	10.28	7.56	998.72	8.59						
JUN30	12:20	3.00	9.94	8.00	998.72	9.43						
JUN30	12:20	6.00	10.28	8.28	998.72	9.60						
							-0.11	0.42	0.06	5.28	-0.17	0.11
JUN30	15:20	1.00	12.22	6.33	998.72	5.65						
JUN30	15:20	3.00	12.61	7.17	998.72	6.51						
JUN30	15:20	6.00	13.06	7.28	998.72	6.37						
							-3.05	0.43	-0.05	7.22	0.19	0.15
JUL 1	12:00	1.00	14.67	9.83	994.99	8.93						
JUL 1	12:00	3.00	15.22	11.50	994.99	11.09						
JUL 1	12:00	6.00	16.44	14.06	994.99	14.44						
							0.23	1.08	1.12	9.67	0.28	0.41
JUL 1	14:00	1.00	15.61	9.00	994.99	7.09						
JUL 1	14:00	3.00	15.67	9.31	994.99	7.49						
JUL 1	14:00	6.00	17.11	9.56	994.99	6.90						
							-1.61	0.20	-0.20	10.61	0.03	0.48
JUL 3	16:40	1.00	16.11	11.89	994.99	11.10						
JUL 3	16:40	3.00	16.72	12.61	994.99	11.85						
JUL 3	16:40	6.00	16.67	13.06	994.99	12.62						
							2.40	0.37	0.25	11.11	0.31	-0.02
JUL 3	18:00	1.00	14.89	13.22	994.99	14.08						
JUL 3	18:00	3.00	15.61	14.67	994.99	16.05						
JUL 3	18:00	6.00	15.50	14.44	994.99	15.74						
							5.38	0.99	-0.10	9.89	0.36	-0.04

JUL 3	19:20	1.00	16.67	13.17	994.99	12.80						
JUL 3	19:20	3.00	18.22	14.94	994.99	14.79						
JUL 3	19:20	6.00	18.22	15.11	994.99	15.09						
							4.10	1.00	0.10	11.67	0.78	0.0
JUL 4	11:20	1.00	16.67	12.78	992.32	12.17						
JUL 4	11:20	3.00	18.00	13.61	992.32	12.66						
JUL 4	11:20	6.00	18.00	13.44	992.32	12.38						
							3.47	0.25	-0.09	11.67	0.67	0.0
JUL 4	12:00	1.00	15.83	12.44	992.32	12.18						
JUL 4	12:00	3.00	16.33	13.44	992.32	13.49						
JUL 4	12:00	6.00	16.94	13.39	992.32	12.99						
							3.48	0.65	-0.17	10.83	0.25	0.20
JUL 4	13:00	1.00	18.17	13.83	992.32	12.92						
JUL 4	13:00	3.00	18.44	14.11	992.32	13.21						
JUL 4	13:00	6.00	19.03	14.22	992.32	13.01						
							4.22	0.14	-0.07	13.17	0.14	0.19
JUL 5	13:20	1.00	21.00	14.50	991.65	12.18						
JUL 5	13:20	3.00	21.56	14.56	991.65	11.90						
JUL 5	13:20	6.00	21.89	14.78	991.65	12.07						
							3.48	-0.14	0.05	16.00	0.28	0.11
JUL 5	15:00	1.00	21.78	14.03	991.65	10.85						
JUL 5	15:00	3.00	22.78	14.11	991.65	10.33						
JUL 5	15:00	6.00	23.17	14.22	991.65	10.26						
							2.15	-0.26	-0.02	16.78	0.50	0.13
JUL 5	17:00	1.00	19.44	13.94	991.65	12.26						
JUL 5	17:00	3.00	19.61	14.06	991.65	12.34						
JUL 5	17:00	6.00	20.00	14.11	991.65	12.18						
							3.56	0.04	-0.05	14.44	0.08	0.13
JUL 5	19:00	1.00	17.44	12.78	991.65	11.65						
JUL 5	19:00	3.00	17.61	12.89	991.65	11.72						
JUL 5	19:00	6.00	17.83	12.94	991.65	11.67						

							2.95	0.04	-0.02	12.44	0.08	0.07
JUL 5	21:00	1.00	13.89	11.22	991.65	11.55						
JUL 5	21:00	3.00	14.00	11.28	991.65	11.56						
JUL 5	21:00	6.00	14.44	11.28	991.65	11.26						
							2.85	0.01	-0.10	8.89	0.04	0.15
JUL 5	24:00	1.00	12.50	10.28	991.65	11.03						
JUL 5	24:00	3.00	13.00	10.50	991.65	11.03						
JUL 5	24:00	6.00	13.06	10.56	991.65	11.08						
							2.33	0.00	0.02	7.50	0.25	0.02
JUL10	14:20	1.00	22.22	14.44	987.52	11.29						
JUL10	14:20	3.00	22.50	14.72	987.52	11.59						
JUL10	14:20	6.00	22.72	15.50	987.52	12.81						
							2.59	0.15	0.41	17.22	0.14	0.07
JUL10	16:00	1.00	22.22	14.94	987.52	12.16						
JUL10	16:00	3.00	22.56	15.11	987.52	12.23						
JUL10	16:00	6.00	22.83	15.33	987.52	12.44						
							3.46	0.04	0.07	17.22	0.17	0.09
JUL10	18:00	1.00	24.39	15.14	987.52	11.06						
JUL10	18:00	3.00	25.00	15.78	987.52	11.80						
JUL10	18:00	6.00	25.22	15.94	987.52	11.95						
							2.36	0.37	0.05	19.39	0.31	0.07
JUL10	20:00	1.00	23.89	15.00	987.52	11.15						
JUL10	20:00	3.00	24.56	15.17	987.52	11.00						
JUL10	20:00	6.00	24.72	15.33	987.52	11.19						
							2.45	-0.07	0.06	18.89	0.33	0.06
JUL10	22:00	1.00	22.33	15.00	987.52	11.85						
JUL10	22:00	3.00	23.33	15.28	987.52	12.01						
JUL10	22:00	6.00	23.78	15.56	987.52	12.21						
							3.15	0.08	0.07	17.83	0.25	0.15
JUL10	24:00	1.00	17.78	13.06	987.52	11.90						
JUL10	24:00	3.00	19.50	13.56	987.52	11.59						

JUL10	24:00	6.00	20.89	14.17	987.52	11.70						
							3.20	-0.16	0.04	12.78	0.86	0.46
JUL11	02:00	1.00	14.83	11.56	990.05	11.44						
JUL11	02:00	3.00	16.94	12.50	990.05	11.54						
JUL11	02:00	6.00	18.50	13.33	990.05	11.87						
							2.74	0.05	0.11	9.83	1.06	0.52
JUL11	04:00	1.00	15.06	11.67	990.05	11.47						
JUL11	04:00	3.00	16.17	12.17	990.05	11.52						
JUL11	04:00	6.00	16.94	12.33	990.05	11.27						
							2.77	0.03	-0.08	10.06	0.56	0.26
JUL11	06:00	1.00	14.72	11.56	990.05	11.51						
JUL11	06:00	3.00	15.83	11.94	990.05	11.39						
JUL11	06:00	6.00	16.17	12.06	990.05	11.35						
							2.81	-0.06	-0.01	9.72	0.56	0.11
JUL11	08:00	1.00	15.17	12.89	990.05	13.35						
JUL11	08:00	3.00	15.33	13.28	990.05	13.88						
JUL11	08:00	6.00	15.67	13.33	990.05	13.75						
							4.65	0.26	-0.04	10.17	0.08	0.11
JUL11	10:00	1.00	16.72	13.61	990.05	13.51						
JUL11	10:00	3.00	17.22	13.72	990.05	13.37						
JUL11	10:00	6.00	17.39	13.83	990.05	13.44						
							4.81	-0.07	0.03	11.72	0.25	0.06
JUL11	12:00	1.00	20.56	14.72	990.05	12.87						
JUL11	12:00	3.00	21.11	15.11	990.05	13.18						
JUL11	12:00	6.00	21.11	15.11	990.05	13.18						
							4.17	0.16	0.0	15.56	0.28	0.0
JUL11	14:00	1.00	22.44	15.06	990.05	12.19						
JUL11	14:00	3.00	22.61	15.22	990.05	12.38						
JUL11	14:00	6.00	23.00	15.28	990.05	12.22						
							3.49	0.09	-0.05	17.44	0.08	0.13
JUL11	16:00	1.00	22.22	15.06	990.05	12.34						

JUL11	16:00	3.00	23.50	15.78	990.05	12.78						
JUL11	16:00	6.00	23.72	15.61	990.05	12.33						
							3.64	0.22	-0.15	17.22	0.64	0.07
JUL12	10:00	1.00	13.50	10.83	993.12	11.20						
JUL12	10:00	3.00	13.61	13.61	993.12	15.58						
JUL12	10:00	6.00	13.83	11.28	993.12	11.67						
							2.50	2.19	-1.30	8.50	0.06	0.07
JUL12	12:00	1.00	13.33	11.22	993.12	11.91						
JUL12	12:00	3.00	13.89	11.33	993.12	11.72						
JUL12	12:00	6.00	14.28	11.67	993.12	11.98						
							3.21	-0.10	0.09	8.33	0.28	0.13
JUL12	14:00	1.00	13.89	11.11	993.12	11.37						
JUL12	14:00	3.00	14.22	11.25	993.12	11.37						
JUL12	14:00	6.00	14.33	11.39	993.12	11.51						
							2.67	-0.00	0.05	8.89	0.17	0.04
JUL12	16:00	1.00	13.33	11.67	993.12	12.60						
JUL12	16:00	3.00	13.56	11.67	993.12	12.46						
JUL12	16:00	6.00	13.61	11.94	993.12	12.86						
							3.90	-0.07	0.13	8.33	0.11	0.02
JUL12	18:00	1.00	13.56	11.67	993.12	12.46						
JUL12	18:00	3.00	13.61	11.78	993.12	12.60						
JUL12	18:00	6.00	13.56	11.67	993.12	12.46						
							3.76	0.07	-0.05	8.56	0.03	-0.02
JUL13	09:20	1.00	13.33	12.06	1002.72	13.21						
JUL13	09:20	3.00	13.33	12.22	1002.72	13.48						
JUL13	09:20	6.00	13.50	12.50	1002.72	13.81						
							4.51	0.13	0.11	8.33	0.0	0.06
JUL13	12:00	1.00	16.00	12.78	1002.72	12.59						
JUL13	12:00	3.00	16.39	12.78	1002.72	12.33						
JUL13	12:00	6.00	16.22	12.78	1002.72	12.44						
							3.89	-0.13	0.04	11.00	0.19	-0.06

JUL13	14:00	1.00	17.06	12.06	1002.72	10.71						
JUL13	14:00	3.00	17.56	12.39	1002.72	10.91						
JUL13	14:00	6.00	17.50	12.61	1002.72	11.31						
							2.01	0.10	0.13	12.06	0.25	-0.02
JUL13	16:00	1.00	19.22	12.22	1002.72	9.53						
JUL13	16:00	3.00	19.78	12.64	1002.72	9.83						
JUL13	16:00	6.00	20.22	12.72	1002.72	9.66						
							0.83	0.15	-0.05	14.22	0.28	0.15
JUL14	10:20	1.00	15.56	12.78	1002.05	12.89						
JUL14	10:20	3.00	16.33	13.22	1002.05	13.10						
JUL14	10:20	6.00	16.89	13.33	1002.05	12.91						
							4.19	0.11	-0.06	10.56	0.39	0.19
JUL14	14:00	1.00	19.17	12.44	1002.05	9.92						
JUL14	14:00	3.00	20.50	13.06	1002.05	10.03						
JUL14	14:00	6.00	21.00	12.78	1002.05	9.23						
							1.22	0.05	-0.26	14.17	0.67	0.17
JUL14	18:00	1.00	21.61	12.67	1002.05	8.64						
JUL14	18:00	3.00	22.28	13.00	1002.05	8.74						
JUL14	18:00	6.00	22.50	12.78	1002.05	8.23						
							-0.06	0.05	-0.17	16.61	0.33	0.07
JUL14	20:00	1.00	22.22	13.22	1002.05	9.15						
JUL14	20:00	3.00	22.44	13.28	1002.05	9.09						
JUL14	20:00	6.00	23.22	13.39	1002.05	8.75						
							0.45	-0.03	-0.11	17.22	0.11	0.26
JUL15	09:20	1.00	14.78	12.00	998.45	12.16						
JUL15	09:20	3.00	15.17	12.22	998.45	12.26						
JUL15	09:20	6.00	15.28	12.06	998.45	11.92						
							3.46	0.05	-0.11	9.78	0.19	0.04
JUL15	12:00	1.00	15.61	13.00	998.45	13.22						
JUL15	12:00	3.00	16.89	13.39	998.45	13.01						
JUL15	12:00	6.00	17.39	13.67	998.45	13.14						

							4.52	-0.11	0.04	10.61	0.64	0.17
JUL15	14:00	1.00	18.44	14.22	998.45	13.38						
JUL15	14:00	3.00	19.56	14.61	998.45	13.31						
JUL15	14:00	6.00	19.86	14.72	998.45	13.30						
							4.68	-0.04	-0.00	13.44	0.56	0.10
JUL15	16:00	1.00	18.89	13.72	998.45	12.23						
JUL15	16:00	3.00	19.44	14.39	998.45	13.00						
JUL15	16:00	6.00	20.00	14.50	998.45	12.82						
							3.53	0.38	-0.06	13.89	0.28	0.19
JUL15	18:00	1.00	19.61	14.50	998.45	13.08						
JUL15	18:00	3.00	20.00	14.67	998.45	13.11						
JUL15	18:00	6.00	20.83	14.72	998.45	12.65						
							4.38	0.01	-0.15	14.61	0.19	0.28
JUL15	20:00	1.00	19.72	14.11	998.45	12.33						
JUL15	20:00	3.00	20.67	14.33	998.45	12.08						
JUL15	20:00	6.00	21.67	14.33	998.45	11.41						
							3.63	-0.13	-0.22	14.72	0.47	0.33
JUL15	22:00	1.00	20.17	13.33	998.45	10.73						
JUL15	22:00	3.00	20.56	13.72	998.45	11.12						
JUL15	22:00	6.00	20.89	13.72	998.45	10.89						
							2.03	0.20	-0.07	15.17	0.19	0.11
JUL15	24:00	1.00	15.89	12.06	998.45	11.51						
JUL15	24:00	3.00	17.72	12.78	998.45	11.45						
JUL15	24:00	6.00	18.44	12.56	998.45	10.60						
							2.81	-0.03	-0.29	10.89	0.62	0.24
JUL16	02:00	1.00	15.44	11.67	990.19	11.21						
JUL16	02:00	3.00	16.00	11.67	990.19	10.84						
JUL16	02:00	6.00	16.17	11.72	990.19	10.82						
							2.51	-0.18	-0.01	10.44	0.29	0.06
JUL16	04:00	1.00	13.33	9.83	990.19	9.82						
JUL16	04:00	3.00	14.03	10.28	990.19	10.02						

JUL16	04:00	6.00	14.17	10.28	990.19	9.93						
							1.12	0.10	-0.03	8.33	0.35	0.05
JUL16	06:00	1.00	11.11	9.72	990.19	11.13						
JUL16	06:00	3.00	11.78	9.72	990.19	10.69						
JUL16	06:00	6.00	11.78	9.72	990.19	10.69						
							2.43	-0.22	0.0	6.11	0.33	0.0
JUL16	08:00	1.00	13.44	9.94	990.19	9.91						
JUL16	08:00	3.00	13.78	10.50	990.19	10.52						
JUL16	08:00	6.00	13.94	10.50	990.19	10.41						
							1.21	0.30	-0.04	8.44	0.17	0.06
JUL16	10:00	1.00	17.50	12.00	990.19	10.37						
JUL16	10:00	3.00	18.19	12.33	990.19	10.44						
JUL16	10:00	6.00	18.78	12.22	990.19	9.88						
							1.67	0.04	-0.19	12.50	0.35	0.19
JUL16	12:00	1.00	19.89	13.33	990.19	10.95						
JUL16	12:00	3.00	20.39	13.61	990.19	11.08						
JUL16	12:00	6.00	20.61	13.33	990.19	10.47						
							2.25	0.07	-0.20	14.89	0.25	0.07
JUL16	14:00	1.00	21.50	12.83	990.19	9.06						
JUL16	14:00	3.00	22.56	13.22	990.19	9.00						
JUL16	14:00	6.00	22.78	13.22	990.19	8.85						
							0.36	-0.03	-0.05	16.50	0.53	0.07
JUL16	16:00	1.00	22.22	13.28	990.19	9.31						
JUL16	16:00	3.00	23.22	13.75	990.19	9.43						
JUL16	16:00	6.00	23.94	13.83	990.19	9.09						
							0.61	0.06	-0.11	17.22	0.50	0.24
JUL16	18:20	1.00	17.44	13.22	990.19	12.39						
JUL16	18:20	3.00	17.89	13.78	990.19	13.02						
JUL16	18:20	6.00	18.44	13.33	990.19	11.91						
							3.69	0.32	-0.37	12.44	0.22	0.19
JUL16	20:00	1.00	15.94	13.06	990.19	13.11						

JUL16	20:00	3.00	16.67	13.33	990.19	13.09						
JUL16	20:00	6.00	16.89	13.39	990.19	13.03						
							4.41	-0.01	-0.02	10.94	0.36	0.07
JUL16	22:00	1.00	14.39	12.83	990.19	13.77						
JUL16	22:00	3.00	14.94	13.28	990.19	14.14						
JUL16	22:00	6.00	15.06	13.22	990.19	13.97						
							5.07	0.18	-0.06	9.39	0.28	0.04
JUL16	24:00	1.00	13.61	12.33	990.19	13.48						
JUL16	24:00	3.00	13.89	12.33	990.19	13.30						
JUL16	24:00	6.00	14.06	12.94	990.19	14.18						
							4.78	-0.09	0.29	8.61	0.14	0.06
JUL17	07:00	1.00	13.61	12.22	993.92	13.30						
JUL17	07:00	3.00	14.22	12.22	993.92	12.89						
JUL17	07:00	6.00	14.17	12.22	993.92	12.93						
							4.60	-0.20	0.01	8.61	0.31	-0.02
JUL17	10:00	1.00	13.67	12.50	993.92	13.71						
JUL17	10:00	3.00	14.50	12.94	993.92	13.88						
JUL17	10:00	6.00	14.22	12.94	993.92	14.06						
							5.01	0.08	0.06	8.67	0.42	-0.09
JUL17	12:00	1.00	16.39	13.89	993.92	14.20						
JUL17	12:00	3.00	16.39	14.17	993.92	14.67						
JUL17	12:00	6.00	16.44	14.22	993.92	14.73						
							5.50	0.24	0.02	11.39	0.0	0.02
JUL17	16:00	1.00	13.33	9.44	993.92	9.24						
JUL17	16:00	3.00	15.67	13.39	993.92	13.84						
JUL17	16:00	6.00	15.89	13.33	993.92	13.60						
							0.54	2.30	-0.08	8.33	1.17	0.07
JUL17	18:00	1.00	18.06	14.44	993.92	14.04						
JUL17	18:00	3.00	19.33	14.67	993.92	13.57						
JUL17	18:00	6.00	19.44	14.44	993.92	13.11						
							5.34	-0.23	-0.15	13.06	0.64	0.04

TABLE D-1

RADIATION DATA JUNE 21/74 (LY/HR)
(FORT SIMPSON TEST SITE)

TIME (HOURS)	STA 1	STA 2	STA 3	STA 4	STA 5	STA 6
1:00	0.9	1.0	2.7	0.4	-2.0	0.1
2:00	1.5	1.8	3.6	1.1	-1.2	-
3:00	1.7	1.9	3.9	1.4	-0.6	-
4:00	0.9	1.1	5.8	0.6	-2.1	-
5:00	-0.4	-	2.5	0.9	-3.9	0.9
6:00	0.6	1.2	4.6	4.5	-2.0	3.6
7:00	1.7	3.1	10.2	13.3	-1.7	9.3
8:00	2.8	6.0	11.6	15.3	5.7	11.8
9:00	2.5	5.0	14.3	36.1	21.2	25.6
10:00	3.3	7.6	21.2	46.1	37.1	39.4
11:00	6.6	7.3	16.6	31.2	43.8	45.0
12:00	5.4	10.6	14.0	17.6	53.7	55.3
13:00	17.4	9.1	11.3	38.1	56.0	59.2
14:00	18.6	9.9	12.5	52.7	58.0	62.4
15:00	28.5	5.9	12.1	43.6	58.4	62.0
16:00	20.0	10.1	11.1	31.3	55.6	58.5
17:00	20.5	7.0	5.1	11.7	34.6	36.3
18:00	14.3	13.7	13.9	9.2	35.7	38.5
19:00	28.6	18.8	17.2	8.8	24.7	27.2
20:00	21.1	16.0	15.9	6.9	16.7	18.6
21:00	38.2	26.1	22.1	4.3	18.3	21.6
22:00	18.5	26.3	25.2	4.5	7.8	13.8
23:00	19.5	19.5	17.6	1.5	-2.1	6.0
24:00	3.5	5.1	7.9	-	-5.4	1.0
AVE	11.5	8.9	11.8	15.9	21.1	24.8

TABLE D-1 (CONTINUED)

RADIATION DATA JULY 11/74 (Ly/Hr)
(FORT SIMPSON TEST SITE)

TIME (HOURS)	STA 1	STA 2	STA 3	STA 4	STA 5	STA 6
1:00	0.9	-	-0.6	1.3	-5.1	1.9
2:00	1.1	-	-0.7	1.0	-4.8	1.9
3:00	1.5	0.2	-0.5	1.2	-4.3	1.9
4:00	2.1	0.8	-0.2	1.6	-3.7	1.9
5:00	2.1	0.7	-0.4	2.0	-3.9	2.3
6:00	2.9	1.6	0.7	7.3	1.3	5.1
7:00	3.4	2.6	2.0	15.6	2.2	12.2
8:00	4.3	4.1	4.0	10.0	2.8	10.3
9:00	5.5	5.2	8.1	19.1	11.7	18.7
10:00	7.4	7.6	12.1	24.0	19.2	26.4
11:00	7.6	7.1	18.6	30.9	38.0	44.5
12:00	7.4	6.6	16.2	23.8	44.0	52.0
13:00	13.3	11.5	16.1	29.8	46.0	55.6
14:00	15.3	12.0	29.0	33.2	49.9	59.3
15:00	14.6	10.5	29.6	24.4	38.0	47.4
16:00	21.1	9.9	53.2	17.9	45.0	54.1
17:00	8.2	4.4	10.8	4.4	2.2	4.7
18:00	15.0	14.0	20.3	11.4	16.3	22.3
19:00	18.6	15.5	18.1	11.5	13.5	19.4
20:00	32.1	22.2	25.7	8.2	17.9	24.1
21:00	41.5	30.0	29.2	8.1	17.8	24.1
22:00	19.8	16.4	13.1	6.5	5.5	12.4
23:00	10.3	9.7	4.7	3.7	-1.2	5.4
24:00	8.8	8.5	2.1	1.9	-3.6	3.0
AVE	10.9	8.5	13.1	12.6	14.6	21.6

TABLE D-1 (CONTINUED)

RADIATION DATA JULY 19/74
(FORT SIMPSON TEST SITE)

TIME (HOURS)	STA 1	STA 2	STA 3	STA 4	STA 5	STA 6
1:00	-1.6	0.8	0.3	-0.3	-5.9	1.9
2:00	-1.8	-1.0	-0.3	-0.7	-6.2	1.9
3:00	-1.8	-1.1	-0.6	-0.8	-6.2	1.9
4:00	-1.8	-1.1	-0.7	-1.0	-6.1	2.0
5:00	-1.6	-0.9	-0.6	-0.7	-5.6	2.1
6:00	-0.1	1.1	1.8	3.5	-3.2	4.8
7:00	1.9	3.2	4.0	4.4	-0.7	6.0
8:00	4.5	6.1	7.4	8.5	4.1	10.2
9:00	6.5	9.2	11.9	39.2	40.6	31.6
10:00	4.5	6.0	7.1	27.2	19.9	19.2
11:00	3.7	4.7	5.3	54.3	40.3	47.2
12:00	5.5	4.8	5.8	32.8	45.4	54.0
13:00	6.3	4.9	6.0	41.5	47.9	60.9
14:00	18.3	5.6	6.7	45.7	49.7	62.3
15:00	26.5	6.0	7.0	24.0	49.6	62.4
16:00	7.5	6.0	6.6	12.5	46.5	59.8
17:00	24.1	8.0	8.6	13.3	37.9	50.2
18:00	28.7	13.6	10.8	5.7	19.9	29.9
19:00	22.3	13.2	10.8	4.4	9.7	18.8
20:00	18.9	15.6	14.1	7.5	8.9	14.5
21:00	8.2	8.5	9.4	5.9	2.5	8.6
22:00	6.7	5.0	8.7	5.6	-1.9	5.6
23:00	2.1	3.4	4.2	2.3	-2.9	4.1
24:00	1.4	2.2	3.1	2.0	-2.7	2.1
AVE	7.9	5.2	5.8	14.2	16.1	23.7

B30166